For Reference

NOT TO BE TAKEN FROM THIS ROOM

For Reference

NOT TO BE TAKEN FROM THIS ROOM

Ex libris
universitatis
albertaensis

University of Alberta
Printing Department

Digitized by the Internet Archive
in 2018 with funding from
University of Alberta Libraries

https://archive.org/details/Truch1963

Thesis
1963
#70

THE UNIVERSITY OF ALBERTA

FRAME DEFLECTIONS IN THE PLASTIC RANGE

by

WILLIAM PATRICK TRUCH

A THESIS
SUBMITTED TO THE FACULTY OF GRADUATE STUDIES
IN PARTIAL FULFILMENT OF THE REQUIREMENTS FOR THE DEGREE
OF MASTER OF SCIENCE

DEPARTMENT OF CIVIL ENGINEERING

EDMONTON, ALBERTA

APRIL, 1963

ABSTRACT

Theoretical load-deflection calculations for steel structures, based on the simple plastic theory, provide a good comparison with experimental values up to the formation of the first plastic hinge. Thereafter, a considerable departure between theoretical and experimental values is usually observed, due to the effects of strain-hardening.

A method for the analysis of steel frames which includes the non-linear characteristics of the stress-strain diagram, is presented for the cases wherein single concentrated loads are applied. Experimental verification is provided from results of load tests on two frames. One frame was loaded with a concentrated vertical load at midspan, the other with a concentrated horizontal load at the top of one column. Theoretical load-deflection values derived by this method, which is based on the "moment end-slope" relationships for a given section, provided very close agreement with experimental values.

Results of tests conducted to define the material properties pertinent to the derivation of the "moment end-slope" relationships are also presented.

In addition, test results are presented for two frames which were subjected to horizontal and vertical concentrated loads. These results will provide information for an experimental check in a future extension of this project which will incorporate the "moment end-slope" relationships into an analysis for the case of combined loadings.

ACKNOWLEDGMENTS

The author wishes to express his sincere thanks to the following persons for their cooperation towards the successful completion of the studies reported herein.

Professor J. Longworth, Department of Civil Engineering, for his guidance, advice and criticism in carrying out the testing program and in preparation of the report.

W. B. McMinn, Assistant Professor, Computing Center, University of Alberta, for his assistance in compiling the computer program.

D. W. Murray, Associate Professor, Department of Civil Engineering, for his guidance in the theoretical frame analyses.

The Canadian Institute of Steel Construction, Western Regional Committee, Alberta Division, for providing the test specimens.

H. Panse, A. L. Ekman, K. Lazenby, B. Aves, D. McGowan, W. Sadoway, W. J. Gregg, and P. B. Makowichuk for their assistance during the testing program.

Miss G. Misura, for her untiring effort in typing and proof reading the manuscript.

The author is also indebted to his wife for her moral support throughout the entire project.

TABLE OF CONTENTS

ABSTRACT i

ACKNOWLEDGMENTS ii

LIST OF FIGURES v

LIST OF PLATES ix

CHAPTER I INTRODUCTION

1-1 Analysis of Structures Beyond the Elastic Limit 1
1-2 Analysis of Deflections Beyond the Elastic Limit 4
1-3 Previous Investigations at the U. of A. 9
1-4 Present Investigation 11

CHAPTER II SCOPE OF INVESTIGATION 13

CHAPTER III MATERIAL PROPERTIES

3-1 Definitions 16
3-2 Tensile Test Specimens 17
3-3 Loading and Instrumentation 18
3-4 Tensile Test Results 19

CHAPTER IV RESIDUAL STRESSES

4-1 Sectioning Method for Residual Stress Measurements .. 25
4-2 Stub Column Tests 26
4-3 Results of Residual Stress Measurements 26

CHAPTER V MOMENT-END-SLOPE RELATIONSHIP

5-1 Moment-Curvature Relationship 32
5-2 Moment End-Slope Relationship 37
5-3 Method of Analysis 40

CHAPTER VI BEAM TESTS

6-1 Beam Specimens 48
6-2 Loading System 48
6-3 Beam Instrumentation 50
6-4 Experimental Procedure 55
6-5 Test Results 55

CHAPTER VII FRAME TESTS

7-1 Frame Specimens 64
7-2 Loading System 68
7-3 Frame Instrumentation 69
7-4 Experimental Procedure 76
7-5 Frame Test Results 77

CHAPTER VIII DISCUSSION

8-1 Material Properties 113
8-2 Residual Stresses 115
8-3 Beam Test Results 117
8-4 Frame Test No. 1 122
8-5 Frame Test No. 2 127
8-6 Frame Test No. 3 131
8-7 Frame Test No. 4 134

CHAPTER IX CONCLUSIONS 138

BIBLIOGRAPHY 141

APPENDIX A CALCULATIONS BASED ON SIMPLE PLASTIC THEORY

A-1 Section Properties (4 I 9.5) A1
A-2 Ultimate Load Calculations A1
A-3 Elastic Analysis A14
A-4 Deflection Calculations A20
A-5 Theoretical Moment-Curvature Relationship A36
A-6 Calculated Moment-Curvature Relationships A37
A-7 Calculated Horizontal Reactions A39

APPENDIX B CALCULATIONS BASED ON MOMENT END-SLOPE RELATIONSHIPS

B-1 Moment-Curvature Relationship B1
B-2 Deflection Calculations B2
Table B B13

APPENDIX C COMPUTER PROGRAM FOR MOMENT END-SLOPE RELATIONSHIPS C1

APPENDIX D TEST RESULTS FROM TENSION TESTS D1

LIST OF FIGURES

Figure Page

1 Stress Distributions Assumed for Calculating Deflections Beyond the Elastic Limit 6

2 Assumed Stress-Strain and Moment-Curvature Relationships Used in Deflection Calculations 8

3 Test Coupon Dimensions 20

4 Stress-Strain Curves for Web Coupons 22

5 Stress-Strain Curves for Flange Coupons 23

6 Average Stress-Strain Curve Derived from Tension Tests ... 24

7 Sectioning Method for Measuring Residual Strains 28

8 Distribution of Residual Stresses after Final Sectioning 29

9 Stress-Strain Curves for Stub Columns 30

10 Non-Dimensional Moment-Curvature Relationship 35

11 Non-Dimensional Stress-Strain Relationship Derived from Tension Tests 36

12 Designation of Moments and Deformations of a Simply-Supported Beam 38

13 Moment End-Slope Relationships 4 I 9.5, Double Curvature, Derived from Theoretical Moment-Curvature Relation 41

14 Moment End-Slope Relationships 4 I 9.5, Double Curvature, Derived from Experimental Moment-Curvature Relation 42

15 Moment End-Slope Relationships 4 I 9.5, Single Curvature, Derived from Theoretical Moment-Curvature Relation 43

16 Moment End-Slope Relationships 4 I 9.5, Single Curvature, Derived from Experimental Moment-Curvature Relation ... 44

17 Details of Test Beams 49

18 Load vs. Deflection at Midspan, Beam Test No. 1 57

19 Load vs. Deflection at Midspan, Beam Test No. 2 58

20 Moment vs. Curvature at Midspan, Beam Test No. 1 59

21 Moment vs. Curvature at Midspan, Beam Test No. 2 60

22 Average Moment vs. Curvature Relationship (4 I 9.5) 61

23 Details of Test Frames 65

24 Details of Test Frame Connections 66

25 Details of Hinge Connections and Rotation Indicator Brackets .. 67

26 Strain Gauge Locations on Frames 75

27 Load vs. Deflection at Midspan, Frame No. 1 79

28 Load vs. Curvature at Midspan, Frame No. 1 80

29 Load vs. Curvature at Tops of Columns, Frame No. 1 81

30 Load vs. Curvature at Ends of Beam, Frame No. 1 82

31 Load vs. Horizontal Reaction, Frame No. 1 83

32 Moment vs. Curvture at Midspan, Frame Test No. 1 84

33 Moment vs. Curvature at Top of Left Column, Frame No. 1 ... 85

34 Moment vs. Curvature at Top of Right Column, Frame No. 1 ... 86

35 Load vs. Deflection at Top of Columns, Frame No. 2 87

36 Load vs. Curvature at Ends of Beam, Frame No. 2 88

37 Load vs. Curvature at Tops of Columns, Frame No. 2 89

38 Load vs. Horizontal Reactions, Frame No. 2 90

39 Moment vs. Curvature at Top of Left Column, Frame No. 2 91

40 Moment vs. Curvature at Top of Right Column, Frame No. 2 92

41 Load vs. Horizontal Deflection at Top of Columns, Frame No. 3 97

42 Load vs. Deflection at Midspan, Frame No. 3 98

43 Load-Curvature Relationships of Beam, Frame No. 3 99

44 Load vs. Curvature at Tops of Columns, Frame No. 3 100

45 Load vs. Horizontal Reactions, Frame No. 3 101

46 Moment vs. Curvature at Top of Left Column, Frame No. 3 102

47 Moment vs. Curvature at Top of Right Column, Frame No. 3 103

48 Load vs. Horizontal Deflection at Top of Columns, Frame No. 4 104

49 Load vs. Deflection at Midspan, Frame No. 4 105

50 Load vs. Curvature at Midspan, Frame No. 4 106

51 Load-Curvature Relationships at Top of Left Column and Ends of Beam, Frame No. 4 107

52 Load vs. Curvature at Top of Right Column, Frame No. 4 .. 108

53 Load vs. Horizontal Reactions, Frame No. 4 109

54 Moment vs. Curvature at Midspan, Frame No. 4 110

55 Moment vs. Curvature at Top of Right Column, Frame No. 4 111

A1 Ultimate Load Analysis, Frame No. 1 .... A3

A2 Ultimate Load Analysis, Frame No. 2 .... A6

A3 Ultimate Load Analysis, Frame No. 3 .... A9

A4 Ultimate Load Analysis, Frame No. 4 .... A11

A5 Ultimate Load Analysis, Beams A13

A6 Moments and Reactions for Unit Load, Frame No.1 .... A15

A7 Moments and Reactions for Unit Load, Frame No. 2 .... A17

A8 Moments and Reactions for Unit Load, Frame No.3 .... A18

A9 Moments and Reactions for Unit Load, Frame No.4 .... A19

A10 Deflection Analysis, Frame No.1 .... A23

A11 Deflection Analysis, Frame No.2 .... A24

A12 Deflection Analysis, Frame No. 3 .... A29

A13 Deflection Analysis, Frame No. 3 .... A30

A14 Deflection Analysis, Frame No.4 .... A34

A15 Deflection Analysis, Frame No.4 .... A35

B1 Moments and Deformations for Beam Analysis B5

B2 Moments and Deformations for Frame No.1 .... B9

B3 Moments and Deformations for Frame No.2 .... B12

LIST OF PLATES

PLATE PAGE

1 Model TS-M Dual Extensometer used in Tension Tests 21

2A Stub Column Before Testing 31

2B Stub Column After Testing 31

3A Loading System for Beam Tests 51

3B Bracing System for Hydraulic Jacks 51

4 Overall View of Beam Instrumentation 52

5 Typical Beam After Test 62

6A Plastic Hinge at Beam Midspan 63

6B Buckled Compression Flange in Beam 63

7A Loading System for Frame No. 1 70

7B Loading System for Frame No. 2 70

8A Loading System for Frame No. 3 71

8B Loading System for Frame No. 4 71

9 Lateral Support System for Frames 72

10A Frame No. 1 After Test 93

10B Frame No. 2 After Test 93

11 Tension Failure in Throat of Weld 94

12A Frame No. 3 After Test 112

12B Frame No. 4 After Test 112

CHAPTER I

INTRODUCTION

1-1 Analysis of Structures Beyond the Elastic Limit

Except in problems of elastic stability, structural design methods, based on the theory of elasticity, define the limiting load as the load producing initial yield at the most highly stressed section in a structure. The working load is taken as a certain fraction of this yield load. In the design of a frame, for example, members are proportioned so that working loads produce maximum stresses, as computed by elastic procedures, which do not exceed a permissible working stress. This theoretically implies that the entire structure is well within the so-called elastic range. Deflections, in most cases, are readily determined by such methods as "slope-deflection", "method of work", or "moment-area".

The advent of plastic design within the past few years has resulted in a basic change in design philosophy.(1)* Whereas elastic design is based on the concepts of working load and a working unit stress, plastic design is based on the concepts of ultimate load and

---

*Numbers in parentheses refer to references listed in the Bibliography.

ultimate moments. A margin of safety is provided by proportioning members such that working loads, when multiplied by a specified load factor, produce collapse loads. Plastic design recognizes the fact that initial yield at some location in a redundant structure does not render the structure incapable of carrying additional load; imminent collapse is obviated by the fact that such structures may draw on the reserve strength of their less heavily stressed portions through the capacity of structural steel to deform plastically.

Plastic methods of structural analysis have been developed for the purpose of calculating collapse loads, particularly for indeterminate structures, with the ultimate objective of establishing a rational and economical design procedure. These methods are now as fully developed as the elastic methods. According to simple plastic design theory, collapse of a structure is said to occur when a sufficient number of cross-sections have completely yielded, thus causing the entire structure or part of it to act as a mechanism or unstable linkage. The theoretical collapse load is defined as the load at which a small load increment would cause a very large increase in deformation.

Since structural steel sections are elastic for a relatively small range of curvature, it is generally recognized that a non-linear moment-curvature relationship must be used to even approximate the true behavior of steel structures. In simple plastic design theory, a two-segment approximation consisting of the elastic line and an

infinitely long, horizontal plastic line, is thus generally used as the starting point for deflection computations. This appriximation represents an ideal elasto-plastic material for which there is a purely elastic range and a purely plastic range. With the exception of strain-hardening, this basically typifies the actual behavior of structural steel, hence, a prediction of deflections nearer to true structural behavior than those calculated by the elastic theory is obtained.

For practical structural design problems, the simplifying assumptions underlying simple plastic theory are justifiable. However, at least four important factors which affect the strength and deformations of steel members are neglected; shear, axial load, and instability or buckling which tend to reduce the load-carrying capacity, and strain-hardening which increases the margin between initial yield and ultimate collapse. In general, the increase in strength due to strain-hardening outweighs the decrease resulting from the other effects. The simple plastic theory may, by coincidence, give close results for certain structures,(2) but for precise predictions of strength and deformations of any structure, a more accurate moment-curvature relationship must be used.

It would be reasonable to presume that if a theory should be developed that would account for all secondary factors, it would be so complex as to be of little practical use. It may, however, be of advantage, especially in research studies, to be able to assess the

benefits associated with strain-hardening. This would necessitate a close look at deflections.

1-2 Analysis of Deflections Beyond the Elastic Limit

In essence, structural deflections are calculated by integration, with appropriate boundary conditions, of the differential equation:(3)

$$\frac{d^2y}{dx^2} = \phi$$

where, y = deflection from original straight line of member

x = distance along member

$\frac{d^2y}{dx^2}$ = approximate curvature of member

ϕ = curvature produced by bending.

In the elastic range, the expression for curvature, ϕ, is given by the linear expression:

$$\phi = \frac{M}{EI}$$

where, M = bending moment as a function of x

E = modulus of elasticity

I = moment of inertia of the cross-section of the member

This simple linear relationship between load and deflection becomes invalid as soon as initial yield is reached anywhere in the

structure, consequently the calculation of deflections in the plastic range becomes more involved. Several methods for calculating deflections in the plastic range are available,(4) of which five will be discussed and compared briefly. In these methods, the moment-curvature relationship derived from the stress-strain relationship is substituted into the above differential equation, and deflections are obtained by integration, using particular boundary conditions. The methods differ only in assumptions made in the moment-curvature relationship to simplify the computation. FIGURE 1 shows the stress distribution associated with the assumptions for each method.

The first method, namely, the "plastic hinge" method, is the simplest approach, and is the method commonly used for design purposes. It assumes that yielding is limited to the cross-sections at which the fully-plastic moment is reached. Hence, at collapse load, a structure is assumed to consist of elastic portions connected by loacalized plastic hinges. Strain-hardening is neglected, since in this method, a two-segment stress-strain diagram as shown by FIGURE 2A is assumed. Deflections are calculated by using any one of the elastic methods such as "slope-deflection," "moment area," or "method of work" with suitable handling of the boundary conditions, to allow for freedom of rotation at plastic hinges. Because of the basic assumptions underlying this method, values of deflections so obtained tend to be overly conservative. Moreover, since this method

STRESS DISTRIBUTIONS ASSUMED FOR CALCULATING DEFLECTIONS BEYOND THE ELASTIC LIMIT

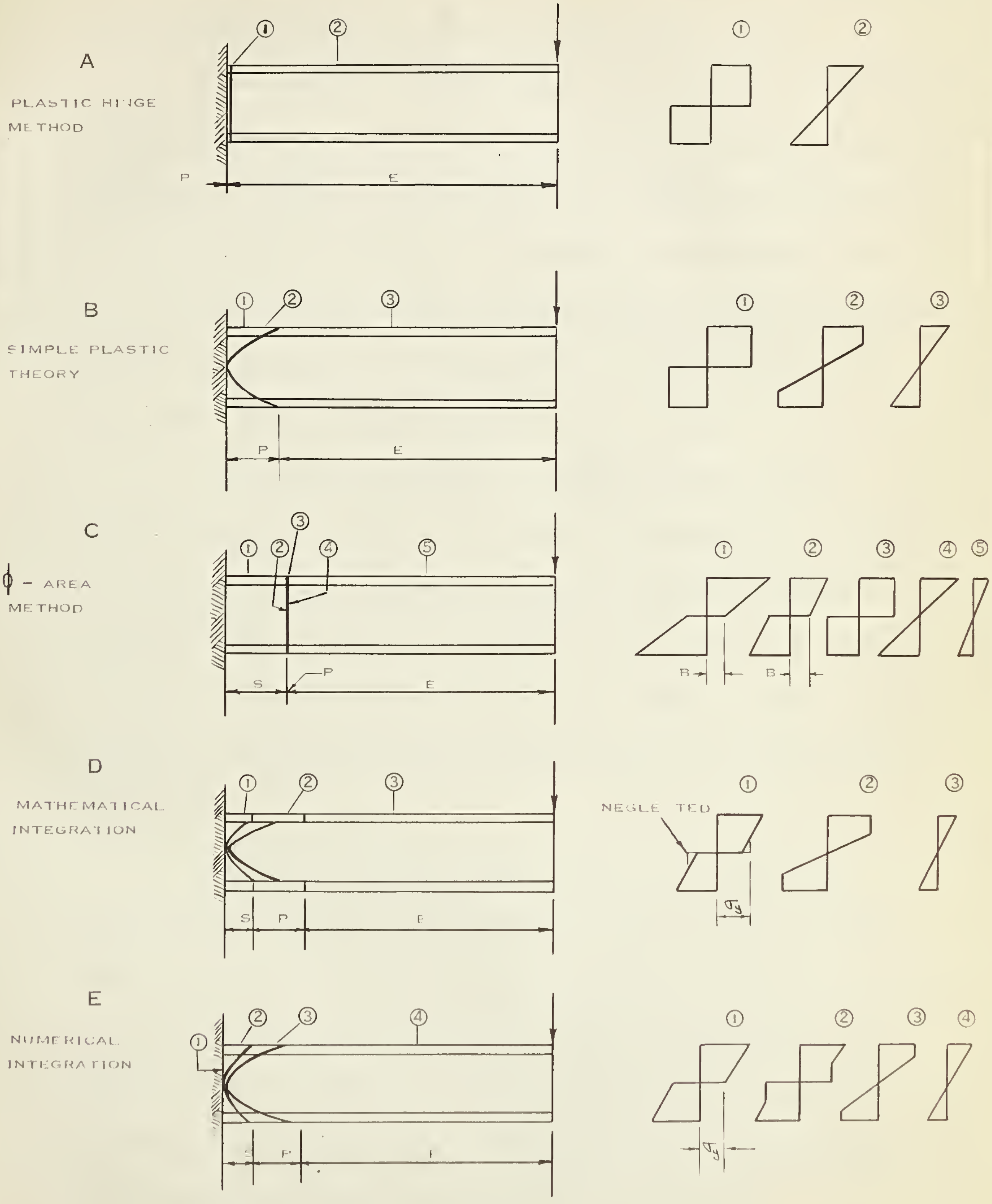

FIGURE 1

is based on an ideal elasto-plastic material, computation of deflections becomes indeterminate once the last plastic hinge forms.

The other four methods utilize more realistic representations of the properties of steel in order to increase the accuracy in deflection calculations. However, this increase in accuracy is accompanied by a corresponding increase in the complexity of computations, since a trial-and-error process must be used to satisfy not only the boundary conditions, but also the curvatures and hence the moments. For this reason, these methods have been used sparingly.

Of these four methods, the "simple plastic theory" method is the least complex. The same basic assumptions contained in the "plastic hinge" method are used except that the spread of the plastic hinge is considered (FIGURE 1B), resulting in a slight increase in accuracy. As in the case of the "plastic hinge" method, deflection computations become indeterminate once the last plastic hinge forms.

As with the "plastic hinge" method, the " ϕ - area" method neglects the spread of the plastic hinge; however, the two differ in that the " ϕ - area " method considers the hinge to be formed in a strain-hardened zone in a manner shown in FIGURE 2C. At collapse loads, therefore, a structure consists of elastic portions and strain-hardened portions. As expected, calculated deflections are more accurate than those obtained from the above

ASSUMED STRESS - STRAIN AND MOMENT-CURVATURE RELATIONSHIPS USED IN DEFLECTION CALCULATIONS

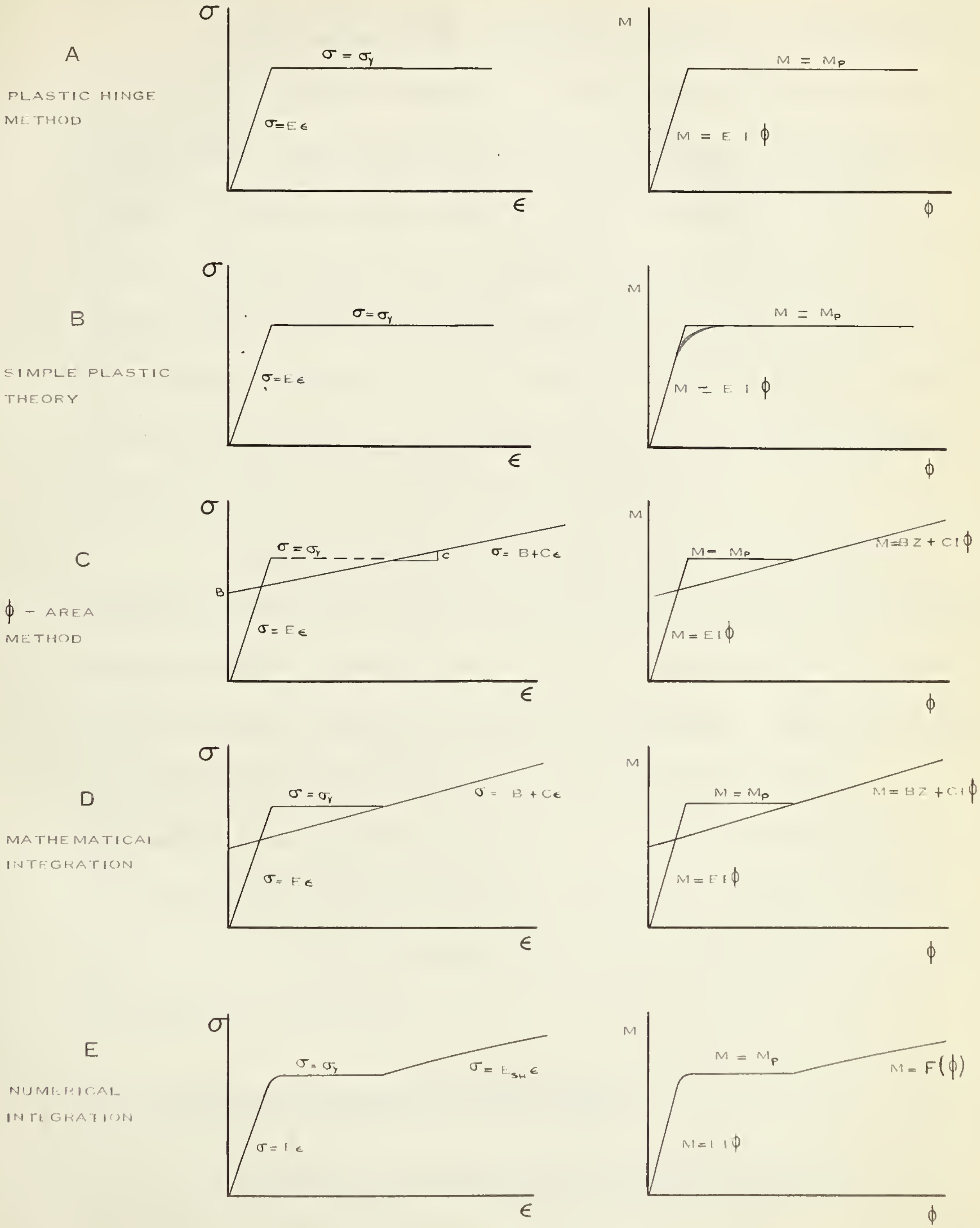

FIGURE 2

two methods.

The "mathematical integration" method is a more refined version of the "ϕ-area" method in that the spread of the plastic hinge is considered. Stress-strain and moment-curvature relationships are simplified to functions which may be expressed mathematically, as shown by FIGURE 2D. This method also neglects the short curved portion of the moment-curvature relationship near yield, as well as the triangular portion of the stress diagram (FIGURE 1D). Increased accuracy as compared to the "ϕ-area" method is of course obtained, since the spread of the plastic hinge is considered.

The most precise method, the "numerical integration" method, gives the exact values for deflections in so far as the moment-curvature diagram used is correct, since all simplifying assumptions of the previously described methods are eliminated. FIGURES 1E and 2E show the stress distributions and curvature relationships, respectively, used for mild structural steel. A detailed discussion of a modified version of the "numerical integration" method of analysis, namely, the "moment end-slope relationship", as proposed by Ang, (5) is included in Chapter V.

1-3 Previous Investigations at the U. of A.

A series of investigations in plastic analysis was

introduced at the University of Alberta in 1961, by Channon.(6) Results were reported on four rectangular two-hinged portal frames, loaded with various combinations of concentrated vertical and horizontal forces. Since this was a pilot project, a major portion of the program consisted in the design of the loading frame. Consequently, the results were presented with a view to substantiating the basic simple plastic theory. However, these initial tests did reveal one pertinent point. Except for one frame which failed at a load slightly lower than its predicted capacity due to insufficient lateral support, the remaining three test frames exhibited ultimate load carrying capacities greater than those predicted by simple plastic theory. This increased capacity was attributed to the effects of strain-hardening.

Kraemer (7) continued this project the following year by testing two similar rectangular portal frames with a view to examining the effects of strain-hardening on the ultimate moment capacity. One frame was loaded with a concentrated vertical force at the midspan; the second was loaded with a combination of vertical load at beam midspan and horizontal load at the top of one column. The ratio of vertical load to horizontal load was maintained throughout the test at 2:1. Three improvements were implemented in frame instrumentation; the horizontal reaction was measured at one support, a mechanical device was used to measure curvature, and newly acquired load cells were used to measure applied loads. In addition to the frame tests,

residual stress measurements were determined by the "method of sections". A beam test was also conducted in order to obtain the moment-curvature relationship for the section used.

As in the previous investigation, both frames developed ultimate capacities greater than those predicted by simple plastic theory. Strain-hardening developed at approximately ultimate load and resulted in an increase in load carrying capacity that was proportional to deformation.(7) Values of the strain-hardening modulus (E_{st}) and the strain at the onset of strain-hardening (e_{st}), as determined from tension tests, were lower than those normally expected, and the residual stress distribution obtained was not of the type usually expected. In the second frame test, measured values of the horizontal reaction did not compare favorably with theoretical values.

The theoretical analysis used by both investigators was based on the simple plastic theory and deflections were estimated by the "plastic hinge" method.

1-4 Present Investigation

Although the "plastic hinge" method is fairly well-known, very little published material is available on the subject of analysis of a statically indeterminate structure incorporating the non-linear

behavior of its component parts. For this reason, and on the basis of results obtained from the previous investigations at the University of Alberta, the present investigation was initiated to provide a more comprehensive examination of the effects of strain-hardening, with particular emphasis on deflections.

CHAPTER II

SCOPE OF INVESTIGATION

The investigation described in this thesis was devised to examine the effects of strain-hardening on the ultimate load capacity of steel frames, with particular emphasis on the load-deflection relationships.

The major portion of the testing program consisted of load tests on four hinge-supported rectangular frames. One frame was loaded with a vertical force at beam midspan, another was loaded with a horizontal force applied at the top of one column. Two frames were loaded with a combined vertical and horizontal loading; one with a ratio of vertical to horizontal load of unity, and the other with a vertical load equal to twice the horizontal load.

Two beam tests were conducted in order to obtain an experimental moment-curvature relationship which would include residual stress effects. In addition, thirty-two tensile tests were performed to provide an accurate stress-strain curve for the 4I9.5 material used throughout the tests.

Four residual stress measurements were performed by

the "method of sections". Two stub column tests were conducted to provide a check on the magnitude of the maximum compressive residual stress.

A program was compiled for the IBM 1620 digital computer to derive the "moment end-slope" relationships for the 4 I 9.5 section. A "theoretical" set of curves was obtained from the tensile tests and an "experimental" set of curves was derived from the beam tests.

For Frame Nos. 1 and 2, and the beam tests, attention was focussed on the following:

1) Actual deflections as compared to theoretical deflections based on the "moment end-slope" relationships, as well as on the "plastic-hinge" method.
2) Actual load-carrying capacity as compared to the calculated capacity.
3) Actual moment-curvature relationships as compared to computed values.
4) Failure mechanism in each frame at ultimate load.

For the tensile tests, attention was focussed on the following:

1) Values of the modulus of elasticity, yield strain, static level of yield stress, strain at onset of strain-hardening, and the strain-hardening modulus.

Frame Nos. 3 and 4 were tested with a view to providing sufficient experimental data for a future extension of this project to incorporate the "moment end-slope" relationships into an analysis for the case of combined loadings. Hence, for these two frames, attention was focussed on the following:

1) Actual deflections as compared to theoretical deflections based on the "plastic-hinge" method.
2) Actual load-carrying capacity as compared to the calculated capacity.
3) Actual moment-curvature relationships as compared to computed values.
4) Failure mechanism in each frame at ultimate load.

CHAPTER III

MATERIAL PROPERTIES

3-1 Definitions

The first step in developing a method for determining deflections which includes the effects of strain-hardening, is to establish appropriate bending moment-curvature relations. Since these relations are dependent mainly upon the stress-strain characteristics of the material, it is apparent that an accurate determination of the stress-strain relationship is essential. For this reason, the first stage of the testing program involved the determination of the stress-strain relationship for the steel used in the beam and frame specimens. The following terms are relevant in defining pertinent values of the stress-strain curve:

(a) Yield stress (σ_y)

Although mild structural steel usually exhibits more than one level of yield stress, a logical choice for this value is the stress at the static level (zero strain rate). This value best simulates most structural loadings, is independent of time (and is therefore constant), and is the easiest to obtain.(8) Thus, in this report, the term "yield

stress" applies to the static level of yield stress.

(b) Yield strain (e_y)

The value for the yield strain refers to the intersection between the elastic portion of the stress-strain diagram and the horizontal line representing the static yield stress.

(c) Strain at the onset of strain-hardening (e_{st})

The value of strain at the onset of strain-hardening refers to the intersection of the horizontal line denoting the static yield stress with the stress-strain curve in the strain-hardening region.

(d) Strain-hardening modulus (E_{st})

The slope at the initial portion of the strain-hardening region is defined as the value of the strain-hardening modulus. For this investigation, calculation of the moment-curvature relationship depended upon the actual stress-strain values at all levels of strain, consequently the value of the strain-hardening modulus was only a matter of interest.

3-2 Tensile Test Specimens

A total of 32 coupons, cut from the 4 I 9.5 sections, were tested in tension; 16 were cut from the web and 16 from the flanges. Of these, two web coupons and two flange coupons were used to determine the modulus of elasticity; the remainder were tested to obtain average values for yield stress, yield strain, strain at the onset of

strain-hardening, strain-hardening modulus, and the stress-strain curve in the strain-hardening region. FIGURE 3 shows the dimensions of these coupons which were cut to conform as nearly as possible to A.S.T.M. Designation A 9-36.

3-3 Loading and Instrumentation

All specimens were tested in the "Baldwin-Tate-Emery Universal Testing Machine" of 200, 000 pound capacity. Two electrical resistance "SR-4" strain gauges were mounted on each specimen for the purpose of obtaining data in the elastic range. Load was applied in 500 pound increments, thereby simulating the incremental loading used in the frame and beam tests.

To determine values in the plastic and strain-hardening ranges, a "Model TS-M Dual Extensometer" (PLATE 1), with an 8-inch gauge length, was attached to the specimens and connected to an electrical load-deformation recorder. This system provided an autographic plot of the stress-strain diagram for each specimen. From previous preliminary tests, it was determined that magnification factors of 20, 40 and 80 were most suitable in obtaining the strain-hardening curve, the strain at onset of strain-hardening, the yield stress and the yield strain. Load was applied continuously at a very slow rate until yielding occurred, at which point the load control vernier was turned off to allow the load to decrease to a

minimum. Care was excercised to ensure that strain reversal did not occur. The static yield stress was thus read from the load dial on the testing machine. After three such readings were obtained for each specimen, the loading rate was set at the original value and the test was continued to ultimate load.

3-4 Tensile Test Results

The two web specimens yielded an average modulus of elasticity of 29.55×10^6 psi (FIGURE 4), whereas the two flange specimens gave an average value of 29.25×10^6 psi (FIGURE 5). From these values, a weighted average value (by areas) of 29.35×10^6 psi was determined and used for all subsequent calculations. FIGURE 6 shows an average stress-strain curve obtained from the remaining 28 tension tests. Test data is presented in Appendix D. Pertinent values were as follows:

σ_y	41, 100 psi
e_y	0.00144 in./in.
e_{st}	0.0143 in./in.
e_{st} / e_y	10.0

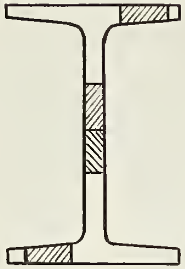

COUPON LOCATIONS ON CROSS-SECTION

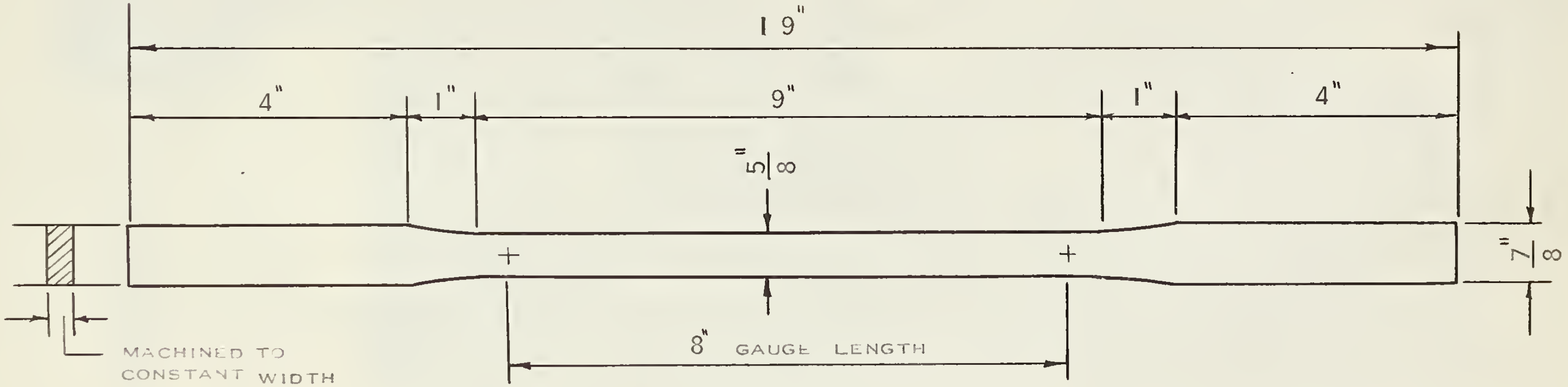

SCALE - $\frac{3''}{8}$ = 1' - 0

TEST COUPON DIMENSIONS

FIGURE 3

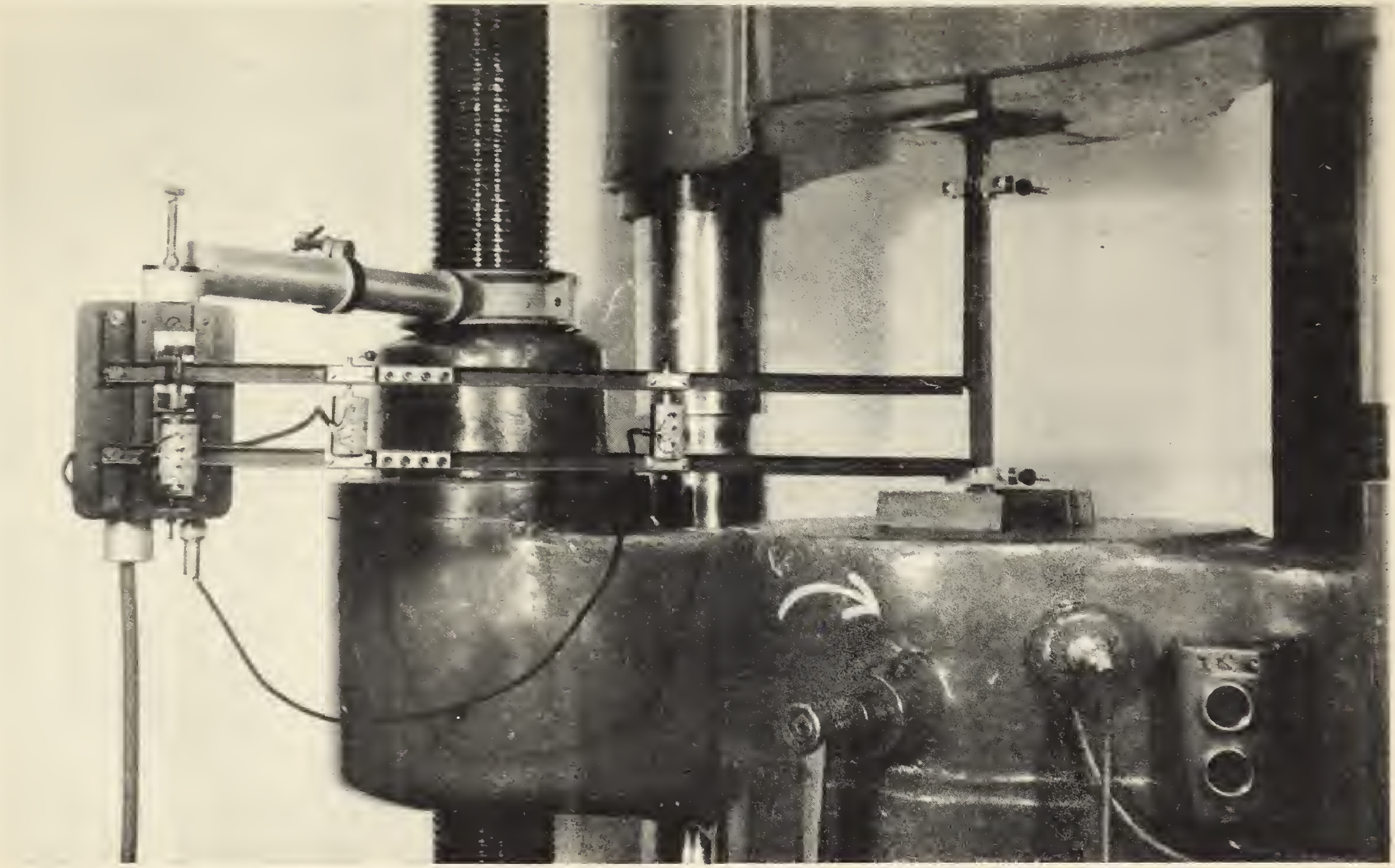

MODEL TS-M DUAL EXTENSOMETER USED IN TENSION TESTS

PLATE I

[illegible]

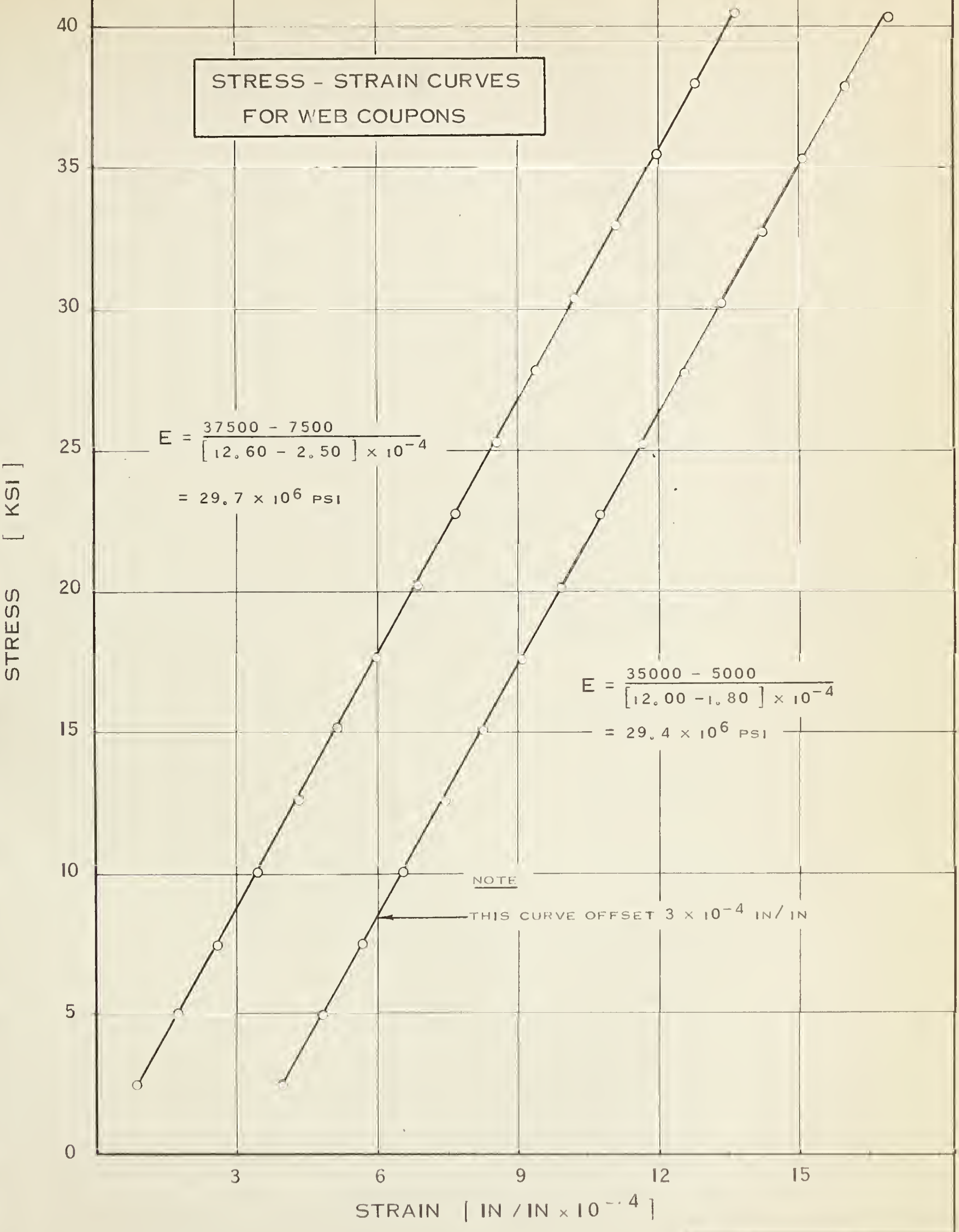

STRESS - STRAIN CURVES FOR WEB COUPONS

$$E = \frac{37500 - 7500}{[12.60 - 2.50] \times 10^{-4}} = 29.7 \times 10^{6} \text{ PSI}$$

$$E = \frac{35000 - 5000}{[12.00 - 1.80] \times 10^{-4}} = 29.4 \times 10^{6} \text{ PSI}$$

NOTE

THIS CURVE OFFSET 3×10^{-4} IN/IN

FIGURE 4

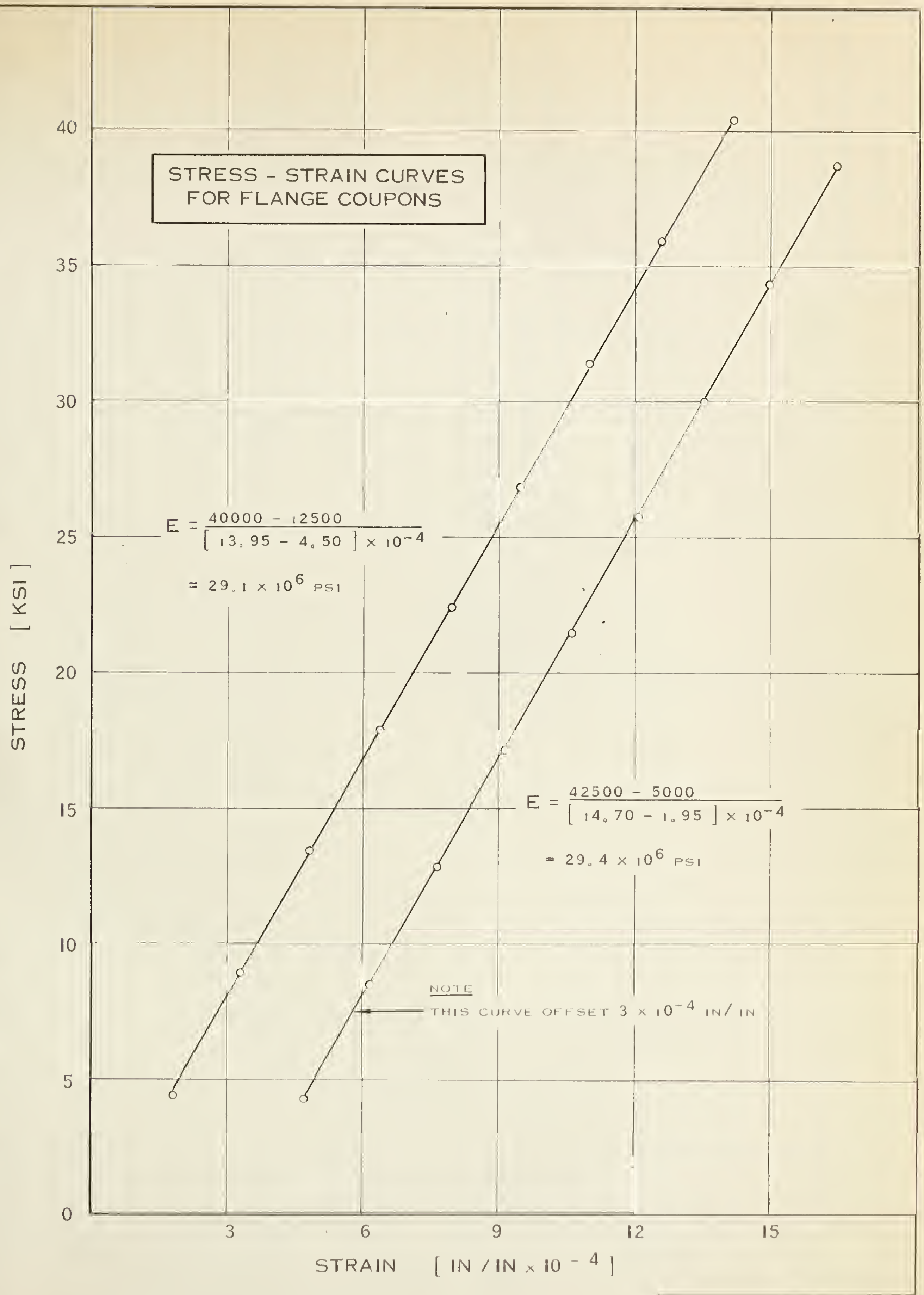
STRESS - STRAIN CURVES FOR FLANGE COUPONS
E = (40000 - 12500) / ([13.95 - 4.50] x 10^-4)
= 29.1 x 10^6 PSI
E = (42500 - 5000) / ([14.70 - 1.95] x 10^-4)
= 29.4 x 10^6 PSI
NOTE
THIS CURVE OFFSET 3 x 10^-4 IN/IN
STRESS [KSI]
0
5
10
15
20
25
30
35
40
3
6
9
12
15
STRAIN [IN/IN x 10^-4]

FIGURE 5

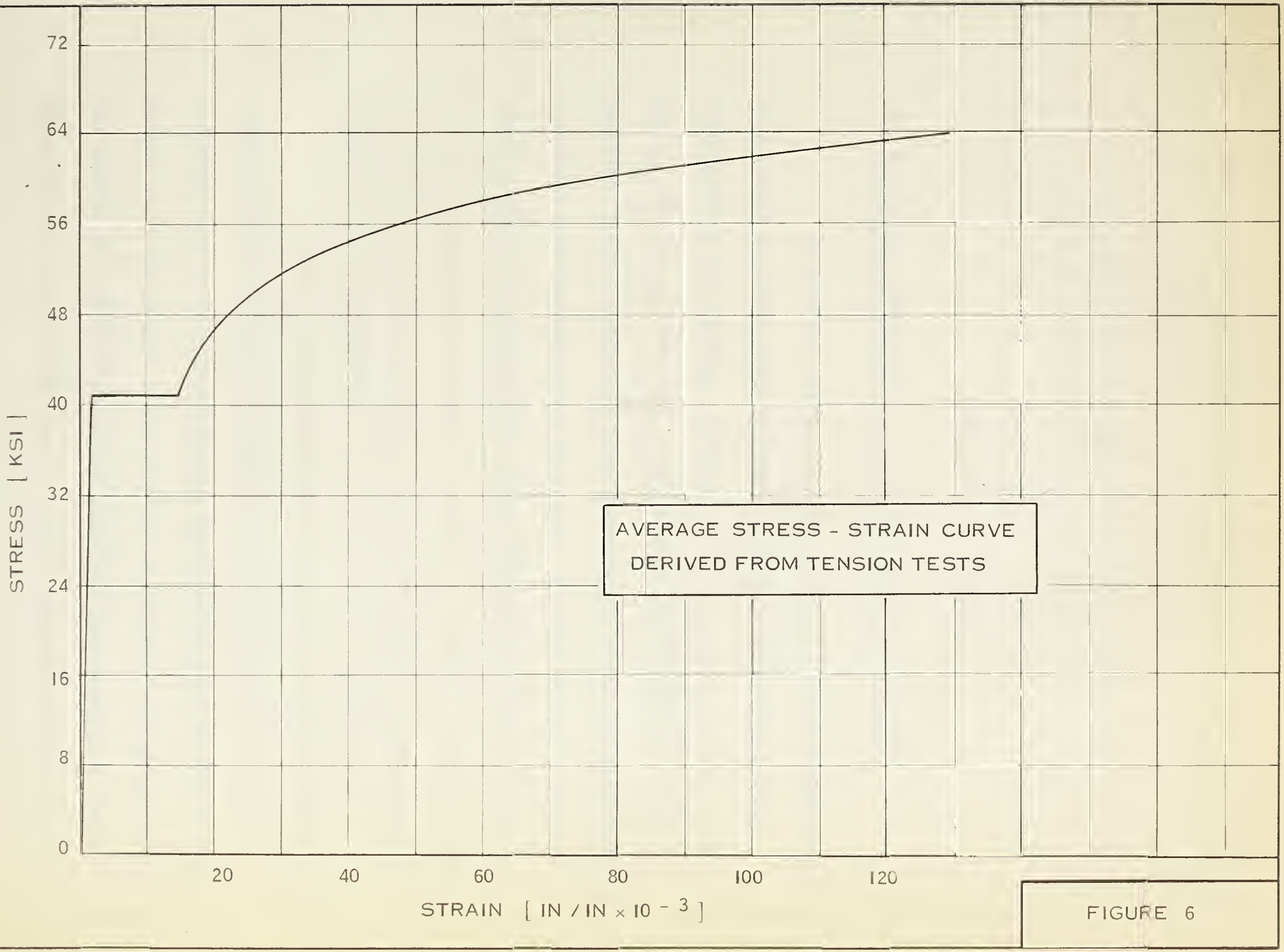

AVERAGE STRESS - STRAIN CURVE
DERIVED FROM TENSION TESTS

FIGURE 6

CHAPTER IV

RESIDUAL STRESSES

4-1 Sectioning Method for Residual Stress Measurements

In general, residual stresses are present in rolled shapes as a result of plastic deformations caused by differential cooling, cold-bending and welding. Although the presence of residual stresses has no effect on the ultimate moment capacity,(9) these stresses do however, cause a departure from the linearity of the assumed moment-curvature and load-deflection diagrams. In other words, a section under applied load experiences initial yielding at a load that is less than the theoretical yield load. In order to predict the value of load at which first yield will occur, it is thus necessary to determine the residual stress distribution in the section under consideration.

The "method of sections" as devised at Lehigh University(10) was employed to obtain the residual stress pattern for the 4 I 9.5 material used in this investigation. Small holes were drilled in the flanges and webs of four 4-foot sections to properly seat gauge points. The distances between these holes were then measured by a "Demec Gauge" measuring to 0.0001 inch. After longitudinal saw cuts,

straddling the gauge holes, were made (FIGURE 7), the distances between the gauge points were again measured. The differences in lengths between final and initial readings (including temperature effects) were thus equal to the values of the residual strains in the sections.

4-2 Stub Column Tests

Stub column tests may be used to provide a check on the magnitude of the residual stress in the flange tips of a particular section. This indirect method is dependent upon the fact that the difference between the yield stress and the proportional limit, is equal to the value of the compressive residual stress in the flange tips.

Two stub columns were tested to substantiate residual stress measurements taken by the "sectioning method". Both 18-inch columns were tested in the "Baldwin-Tate-Emery Universal Testing Machine" with load increments of 5,000 pounds. Strain readings were recorded at each increment of load on eight "SR-4" electrical resistance strain gauges, symmetrically mounted at mid-height. PLATE 2A shows a typical stub column before testing.

4-3 Results of Residual Stress Measurements

FIGURE 8 shows the average magnitude and distribution

of the residual stresses as obtained by the "method of sectioning." Stresses were calculated using the elastic modulus of 29.35 x 10^6 psi obtained from the tension tests. A value of 5,600 psi was obtained for the maximum compressive residual stress in the flange tips, and a value of 9,400 psi was obtained for the maximum compressive residual stress in the section. This maximum value occurred at the center of one flange.

Results from the stub column tests are shown in FIGURE 9. An average value of 9,500 psi was obtained for the magnitude of the maximum compressive residual stress, and the average value for the modulus of elasticity in compression was found to be 30 x 10^6 psi.

The yield pattern for a test of this type is shown in PLATE 2B.

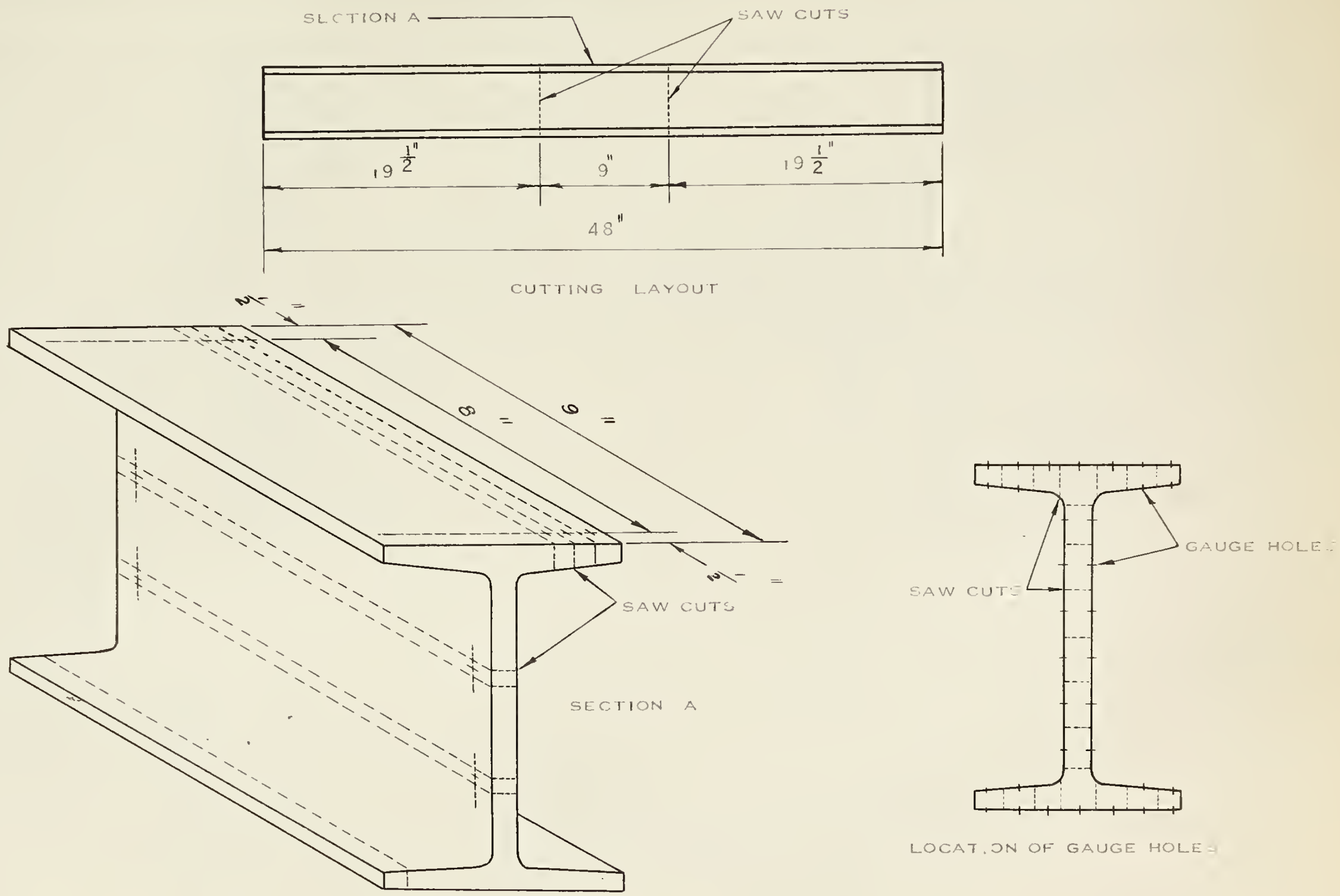

SECTIONING METHOD FOR MEASURING RESIDUAL STRAINS

FIGURE 7

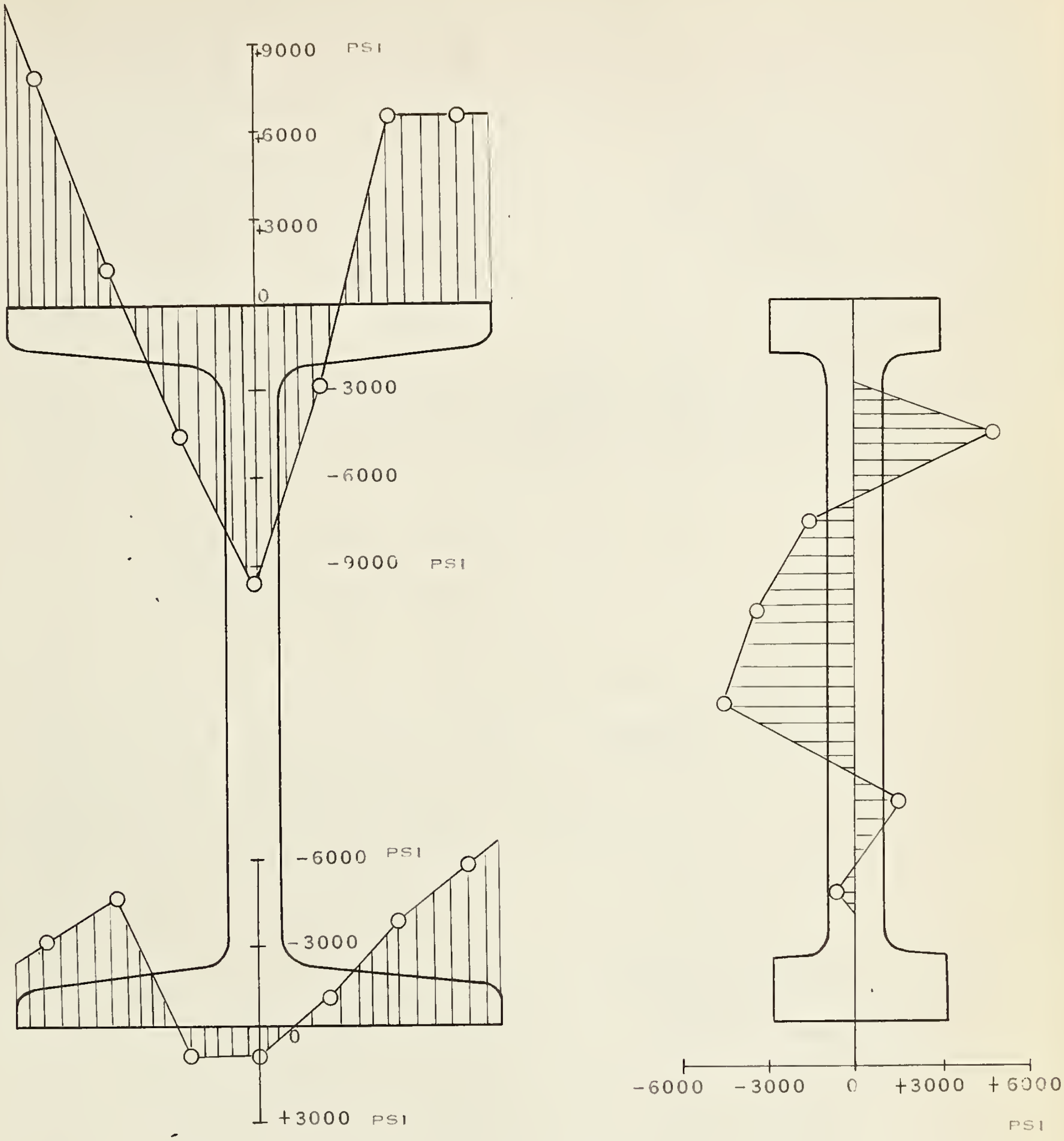

CROSS SECTION SCALE
FULL SIZE

DISTRIBUTION OF RESIDUAL STRESSES
AFTER FINAL SECTIONING

FIGURE 8

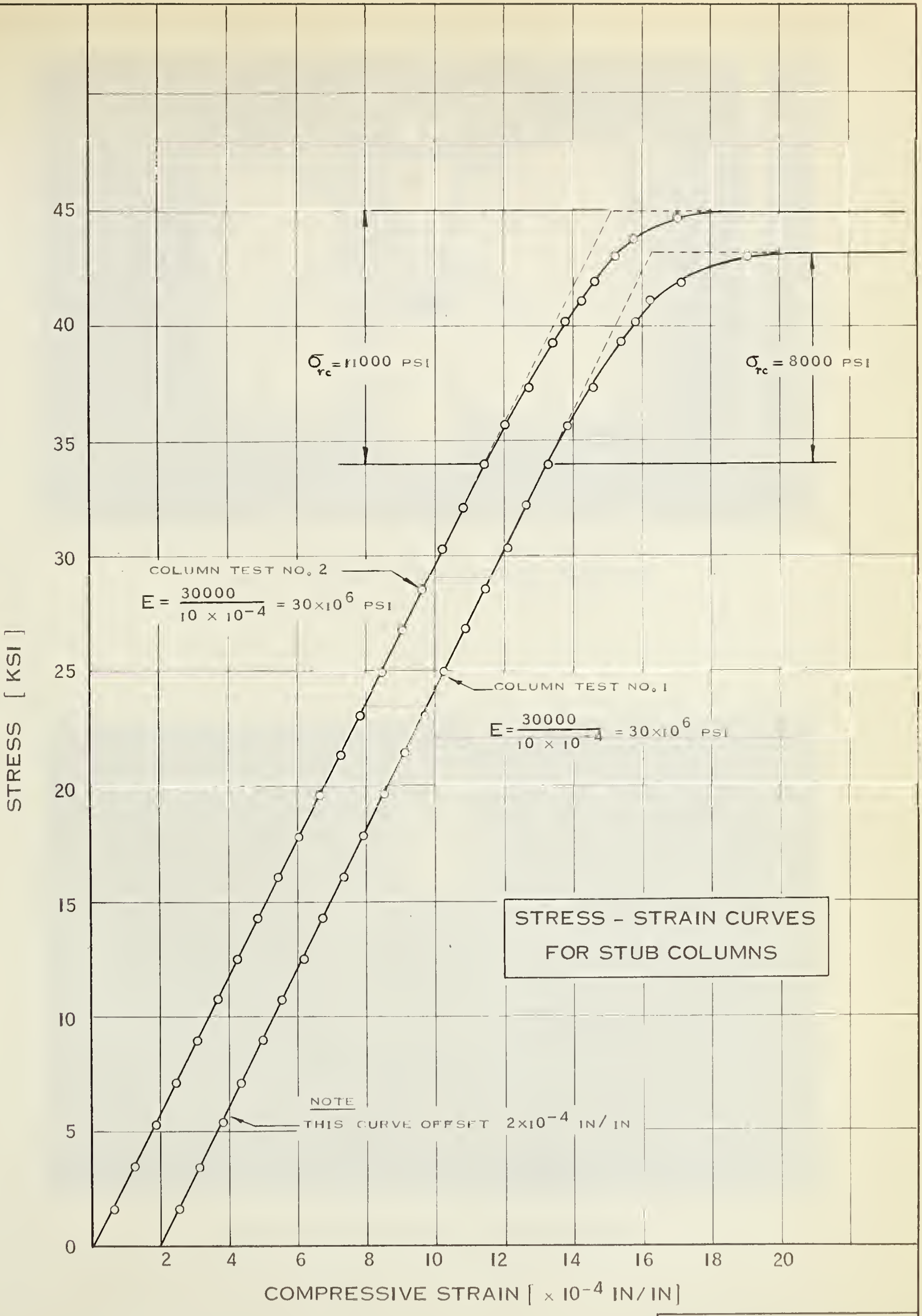

STRESS - STRAIN CURVES
FOR STUB COLUMNS

FIGURE 9

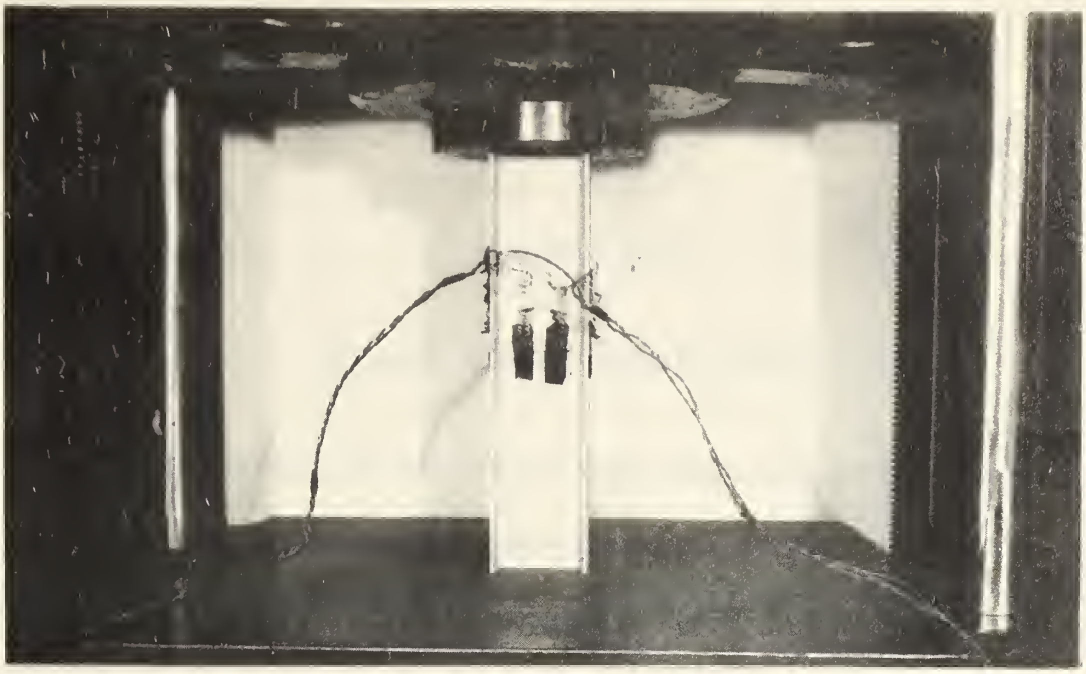

[A] STUB COLUMN BEFORE TESTING

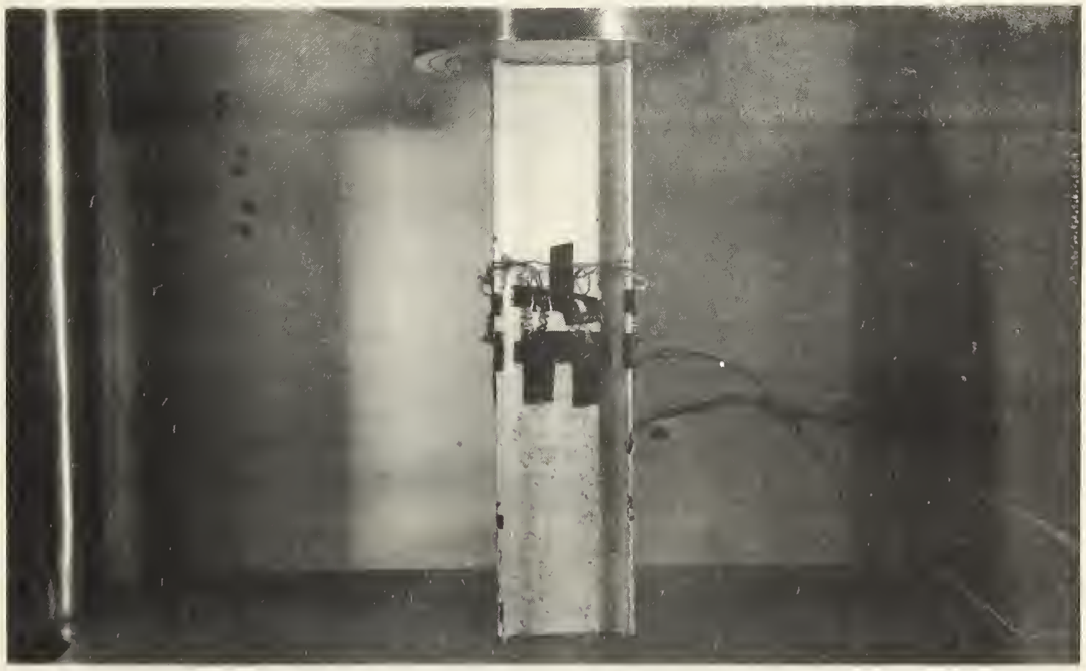

[B] STUB COLUMN AFTER TESTING

PLATE 2

[illegible]

[illegible]

CHAPTER V

MOMENT END-SLOPE RELATIONSHIP

If buckling or fracture of individual members of a steel structure does not occur, the behavior of the structure is largely a function of the stress-strain characteristics of the material, and strengths greater than the fully-plastic resistance can be obtained as a result of strain-hardening. Since simple plastic theory does not account for strain-hardening, deflections in excess of those predicted by this theory are usually observed in tests to ultimate load. (6, 7)

A method developed by Ang, (5) was adopted in this investigation to include the effects of strain-hardening in the frame analyses. This method is a modified version of the numerical integration method discussed in Chapter I. Its practicability depends upon a means of relating the resisting moments at the ends of a member to the corresponding end-slopes, hence the term "moment end-slope relationship" is applied to this method.

5-1 Moment-Curvature Relationship

The first step involved in the derivation of the moment

end-slope relationships, is the determination of the moment-curvature relations for a particular section. A convenient means of obtaining this relationship in a dimensionless form is based on the following assumptions:

1) Strains are distributed linearly through the depth of a section.

2) The stress-strain relationship for the material is the same in tension and compression, and the resistance of a member in flexure is dependent upon this relationship.

3) A wide flange section can be idealized as being composed of three rectangular components.

4) The average stress in the flange, σ_{fl}, is the stress at the centroidal axis of the flange.

With these assumptions, the value for the moment (M) in a section may be expressed in dimensionless form.

$$\frac{M}{M_y} = \frac{N \frac{A_w}{A_{fl}} + \frac{1}{2} \frac{\sigma_{fl}}{\sigma_y} \frac{(d-t)}{d}}{\frac{1}{6} \frac{A_w}{A_{fl}} + \frac{1}{2} \left(\frac{d-t}{d}\right)^2} \quad \ldots\ldots\ldots\ldots (1)$$

where, M_y = moment which produces first yield

$N = \frac{\text{moment contributed by web}}{\sigma_y A_w d}$

A_w = area of web

A_{fl} = total flange area

d = section depth

t = flange thickness

The shape factor (S.F.), which is the ratio of the fully plastic moment of a section (M_{fp}) to the yield moment (M_y), can also be expressed in dimensionless form.

$$\text{S.F.} = \frac{M_{fp}}{M_y} = \frac{\frac{1}{4}\frac{A_w}{A_{fl}} + \frac{1}{2}\left(\frac{d-t}{d}\right)}{\frac{1}{6}\frac{A_w}{A_{fl}} + \frac{1}{2}\left(\frac{d-t}{d}\right)^2} \quad \ldots\ldots\ldots\ldots(2)$$

Using the above two equations, the resisting moment can be expressed in terms of the fully-plastic moment of a section.

$$\frac{M}{M_{fp}} = \frac{M}{M_y} \times \frac{M_y}{M_{fp}} = \frac{M}{M_y} \times \frac{1}{\text{S.F.}}$$

or,

$$\frac{M}{M_{fp}} = \frac{N\frac{A_w}{A_{fl}} + \frac{1}{2}\frac{\sigma_{fl}}{\sigma_y}\left(\frac{d-t}{d}\right)}{\frac{1}{4}\frac{A_w}{A_{fl}} + \frac{1}{2}\left(\frac{d-t}{d}\right)} \quad \ldots\ldots.(3)$$

For the 4 I 9.5 section, Equation (3) takes the form:

$$\frac{M}{M_{fp}} = 1.334\,N + 0.666\,\frac{\sigma_{fl}}{\sigma_y} \quad \ldots\ldots\ldots(4)$$

A dimensionless plot of the moment-curvature relationship, derived from Equation (4), is shown in FIGURE 10. Sample calculations are given in Appendix B. The stress-strain diagram used in the computations of this relationship is shown in dimensionless form in FIGURE 11.

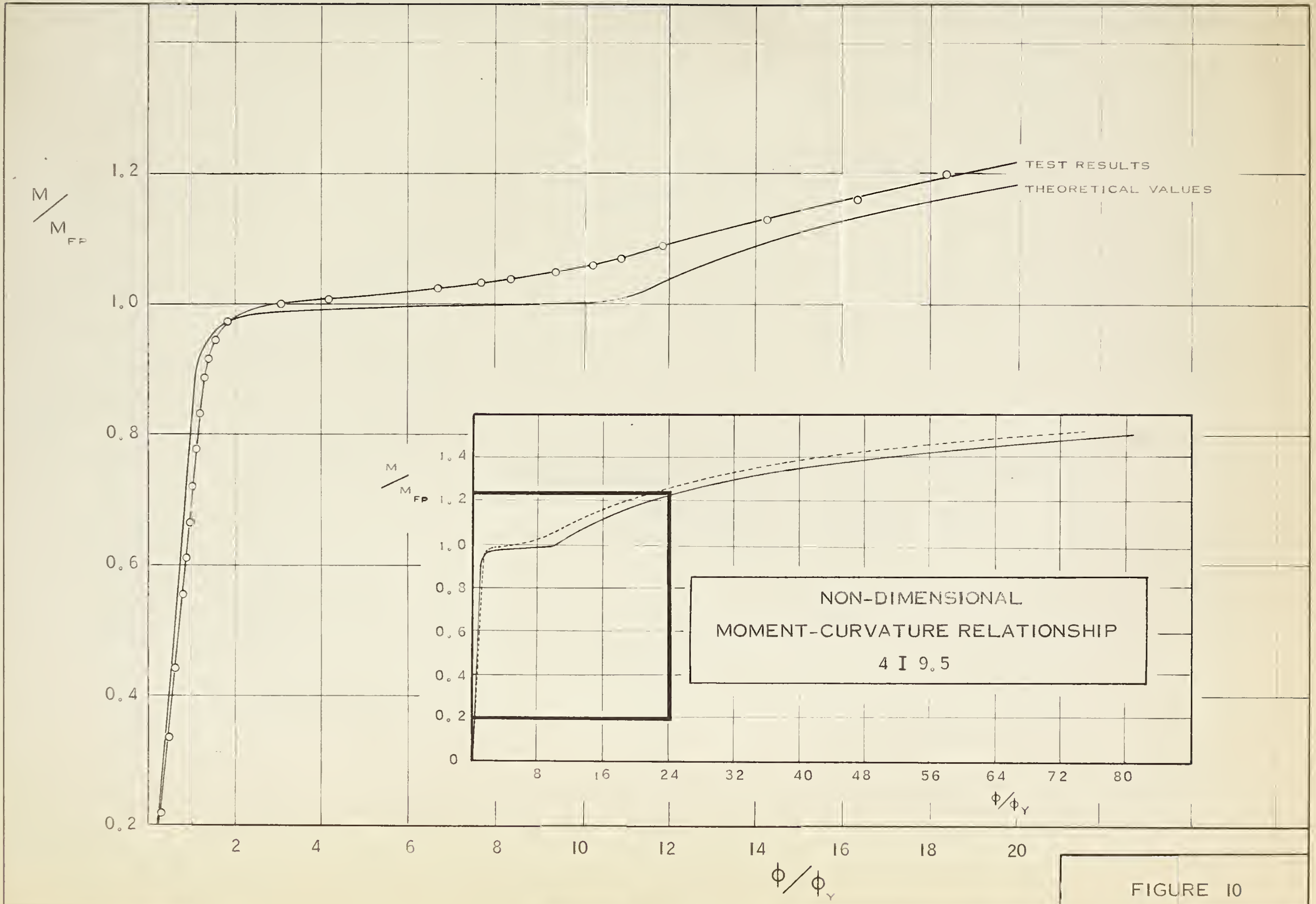

NON-DIMENSIONAL
MOMENT-CURVATURE RELATIONSHIP
4 I 9.5

FIGURE 10

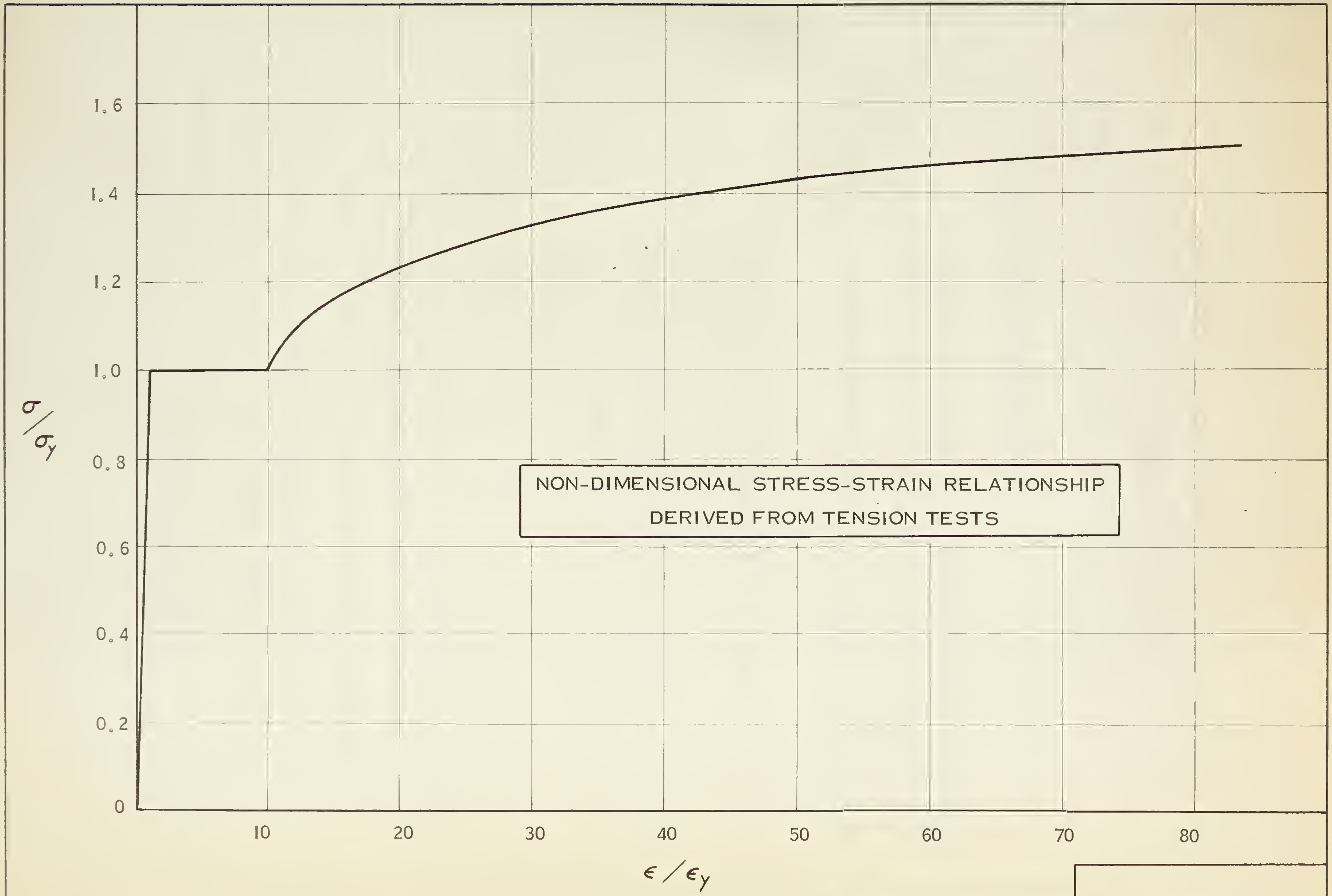

NON-DIMENSIONAL STRESS-STRAIN RELATIONSHIP
DERIVED FROM TENSION TESTS

FIGURE II

In addition to this theoretical plot, a dimensionless form of the moment-curvature relationship determined from the beam tests (Chapter VI), is also shown in FIGURE 10.

5-2 Moment End-Slope Relationship

Having thus obtained the moment-curvature relationship, it is now necessary to derive the moment end-slope relations, which are those of a simply-supported beam with moments applied at both ends.

Derivation of these relationships is based on the following assumptions:

1) An end slope is positive if the direction of its rotation from the original position is the same as the end moment.
2) Relative lateral displacement is the product of an angle change times the original length of a member.

A simply-supported beam with moments applied at both ends is shown in FIGURE 12A. The moment diagram and its corresponding curvature diagram, derived from the moment-curvature relationship, are shown in FIGURE 12B. By the "conjugate-beam" method of analysis,(11) the end slopes for any given set of end moments, are the corresponding reactions at the supports with the curvature

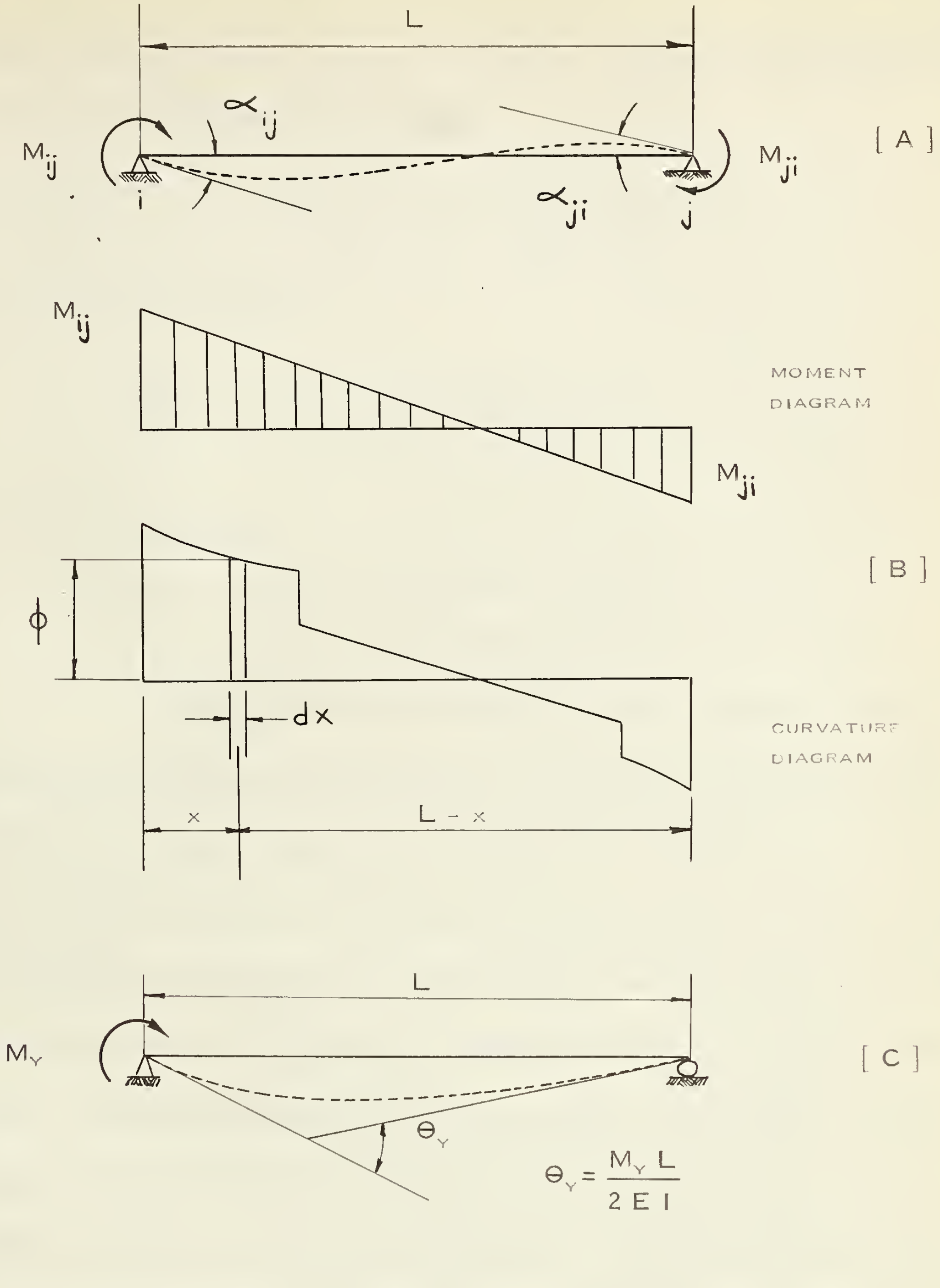

DESIGNATION OF MOMENTS AND DEFORMATIONS
OF A SIMPLY-SUPPORTED BEAM

FIGURE 12

diagram applied as the load on the beam. This can be expressed with reference to FIGURE 12B as follows:

$$\alpha_{ij} = \int_{i}^{j} \phi \left(\frac{L-x}{L}\right) dx,$$

and,
$$\alpha_{ji} = \int_{j}^{i} \phi \left(\frac{x}{L}\right) dx$$

in which,

α_{ij} = end slope at end "i" of member ij

α_{ji} = end slope at end "j" of member ij

A program for the IBM 1620 digital computer was compiled using the above relationships, and values of end-slopes were obtained for varying values of end moments. Two series of curves were obtained; the first was based on the theoretical moment-curvature relationship derived from the tension tests, and the second series was based on the moment-curvature relationship derived from the beam tests. A dimensionless plot of the end-slope relationships, for the simply-supported beam with end moments applied so as to produce double curvature, is shown in FIGURE 13. The abscissa was derived in dimensionless form by relating the end slopes to the total angle change, θ_y, of a simply-supported beam with a moment M_y applied at one end. (FIGURE 12C) The case of a simply-supported beam

with end moments applied so as to produce single curvature, is shown in FIGURE 15. FIGURES 14 and 16 show the moment end-slope relationships derived from the experimental moment-curvature values.

5-3 Method of Analysis

Basically, the analysis of statically indeterminate structures involves the solution of the equations of equilibrium and continuity. The equations of equilibrium and continuity at a joint "i" in a given structure may be expressed, respectively as:

$$\sum_{j=i}^{n} M_{ij} = O \quad \ldots\ldots\ldots\ldots\ldots\ldots\ldots\ldots (5)$$

and, $$\Omega_{i1} = \Omega_{i2} = \ldots\ldots \Omega_{ij} = \ldots\ldots \Omega_{in} \ldots\ldots (6)$$

in which $$\Omega_{ij} = F(\psi, \alpha_{ij}) \ldots\ldots\ldots\ldots\ldots\ldots\ldots (7)$$

where:

n = number of members meeting at a joint

Ω_{ij} = total rotation at joint "i" of member ij

ψ = chord displacement angle

M_{ij} = moment at end "i" of member ij

Since the moment end-slope relationships relate end-slopes to end moments, Equation (7) becomes:

$$\Omega_{ij} = F(\psi, M_{ij}, M_{ji})$$

Hence, equations of continuity may be written for each joint in a

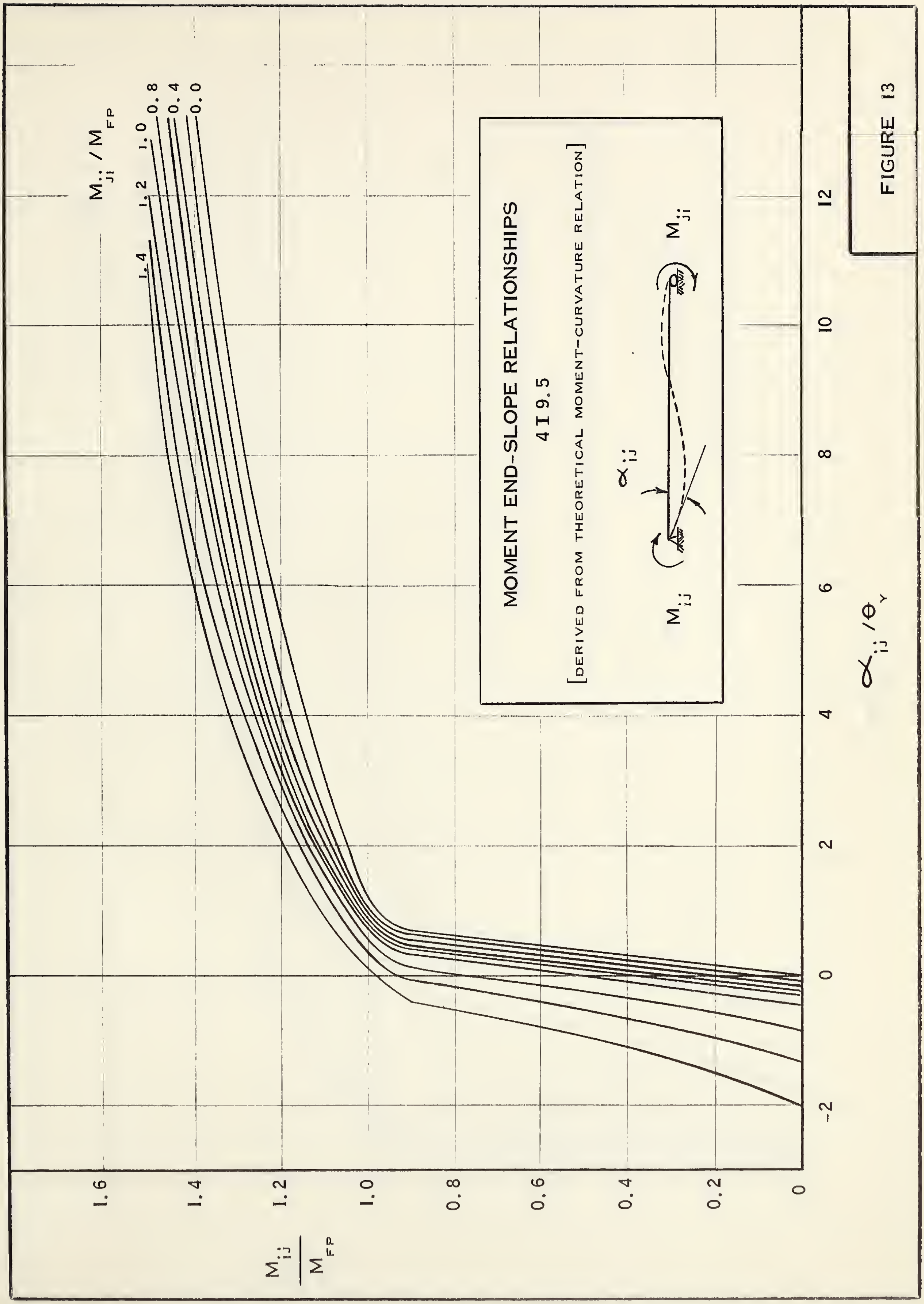

MOMENT END-SLOPE RELATIONSHIPS

4 I 9.5

[DERIVED FROM THEORETICAL MOMENT-CURVATURE RELATION]

FIGURE 13

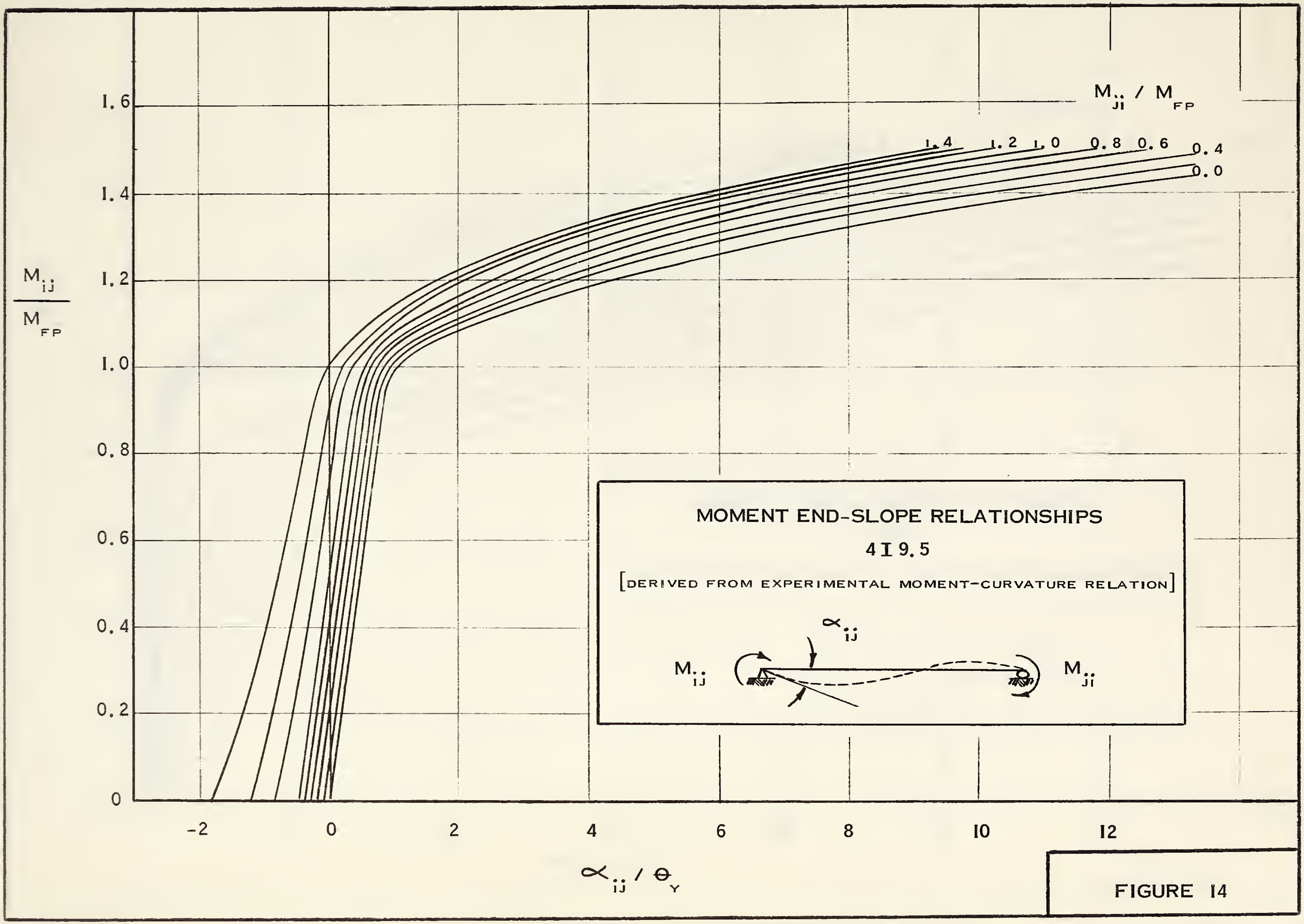
MOMENT END-SLOPE RELATIONSHIPS
4 I 9.5
[DERIVED FROM EXPERIMENTAL MOMENT-CURVATURE RELATION]
M_{ij} / M_{FP}
M_{ji} / M_{FP}
1.4
1.2
1.0
0.8
0.6
0.4
0.0
1.6
1.4
1.2
1.0
0.8
0.6
0.4
0.2
0
-2
0
2
4
6
8
10
12
α_{ij} / θ_Y
α_{ij}
M_{ij}
M_{ji}

FIGURE 14

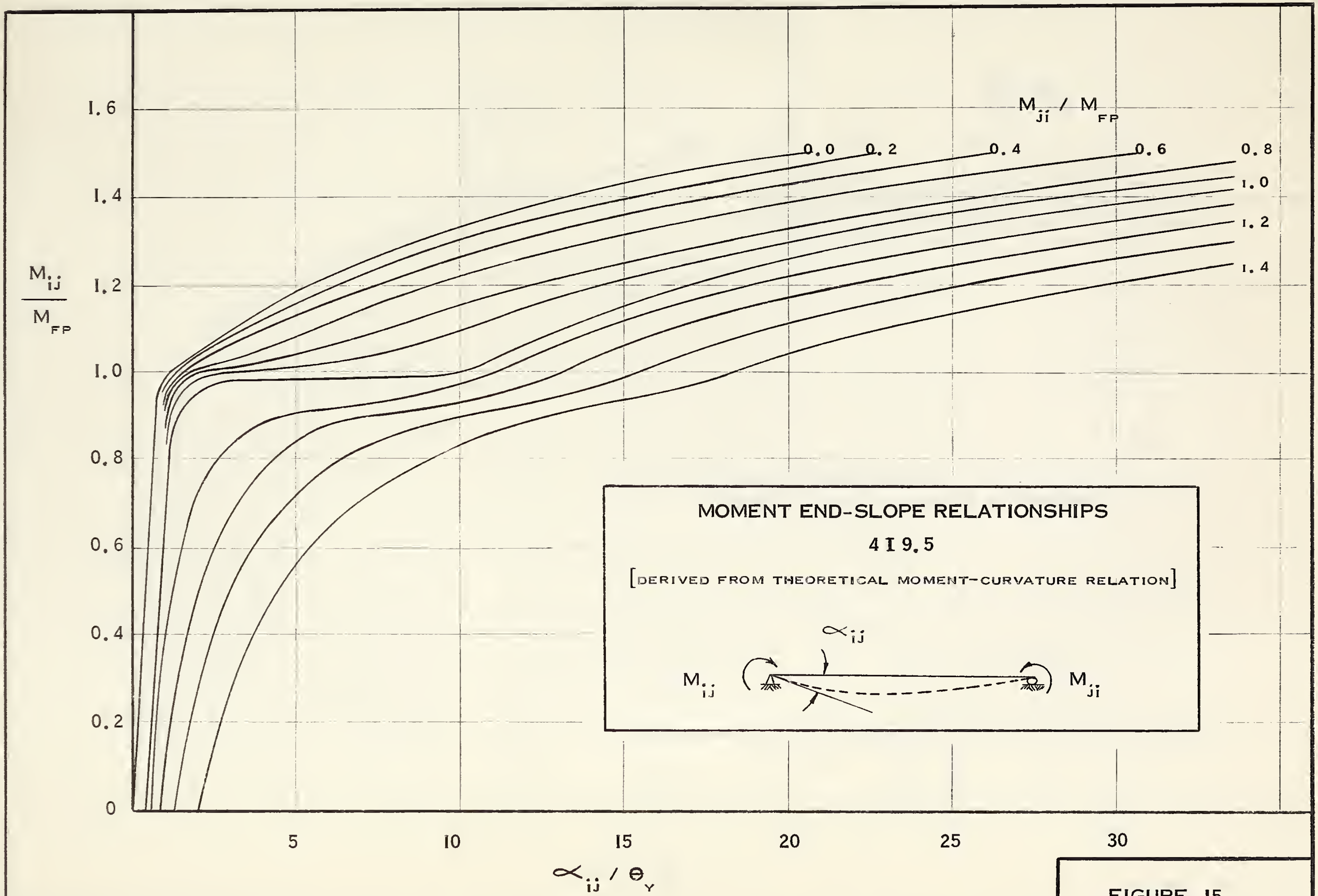

MOMENT END-SLOPE RELATIONSHIPS

4I9.5

[DERIVED FROM THEORETICAL MOMENT-CURVATURE RELATION]

FIGURE 15

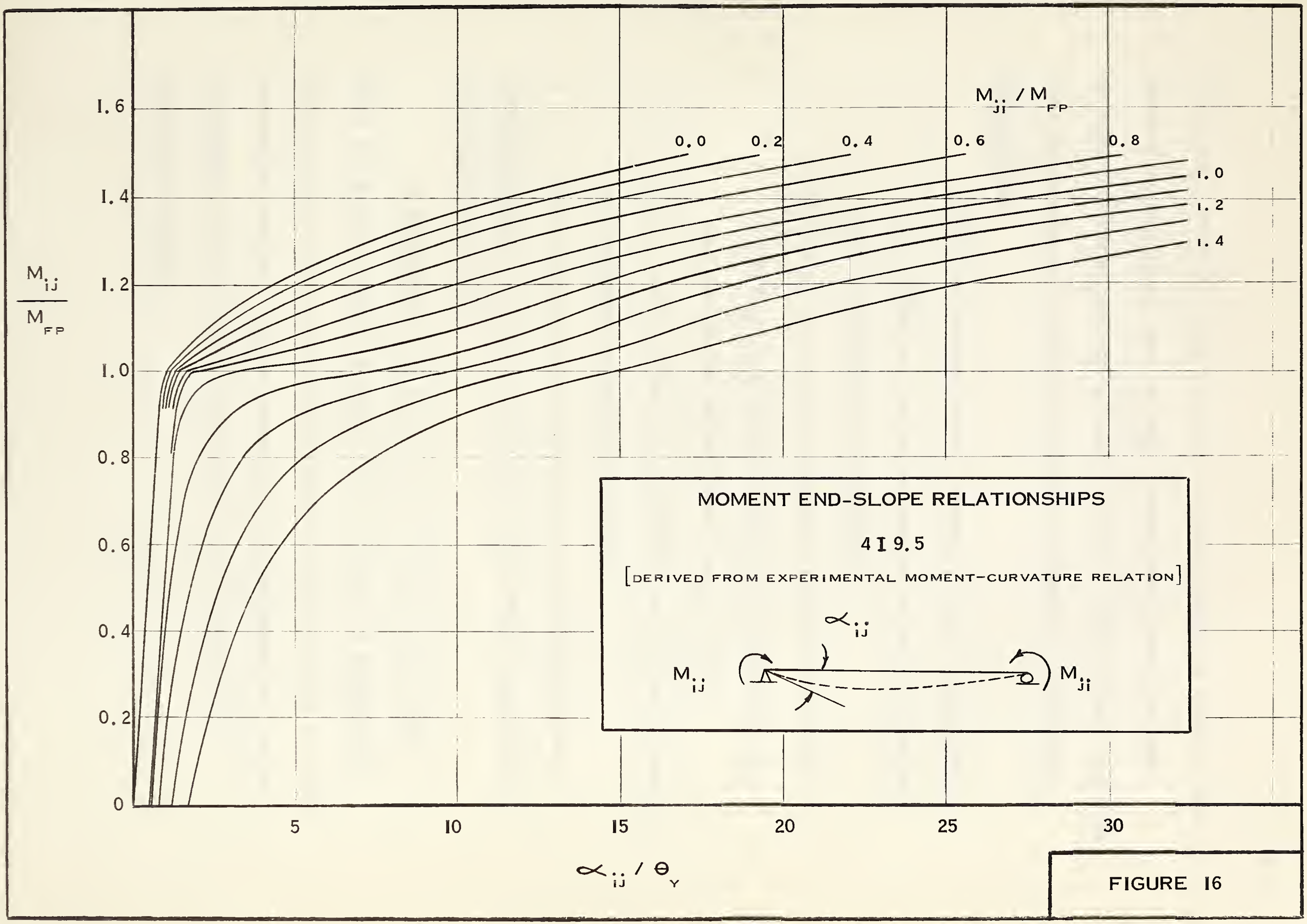

MOMENT END-SLOPE RELATIONSHIPS

4I9.5

[DERIVED FROM EXPERIMENTAL MOMENT-CURVATURE RELATION]

FIGURE 16

structure. To solve these equations, a semi-graphical method must however be employed, since a simple relationship does not exist between end-slopes and end-moments once the yield stress is reached. This semi-graphical method of analysis is based on the following assumptions:

1) Effects of axial forces, shearing forces, and buckling are neglected, hence the moment-curvature relationship corresponds to pure flexure.
2) The joints are rigid, therefore moments up to and including the ultimate moment of the members can be transmitted without destroying continuity.
3) Concentrated loads are applied in an increasing manner.
4) Clockwise moments are positive.

The step-by-step procedure used in the computation of a load-deflection curve for a structure, loaded with a single concentrated load is as follows:

A displacement is assumed at the loaded joint, from which the general deflected shape of the structure is determined. The moments at the ends of every member in the structure are then assumed at random. These moments in all likelihood, will not be compatible with the assumed deformation, hence they must be corrected iteratively.

For a particular member, the moment at the near-end, M_{ij}, is found that will produce the required end-slope, α_{ij}, at the near-end, with the known or assumed far-end moment, M_{ji}. The solution for a joint is obtained once a set of near-end moments and the corresponding near-end rotations is found that satisfies Equations (5) and (6) simultaneously. The determination of this tentative solution for a joint is successively carried out for all joints in the structure with the most recently found moments on the opposite ends of the members used as far-end moments for the joint concerned.

The final solution for the structure is found when the tentative solutions of every joint are the correct solutions. The magnitude of the load which produced the assumed displacement is then obtained by statics, using these correct moment values. The procedure is then repeated for different assumed displacements until the desired number of points are obtained.

For this investigation, computations required in the derivation of theoretical load-deflection curves for Frame Nos. 1 and 2, as well as for the beams, based on the above procedure, are given in Appendix B.

It must, however, be kept in mind that the semi-graphical method outlined above is suitable only for the case of a redundant structure loaded with a single concentrated load. For the case of

combined loadings, as in Frame Nos. 3 and 4, the number of trials necessary to obtain a compatible relationship between moment and end-slope at every joint in the structure becomes unreasonable. At least two displacements must be assumed initially, and after the iterative procedure is followed to obtain compatibility between moments and end-slopes, the final result must be such that the desired ratio between loads is achieved. In all likelihood, a goodly number of iterations would have to be performed before this last criterion is satisfied. For this reason, it was felt that use of the digital computer would be a necessity in dealing with the case of combined loadings. To compile a program of this sort, in itself, is a major undertaking. This task has been left as a future extension of this project.

CHAPTER VI

BEAM TESTS

6-1 Beam Specimens

Two identical simply-supported beams, with a span length of 45 inches, were tested in order to obtain an average moment-curvature relationship which would include the effects of residual stresses, and in order to provide a comparison with theoretical values predicted from the tension tests. As shown in FIGURE 17A, vertical bearing stiffeners were provided on each side of the web at the two load points and at the locations of the end supports. Two rotation indicator brackets, straddling the midspan of the beams, were welded to the web-flange fillets.

6-2 Loading System

Both beams were tested in a loading frame, details of which are described by Channon.(6) Two "Blackhawk RC-161" hydraulic rams, each with a capacity of ten tons and a plunger travel of ten inches, were rigidly attached to the loading frame eighteen inches apart, such that a region of pure moment without

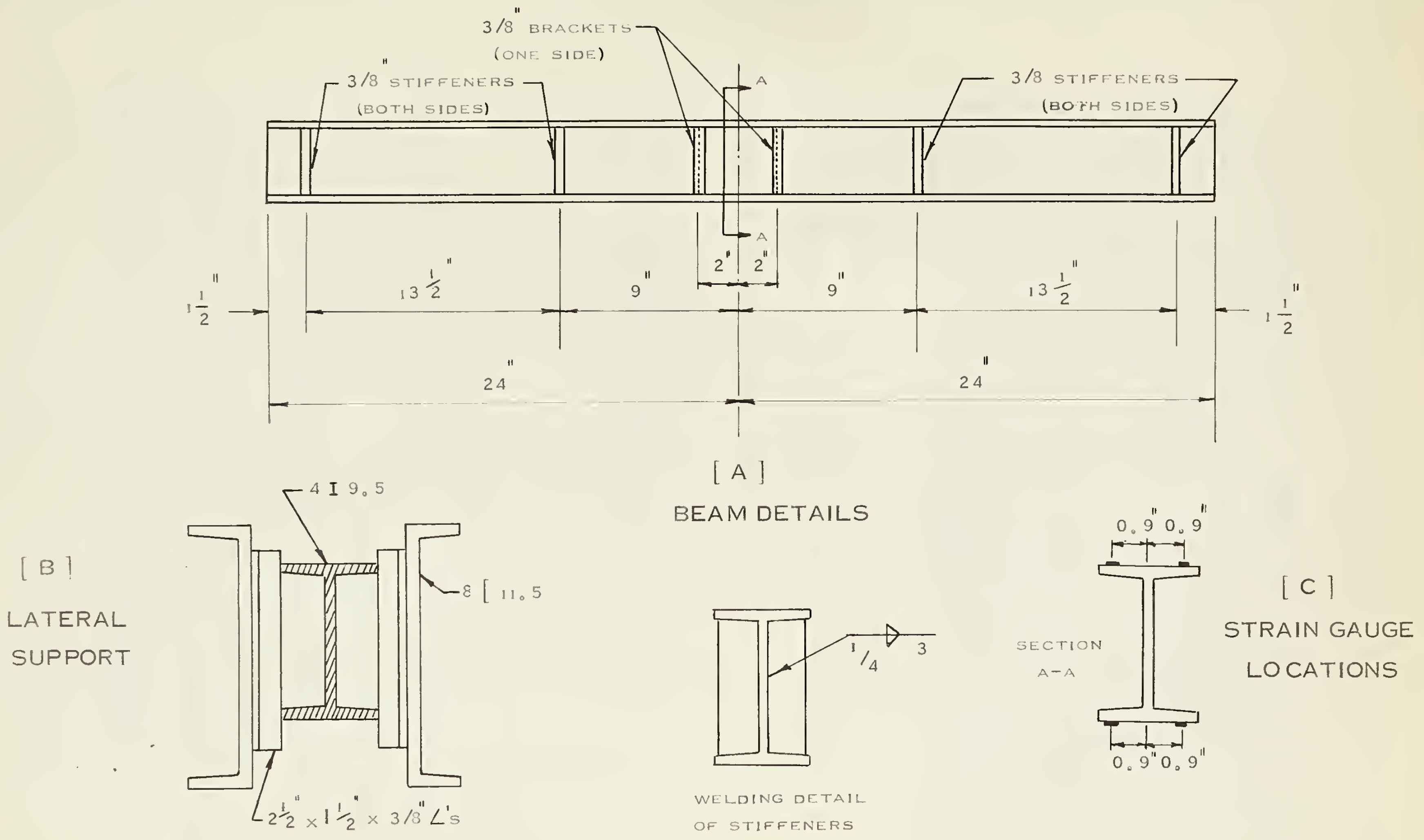

DETAILS OF TEST BEAMS

FIGURE 17

shear, would be achieved in the test beams (PLATE 3A). Both rams were operated with a single "Blackhawk P-59" pump to ensure equal distribution of load throughout the tests. A bracing system as indicated by PLATE 3B was used to prevent any lateral movement in the rams during testing.

Lateral support was provided for the beams by structural angles projecting from the backs of two 8-inch channel sections which were bolted to the columns of the loading frame (FIGURE 17B). Movement of the beams was thereby restricted to the vertical direction only. Friction was reduced to a minimum by greasing the contact surfaces of the projecting angles.

6-3 Beam Instrumentation

(i) Load Measurement

An overall view of the instrumentation employed in the beam tests is shown in PLATE 4. Loads applied through the hydraulic rams were measured by two ten-ton "Kyowa" load cells which were attached to bearing plates screwed to the ends of the hydraulic rams. A 3-point switching box connected these load cells to a "Type SLW-210 PA Kyowa Self-Balancing Indicator", which enabled the direct measurement of applied loads throughout each test.

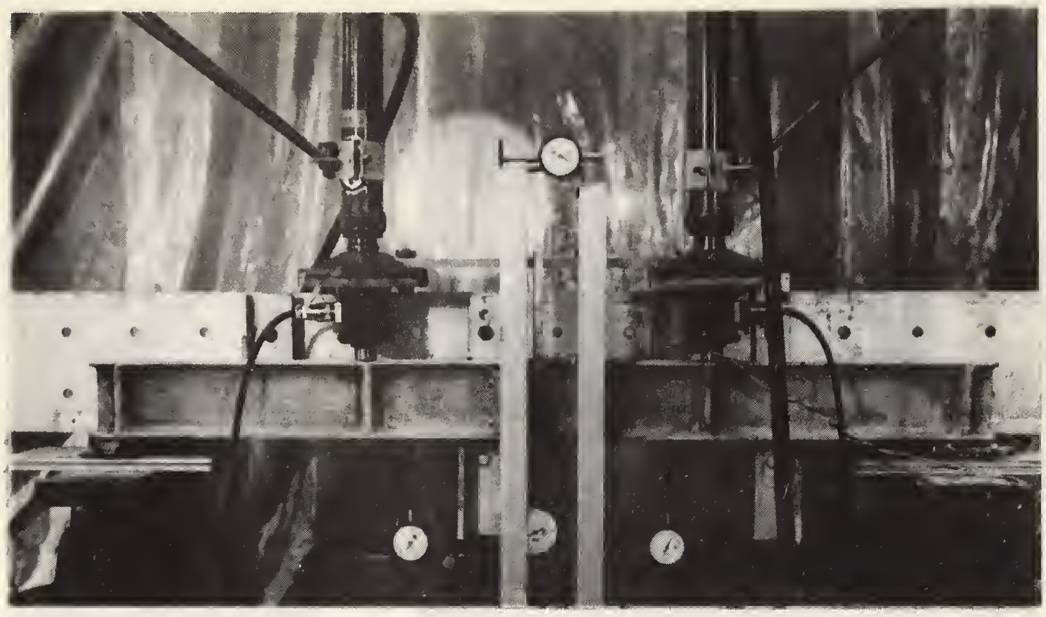

[A] LOADING SYSTEM FOR BEAM TESTS

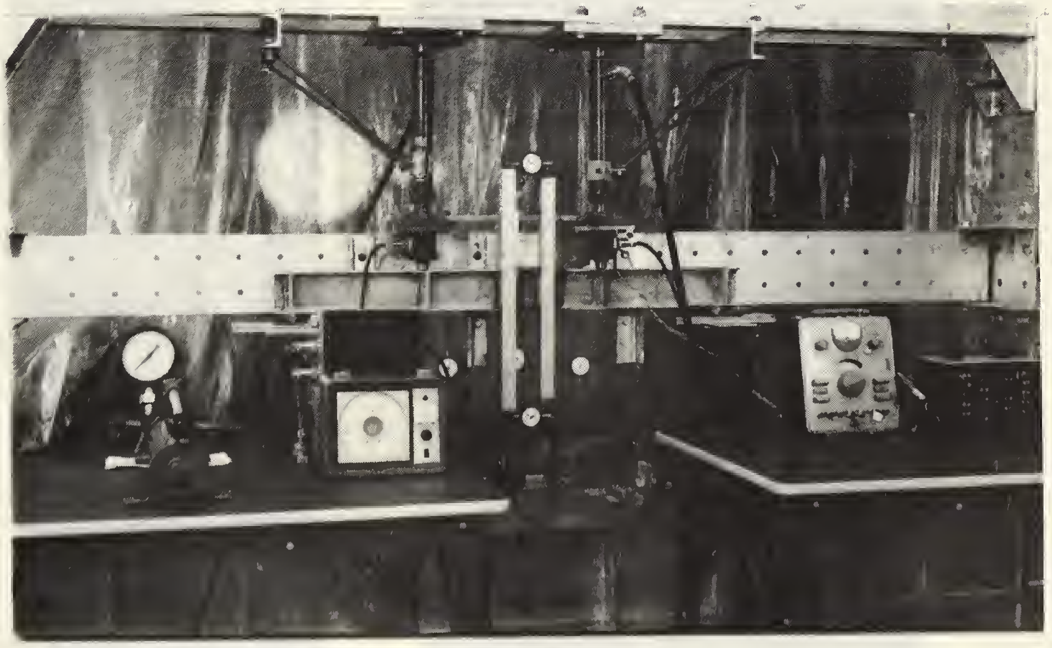

[B] BRACING SYSTEM FOR HYDRAULIC JACKS

PLATE 3

[illegible]

[illegible]

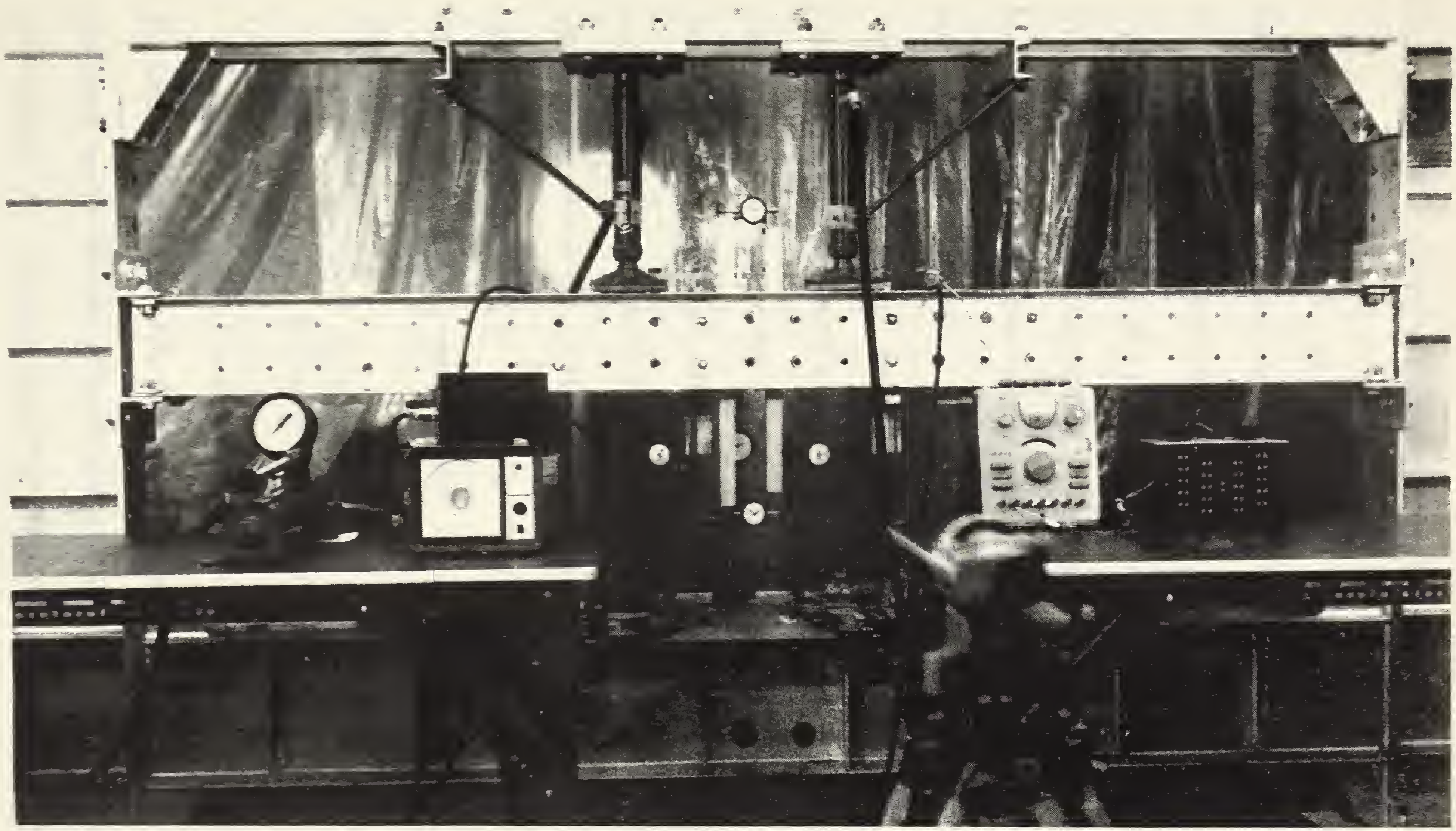

OVERALL VIEW OF BEAM INSTRUMENTATION

PLATE 4

(ii) Curvature Measurement

Curvature was measured at the beam midspan by two methods. The first method employed rotation indicators to measure the relative rotation between two neighbouring cross-sections. Each indicator consisted of two steel angle "arms" approximately twenty-five inches long, two brackets, and two dial gauges reading to 0.001 inch. The brackets were symmetrically placed two inches on either side of the beam midspan, and welded to the beams at the fillets. The steel angle "arms" were then bolted to these brackets and the relative rotation of these arms was measured by the dial gauges mounted at the ends of the angles at a set distance (12.5 inches) above and below the mid-depth of the beams. Since the unit curvature at a section equals the measured angle divided by the distance (4 inches) between the two arms, a simple relationship is obtained between dial readings and curvature. Denoting two average consecutive dial readings as R_1 and R_2 respectively, the change in curvature, $\Delta\phi$, is given by:

$$\Delta\phi = \frac{R_2 - R_1}{4 \times 12.5} = 0.02(R_2 - R_1) \text{ rad./inch}$$

The second method for computing curvatures involved the use of four "Type A3, SR-4" electrical resistance strain gauges, mounted on the flanges of each beam at midspan, in locations shown in FIGURE 17C. Before mounting the strain gauges, a rotary disc

sander was used to obtain a smooth surface on the flanges of each beam. This surface was then polished with emery cloth, after which it was thoroughly cleaned with acetone. The "SR-4" gauges were then carefully cemented in position with C.I.L. Household Cement and any air bubbles in the cement were squeezed out to ensure intimate contact with the flange surfaces. All gauges were checked with an ohmeter before wiring; and defective gauges were replaced immediately. Approximately 24 hours after the gauges were mounted, a liberal quantity of neoprene was applied to waterproof as well as to the protect the gauges. The beam was then whitewashed and tested approximately three weeks later.

After the beam was set in place in the loading frame, lead wires were connected to a "Baldwin-Lima-Hamilton 20-point Switching Unit". Strain readings were taken with a "Baldwin-Lima-Hamilton Type N, SR-4 Strain Indicator". Curvatures were calculated by dividing the average gauge readings by half the section depth.

The curvatures presented herein were the average results obtained by the above two methods of curvature measurement.

(iii) Deflection Measurement

Vertical deflection at midspan of each beam was measured by a dial gauge having a travel of two inches and measuring to 0.001 inch. A check on these deflection measurements was provided by

readings taken with a surveyor's level on a steel scale, graduated to 0.01 inch, mounted at midspan.

6-4 Experimental Procedure

After alignment of each beam in the loading frame was completed, a preliminary test was first performed as a check on the instrumentation. This test consisted of applying loads up to approximately one-third of the predicted yield load and checking readings on all gauges. The loads were then released and the main test was carried out.

Loads were applied in increments of 500 pounds up to a value of 11,000 pounds, after which the increments were reduced to 250 pounds until completion of the test. All gauge readings were taken at each increment of load. In the plastic range, a "waiting period" of at least 45 minutes after load application was necessary, before readings were taken.

Three men were employed in the beam tests; the first maintained the load on the jacks, the second recorded strain readings, and the third recorded the deflection and rotation measurements and plotted a load-deflection curve as the test progressed. The duration of each test was approximately seven hours.

6-5 Test Results

Test results are presented in graphical form for both

beam tests as follows:

(1) Load vs. deflection (FIGURES 18 & 19)

(2) Moment vs. curvature (FIGURES 20 & 21)

A general view of a typical beam after testing is shown in PLATE 5; a closeup view of the plastic hinge is shown in PLATE 6A. The extent to which lateral buckling occurred in Beam Test No. 1 is evident in PLATE 6B.

The experimental load-deflection curves were plotted using dial indicator readings. In addition to the observed deflections, a plot of theoretical deflections was made to provide a means of comparing actual test results with those predicted from computations based on the "moment end-slope" relationships, as well as those predicted by the "plastic-hinge" method. Calculations based on the "plastic-hinge" method appear in Appendix A, and calculations based on the "moment end-slope" relationships are given in Appendix B.

For both beam tests, experimental moment-curvature relationships were plotted from strain gauge readings, as well as from rotation indicator readings. Calculations were based on the methods outlined previously in this chapter. An average moment-curvature relationship derived from the two beam tests is shown in FIGURE 22. Theoretical moment-curvature relationships for the 4 I 9.5 section were plotted for comparison with the above curves. Calculations based on the simple plastic theory are given in Appendix A , and calculations based on Equation (4) (Chapter V), are given in Appendix B.

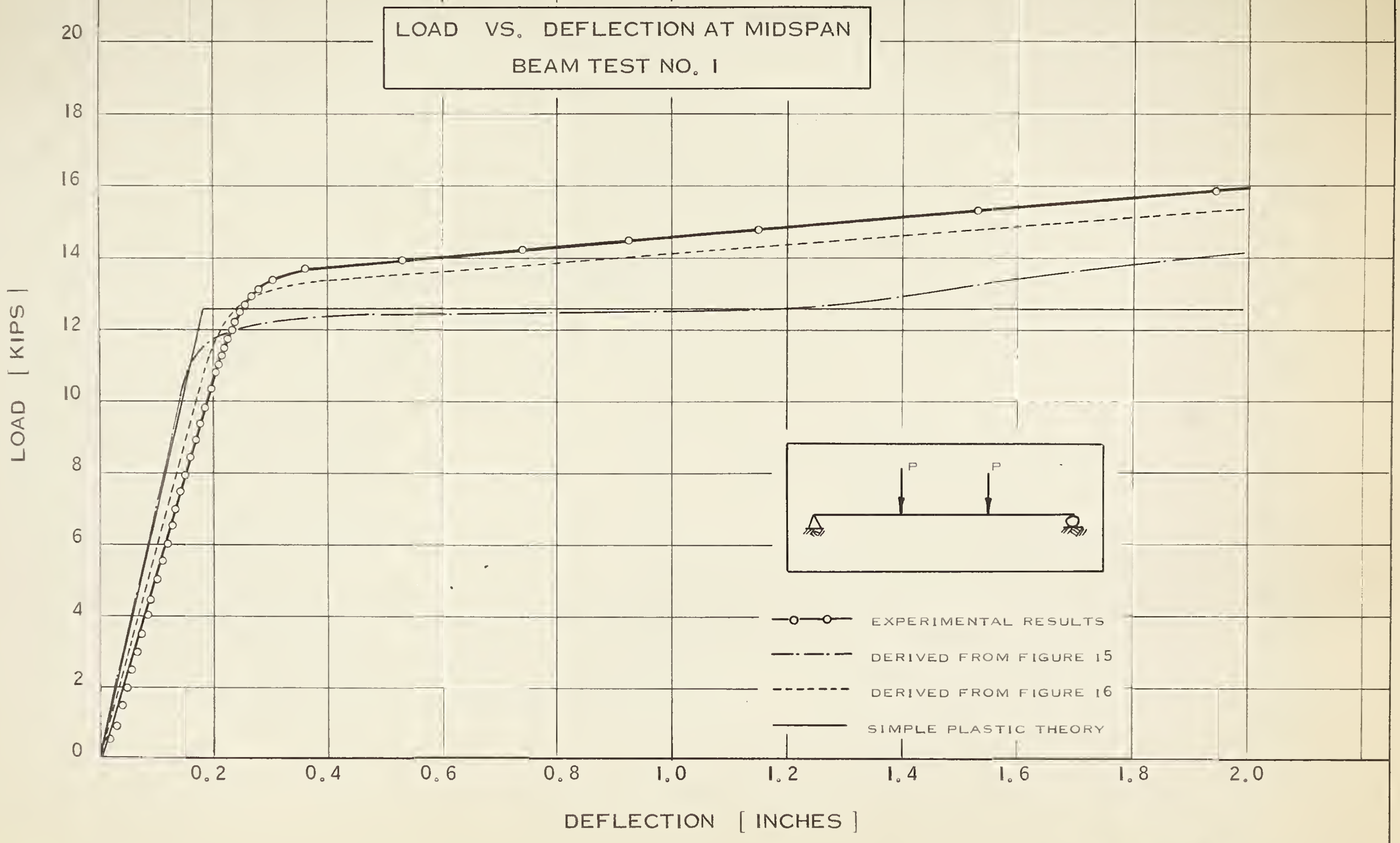
LOAD VS. DEFLECTION AT MIDSPAN
BEAM TEST NO. I
LOAD [KIPS]
20
18
16
14
12
10
8
6
4
2
0
0.2
0.4
0.6
0.8
1.0
1.2
1.4
1.6
1.8
2.0
DEFLECTION [INCHES]
P
P
EXPERIMENTAL RESULTS
DERIVED FROM FIGURE 15
DERIVED FROM FIGURE 16
SIMPLE PLASTIC THEORY

FIGURE 18

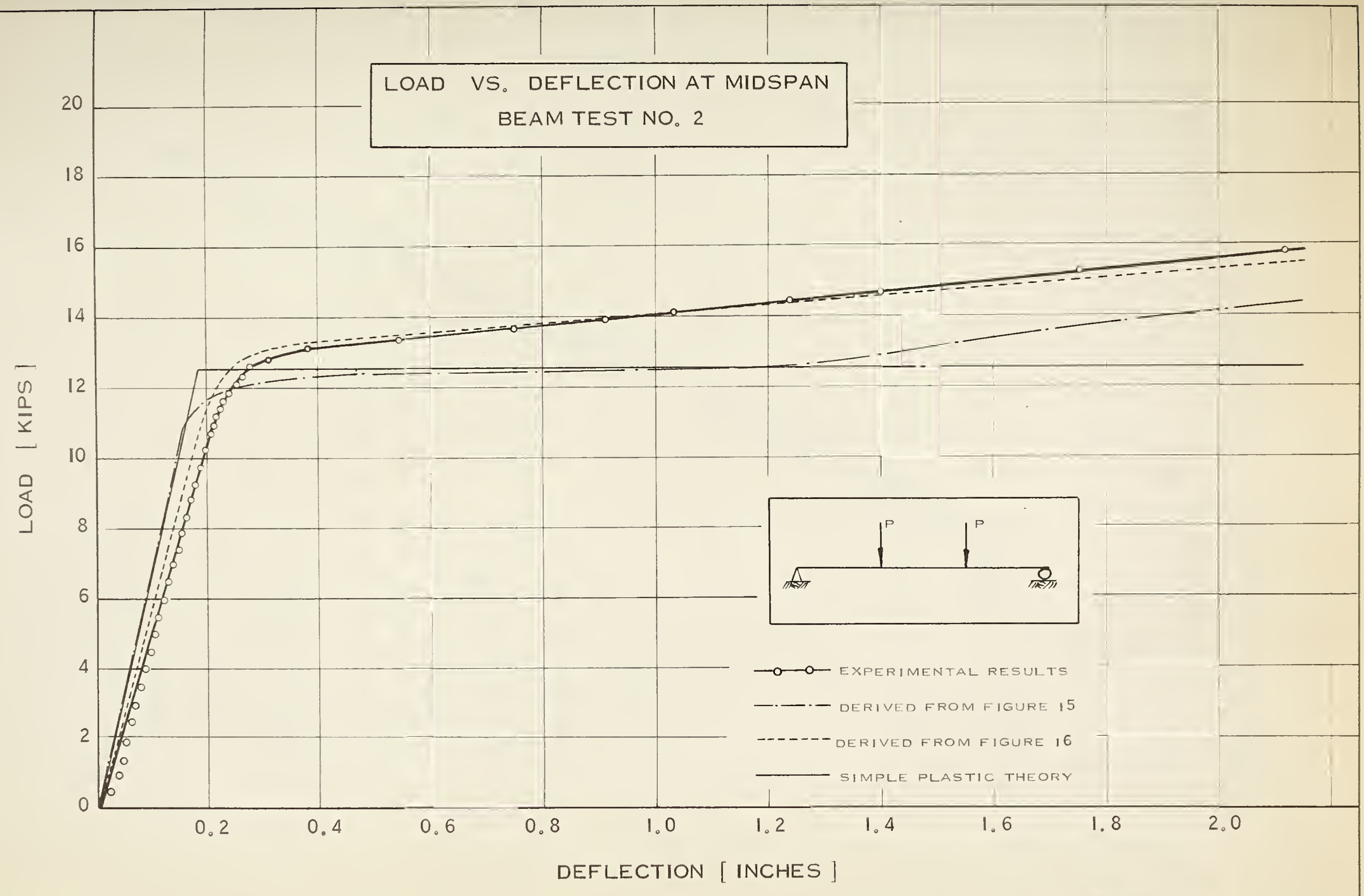

LOAD VS. DEFLECTION AT MIDSPAN
BEAM TEST NO. 2

FIGURE 19

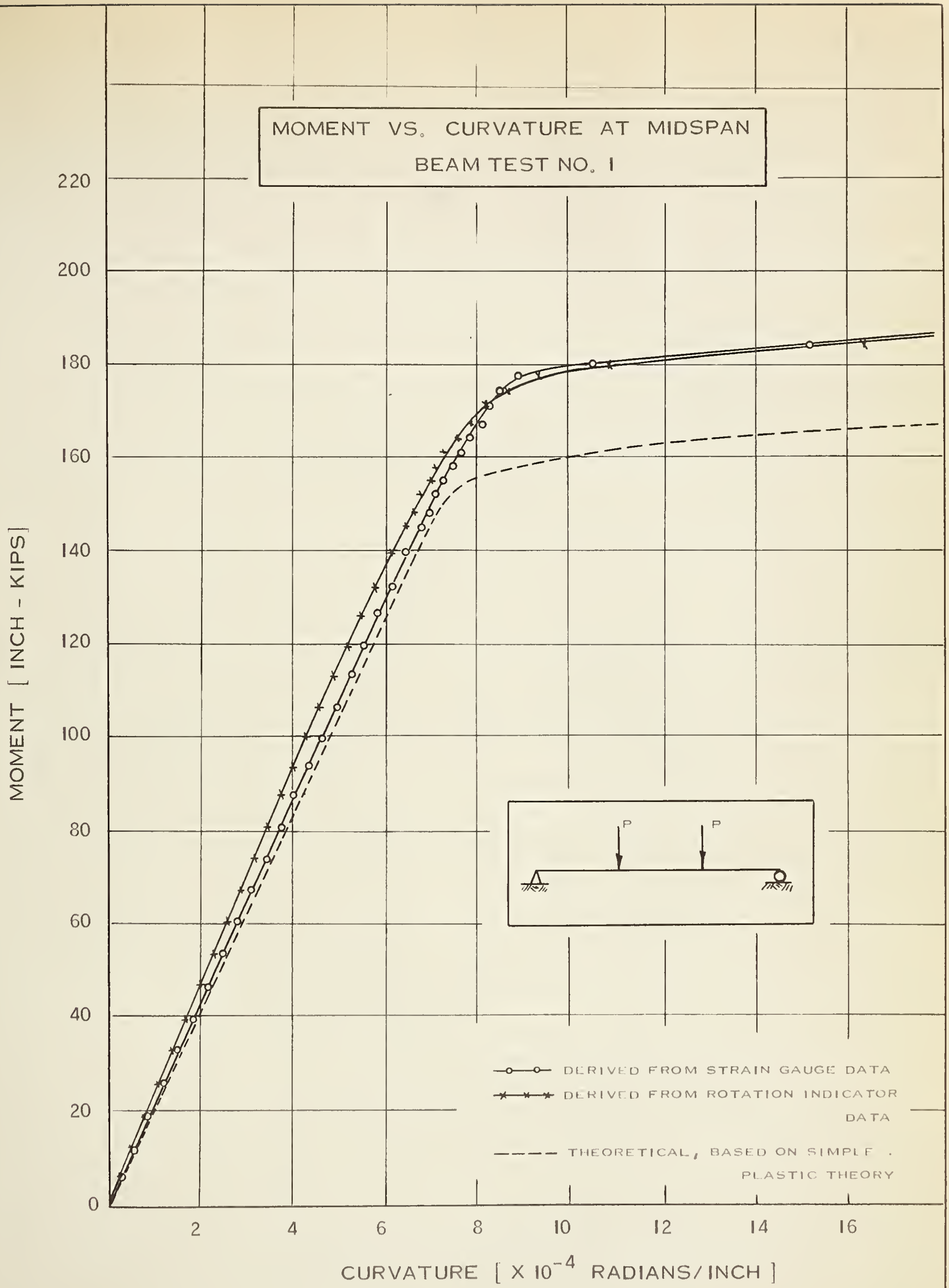
MOMENT VS. CURVATURE AT MIDSPAN
BEAM TEST NO. 1
MOMENT [INCH - KIPS]
0
20
40
60
80
100
120
140
160
180
200
220
2
4
6
8
10
12
14
16
CURVATURE [X 10^{-4} RADIANS/INCH]
P
P
DERIVED FROM STRAIN GAUGE DATA
DERIVED FROM ROTATION INDICATOR DATA
THEORETICAL, BASED ON SIMPLE PLASTIC THEORY

FIGURE 20

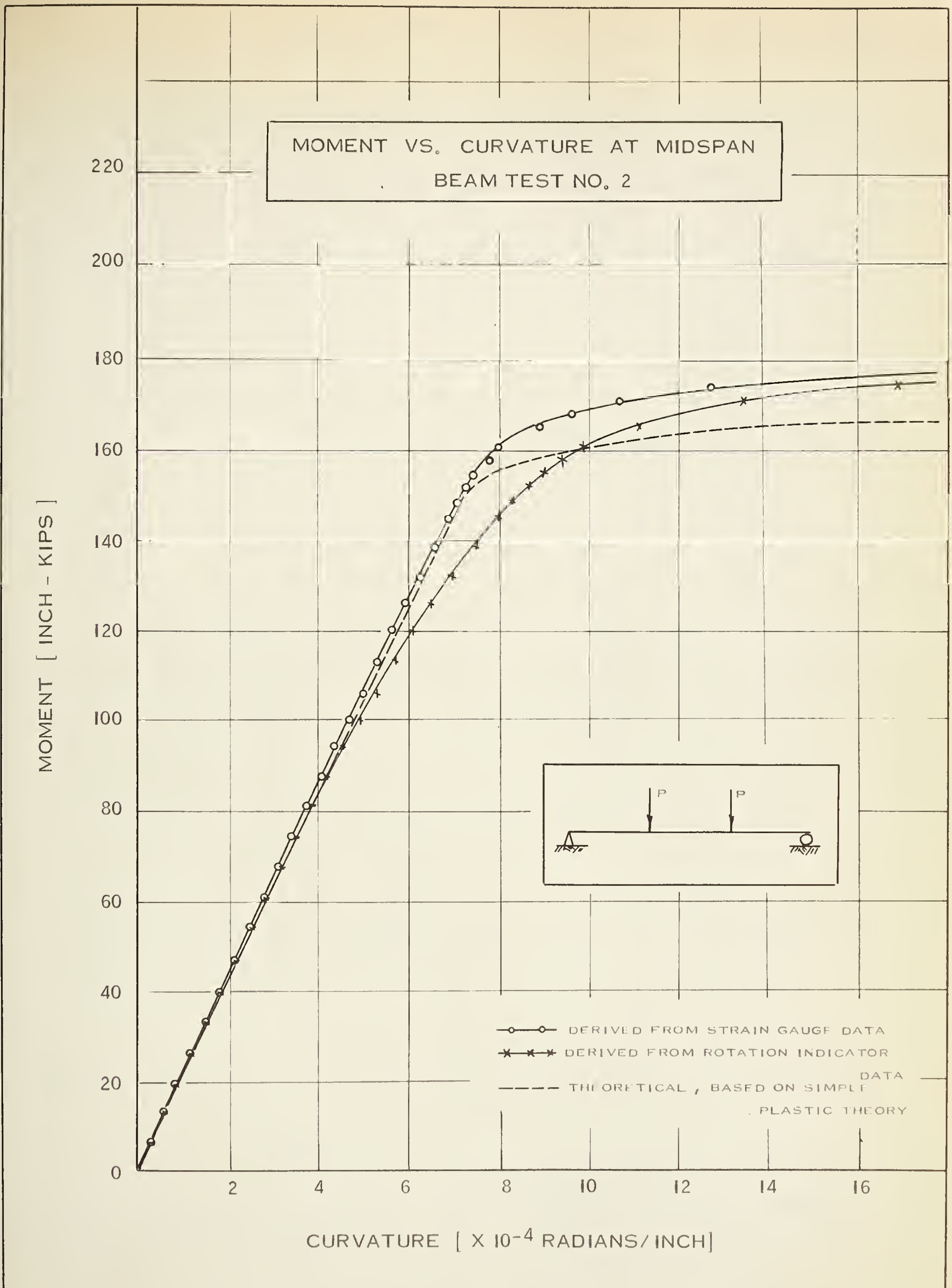
MOMENT VS. CURVATURE AT MIDSPAN
BEAM TEST NO. 2
MOMENT [INCH - KIPS]
0
20
40
60
80
100
120
140
160
180
200
220
CURVATURE [X 10^{-4} RADIANS/ INCH]
2
4
6
8
10
12
14
16
P
P
DERIVED FROM STRAIN GAUGE DATA
DERIVED FROM ROTATION INDICATOR DATA
THEORETICAL , BASED ON SIMPLE PLASTIC THEORY

FIGURE 21

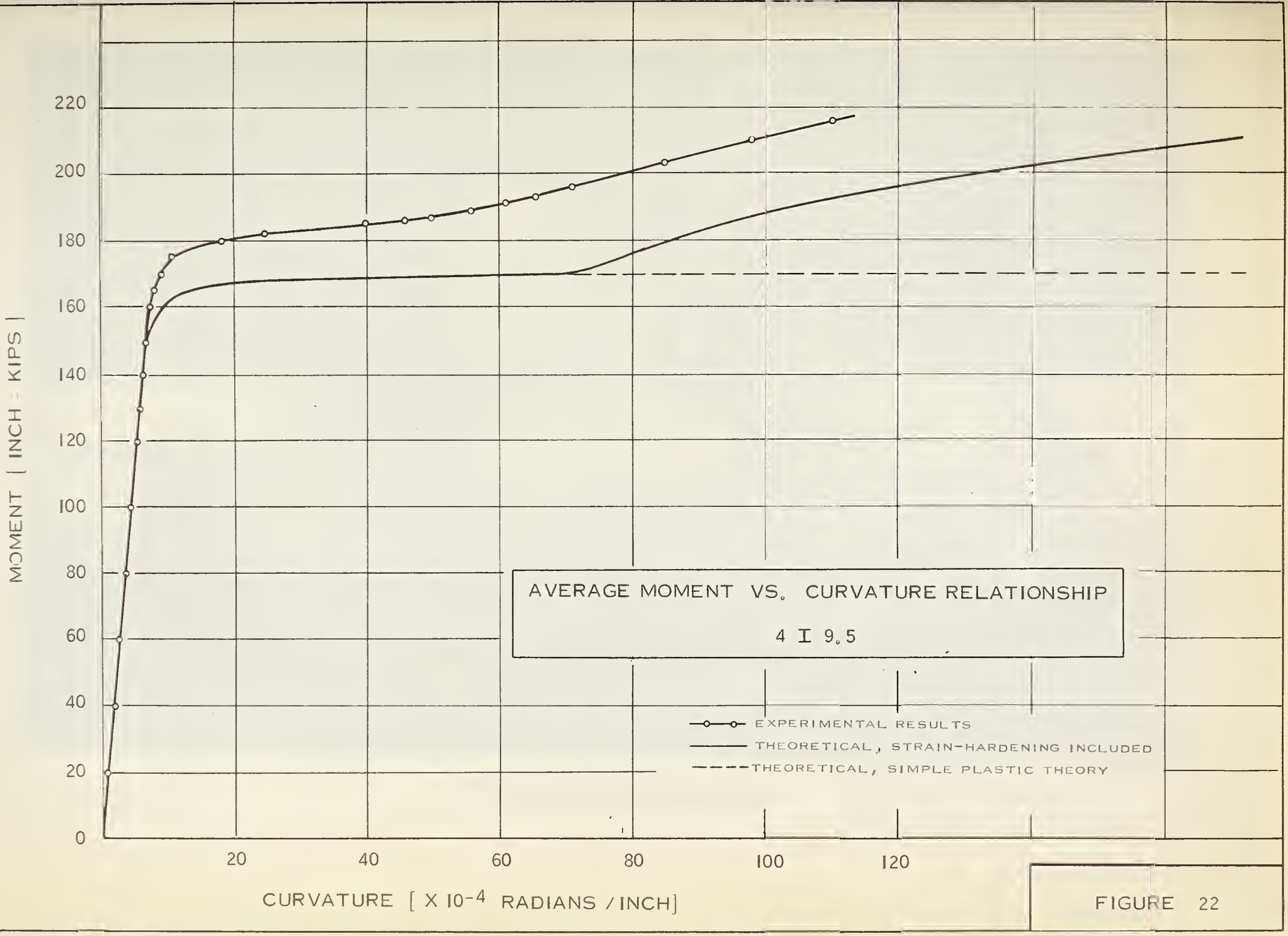

AVERAGE MOMENT VS. CURVATURE RELATIONSHIP

4 I 9.5

FIGURE 22

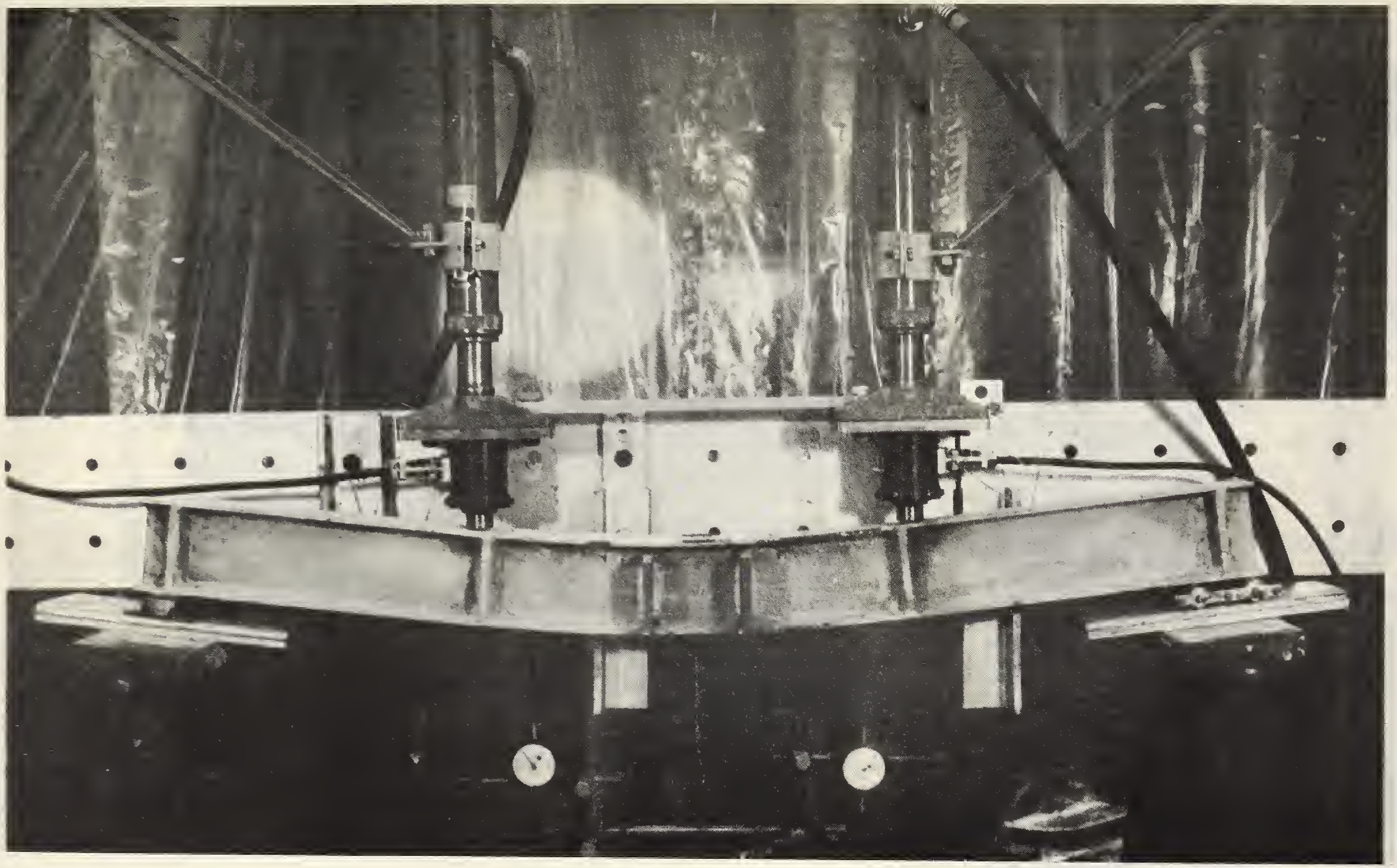

TYPICAL BEAM AFTER TEST

PLATE 5

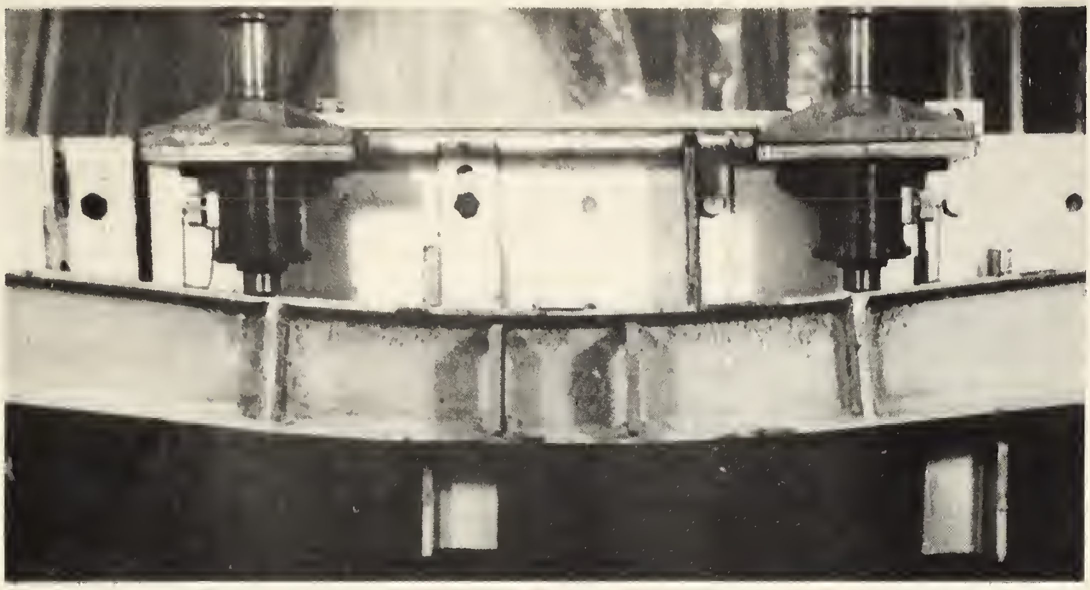

[A] PLASTIC HINGE AT BEAM MIDSPAN

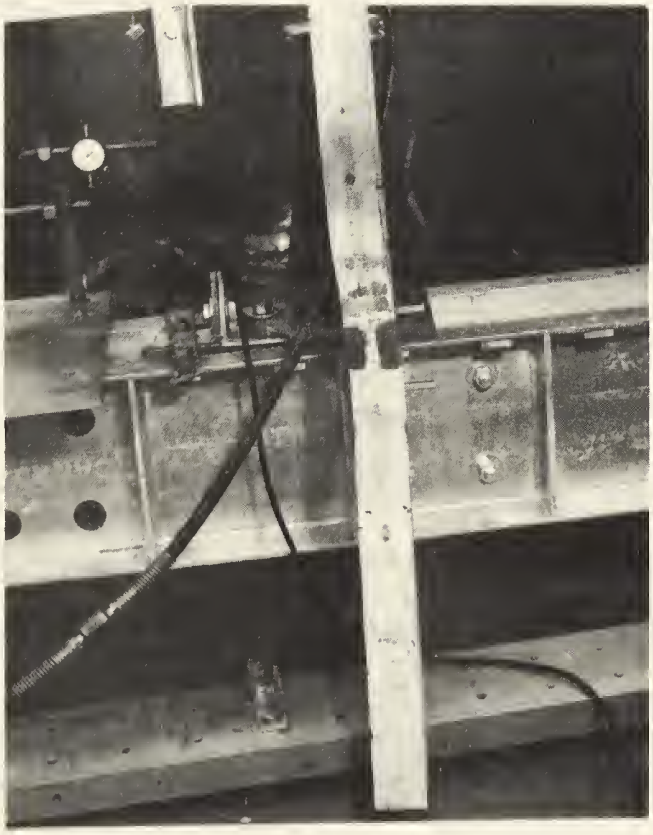

[B] BUCKLED COMPRESSION FLANGE IN BEAM

PLATE 6

[illegible]

[illegible]

[illegible]

CHAPTER VII

FRAME TESTS

7-1 Frame Specimens

The four frames tested in this program were of the same design as those tested by previous investigators at the University of Alberta.(6, 7) Frame dimensions and details are shown in FIGURES 23, 24 and 25. Each frame tested had a column height of four feet and a beam span of six feet. Flange plates, web stiffeners, and welding details were proportioned so as to provide the greatest possible rigidity in the corner connections. Vertical bearing stiffeners were provided at the center of each beam to prevent web crippling under the vertically applied, concentrated load. The column flanges were coped at the base so the frames could be fitted into the hinge supports of the loading frame. Resistance to rotation at these supports was minimized by reaming and greasing the holes provided for the hinge pins. Five pairs of rotation indicator brackets were welded to the web-flange fillets near points where plastic hinges were expected to form.

[illegible]

[illegible]

[illegible]

[illegible]

[illegible]

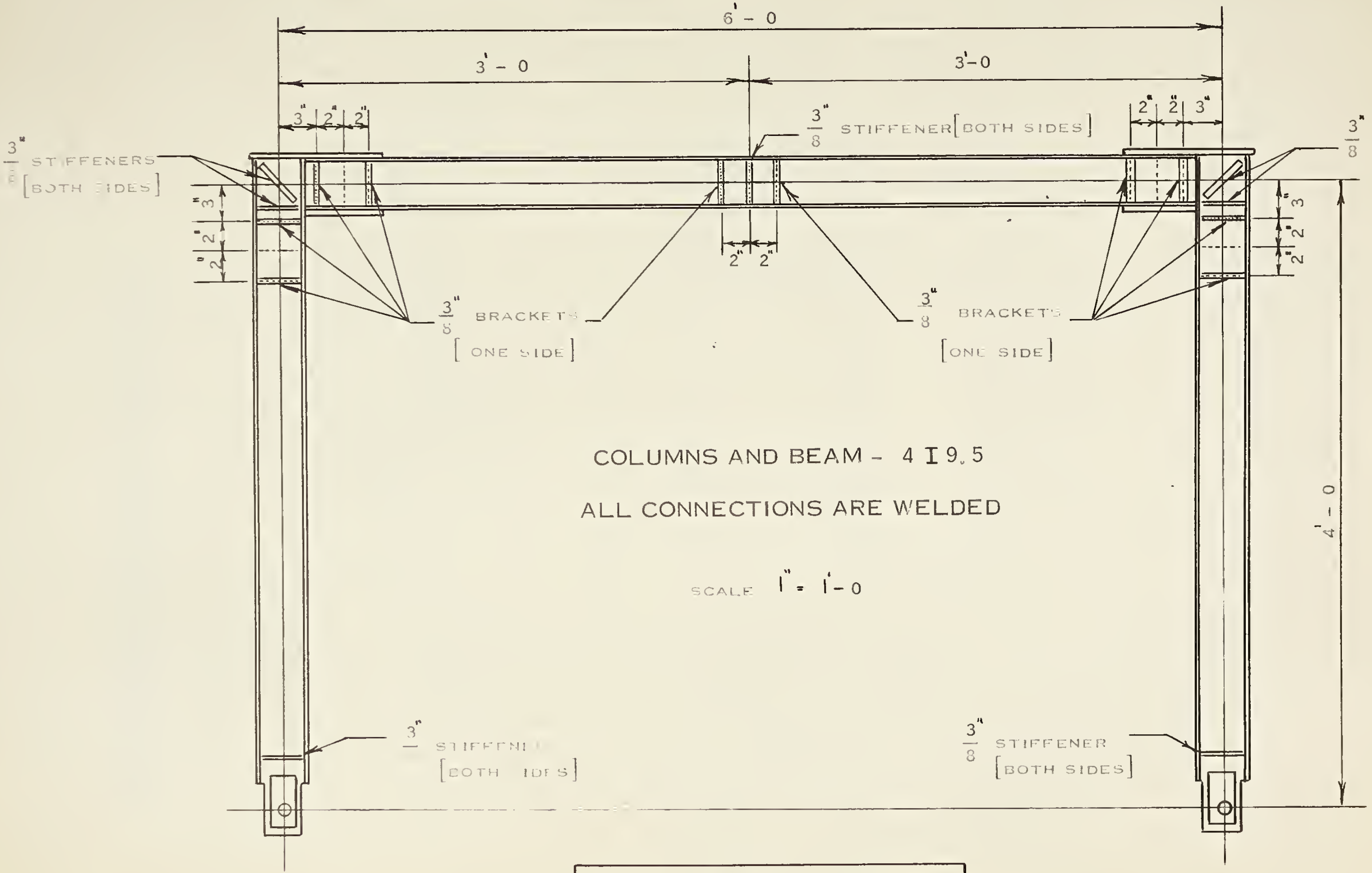
6' - 0
3' - 0
3'-0
3"
2"
2"
2"
2"
3"
$\frac{3}{8}$" STIFFENER [BOTH SIDES]
$\frac{3}{8}$" STIFFENERS [BOTH SIDES]
$\frac{3}{8}$" STIFFENERS [BOTH SIDES]
3"
2"
2"
3"
2"
2"
2"
2"
$\frac{3}{8}$" BRACKETS [ONE SIDE]
$\frac{3}{8}$" BRACKETS [ONE SIDE]
4' - 0
$\frac{3}{8}$" STIFFENER [BOTH SIDES]
$\frac{3}{8}$" STIFFENER [BOTH SIDES]

COLUMNS AND BEAM - 4 I 9.5

ALL CONNECTIONS ARE WELDED

SCALE 1" = 1'-0

DETAILS OF TEST FRAMES

FIGURE 23

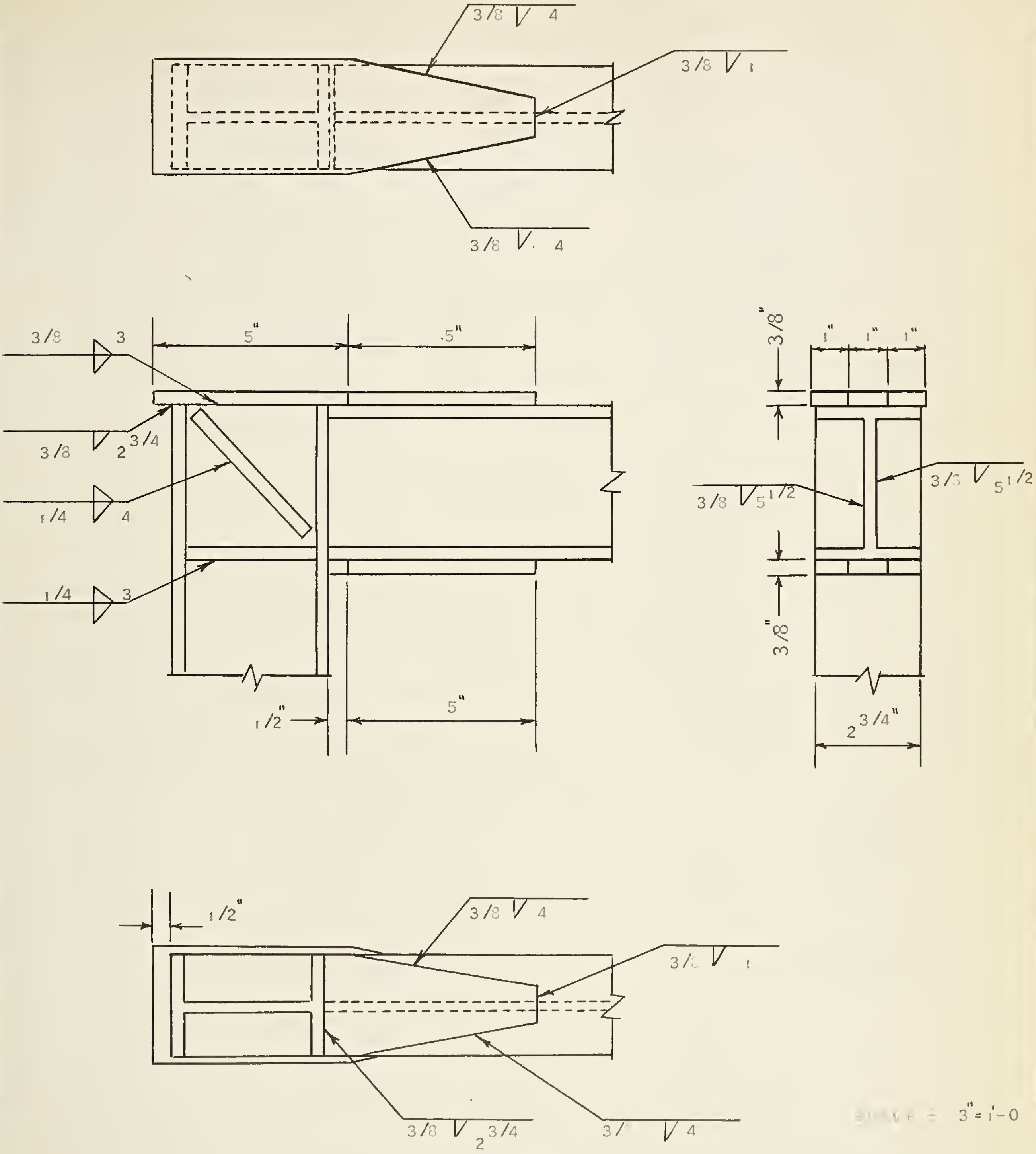

SCALE = 3" = 1'-0

NOTE – ALL STIFFENERS CUT FROM 3/8" PLATE

DETAILS OF TEST FRAME CONNECTIONS

FIGURE 24

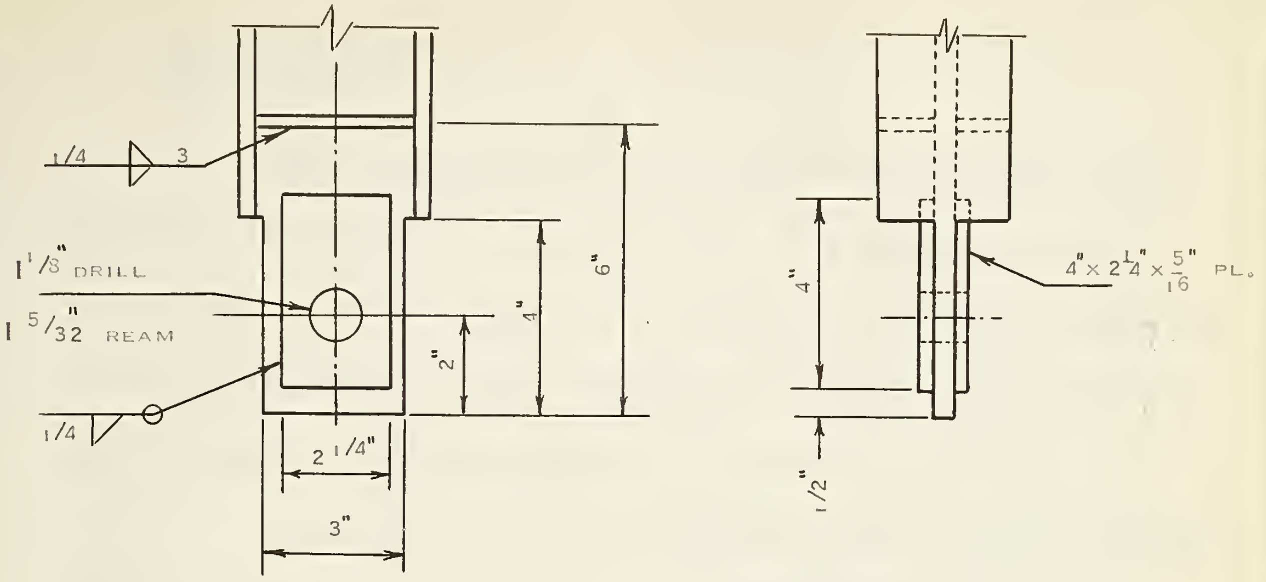

HINGE CONNECTION

BRACKET CONNECTION

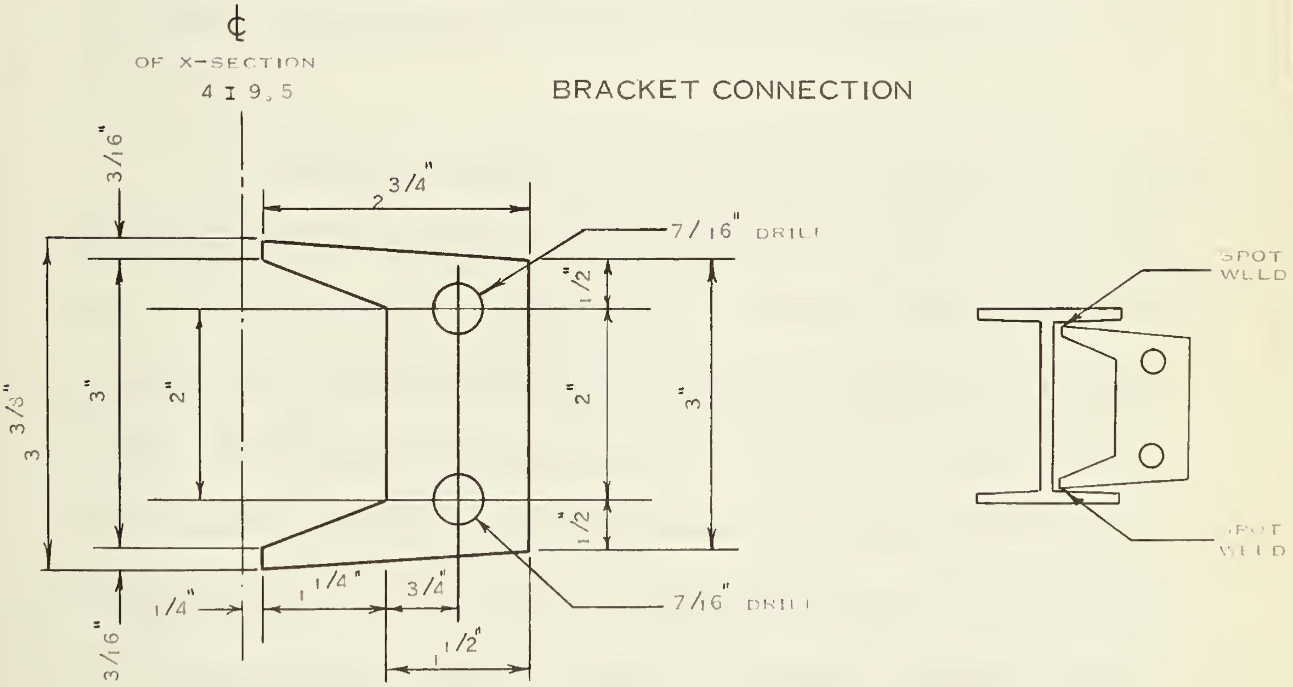

DETAILS OF HINGE CONNECTIONS AND ROTATION INDICATOR BRACKETS

FIGURE 25

7-2 Loading System

Each frame specimen was tested in an upside-down position and the hinge supports were attached to the upper beam of the loading frame. This configuration conveniently eliminated the problem of supporting the heavy roller mechanism which was designed specifically to allow horizontal movement of the vertical jack.(6)

As shown in PLATE 7A, a single vertical load was applied at the beam midspan of Frame No. 1 by a "Blackhawk RC-251" hydraulic ram with a capacity of twenty tons and a plunger travel of six inches. Movement of the roller mechanism did not occur in this particular test.

Frame No. 2 was loaded as shown in PLATE 7B. A single horizontal load was applied to the top of the left column, at the elevations of the mid-depth of the beam, by means of a "Blackhawk RC-159" hydraulic ram with a capacity of ten tons and a plunger travel of six inches. Part way through the test, this ram was replaced by a "Blackhawk RC-161" hydraulic ram of the same capacity but with a plunger travel of ten inches. This replacement was necessary due to the limited clearance between the test specimen and loading frame.

The loading system used in Frame Tests Nos. 3 and 4 is shown in PLATES 8A and 8B, respectively. In both tests, the vertical load was applied by the system as described for Frame No. 1, and the

horizontal load was applied by the system as described for Frame No. 2. For Frame No. 3, the vertical load was equal in magnitude to the horizontal load; for Frame No. 4, the ratio of vertical to horizontal load was 2:1. Movement of the roller mechanism under the vertical load occurred as a result of the horizontal load. As in the test for Frame No. 2, the horizontal ram used at the beginning of the test was replaced by one with a larger plunger travel, part way through each test.

Lateral support was provided for the beam and column portions of the frames in a manner similar to that described for the beam test specimens (PLATE 9).

7-3 Frame Instrumentation

(i) Load Measurements

In testing Frame No. 1, vertical load was measured by a twenty ton "Kyowa" load cell. This load cell was directly connected to the "Type SLW-210PA Kyowa Self-Balancing Indicator". For Frame Test No. 2, the horizontal load was measured by a ten ton "Kyowa" load cell. In testing Frame Nos. 3 and 4, vertical load was measured by a twenty ton "Kyowa" load cell, and the horizontal load was measured by a ten ton "Kyowa" load cell. A three-point switching box connected these load cells to the "Kyowa Self-Balancing Indicator," from which direct measurements of load were obtained.

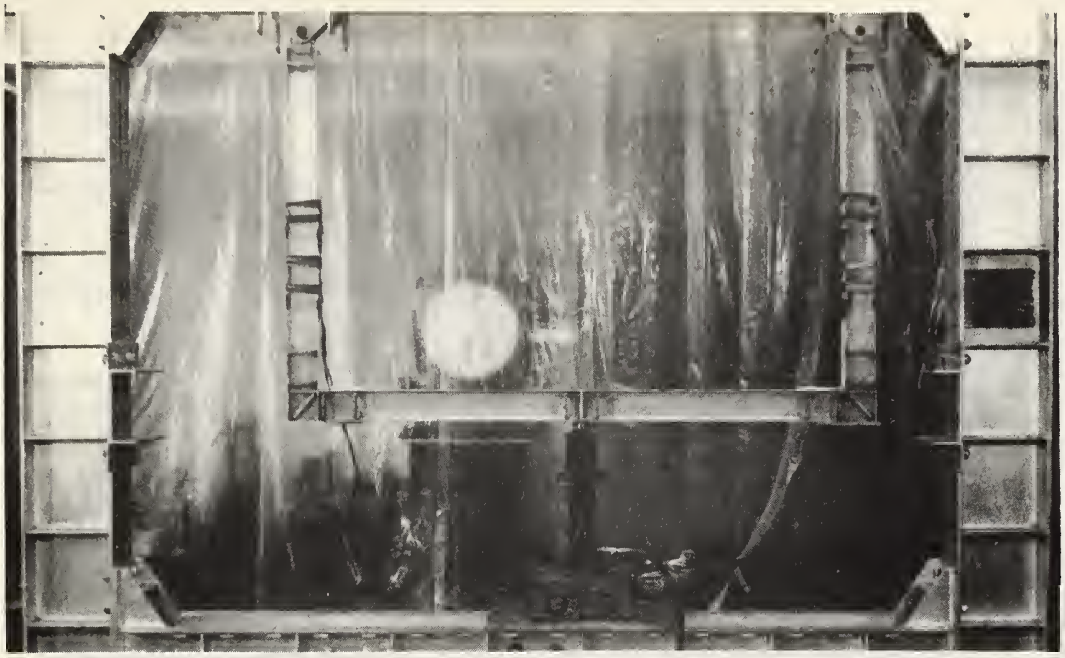

[A] LOADING SYSTEM FOR FRAME NO. 1

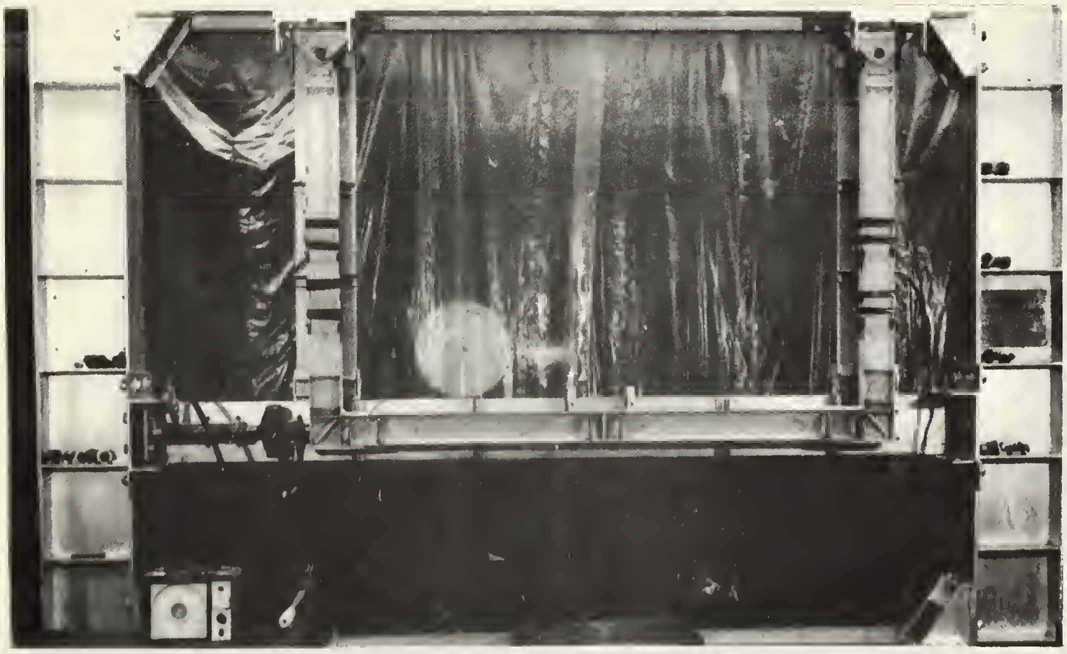

[B] LOADING SYSTEM FOR FRAME NO. 2

PLATE 7

[illegible]

[illegible]

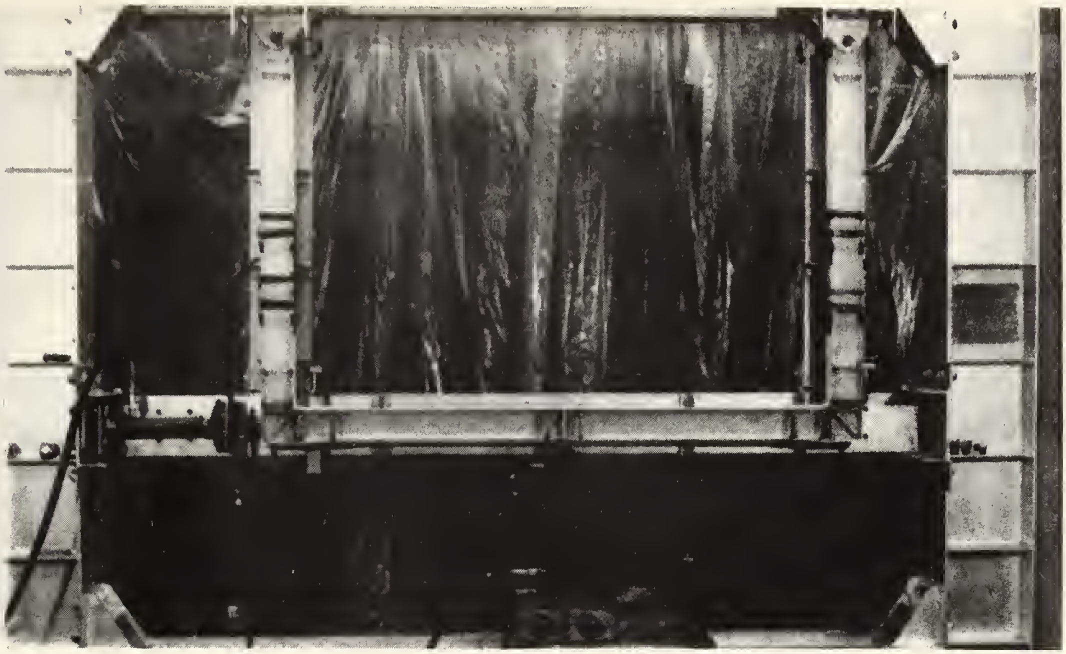

[A] LOADING SYSTEM FOR FRAME NO. 3

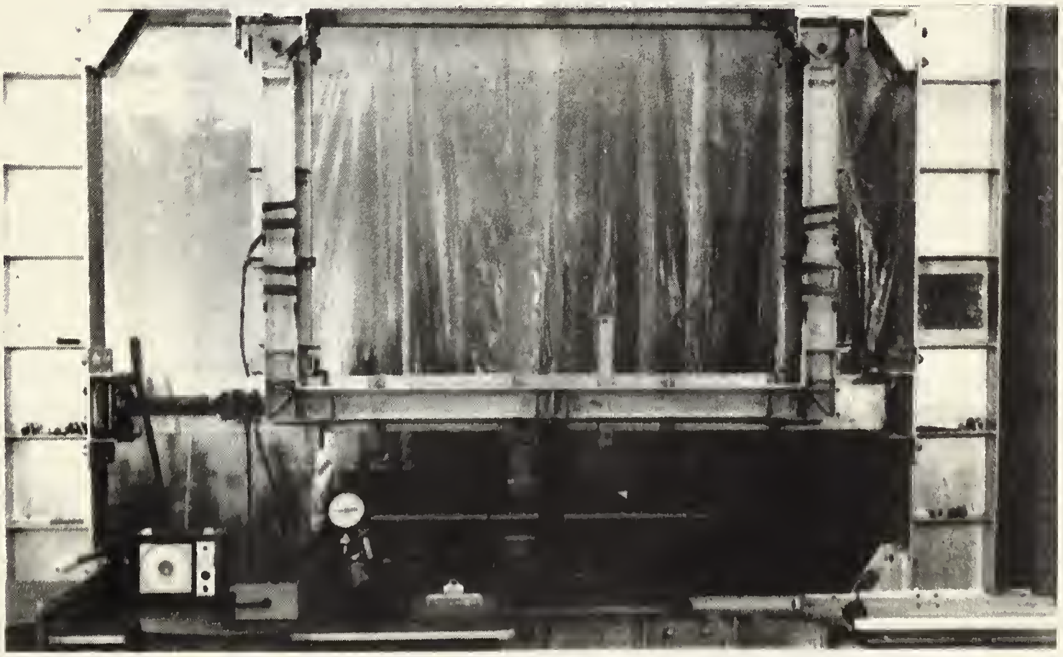

[B] LOADING SYSTEM FOR FRAME NO. 4

[illegible]

[illegible]

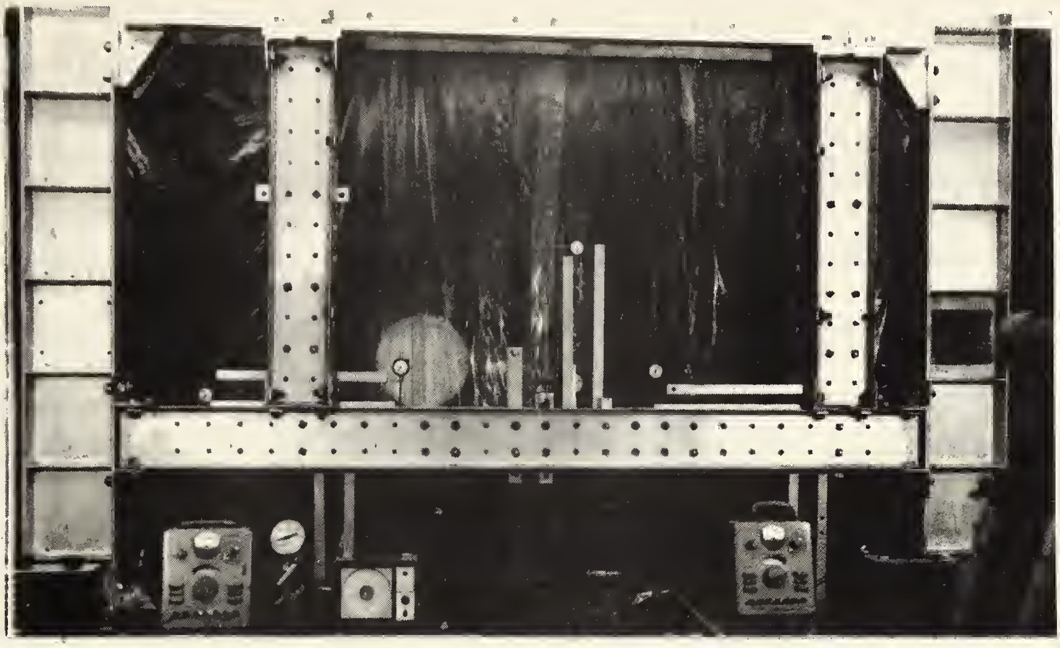

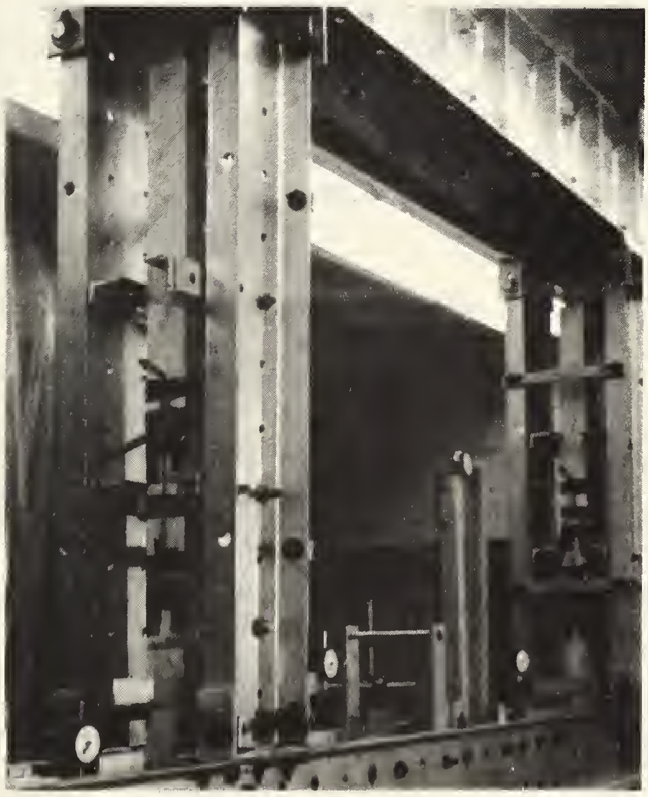

LATERAL SUPPORT SYSTEM FOR FRAMES

PLATE 9

[illegible]

(ii) Curvature Measurements

Five rotation indicators, as described in Chapter VI, were used in each frame test. One indicator was positioned at the midspan of each beam, and four were placed at the corners — two were attached to the columns and the other two were attached near the ends of the beam. Exact positioning is shown in FIGURE 23.

A slight modification to the rotation indicators as used for the beam tests was employed in most cases. Instead of two dial gauges, a single dial mounted at the one end of the steel angles was used to measure rotation increments. The relationship for change in curvature, $\Delta \phi$, is therefore:

$$\Delta \phi = \frac{R_2 - R_1}{4x25} = 0.01 (R_2 - R_1) \text{ radians/in.}$$

(iii) Deflection Measurements

Vertical deflections at beam midspan for Frame No. 1 were taken by means of a two-inch travel dial gauge reading to 0.001 inch. A check on these deflection measurements was provided by readings taken with a surveyor's level on a steel scale mounted at midspan.

For Frame Nos. 2, 3, and 4, vertical deflection readings were taken at beam midspan with the level and scale arrangement only. Horizontal deflections were measured at the upper left column with a two-inch travel dial gauge reading to 0.001 inch. These measurements

were checked with a surveyor's level by readings, taken with the vertical cross-hair, on a scale attached to the column midway between the rotation indicator arms.

(iv) Reaction Measurements

Two groups of four, "Type A-3 SR-4" electrical resistance strain gauges were mounted on each column of the test frame at the locations shown in FIGURE 26. Strain readings from these gauges were used to compute the magnitudes of the horizontal reactions. Mounting and waterproofing of the gauges, as well as whitewashing of the frames was done in the same manner as for the beams (Chapter VI). After each test frame was positioned in the loading frame, lead wires from the gauges on each column were connected to two "Baldwin-Lima-Hamilton 20-point Switching Units". Strain readings were taken with two "Baldwin-Lima-Hamilton Type N, SR-4 Strain Indicators".

For a particular value of applied load, curvature was obtained by dividing the average strain reading at the location of the gauges by half the section depth. For this value of curvature, the magnitude of the moment was then obtained from FIGURE 22, which is an average plot of the moment-curvature relationship derived from the beam tests. The magnitude of the horizontal reaction for Frame Test No. 1 was computed by dividing this value of moment by the distance from the pinned-end to the location of the gauges. An average

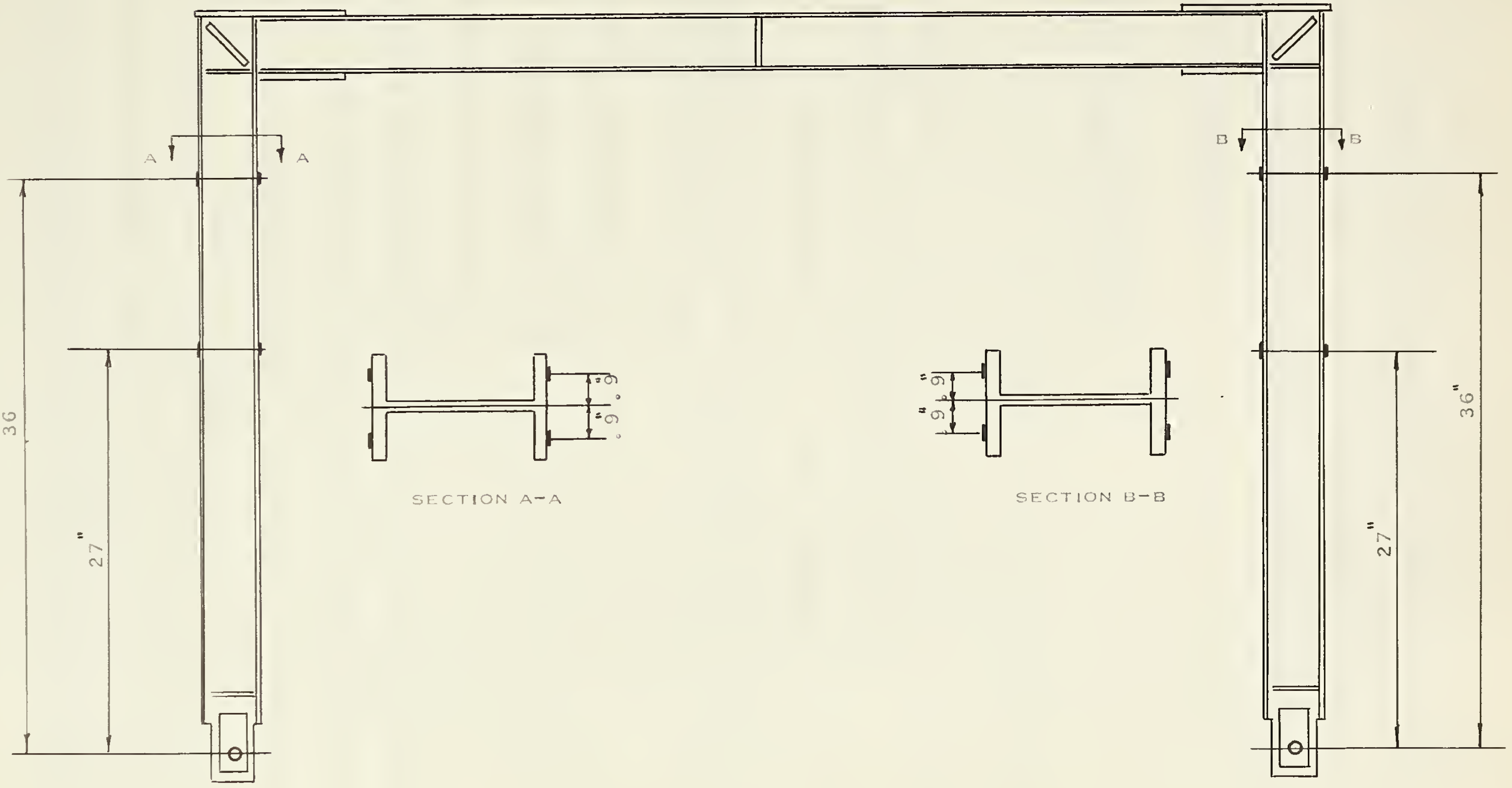

STRAIN GAUGE LOCATIONS ON FRAMES

FIGURE 26

of two such computations was used as the final value for the horizontal reaction. For the other frames tested, a correction to the above procedure was necessary due to the horizontal deflections. The procedure for computing horizontal reactions for these cases is described in Appendix A.

7-4 Experimental Procedure

After each frame alignment was completed, a "friction test", as described in Chapter VI, was performed on instrumentation. The main testing was then carried out for each frame.

In testing Frame No. 1, load was applied in increments of 1, 000 pounds up to a load of 16, 000 pounds, after which the load increment was reduced to 500 pounds until completion of the test. All gauge readings were taken at each load increment. In the plastic range, a "waiting period" of twenty minutes after load application was necessary before each set of readings. For Frame No. 2, load was applied in increments of 1, 000 pounds up to a load of 5. 000 pounds, after which the load increment was reduced to 500 pounds until completion of the test. All gauge readings were taken at each load increment. Four men were employed in testing Frame Nos. 1 and 2; two men recorded strain indicator readings, the third man maintained the load on the jack, and the fourth recorded the deflection and rotation

measurements and plotted a load-deflection curve as the test progressed.

A similar procedure was used in testing the remaining two frames. Horizontal and vertical loads were applied to Frame No. 3 in increments of 1, 000 pounds up to a load of 5, 000 pounds, after which the load increment was reduced to 500 pounds until completion of the test. In testing Frame No. 4, vertical and horizontal loads were applied in increments of 1, 000 and 500 pounds respectively, up to a load of 8, 000 pounds, after which the increments were reduced to 500 and 250 pounds respectively, until test completion. Five men were employed in tests of these frames, since two men were required to maintain the applied loads.

7-5 Frame Test Results

Test results are presented in graphical form for Frame Nos. 1 and 2 as follows:

1) Load vs. deflection (FIGURES 27 and 35)
2) Load vs. curvature (FIGURES 28-30, 36, 37)
3) Load vs. horizontal reactions (FIGURES 31 and 38)
4) Moment vs. curvature (FIGURES 32-34, 39, 40)

PLATES 10A and 10B show a general view of Frame Nos. 1 and 2, respectively, after testing. The tension failure in the throat of the fillet weld at the left corner connection of Frame No. 2 is shown in PLATE 11.

The experimental load-deflection curves were plotted using dial indicator readings. In addition to the observed deflections, a plot of theoretical deflections was made to provide a means of comparing actual test results with those predicted from computations based on the "moment end-slope" relationships, as well as those predicted by the "plastic-hinge" method. Calculations based on the "plastic-hinge" method appear in Appendix A, and calculations based on the "moment end-slope" relationships are given in Appendix B. Load-curvature curves were plotted using actual test data obtained from the rotation indicators located on the frames as shown in FIGURE 23. Load vs. horizontal reaction curves are presented for both frames, and theoretical curves are shown for comparison. These theoretical curves were plotted from the theoretical deflection and ultimate load calculations.

Moment-curvature relationships were plotted for Frame No. 1 at the beam midspan and at the two columns. For Frame No. 2, moment-curvature was plotted for the two columns only. Moments were calculated using the measured horizontal reactions at the supports. The theoretical moment-curvature relationship for the 4 I 9.5 section was plotted for comparison with the above curves. Calculations based on the simple plastic theory are given in Appendix A, and calculations based on Equation 4 (Chapter V), are given in Appendix B.

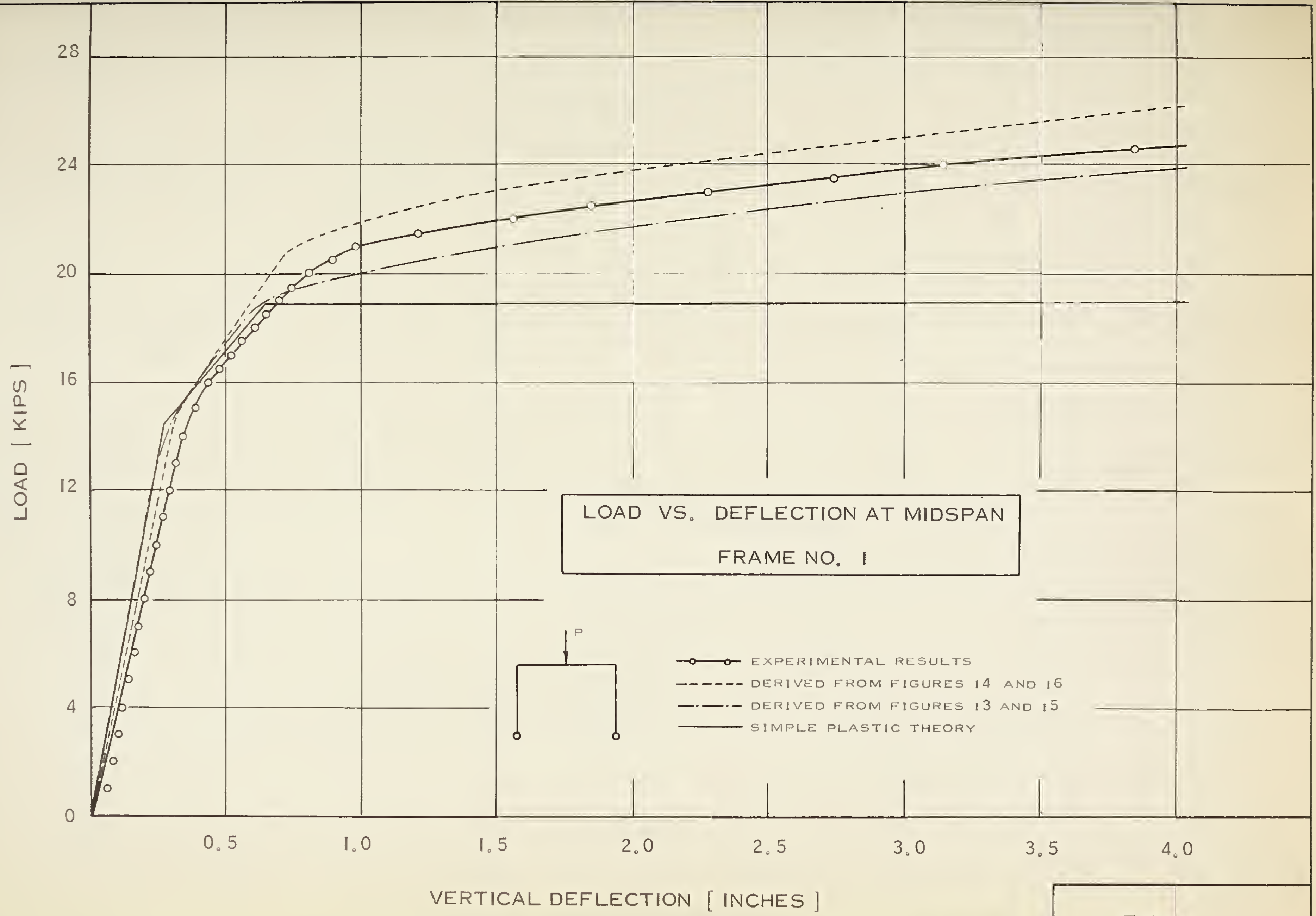
LOAD VS. DEFLECTION AT MIDSPAN
FRAME NO. 1
P
EXPERIMENTAL RESULTS
DERIVED FROM FIGURES 14 AND 16
DERIVED FROM FIGURES 13 AND 15
SIMPLE PLASTIC THEORY
LOAD [KIPS]
0
4
8
12
16
20
24
28
VERTICAL DEFLECTION [INCHES]
0.5
1.0
1.5
2.0
2.5
3.0
3.5
4.0

FIGURE 27

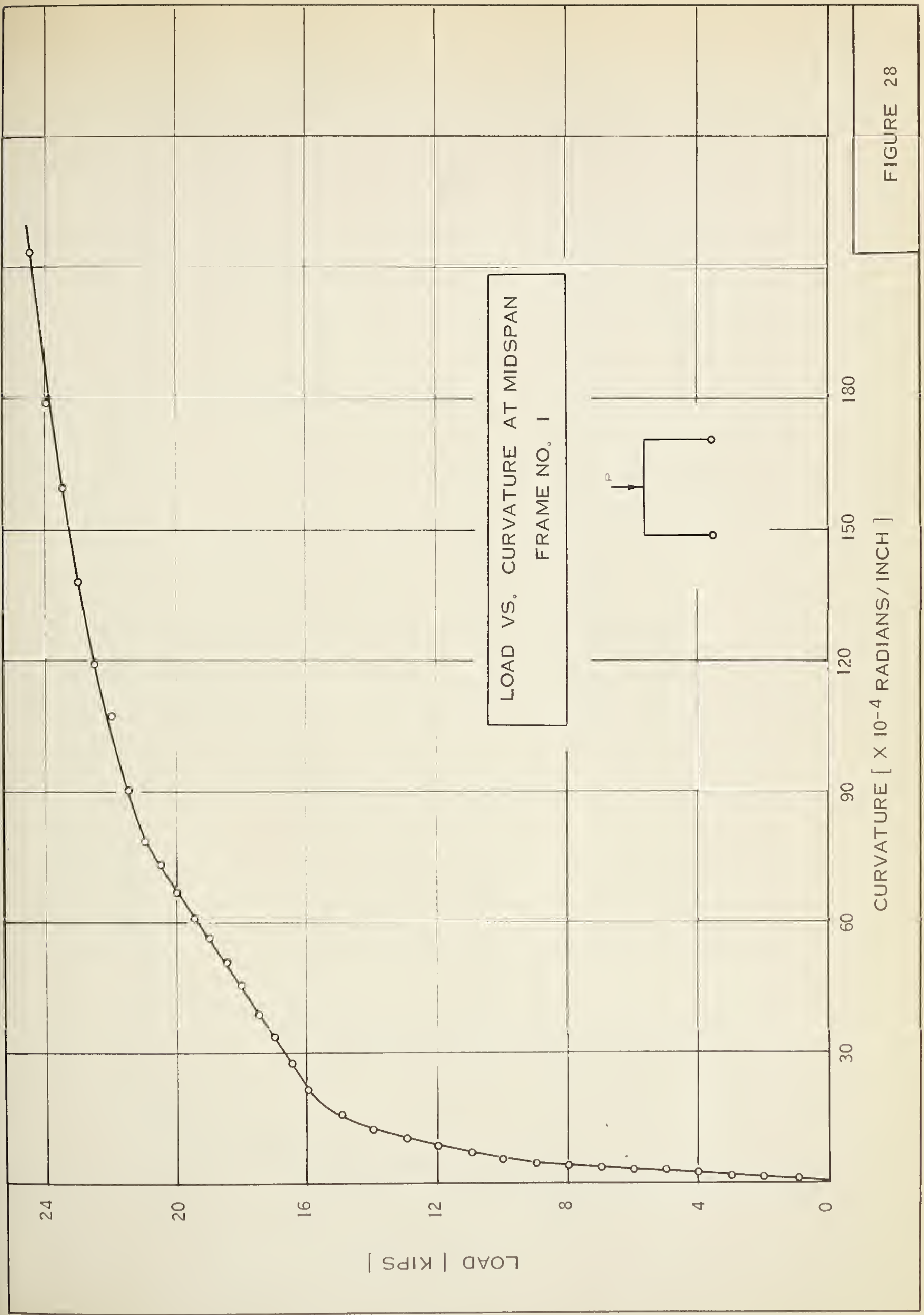
LOAD VS. CURVATURE AT MIDSPAN
FRAME NO. 1
P
LOAD [KIPS]
0
4
8
12
16
20
24
CURVATURE [X 10-4 RADIANS/ INCH]
30
60
90
120
150
180

FIGURE 28

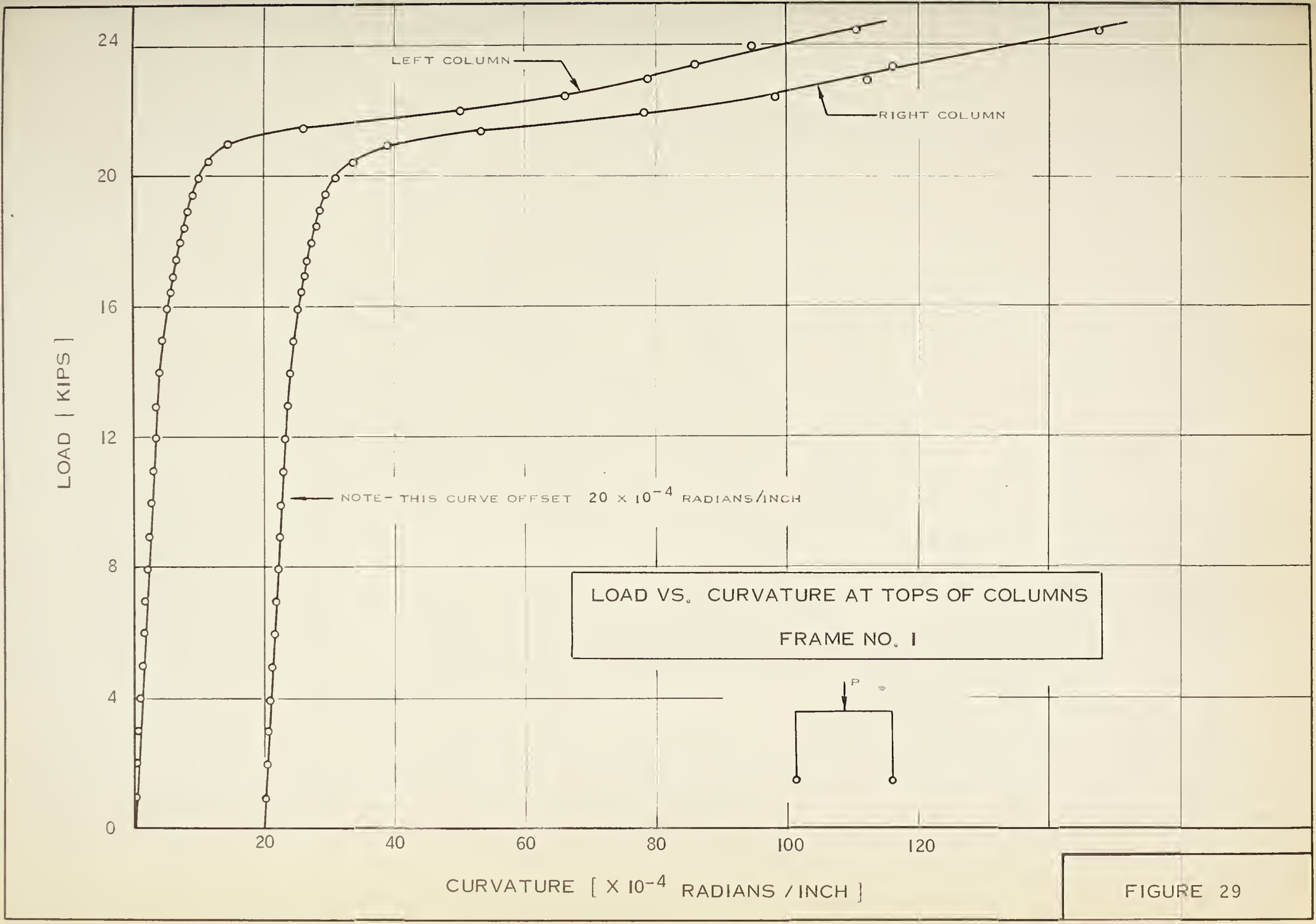

LOAD VS. CURVATURE AT TOPS OF COLUMNS

FRAME NO. I

FIGURE 29

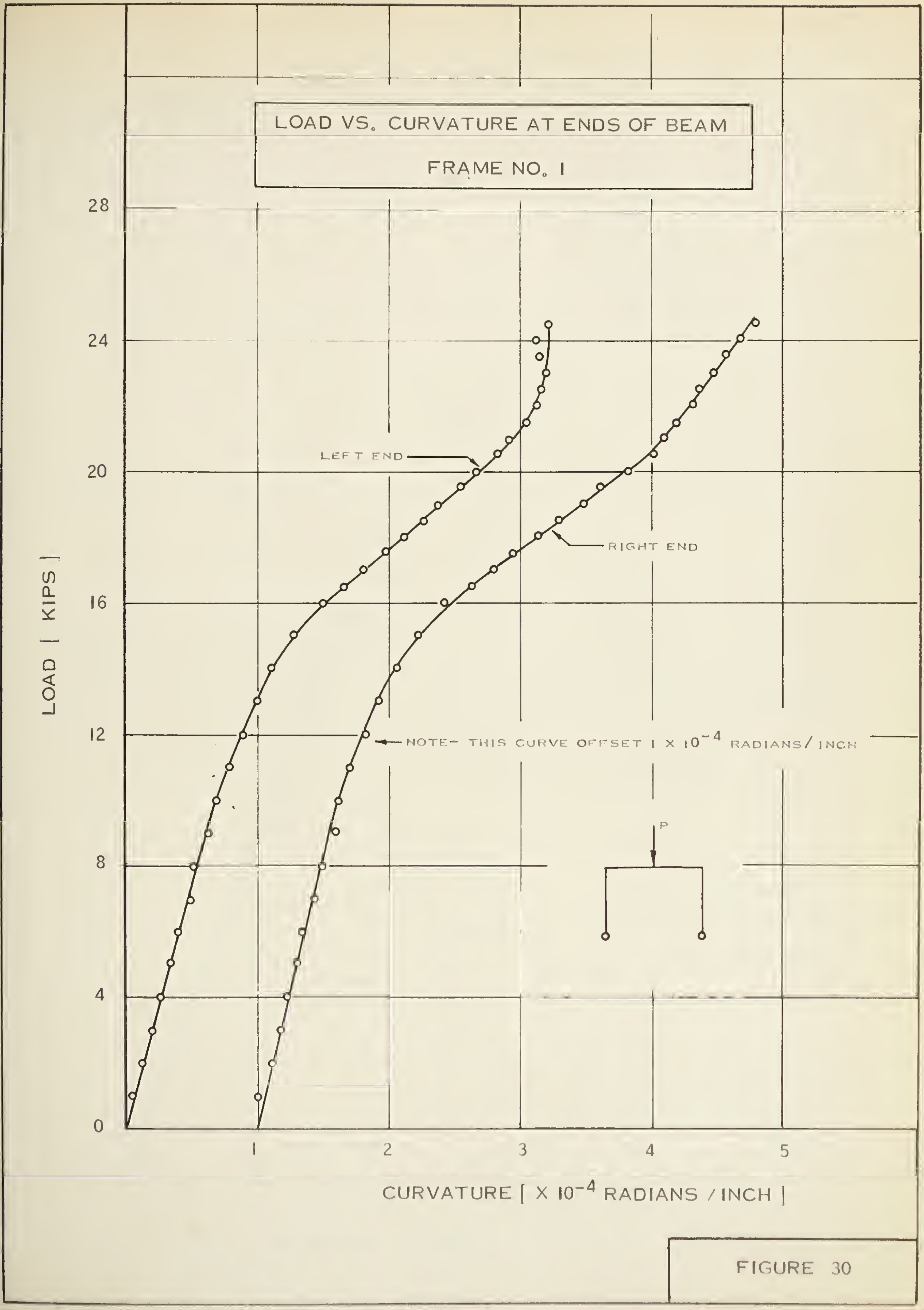
LOAD VS. CURVATURE AT ENDS OF BEAM
FRAME NO. 1
LOAD [KIPS]
0
4
8
12
16
20
24
28
1
2
3
4
5
CURVATURE [X 10^{-4} RADIANS / INCH]
LEFT END
RIGHT END
NOTE- THIS CURVE OFFSET 1 X 10^{-4} RADIANS/INCH
P

FIGURE 30

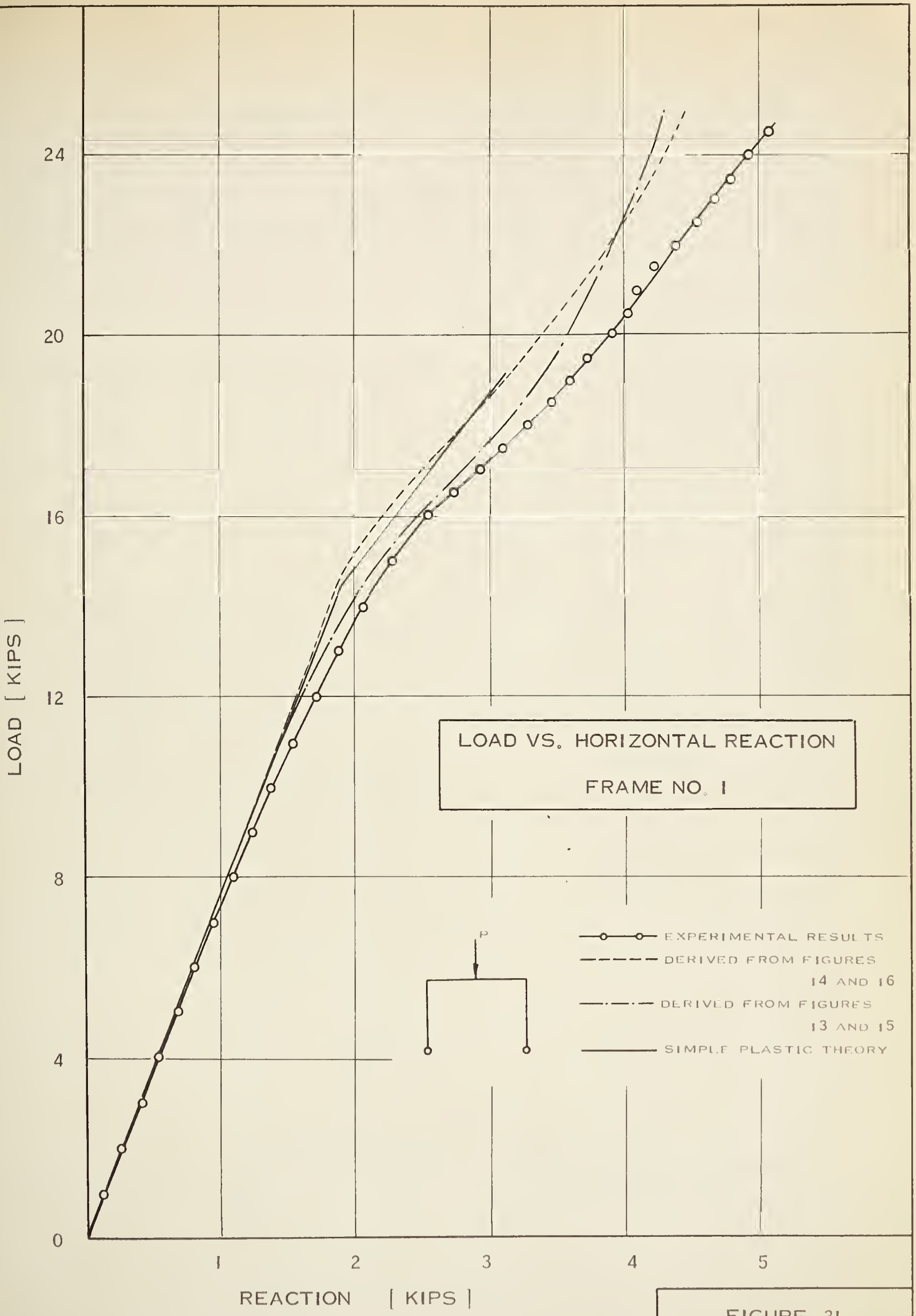
LOAD VS. HORIZONTAL REACTION
FRAME NO. I
LOAD [KIPS]
REACTION [KIPS]
0
4
8
12
16
20
24
1
2
3
4
5
P
EXPERIMENTAL RESULTS
DERIVED FROM FIGURES 14 AND 16
DERIVED FROM FIGURES 13 AND 15
SIMPLE PLASTIC THEORY

FIGURE 31

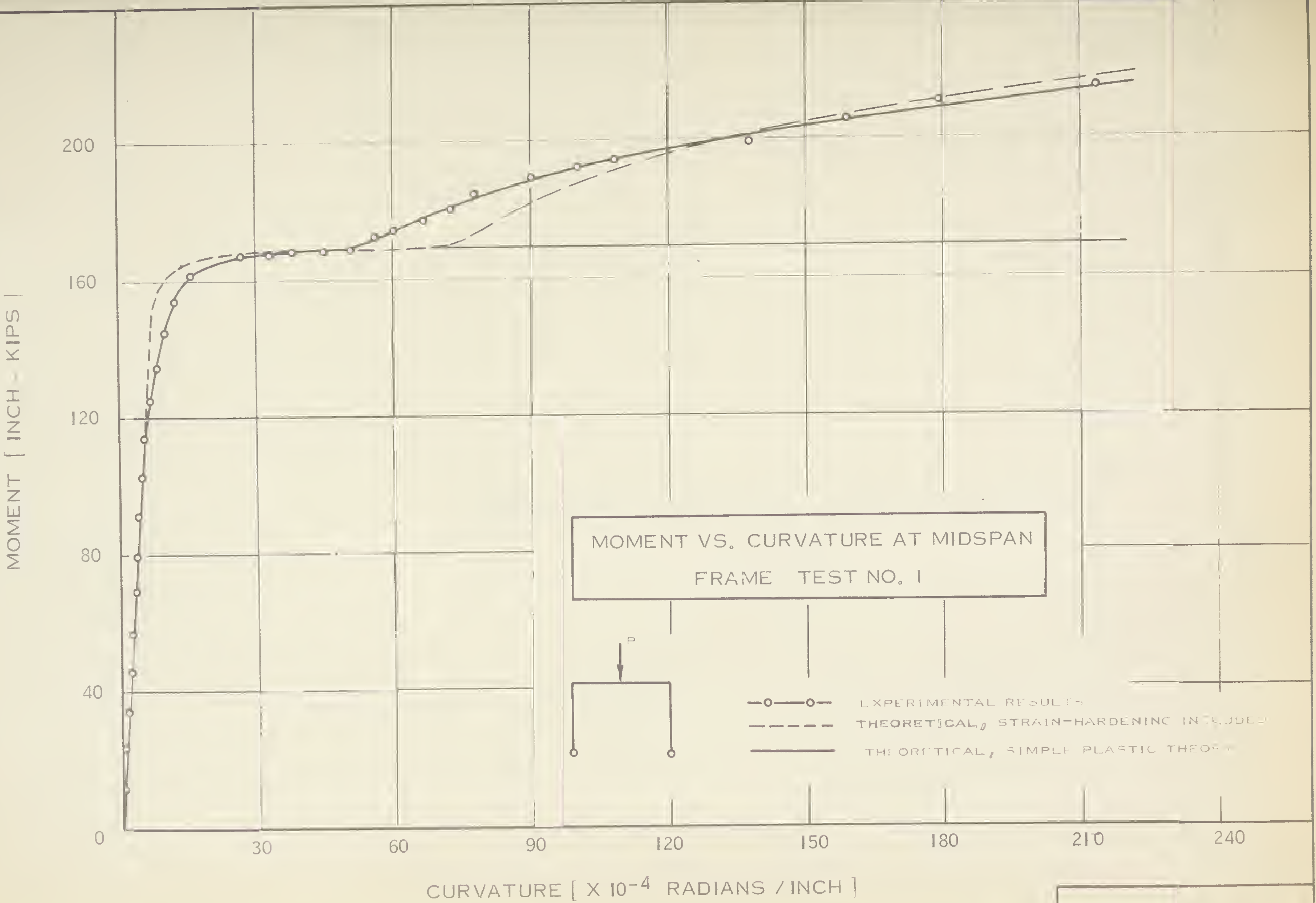

MOMENT VS. CURVATURE AT MIDSPAN
FRAME TEST NO. 1

FIGURE 32

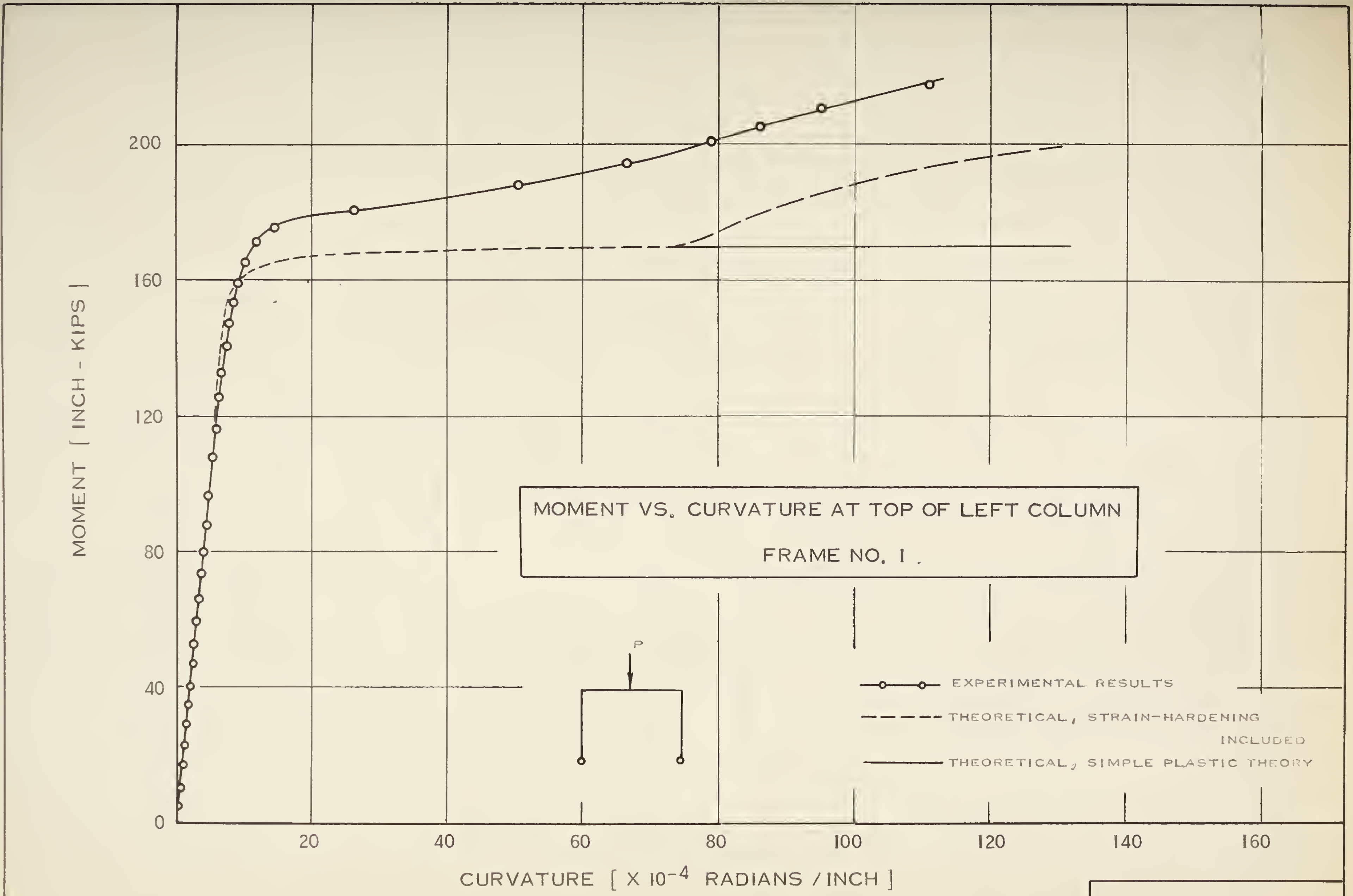

MOMENT VS. CURVATURE AT TOP OF LEFT COLUMN

FRAME NO. I.

FIGURE 33

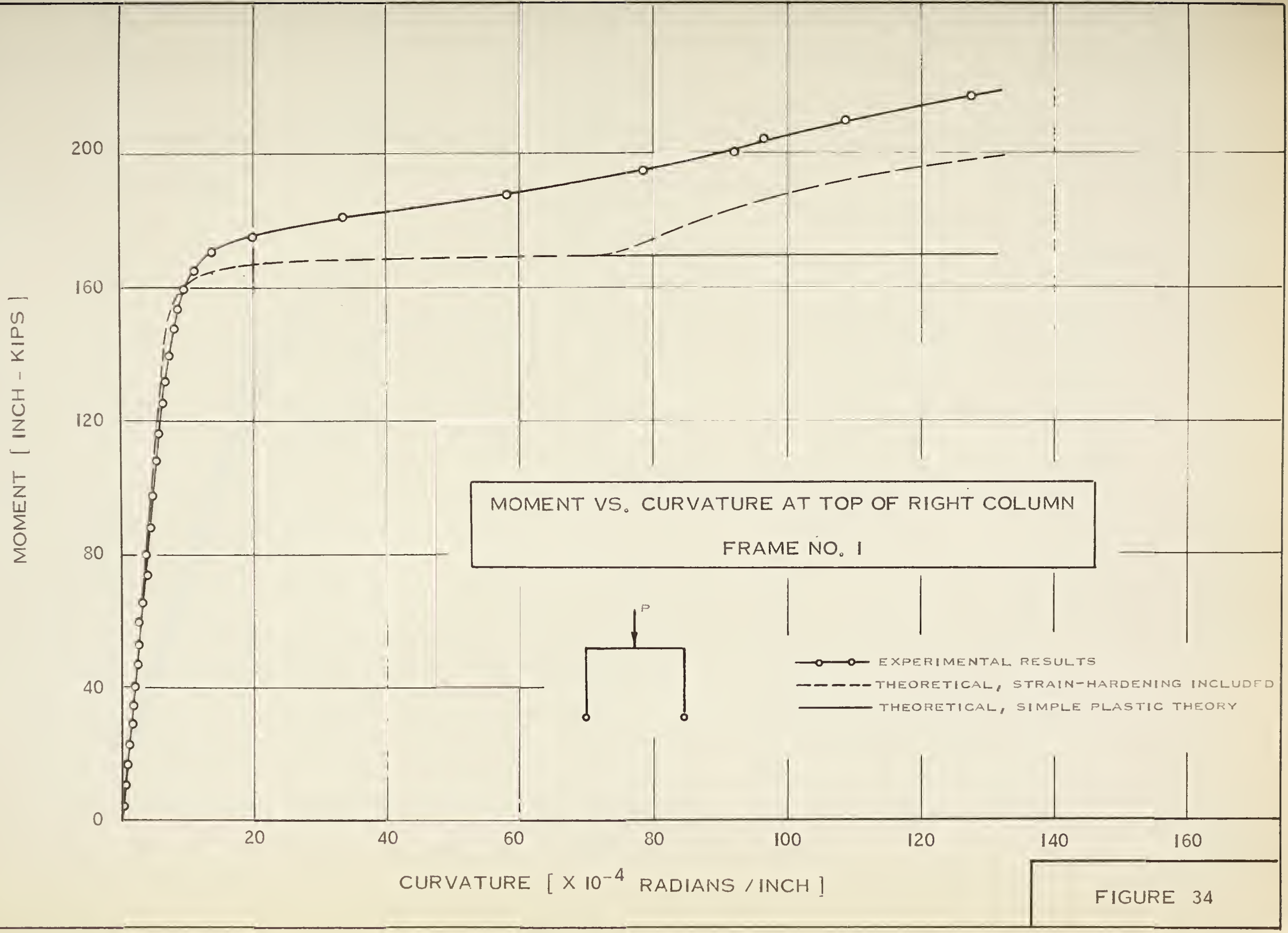

MOMENT VS. CURVATURE AT TOP OF RIGHT COLUMN

FRAME NO. I

FIGURE 34

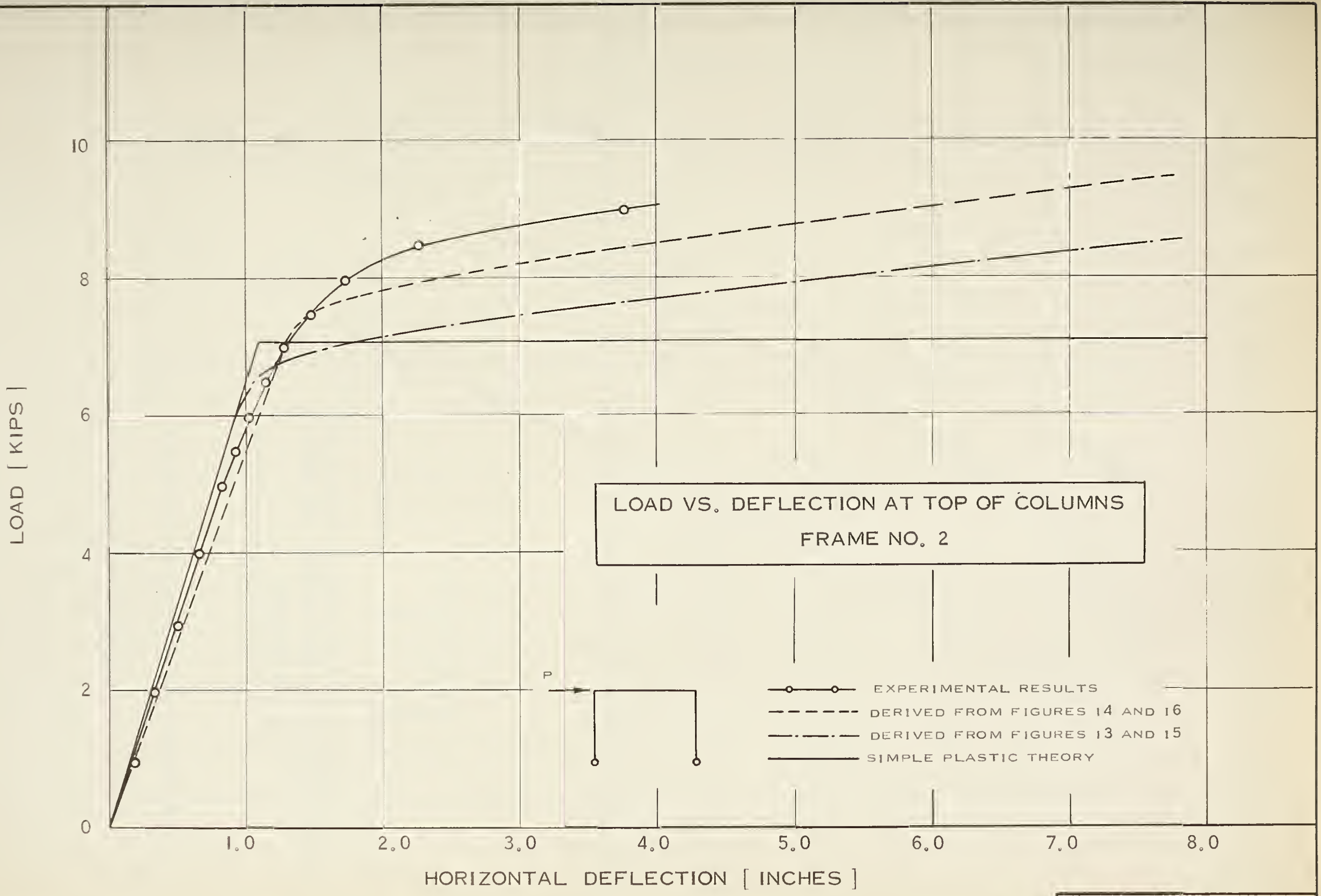
LOAD VS. DEFLECTION AT TOP OF COLUMNS
FRAME NO. 2
LOAD [KIPS]
10
8
6
4
2
0
1.0
2.0
3.0
4.0
5.0
6.0
7.0
8.0
HORIZONTAL DEFLECTION [INCHES]
P
EXPERIMENTAL RESULTS
DERIVED FROM FIGURES 14 AND 16
DERIVED FROM FIGURES 13 AND 15
SIMPLE PLASTIC THEORY

FIGURE 35

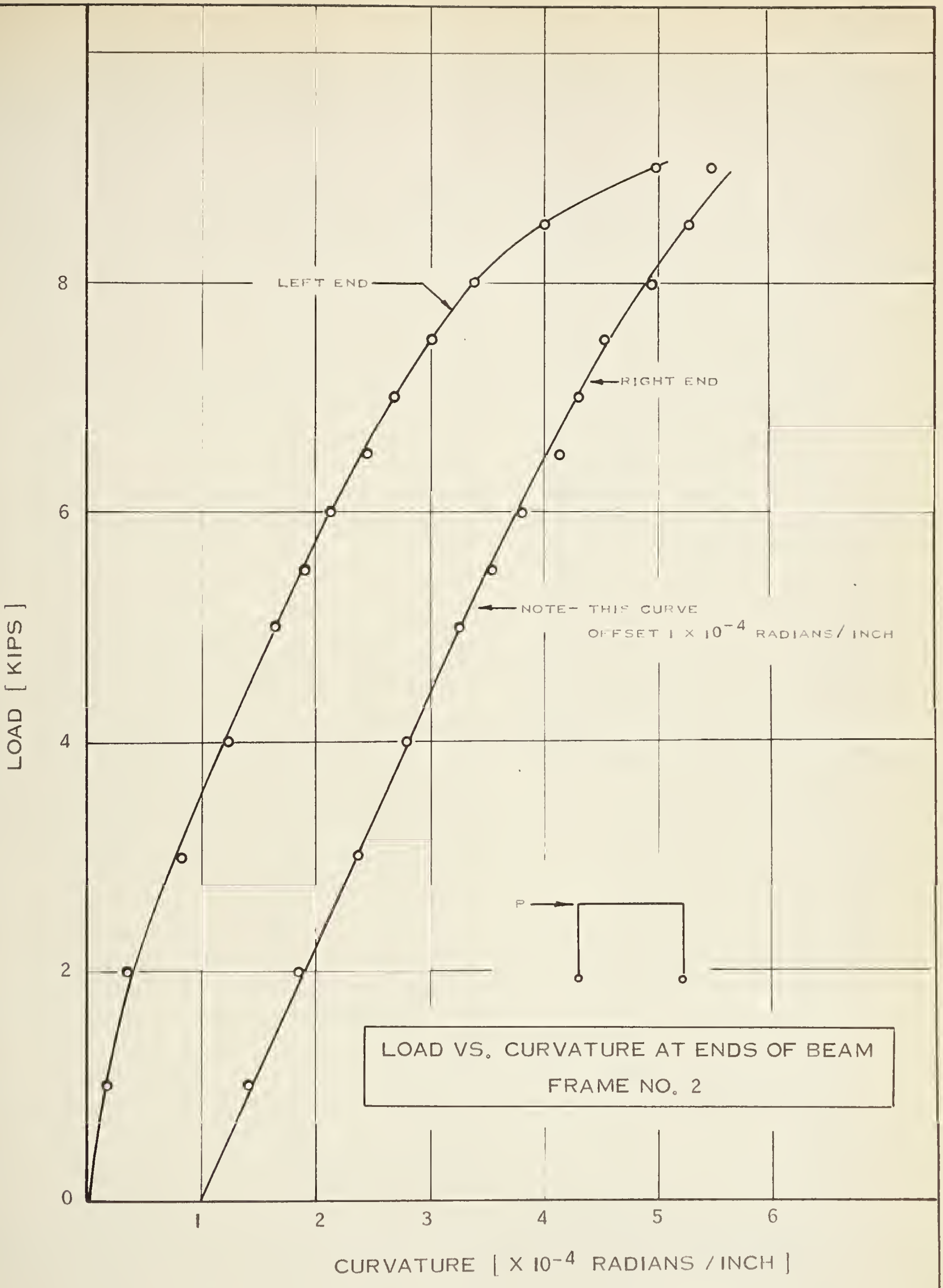

LOAD VS. CURVATURE AT ENDS OF BEAM FRAME NO. 2

FIGURE 36

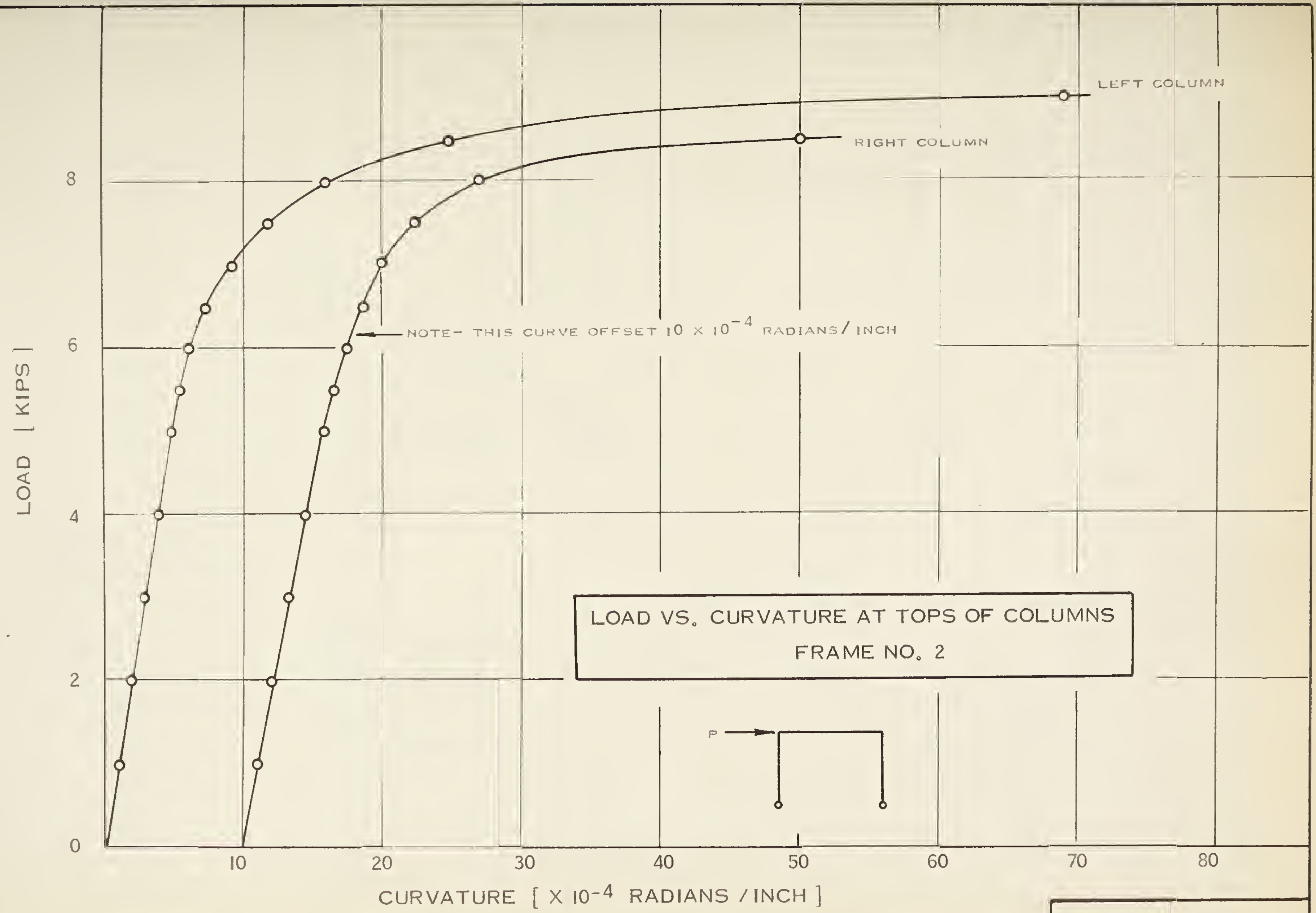

LOAD VS. CURVATURE AT TOPS OF COLUMNS
FRAME NO. 2

FIGURE 37

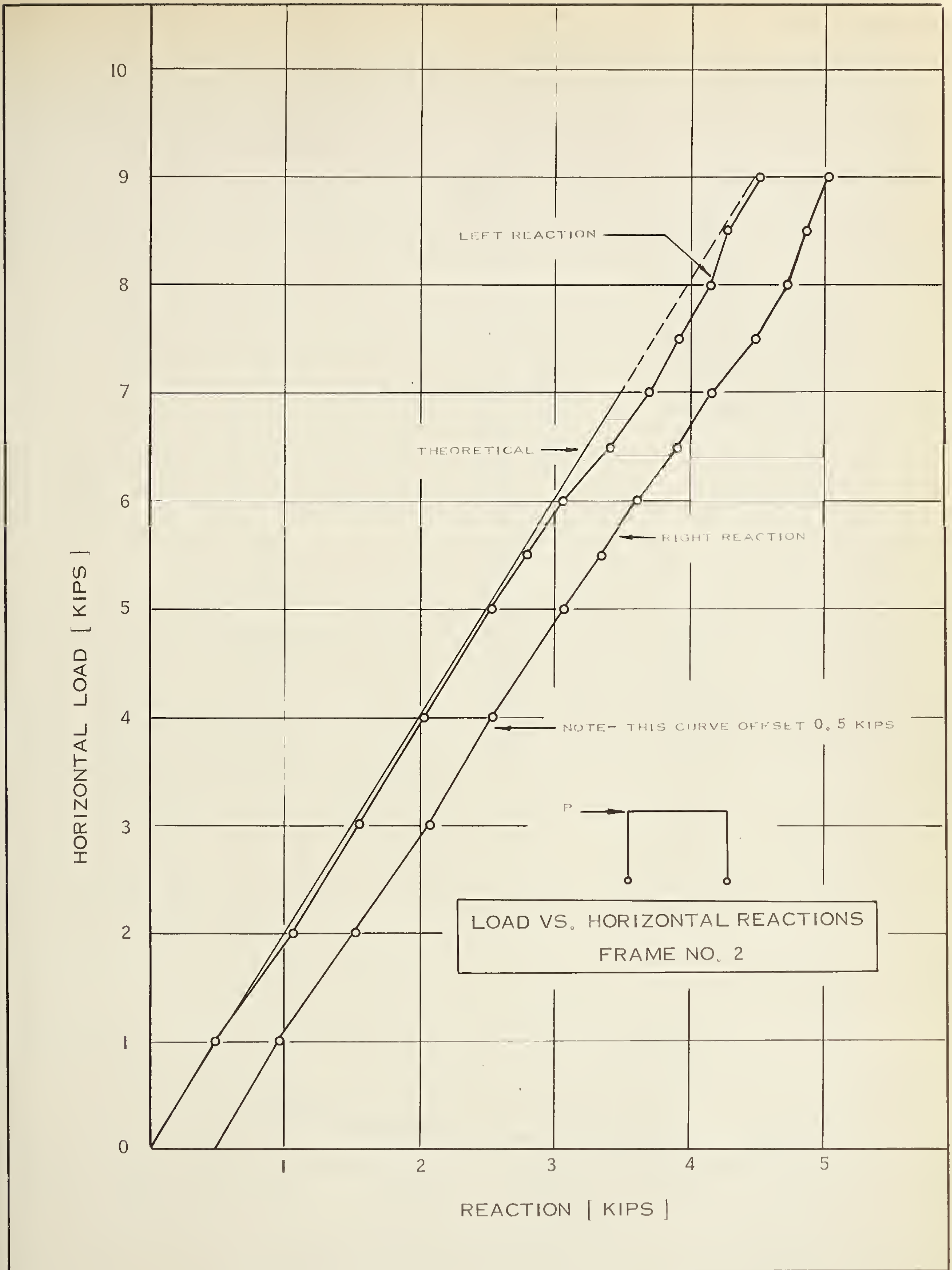
10
9
8
7
6
5
4
3
2
1
0
HORIZONTAL LOAD [KIPS]
1
2
3
4
5
REACTION [KIPS]
LEFT REACTION
THEORETICAL
RIGHT REACTION
NOTE- THIS CURVE OFFSET 0.5 KIPS
P
LOAD VS. HORIZONTAL REACTIONS
FRAME NO. 2

FIGURE 38

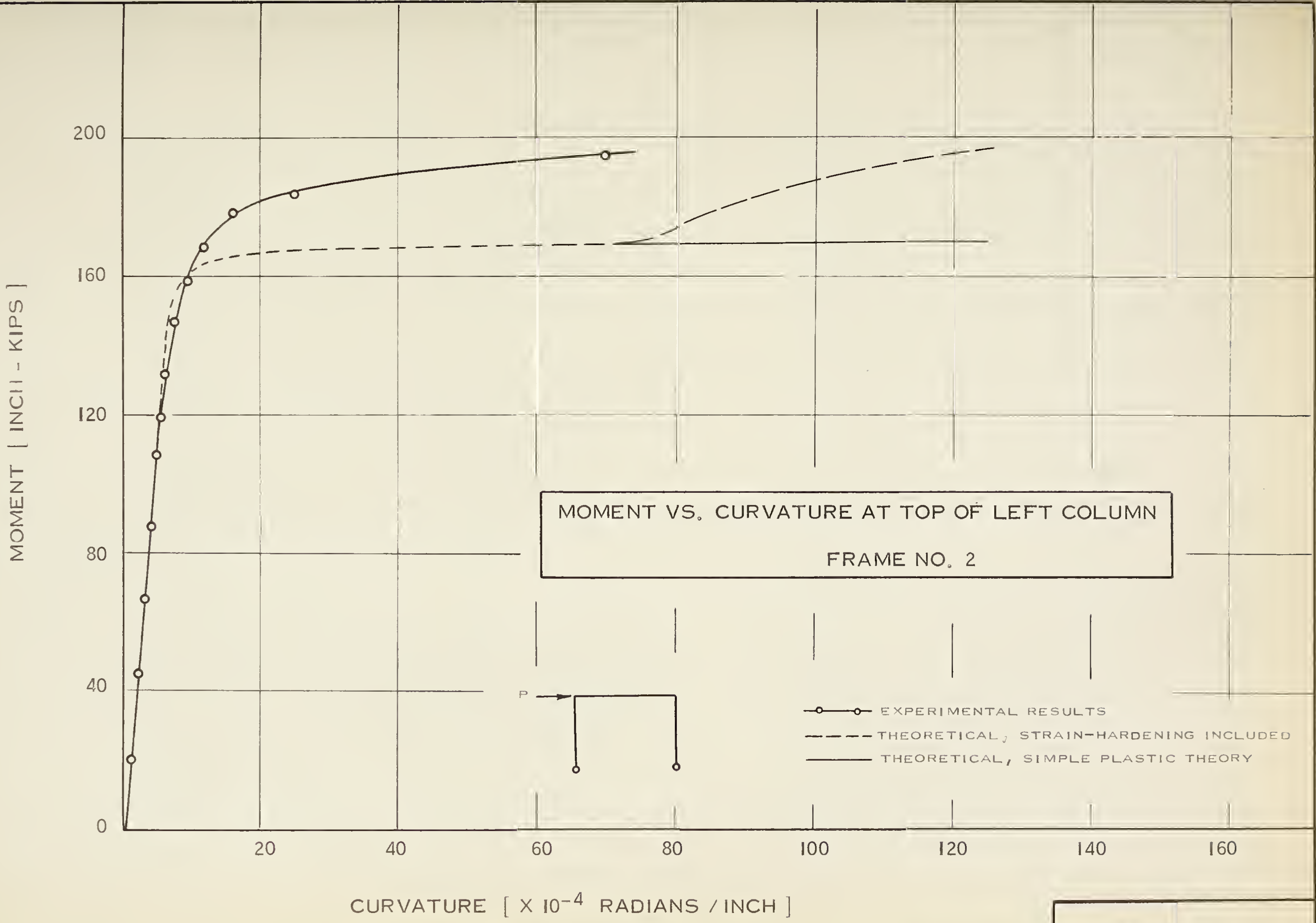
MOMENT VS. CURVATURE AT TOP OF LEFT COLUMN
FRAME NO. 2
MOMENT [INCH - KIPS]
0
40
80
120
160
200
CURVATURE [X 10^{-4} RADIANS / INCH]
20
40
60
80
100
120
140
160
P
EXPERIMENTAL RESULTS
THEORETICAL, STRAIN-HARDENING INCLUDED
THEORETICAL, SIMPLE PLASTIC THEORY

FIGURE 39

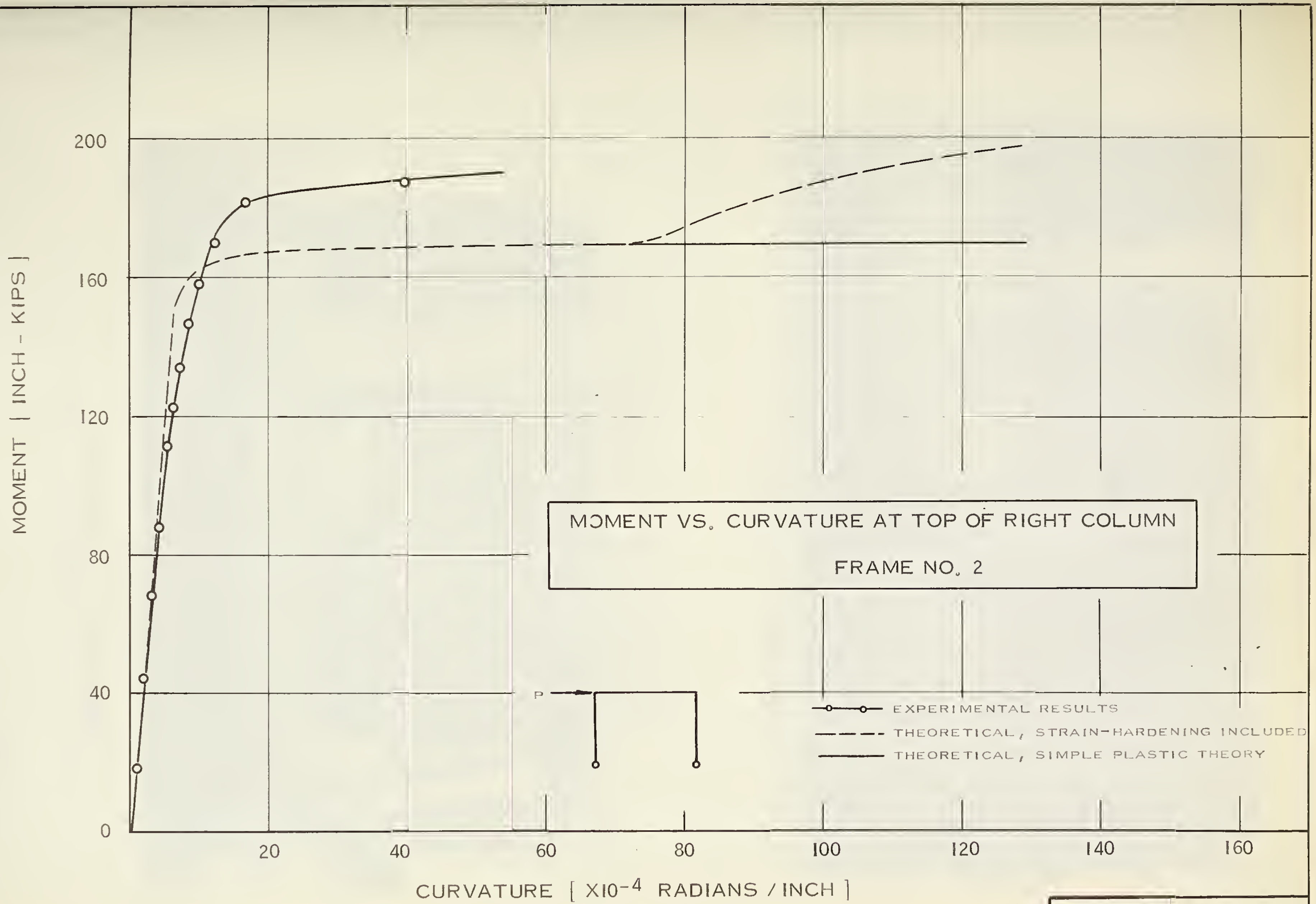

MOMENT VS. CURVATURE AT TOP OF RIGHT COLUMN

FRAME NO. 2

FIGURE 40

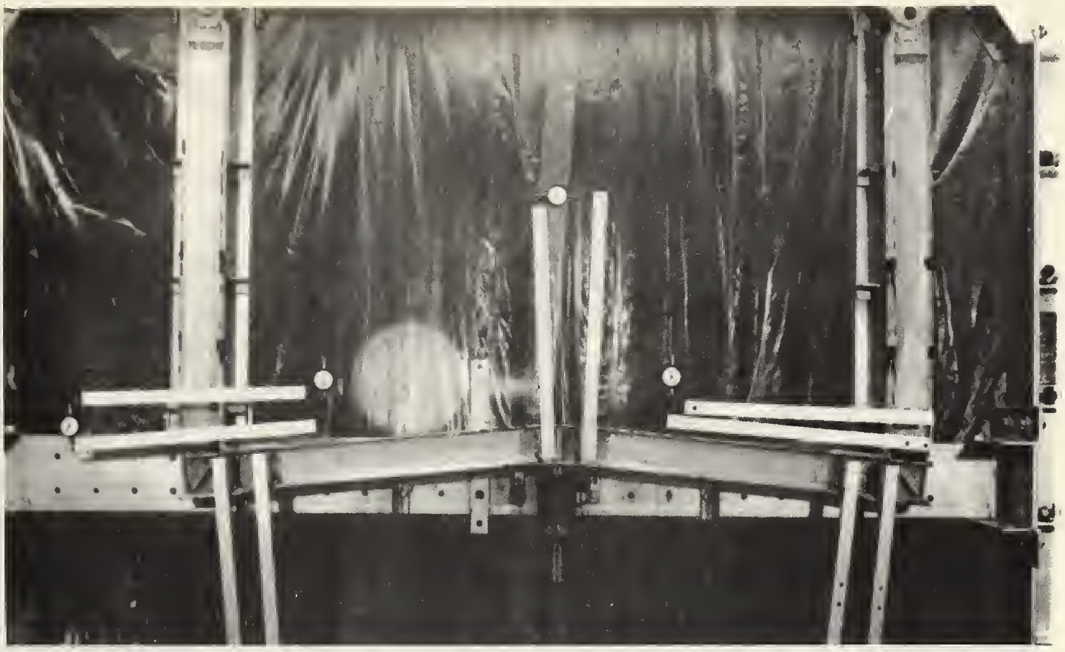

[A] FRAME NO. I AFTER TEST

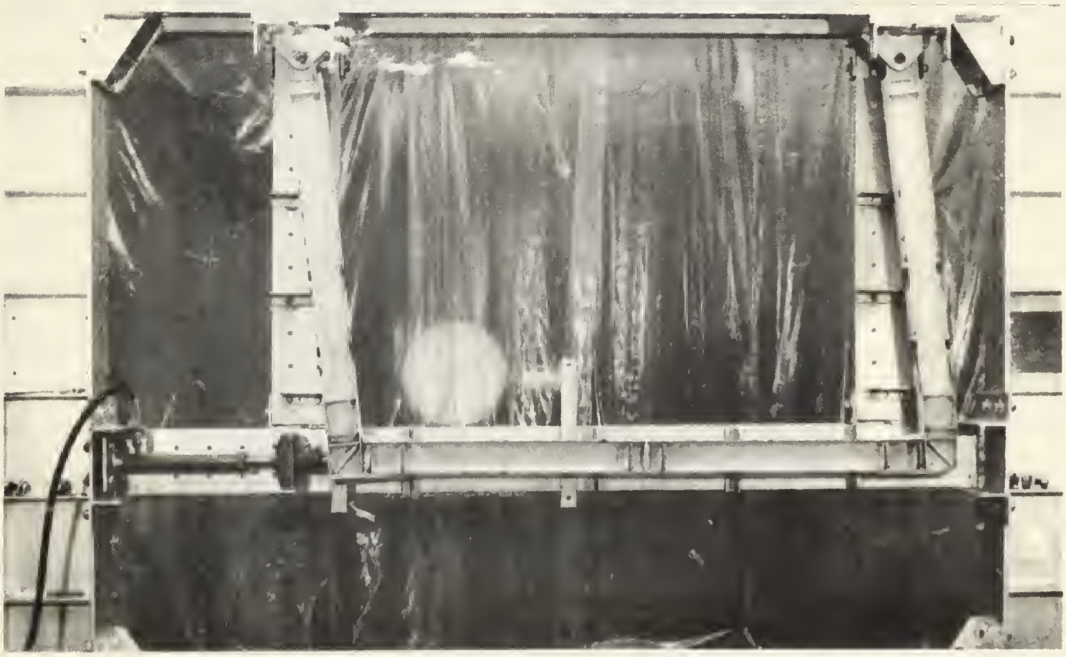

[B] FRAME NO. 2 AFTER TEST

PLATE 10

[illegible]

[illegible]

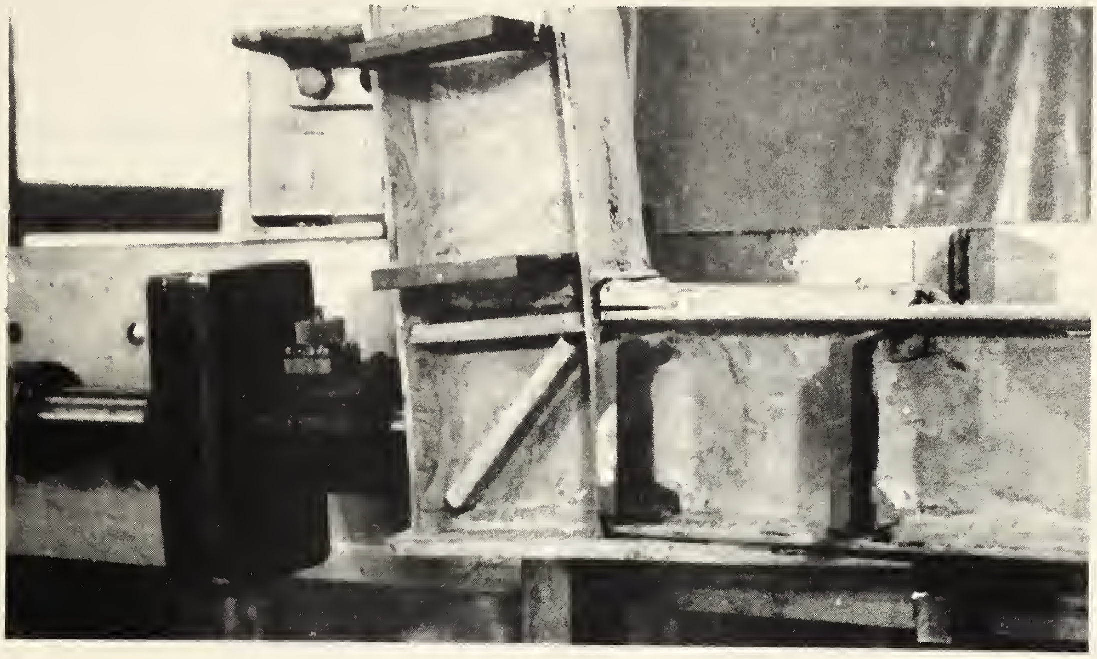

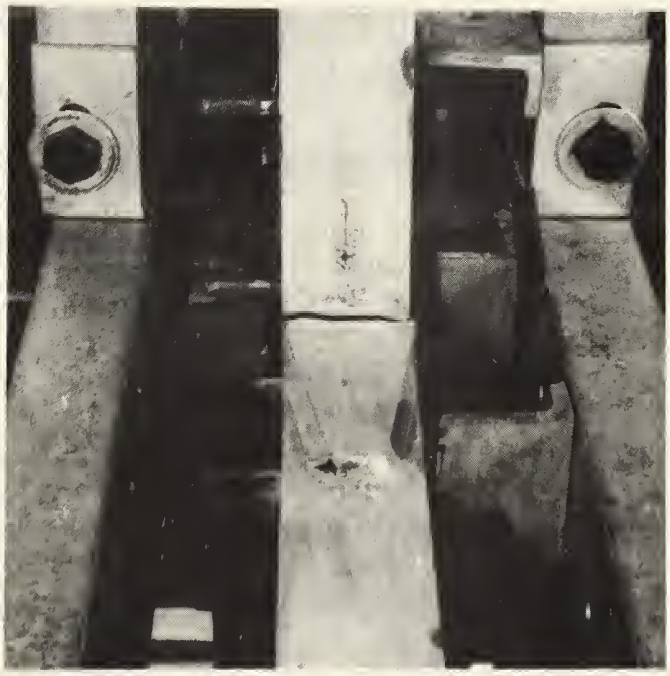

TENSION FAILURE IN THROAT OF WELD

PLATE II

[illegible]

Test results are presented in graphical form for Frame Nos. 3 and 4 as follows:

1) Load vs. deflection (41, 42, 48, 49)
2) Load vs. curvature (43-44, 50-52)
3) Load vs. horizontal reactions (45, 53)
4) Moment vs. curvature (46, 47, 54, 55)

PLATES 12A and 12B show a general view of Frame Nos. 3 and 4, respectively, after testing.

The experimental load-deflection curves were plotted using dial indicator readings wherever possible. Both vertical and horizontal deflections were plotted against load. Theoretical deflection calculations, based on the simple plastic theory appear in Appendix A. Load-curvature curves were plotted using actual test data, obtained from the rotation indicators located on the Frames as shown in FIGURE 23. Load vs. horizontal reaction curves are presented for both frames, and theoretical curves are shown for comparison. On the basis of an elastic analysis, applied load vs. horizontal reaction relationship was assumed to vary linearly up to the formation of the first plastic hinge. From this point, up to the calculated ultimate load, the load-reaction relationship was assumed to vary linearly at a different slope.

Moment-curvature relationships were plotted for both frames at the beam midspans, and at the top of the two columns.

Moments were calculated using the measured horizontal reactions at the supports. The theoretical moment-curvature relationship for the 4 I 9.5 section was plotted for comparison with the above curves.

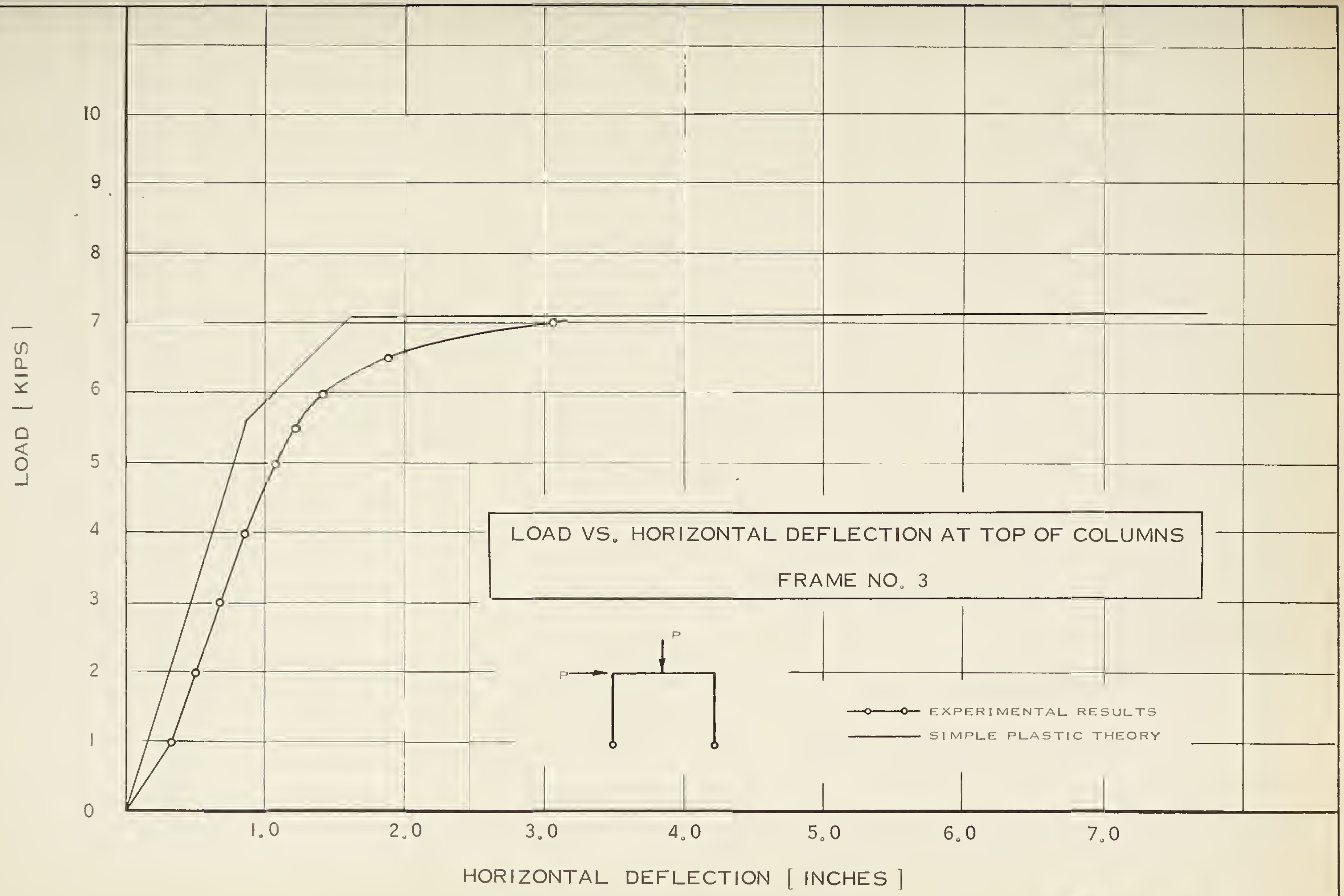
LOAD VS. HORIZONTAL DEFLECTION AT TOP OF COLUMNS

FRAME NO. 3

FIGURE 41

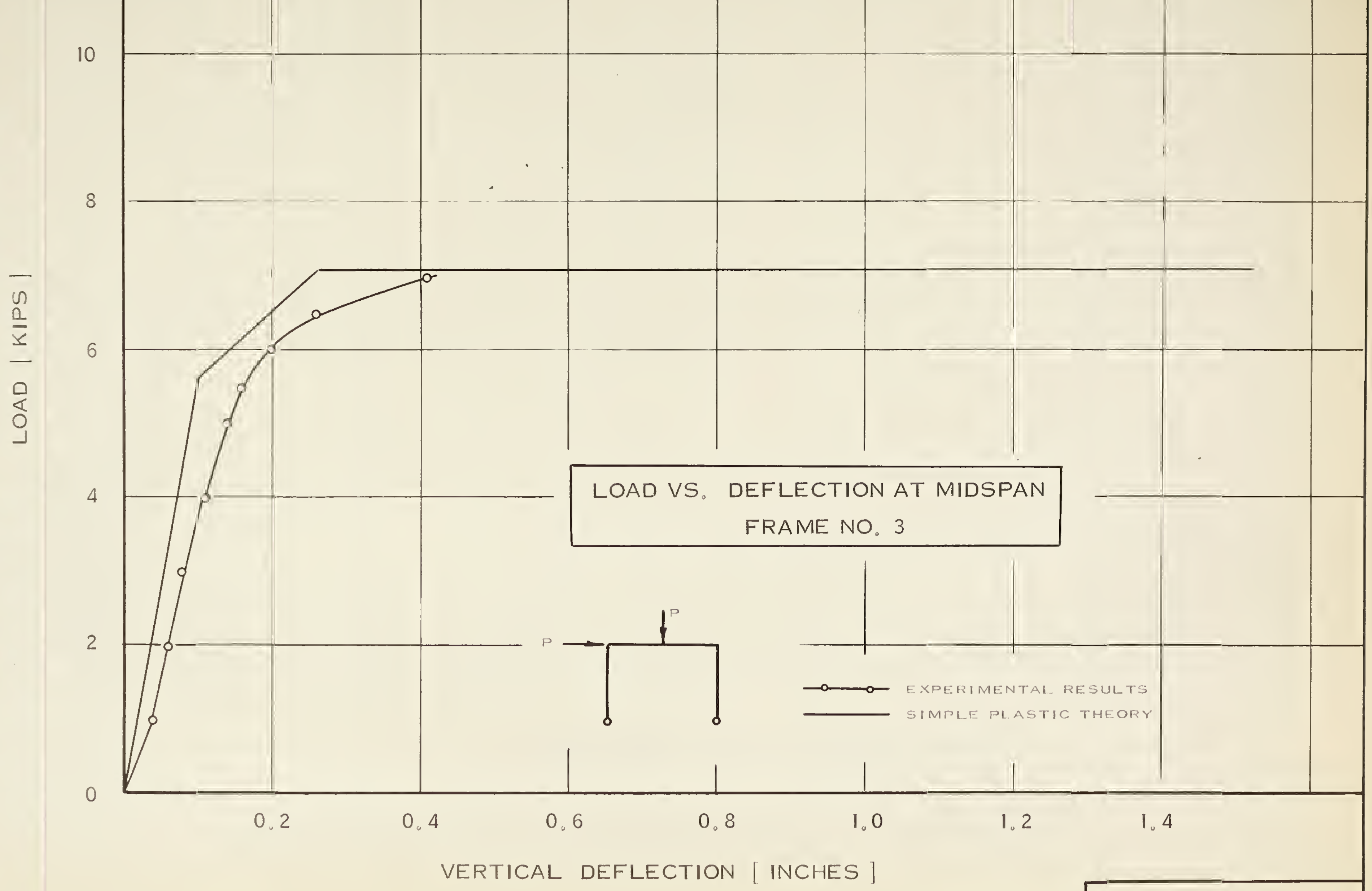
LOAD VS. DEFLECTION AT MIDSPAN
FRAME NO. 3
LOAD [KIPS]
10
8
6
4
2
0
0.2
0.4
0.6
0.8
1.0
1.2
1.4
VERTICAL DEFLECTION [INCHES]
P
P
EXPERIMENTAL RESULTS
SIMPLE PLASTIC THEORY

FIGURE 42

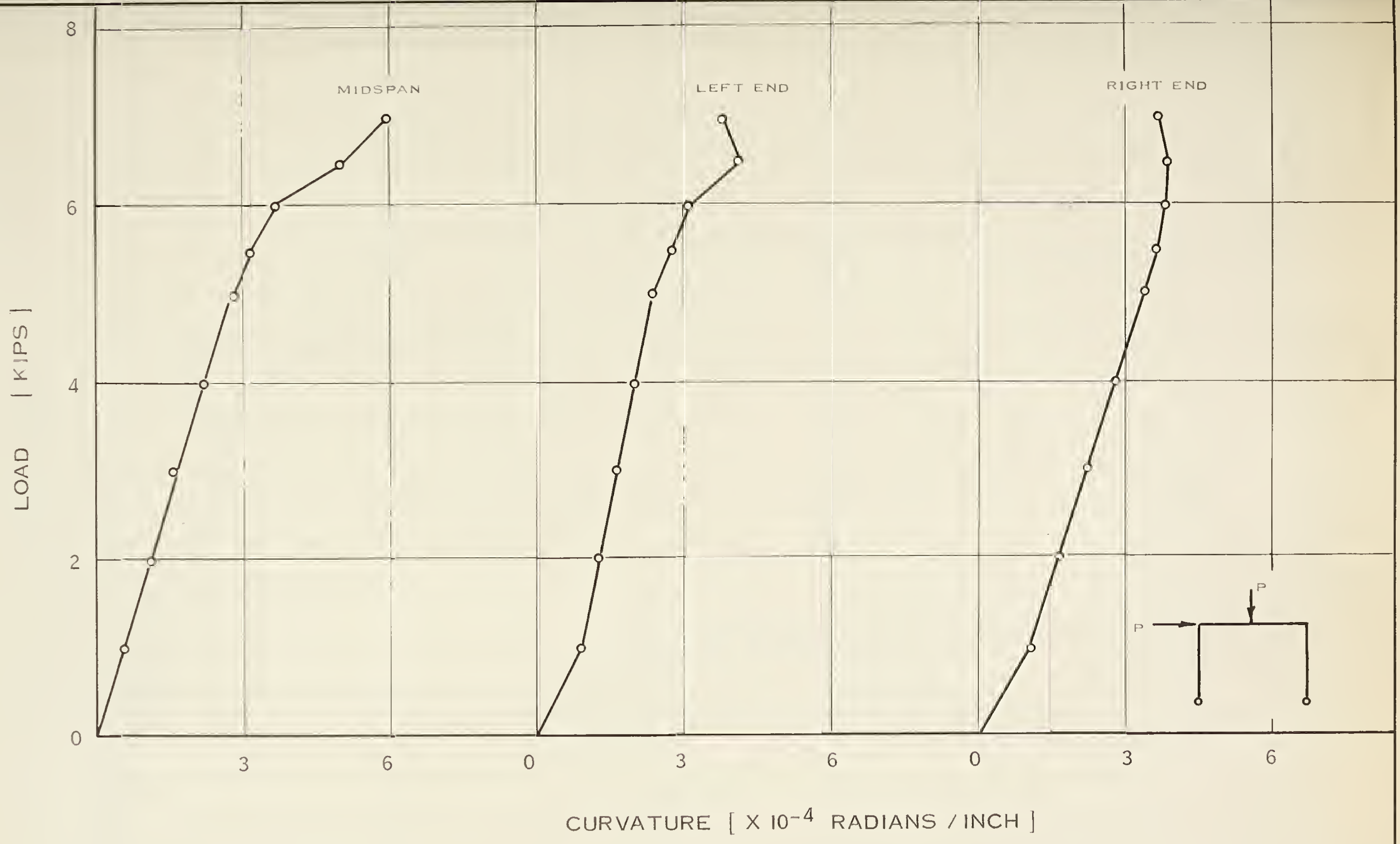

LOAD - CURVATURE RELATIONSHIPS OF BEAM FRAME NO. 3

FIGURE 43

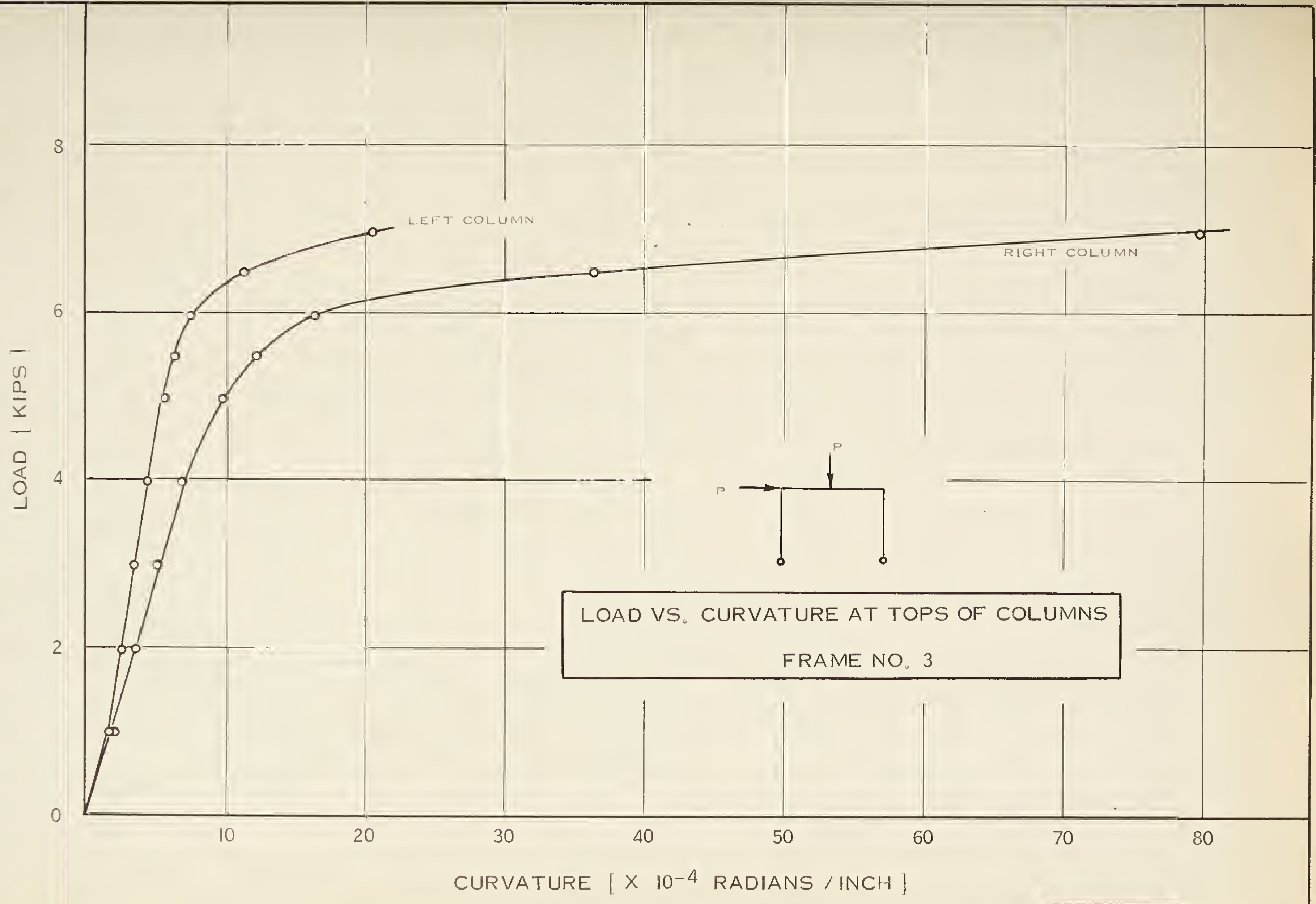

LOAD VS. CURVATURE AT TOPS OF COLUMNS

FRAME NO. 3

FIGURE 44

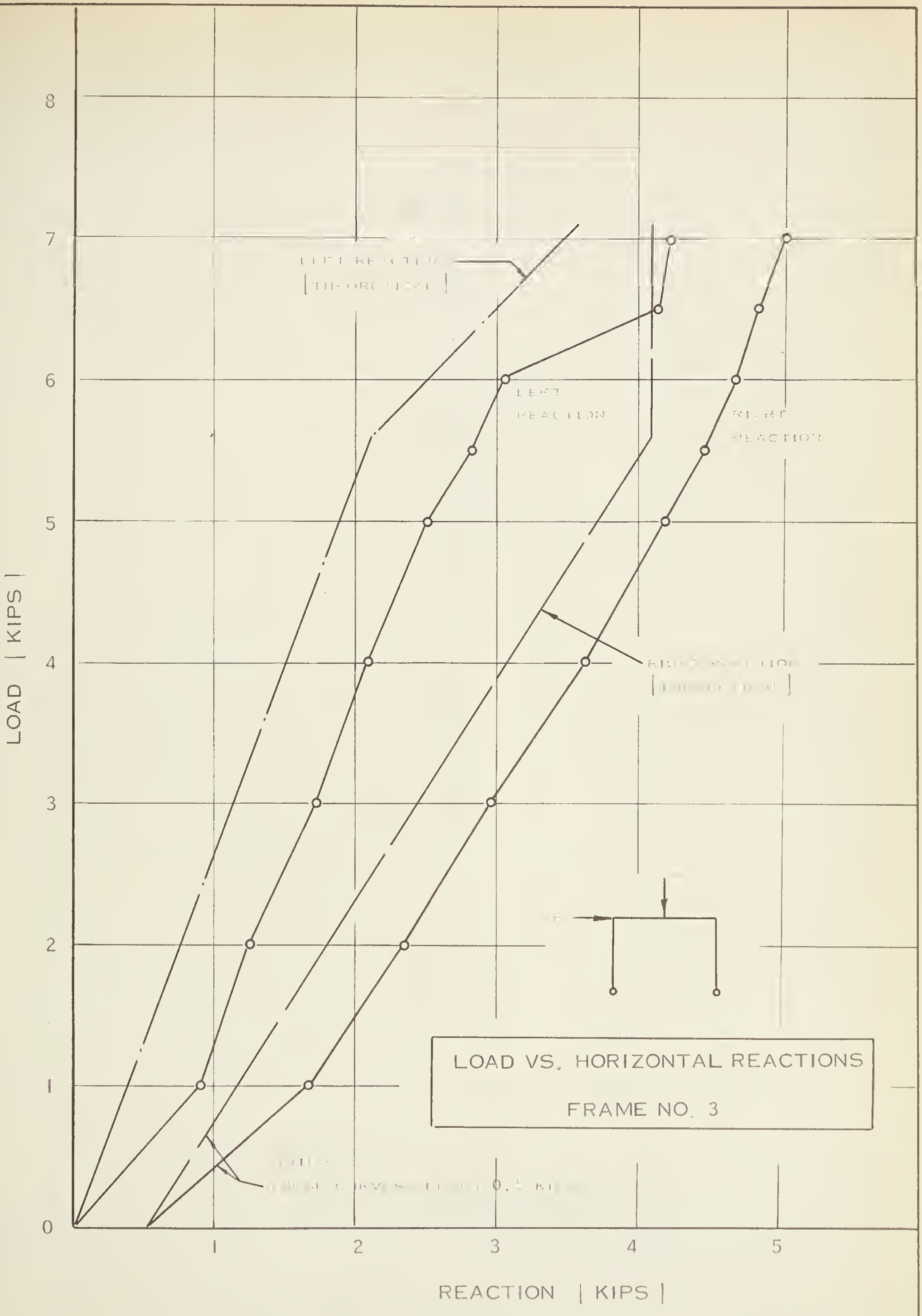

LOAD VS. HORIZONTAL REACTIONS

FRAME NO. 3

FIGURE 45

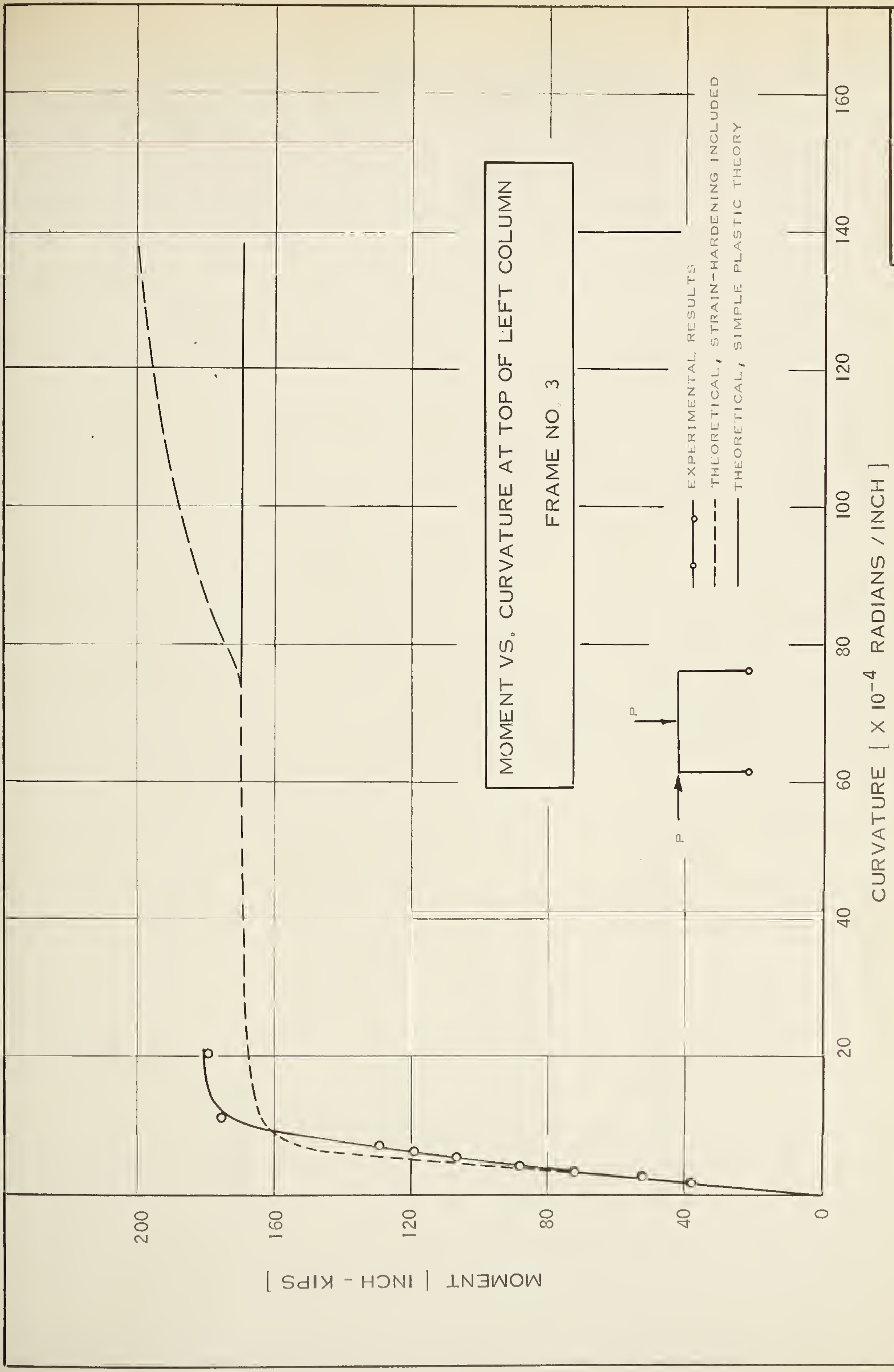
MOMENT VS. CURVATURE AT TOP OF LEFT COLUMN
FRAME NO. 3
EXPERIMENTAL RESULTS
THEORETICAL, STRAIN-HARDENING INCLUDED
THEORETICAL, SIMPLE PLASTIC THEORY
P
P
MOMENT [INCH - KIPS]
0
40
80
120
160
200
CURVATURE [X 10^{-4} RADIANS / INCH]
20
40
60
80
100
120
140
160

FIGURE 46

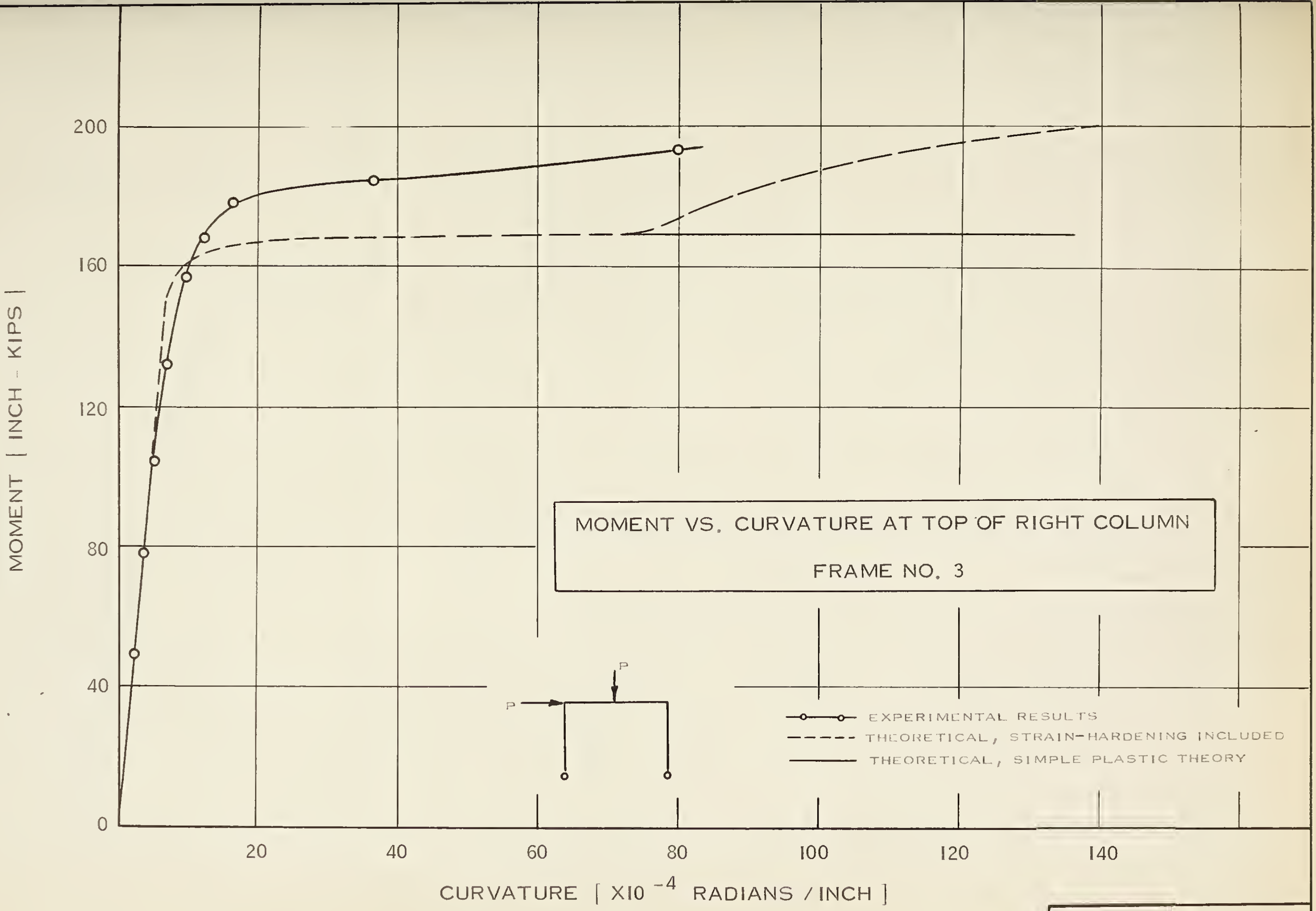

MOMENT VS. CURVATURE AT TOP OF RIGHT COLUMN

FRAME NO. 3

FIGURE 47

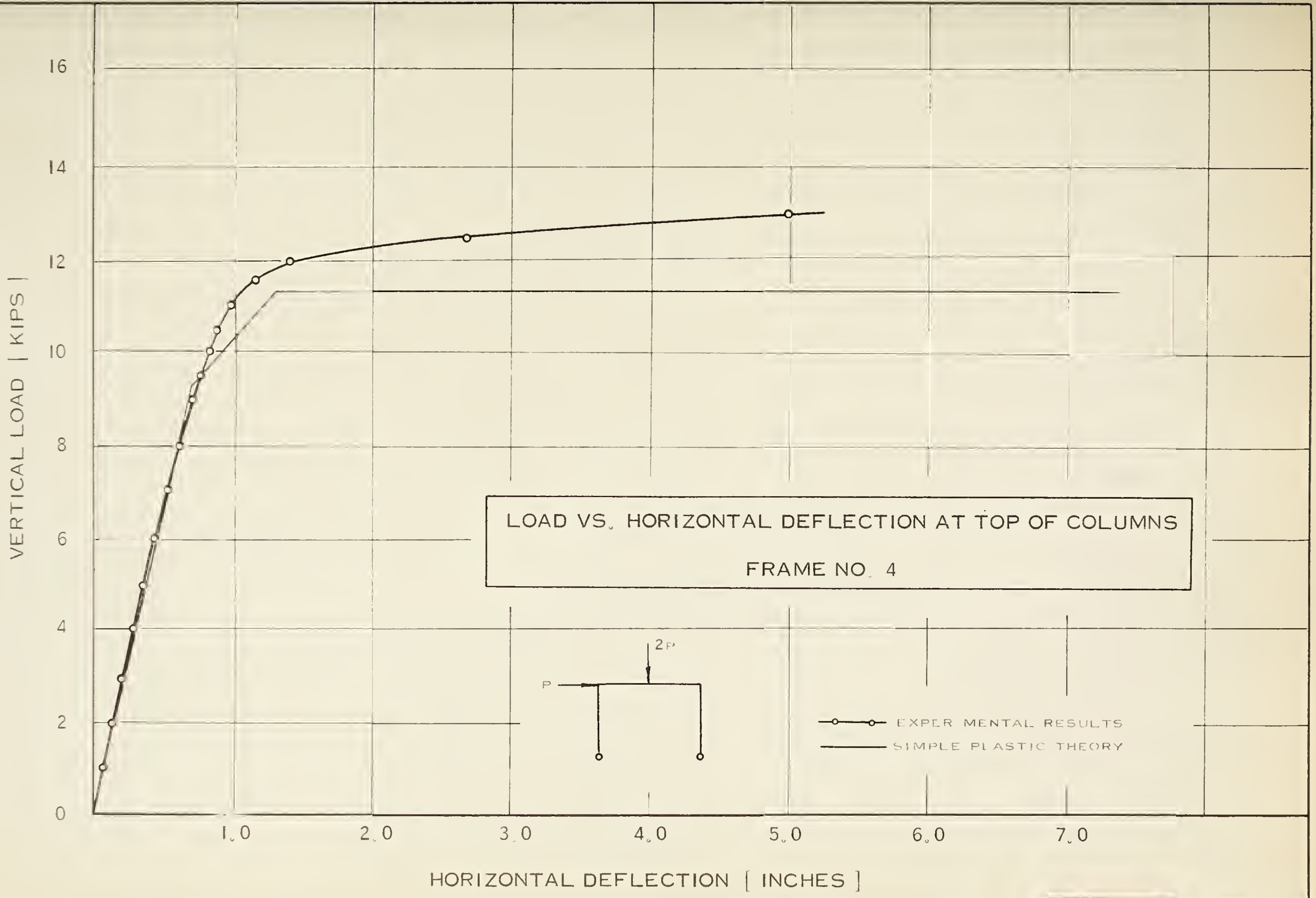
LOAD VS. HORIZONTAL DEFLECTION AT TOP OF COLUMNS
FRAME NO. 4
VERTICAL LOAD [KIPS]
0
2
4
6
8
10
12
14
16
HORIZONTAL DEFLECTION [INCHES]
1.0
2.0
3.0
4.0
5.0
6.0
7.0
2P
P
EXPERIMENTAL RESULTS
SIMPLE PLASTIC THEORY

FIGURE 48

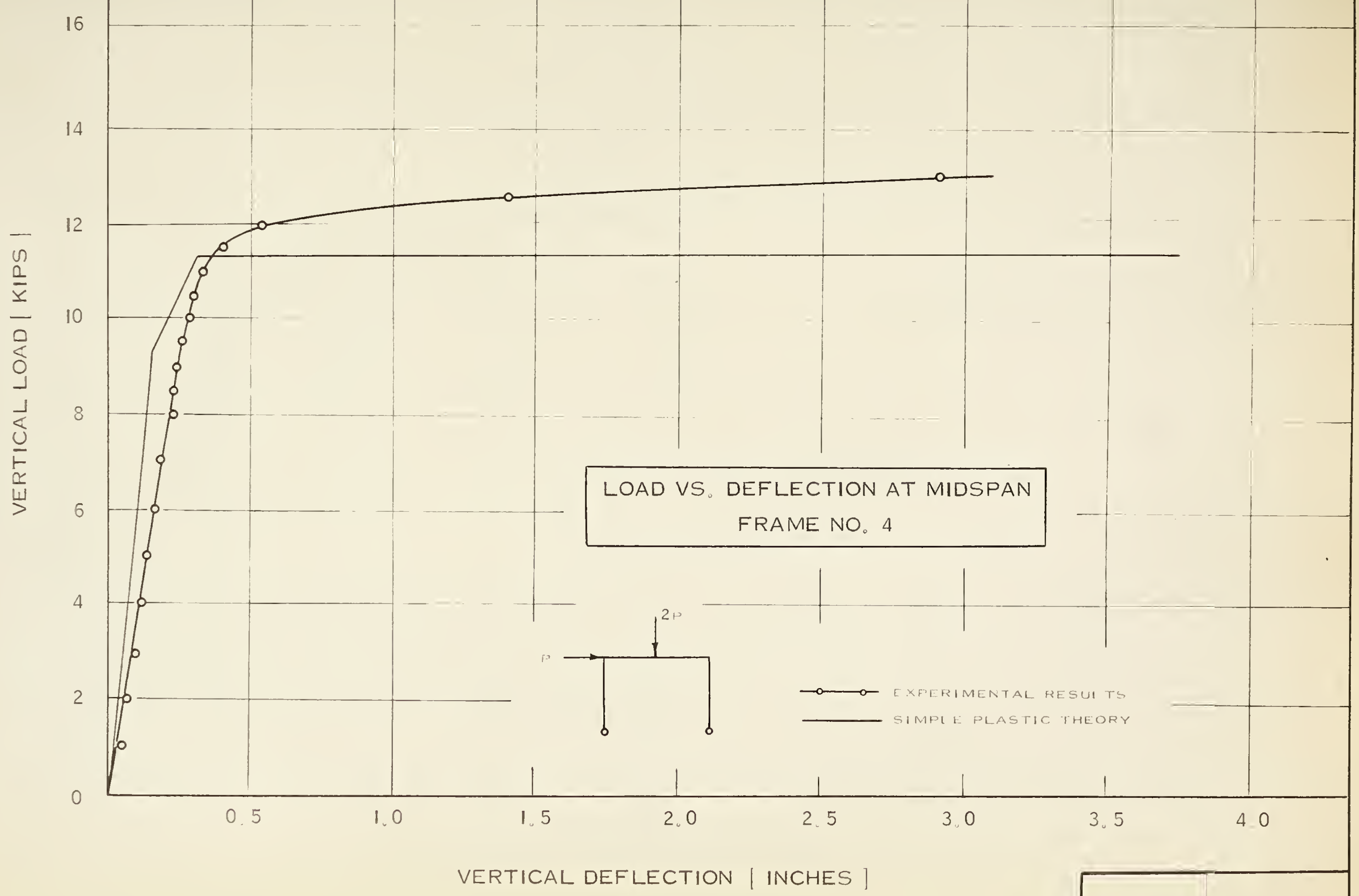
LOAD VS. DEFLECTION AT MIDSPAN
FRAME NO. 4
VERTICAL LOAD [KIPS]
0
2
4
6
8
10
12
14
16
VERTICAL DEFLECTION [INCHES]
0.5
1.0
1.5
2.0
2.5
3.0
3.5
4.0
P
2P
EXPERIMENTAL RESULTS
SIMPLE PLASTIC THEORY

FIGURE 49

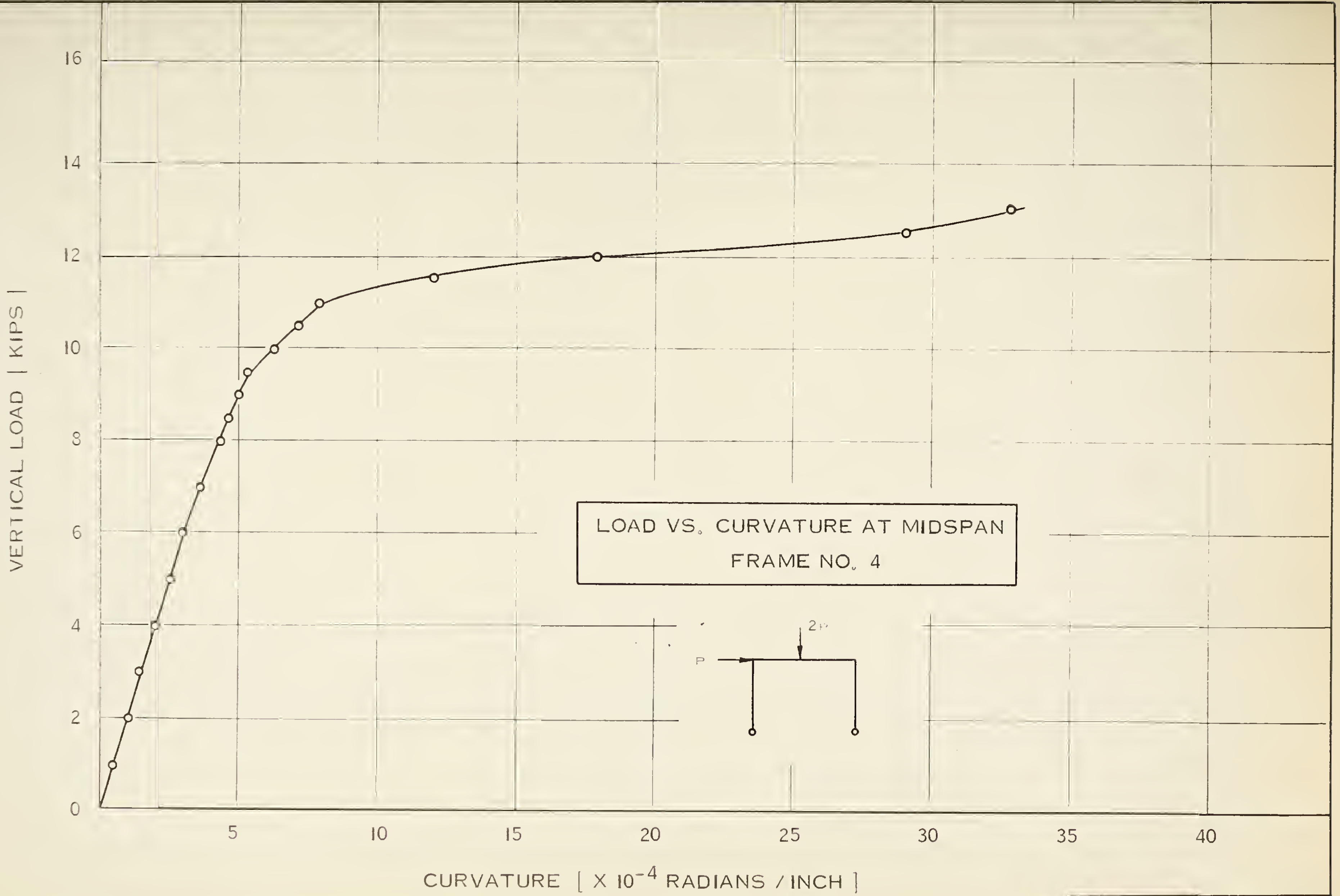

LOAD VS. CURVATURE AT MIDSPAN
FRAME NO. 4

FIGURE 50

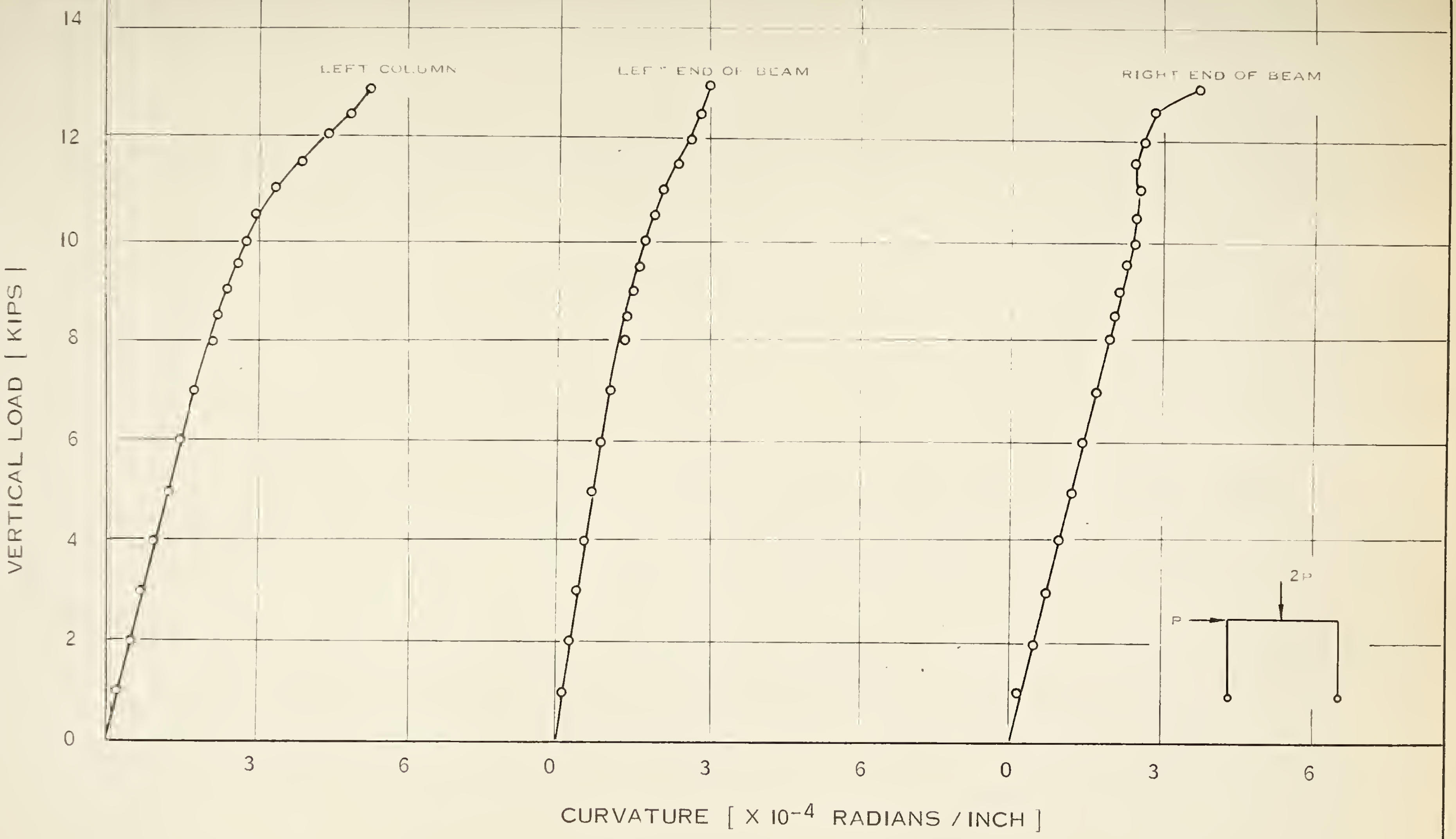

LOAD-CURVATURE RELATIONSHIPS AT TOP OF LEFT COLUMN AND ENDS OF BEAM FRAME NO. 4

FIGURE 51

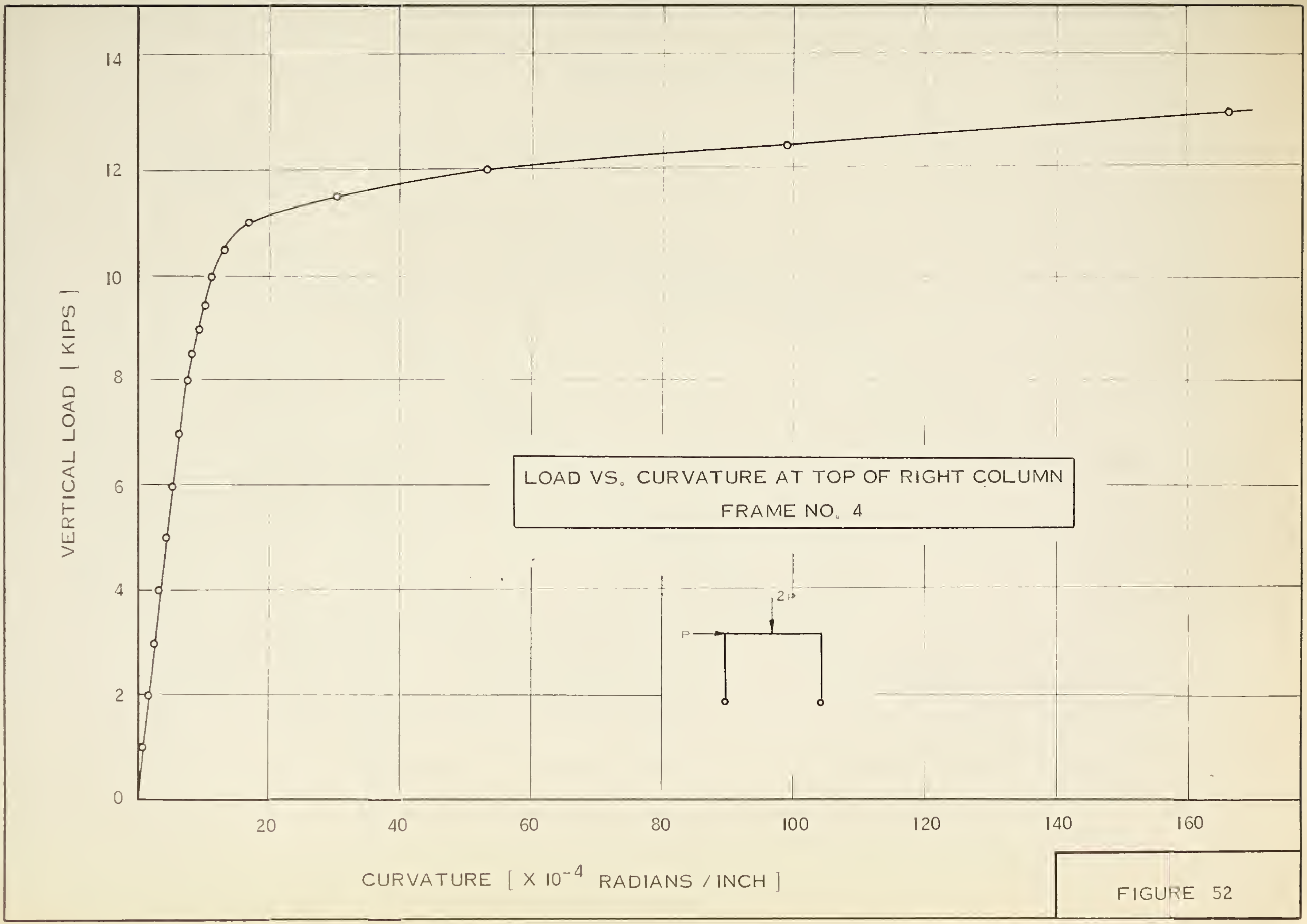
LOAD VS. CURVATURE AT TOP OF RIGHT COLUMN
FRAME NO. 4

FIGURE 52

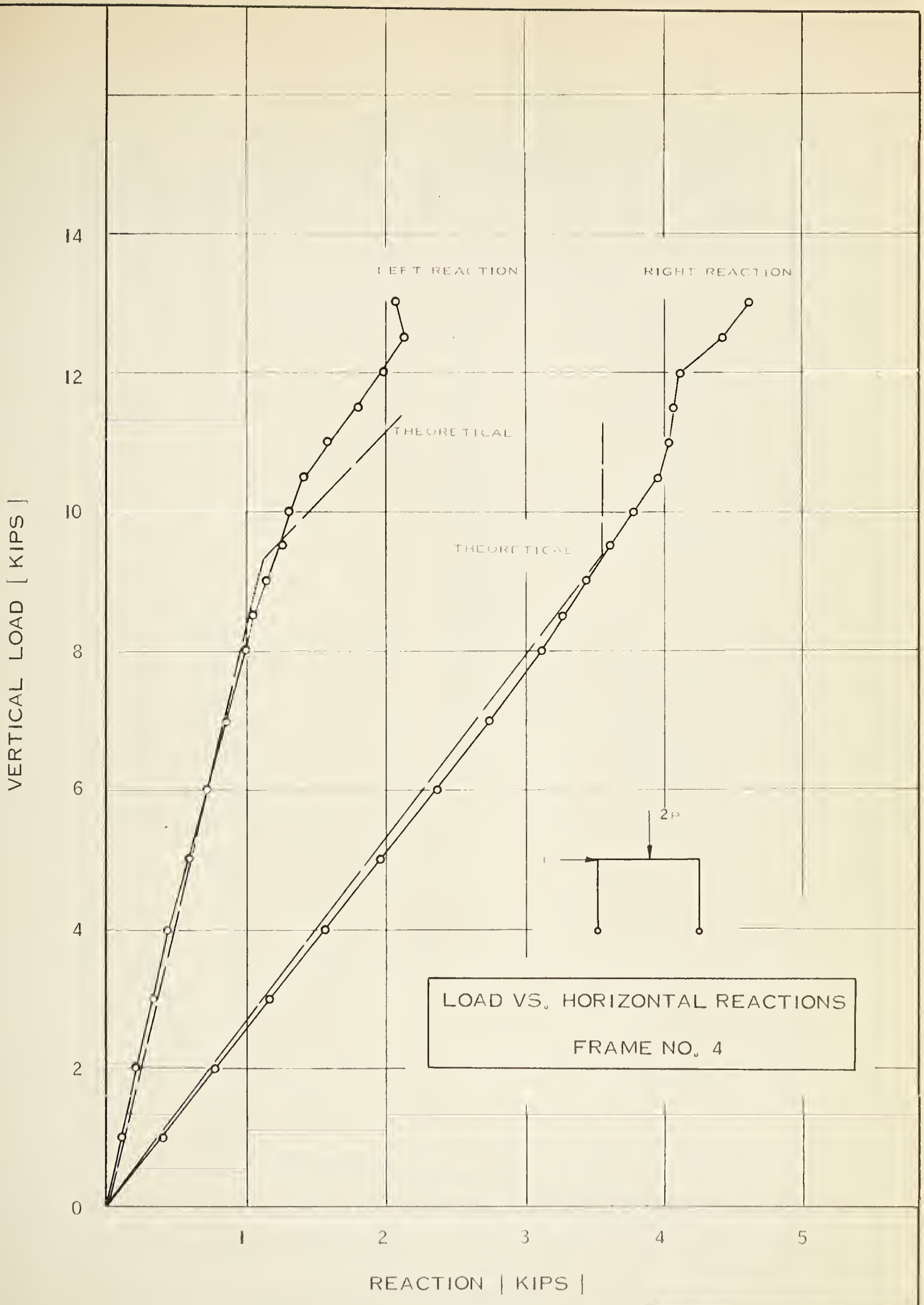

LOAD VS. HORIZONTAL REACTIONS

FRAME NO. 4

FIGURE 53

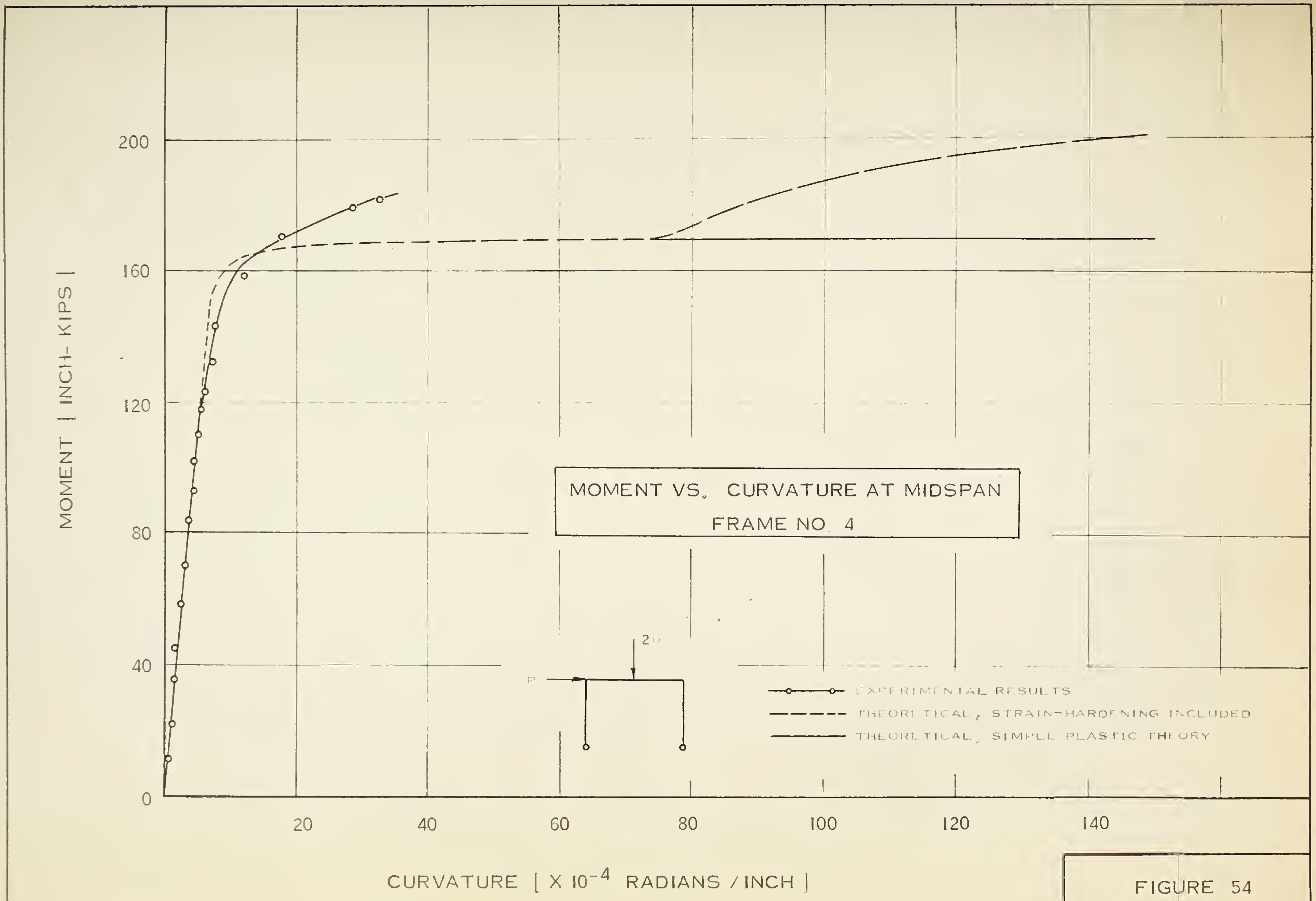

MOMENT VS. CURVATURE AT MIDSPAN
FRAME NO. 4

FIGURE 54

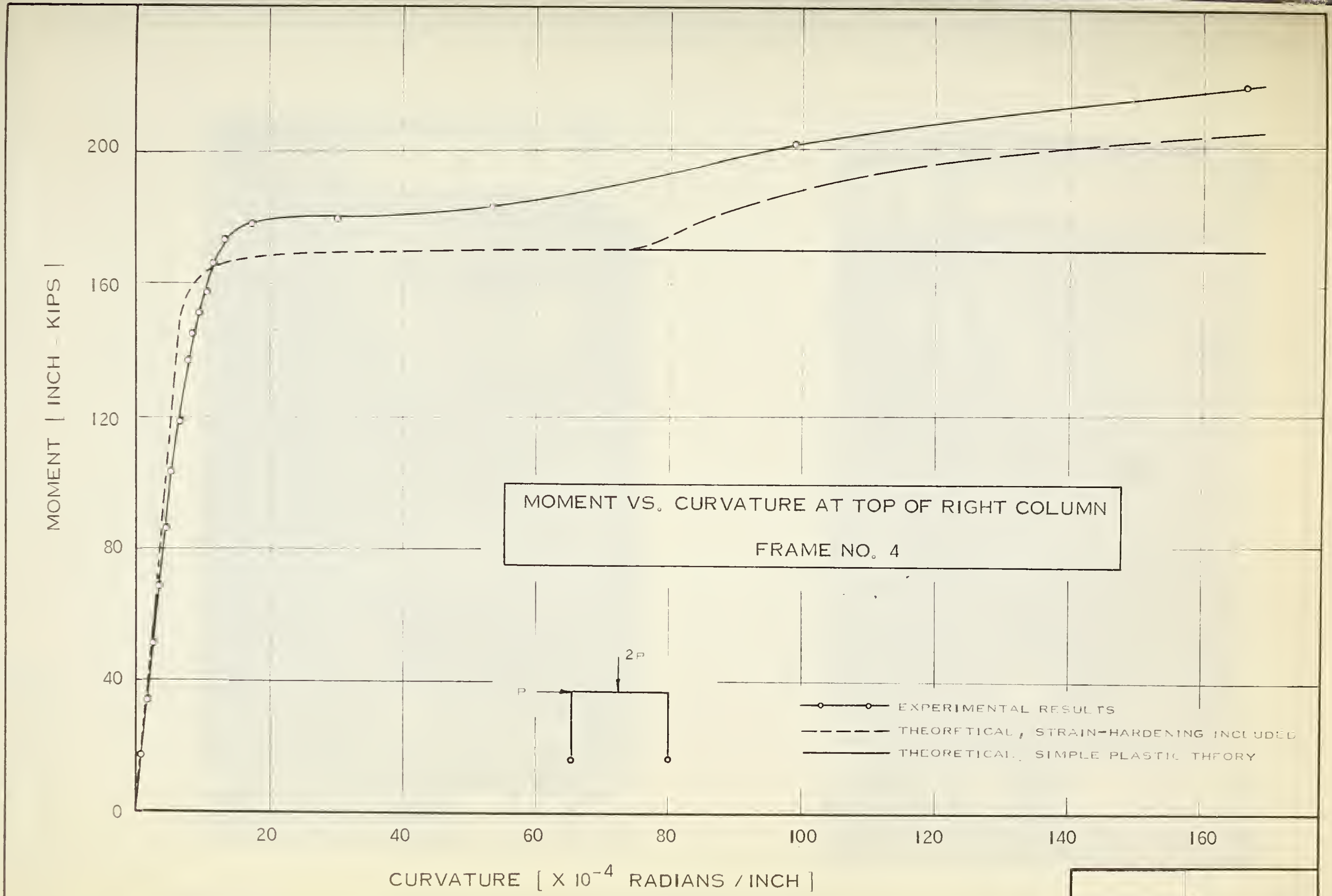

MOMENT VS. CURVATURE AT TOP OF RIGHT COLUMN

FRAME NO. 4

FIGURE 55

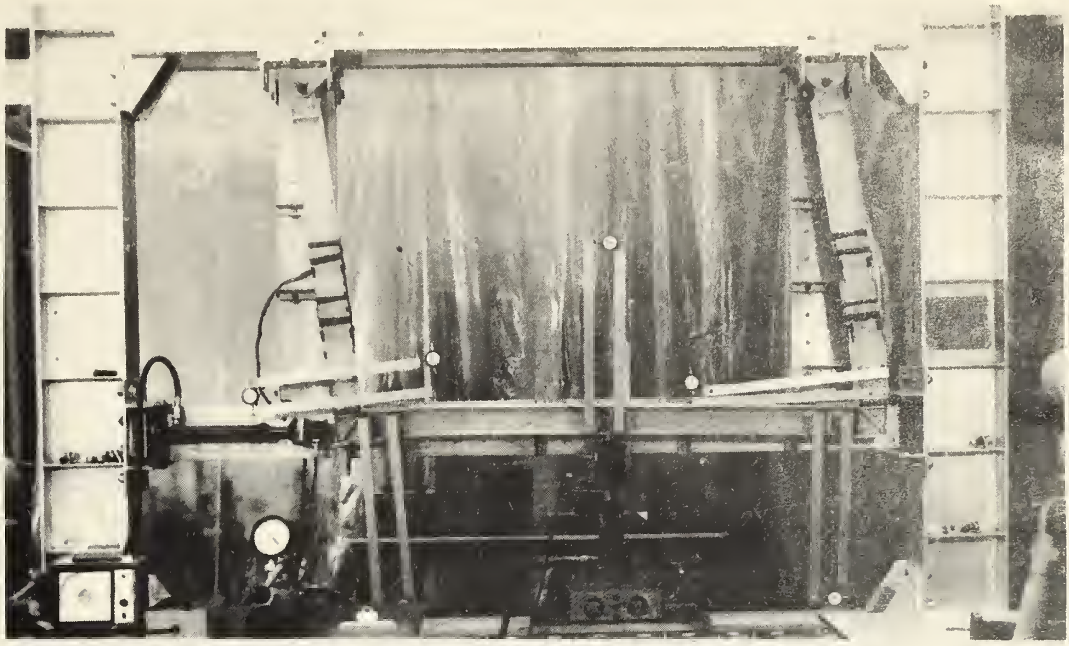

[A] FRAME NO. 3 AFTER TEST

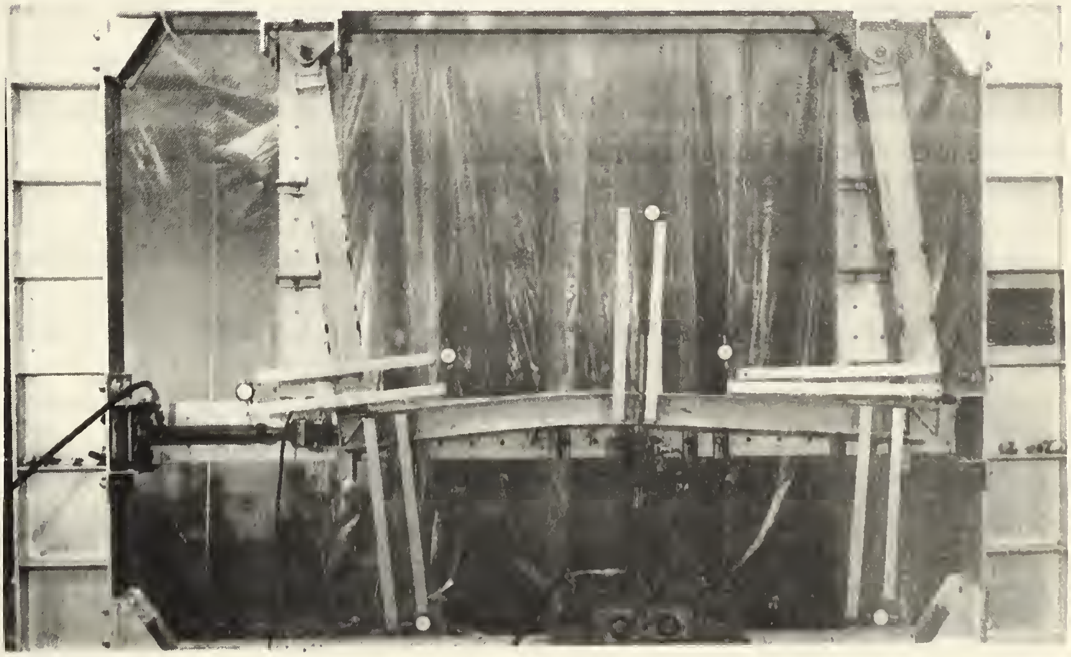

[B] FRAME NO. 4 AFTER TEST

PLATE 12

[illegible]

[illegible]

CHAPTER VIII

DISCUSSION

8-1 Material Properties

The ordinary stress-strain curve is of major importance in determining several of the important mechanical properties, hence, an extensive number of tensile tests were performed to clearly define pertinent values essential in defining the properties of the steel used in this investigation.

Of the various factors influencing yield stress, the rate of strain is most important. Tall(8) suggests that a probable value for the static yield stress is eighty percent of that found at normally accepted mill testing speeds. This discrepancy was attributed to strain rate. The geometry of the test coupon also influences tensile test results. In general, thinner specimens tend to given higher strengths.(12) However, this latter influence is not as pronounced as that of strain rate.

In the present investigation, the average static yield stress obtained for the web coupons was 39,950 psi, while the average value for the flange coupons was 42,200 psi. This difference is to be

expected due to the fact that in the 4 I 9.5 section, the flanges are rolled thinner than the webs. The average weighted value (by areas) of 41,100 psi was used in all calculations. Unfortunately, the mill report was not available, consequently, a comparison with this value could not be made. However, in line with the suggestion made by Tall, a value of 51,400 psi might be expected as the yield stress given in the mill report for the steel used in this investigation. The static level of yield stress is considered as a logical choice for the yield stress value since it best simulates most structural loadings in that they are usually static. Furthermore, it is independent of time (and is therefore constant) and is easy to obtain. A fast method of obtaining this value is to decrease the strain rate to zero in the plastic range (ensuring no strain reversal).

The average value of 29.35×10^6 psi for the modulus of elasticity obtained from the strain gauge data agrees favourably with the usual value for mild steel.

The average value for the yield strain of 0.00144 in./in., obtained from the stress-strain curves drawn by the recorder also agrees favourably with accepted values. Assuming that stress is proportional to strain up to the yield stress, the corresponding yield strain is

$$e_y = \frac{41,100}{29.35 \times 10^6} = 0.00140 \text{ in./in.}$$

The length of the yield zone (or "plastic range") is determined by comparing strain at the onset of strain-hardening, e_{st}, to the yield strain, e_y. For A7 steel, the value of e_{st} is about ten times e_y, varying from a low of about six to a maximum of about sixteen.(12) The average value for e_{st} obtained from the stress-strain curves drawn by the recorder, was 0.0143 in./in., which corresponds to a value of ten times the yield strain.

Although the value of the strain-hardening modulus, E_{st}, was not pertinent to this investigation, it was determined from the slope of the initial portion of the strain-hardening region (FIGURE 6) as being 1.3×10^6 psi. The ratio, E/E_{st} is thus 22.6. For A7 steel, (12) the ratio E/E_{st} varies from about 30 to 100. The fact that this ratio as obtained in this investigation did not fall within the range usually expected suggests that the selection of the initial slope is subject to personal judgment.

8-2 Residual Stresses

In a rolled shape, residual stresses are usually present as a result of plastic deformations caused by differential cooling and cold-bending. Residual stresses cause initial non-linearity of the stress-strain, moment-curvature, or load-deflection relationships as soon as any part of the cross-section starts to yield due to residual

stress effects. Regardless of where yielding first starts, the form of the non-linear stress-strain curve is about the same.(13) The magnitude and distribution of these residual stresses depends on the shape of the cross-section, initial temperature, cooling conditions and material properties. Usually, the fastest cooling portions of the section will be in residual compression and the parts to cool last will be in residual tension. Thus, an ideal residual stress distribution for a W F shape(14) indicates that maximum compressive residual stresses up to 0.3 times the yield stress occur in the flange tips, and that maximum tensile residual stresses occur at the junction of the flange and web. A somewhat uniform distribution of tensile residual stresses usually occurs throughout the web.

In this investigation, the residual stresses calculated from the residual strain measurements were not indicative of the cooling stresses usually observed throughout a section. Although the stress distribution obtained in one flange was of the normal type, the pattern obtained in the other flange was opposite to that usually expected (FIGURE 8). In addition the distribution of stress obtained in the web followed the pattern resulting from cold-bending.(15) The maximum value obtained for the compressive residual stress was 9,400 psi, which corresponds to 0.23 times the yield stress. This value occurred at the web-flange junction in one flange only. A lower value of 5,600

psi was obtained for the maximum compressive residual stress in the flange tips.

From the two stub-column tests, an average value of 9, 500 psi was obtained as the maximum compressive residual stress. This corresponds very favourably with the maximum value obtained by the "method of sections". Hence, a section under an applied load experiences initial yielding at a load approximately 0. 77 times that predicted by theoretical calculations.

For the stub columns, an average value of 30 x 10^6 psi was obtained for the modulus of elasticity in compression, and an average value of 44, 150 psi was obtained for the yield stress. These values are slightly higher than those derived from the tensile tests, but are not unreasonable if the objectives of the two types of tests are considered.

8-3 Beam Test Results

Results of the beam tests are presented in FIGURES 18 to 22 inclusive. FIGURE 18 provides a comparison of the various load-deflection curves for Beam Test No. 1. The theoretical plot based on the "plastic-hinge" method is linear up to the predicted collapse load of 12.6 kips, at which point deflections are assumed to increase indefinitely without further increase in load. In comparison, the

theoretical plot based on the "moment end-slope" relationships derived from the tension tests, follows the same linear relationship up to a load of 11.0 kips. Thereafter, a gradual bend occurs and a considerable range of deflection over which the load remains roughly constant at the theoretical collapse value is observed. At a deflection of 1.1 inches, the load-deflection relation again increases, almost linearly, at a lesser slope than initially, due to strain-hardening. This characteristic curve is to be expected,(16) since it represents the case of a simply-supported beam in which the central portion is subjected to pure moment.

The experimentally derived load-deflection curve is also linear up to a load of 11.0 kips. At this point, a gradual bend occurs up to a load of 13.8 kips. Thereafter, the load-deflection relation increases linearly at a lesser slope than initially. From this, it is apparent that the effects of strain-hardening commence near the 13.8 kip-load at a deflection of approximately 0.35 inches, rather than at a load of 12.6 kips and a deflection of 1.1 inches, as predicted by the theoretical curve. This fact is substantiated by the excellent correlation obtained with the theoretical plot based on the "moment end-slope" relationships derived from the actual average moment-curvature relationship obtained from the beam tests. This theoretical plot closely follows the experimental curve through the entire range of loading. For a given deflection, the difference between the theoretical load and actual load is no greater

than four percent. An even better correlation is shown in FIGURE 19, a plot of load-deflection curves for Beam Test No. 2. Here, the difference between the actual load-deflection curve, and the theoretical plot based on the "moment end-slope" relationships derived from the beam tests, is negligible. The reason that almost perfect correlation was not obtained for both beam tests, is primarily due to the fact that an average moment-curvature relationship, derived from the two beam tests, was used to obtain the "moment end-slope" relationships. In addition, an average experimental value for the fully-plastic moment was used in deflection computations (Appendix B). The theoretical load-deflection curves based on the "plastic-hinge" method and the "moment end-slope" relationships, derived from the tension tests, for Beam Test No. 2, are of course the same as for Beam Test No. 1.

Moment-curvature relationships for the 4 I 9.5 section are shown in FIGURES 20 to 22 inclusive. In FIGURE 20, a plot of moment vs. curvature obtained from the strain gauge readings is compared with the moment-curvature relationship obtained from the rotation indicator data, for Beam Test No. 1. A very close correlation between the two is evident throughout the entire range plotted. Taking the value for the fully-plastic moment as 180 inch-kips, the theoretical moment at which deviation from a linear relationship should begin, as a result of residual stresses, is 0.77 x 180 = 139 inch-kips. The average experimental value, for this same point, was 135 inch-kips. The theoretical moment-

curvature relationship follows the same basic shape as the experimental curves, except that the fully-plastic moment occurs at the lower value of 170 inch kips.

In FIGURE 21, very close agreement between the moment-curvature relationship, derived from the strain gauge readings, and the moment vs. curvature values derived from the rotation indicator data, for Beam Test No. 2, is shown up to a moment value of 80 inch-kips. Thereafter, the moment-curvature relationship derived from the rotation indicator data departs quite gradually from the linear relationship, until at a curvature well into the plastic range, close agreement between the two curves is once again achieved. Excellent correlation between the theoretical plot and the moment vs. curvature values derived from the strain gauge readings is obtained up to a moment of 150 inch-kips. Thereafter, the two curves follow a parallel course with the experimental values for moment at a given curvature being greater than the theoretical.

The average experimental moment-curvature relationship, derived from the two beam tests, is compared with the theoretical curve in FIGURE 22. The experimental value for curvature at which first yield occurred in the outer fibers was determined as being 6.5×10^{-4} radians/inch and the theoretical value was computed as being 6.82×10^{-4} radians/inch. In addition, the theoretical value at which

strain-hardening is said to begin was computed as being 68.2×10^{-4} radians/inch. Experimental verification of this latter value is difficult to obtain. From the experimental plot in FIGURE 22, it would seem that strain-hardening begins at a moment of 180 inch-kips and a corresponding curvature of 18.5×10^{-4} radians/inch. This is even more evident in FIGURE 10, a non-dimensional plot of the same relationship. The assumption that strain-hardening commences at this value provides a plausible explanation of the shape of the experimental load-deflection curves shown in FIGURES 18 and 19. Since the "horizontal plateau" of the theoretical moment-curvature relationship is not obtained experimentally, it must be concluded that indeed, strain-hardening does begin at this early stage. Hence, once the experimental value for the fully plastic moment is reached at a curvature of 18.5×10^{-4} radians/inch, the effects of strain-hardening result in an immediate increase in load-carrying capacity for the beams. An appreciation of the manner in which the "moment end-slope" relationships are derived, further substantiates this argument, since the end-slopes are obtained by an integration of the moment-curvature diagram.

The assumption that strain-hardening commences at the so-called "early stage", is based on the effects of residual stresses. A section-element subject to an initial compressive residual stress reaches the yield strain and consequently the strain at the onset of

strain-hardening, first. At some value of curvature near the predicted yield value, the section is composed of elastic, plastic, and strain-hardened portions. Therefore, an increase in the resisting moment of the section would be obtained at this stage, since the "horizontal plateau" evident in the theoretical relationship is a direct consequence of the assumption that a section behaves as an ideal elasto-plastic material.

8-4 Frame Test No. 1

Test results for Frame No. 1, are presented in FIGURES 27 to 34 inclusive.

In the theoretical calculations, the effect of axial force was neglected. The Commentary on Plastic Design in Steel$^{(3)}$ states that for strong axis bending, the influence of axial force may be neglected if $P/P_y < 0.15$, where "P" is the axial force on the member and "P_y" is the concentric load that would cause yielding of the entire cross-section. The resulting error due to this approximation is less than 5 percent. The maximum axial load to which the columns of Frame No. 1 were subjected, was 12.25 kips. For the 4 I 9.5 section, $P_y = \sigma_y \times A = 41.1 \times 2.80 = 115.0$ kips. Thus, the ratio of P/P_y was 0.106. Hence, the effects of axial load should therefore be less than 5 percent.

Similarly, the effects shear forces were neglected in theoretical calculations. The Commentary$^{(3)}$ suggests that if $V < 18wd$, where "w"

is the web thickness and "d" is the section depth, failure will not be affected by shear. For the 4 I 9.5 section, 18 wd = 24.3 kips. The maximum shear in the columns of Frame No. 1 was 5.08 kips, and the maximum shear in the beam was 12.25 kips, both well within the recommended value of 24.3 kips. Therefore the effects of shearing forces should not be significant.

FIGURE 27 provides a comparison of the various load-deflection curves for Frame Test No. 1. The theoretical curve based on the "plastic-hinge" method is linear up to a load of 14.45 kips, at which point the first plastic hinge is assumed to form. Thereafter, the load-deflection curve follows a linear relationship at a lesser slope, up to the predicted collapse load of 18.9 kips. At this point, deflections are assumed to increase indefinitely without further increase in load. In comparison, the theoretical curve based on the "moment end-slope" relationships derived from the tension tests, closely follows the same shape as for the "plastic-hinge" method up to the theoretical collapse load. Thereafter, the load-deflection curve does not exhibit a sharply defined collapse load, but rather increases in a slightly curved manner at an average slope which is less than either of the preceding straight-line portions. In addition, a gradual change in slope is evident near the values of load at which plastic hinges are assumed to form. This is in contrast to the abrupt changes in slope in evidence in the "plastic-

hinge" method of analysis. The experimental load-deflection plot also bears the same significant characteristics as the theoretical curves up to the predicted collapse load. Thereafter, the load-deflection relationship follows the same average slope as the theoretical curve derived from the "moment end-slope" relationships, only at a slightly greater value of load. For a given deflection, the corresponding actual and theoretical deflections differ by no more than 4 percent. The theoretical load-deflection plot derived from the "moment end-slope" relationships obtained from the beam tests, bears the same characteristics of the two previously described plots. The basic difference between this curve and the experimental plot is that for a given deflection, theoretical values for load are approximately 5 percent greater than experimental values. Thus, in the strain-hardening range, the experimental load-deflection curve falls practically midway between the two theoretical curves derived from the "moment end-slope" relationships. At this point, it should be noted that the value for the fully-plastic moment used to calculate the theoretical curve from the "moment end-slope" relationships derived from the beam tests, was 180 inch-kips. This was the average value obtained experimentally, and was also the value used in deflection computations for the beam tests. It is interesting to note that when a fully-plastic moment value of 170 inch-kips is used, a load-deflection plot for the frame results which is almost identical to the one obtained experimentally.

FIGURES 28 to 30 inclusive are plots of experimental load-curvature data. FIGURE 28, a plot of load vs. curvature at midspan, follows the same characteristic shape as the load-deflection curve. A departure from the initial linear relationship is noted at a load of 9.0 kips. This value does not agree favourably with the theoretical value if residual stresses are taken into account, since theoretically, the formation of the first plastic hinge should begin at a load of 0.77 x 14.45 = 11.43 kips. A departure from the initial linear relationship at a load of 14.0 kips is shown in FIGURE 29, a plot of load vs. curvature at the tops of the columns. Theoretically, the formation of the collapse mechanism should begin at a load of 0.77 x 18.9 = 14.5 kips.

Load vs. curvature at the ends of the beam are plotted in FIGURE 30. A maximum curvature of 3.8×10^{-4} radians/inch was observed, hence it is obvious that the plastic hinges formed in the columns rather that at the ends of the beams.

Vertical load vs. horizontal reaction is plotted in FIGURE 31. The experimental results agree very closely with the theoretical curves up to a load of 8.0 kips. Thereafter, for a given value of load, measured values exceed theoretical values by about 6 percent. It is interesting to note that the theoretical curves as well as the experimental curve bear the same characteristic shape. An initial linear relationship is observed up to the formation of the first plastic hinge, at which point an almost

linear relationship continues at a lesser slope. For the theoretical plot based on the simple plastic theory, the load-reaction relationship was assumed as linear up to the formation of the first plastic hinge. Thereafter, up to the calculated ultimate load, the load-reaction relationship was assumed to vary linearly at a different slope. Theoretical values based on the "moment end-slope"relationships were taken from calculations used to obtain the load-deflection curve (Appendix B).

Moment-curvature relationships at the beam midspan and the tops of the two columns are shown in FIGURES 32 to 34 inclusive. The experimental moment-curvature relationship at midspan coincides with the theoretical curve up to a moment value of 114 inch-kips, after which it begins to depart from the theoretical as a result of residual stresses. The two curves once again coincide at a value of 170 inch-kips, which is the theoretical value for the fully-plastic moment of the section. At a curvature of 52 x 10^{-4} radians/inch, strain-hardening commences, whereas theoretically, strain-hardening begins at a curvature of 68.2 x 10^{-4} radians/inch. The close correlation between the experimental and theoretical curves shown in FIGURE 32 provides a possible explanation of the fact that when a fully-plastic moment value of 170 inch-kips is used with the "moment end-slope" relationships derived from the beam tests, theoretical load-deflection values for Frame No. 1 correspond to experimental values. This suggests that the fully-plastic moment value for the 4 I 9.5 material in this frame, is indeed 170 inch-kips.

rather than the experimentally derived value from the beam tests of 180 inch-kips. FIGURES 33 and 34 are almost identical, indicating that the hinges in each column rotated approximately the same amount. In addition, the experimental curves practically coincide with the average moment-curvature relationship derived from the beam tests. This provides experimental verification that effects of shear and axial forces are almost negligible for this frame.

A general view of Frame No. 1 after testing, is shown in PLATE 10A. As seen from this photograph, all hinges formed approximately at the predicted locations. The connections showed no signs of distress due to the imposed loading. This same observation was made in similar tests of this type.(6, 7)

8-5 Frame Test No. 2

Test results for Frame No. 2 are presented in FIGURES 35 to 40 inclusive. As for Frame No. 1, the effects of axial load and shear forces were neglected in theoretical calculations.

In FIGURE 35, horizontal load is plotted against horizontal deflection at the top of the columns. The theoretical plot, based on the "plastic-hinge" method, is linear up to a load of 7.09 kips, at which point the collapse mechanism is assumed to form. Thereafter, deflections are assumed to increase indefinitely without further increase

in load. In comparison, the theoretical load-deflection curve based on the "moment end-slope" relationships derived from the tension tests, coincides with this curve up to a load of 6.0 kips. At this point, a rather sharp bend occurs, and the load-deflection curve then assumes an almost linear relationship at a lesser slope than initially. A sharply defined collapse load is not evident, due to strain-hardening. The theoretical curve derived from the "moment end-slope" relationships obtained from the beam tests, follows the same characteristic shape as the curve derived from the "moment end-slope" relationships obtained from the tension tests. The basic difference between these two curves is that in the strain-hardening range, for a given deflection, loads are approximately 10 percent greater for the plot based on the beam test results. In the elastic range, the experimental plot falls midway between the theoretical curves up to a load of 5.0 kips. Thereafter, up to a load of 7.5 kips, the experimental curve closely follows the theoretical curve based on the "moment end-slope" relationships derived from the beam tests. In the final stages of loading, for a given deflection, loads in excess of the predicted loads, were observed. This difference was 7 percent greater than the predicted values based on the "moment end-slope" relationships derived from the beam tests, and 17 percent greater than the predicted values based on the "moment end-slope" relationships derived from the tension tests. This difference

is attributed to the value used for the fully-plastic moment in deflection calculations. The same reasoning used in the discussion of the results for Frame No. 1, would apply to this case, in that the theoretical curve is directly dependent upon the value selected for the fully-plastic moment.

At the start of Frame Test No. 2, it was anticipated that a final deflection of approximately 8 inches would be attained. However, in an attempt to increment the load from 9.0 to 9.5 kips, a tension failure in the throat of the fillet weld at the left corner of the frame occurred (PLATE 11). A failure of this type was not expected, since identical frames were tested previously under similar loading conditions,(6) with no visible sign of distress at the connections. A visual examination of the weld revealed poor workmanship in that the throat thickness was not constant throughout. Some undercutting was also evident.

Load vs. curvature relationships are presented in FIGURES 36 and 37. The relationship at the right end of the beam is practically linear throughout, and at the left end, a slight curve is evident. Since the maximum curvature recorded was 4.96×10^{-4} radians/inch, it is obvious that the ends of the beam remained elastic throughout this loading range. In FIGURE 37, the departure from the linear load-curvature relationship at the tops of the columns occurred at a load of approximately 5.5 kips, as a result of residual stresses. Theoretically,

this should occur at a load of 0.77 x 7.09 = 5.45 kips. Since larger curvatures were noted at the tops of the columns, than at the ends of the beams, it is obvious that the plastic hinges formed near these locations.

FIGURE 38, a plot of load vs. horizontal reaction, shows excellent correlation between observed and theoretical values for practically the entire range of loading. A maximum difference of 5 percent occurs near the predicted collapse load, thereby substantiating the assumption, used in theoretical calculations, that the horizontal load is divided equally between the two column reactions.

Moment-curvature relationships are plotted for the tops of the columns in FIGURES 39 and 40. Both curves are almost identical, indicating that the hinges in both columns rotated approximately the same amount. In addition, these curves follow very closely to the average moment-curvature relationship derived from the beam tests. A slight discrepancy does, however, occur in the region of initial yield in that for the columns, a more pronounced transition from the elastic to the plastic range is evident. Otherwise, the curves are coincident, again providing experimental evidence that the influence of shear and axial load is negligible for the frames tested in this investigation.

A general view of Frame No. 2 after testing, is shown in PLATE

10B. From this photograph, it is seen that the predicted sidesway mechanism did indeed form as a result of the formation of plastic hinges near the tops of the two columns.

8-6 Frame Test No. 3

As stated in a previous chapter, Frame Nos. 3 and 4 were tested in this investigation to provide experimental data for a future extension of this project. A very thorough investigation was conducted to clearly define the material properties of the steel used in the fabrication of the frames, and the "moment end-slope" relationships were obtained in accordance with these properties. A theoretical analysis for the case of combined loadings, in all likelihood, will be a major task. The experimental results obtained for Frames 3 and 4 will serve to check this theoretical analysis.

Test results for Frame No. 3 are shown in FIGURES 41 to 47 inclusive. This frame was subjected to a concentrated vertical force at the midspan, and a concentrated horizontal force, of equal magnitude, at the top of the left column. Calculations based on the simple plastic theory indicated that the frame would form a sidesway mechanism at the theoretical collapse load of 7.09 kips. As for the previous two frames, the effects of axial load and shear forces were neglected in theoretical calculations.

FIGURE 41 is a plot of load vs. horizontal deflection at the tops of the columns. A very poor comparison is obtained between the experiment plot and the theoretical plot based on the simple plastic theory. For a given load, deflections vary as much as 33 percent, which is a difference far greater than that observed in the previous two tests.

In FIGURE 42, load is plotted against vertical deflection at the beam midspan. Again, a very poor correlation is obtained between theoretical and observed values. It is noted that the test was discontinued at a load of 7.0 kips. As with Frame No. 2, a tension failure occurred in the throat of the fillet weld at the left corner connection, when the load was incremented from 7.0 to 7.5 kips. Visual examination of the weld indicated that this failure was probably due to the same factors that caused the weld failure in Frame No. 2.

Load vs. curvature relationships at the midspan and ends of the beam are shown in FIGURE 43. Since the maximum curvature observed was 6.0×10^{-4} radians/inch, it is apparent that these portions of the frame remained in the elastic range. Load vs. curvature at the tops of the columns are shown in FIGURE 44. As expected, larger curvatures occurred in the right column since this was the location of the formation of the first plastic hinge.

FIGURE 45, a plot of load vs. horizontal reactions, shows very

poor correlation of observed values with the theoretical curves. All measured reaction values are greater than those predicted. In addition, the summation of the two measured reaction values, at a given load, are approximately 1, 000 pounds in excess of the horizontally applied load. Since excellent correlation was obtained between predicted and measured values in the other frame tests, there is reason to believe that the ratio of horizontal to vertical load was not unity but a somewhat greater value. This is further substantiated by the fact that prior to testing Frame No. 4, it was necessary to replace the twenty-ton load cell, since a preliminary test run on this frame revealed that this equipment was not functioning properly. The only possible time at which this load cell could have been damaged was during the actual testing of Frame No. 3, since a preliminary test run on this frame did not indicate any discrepancies.

Moment vs. curvature relationships for Frame No. 3 are shown in FIGURES 46 and 47. The moment-curvature relationship at the top of the left column (FIGURE 46), shows that a plastic hinge had just formed in this frame prior to the weld failure. In comparison, the moment-curvature relationship at the top of the right column (FIGURE 47), indicates that the formation of the plastic hinge at this location was well advanced, as expected. It is interesting to note that despite the fact that poor correlation was obtained in the load-deflection curves,

the moment-curvature relationships practically coincide with the average moment-curvature relationship derived from the beam tests. On this basis, it seems reasonable to presume that the measured horizontal reaction values are indeed correct, since the moment-curvature relationships were computed from these measured values.

A general view of Frame No. 3 after testing, is shown in PLATE 12A. From this photograph, it is evident that the predicted sidesway mechanism did indeed form as a result of the formation of plastic hinges near the tops of the two columns.

8-7 Frame Test No. 4

Test results for Frame No. 4 are shown in FIGURES 48 to 55 inclusive. This frame was subjected to a concentrated vertical force at the midspan of the beam and a concentrated horizontal force at the top of the left column. The ratio of vertical to horizontal load was 2:1. Calculations based on the simple plastic theory indicated that the frame would form a combined mechanism when the magnitude of the vertical and horizontal loads reached 11.32 and 5.66 kips, respectively. As with previous calculations, the effects of axial load and shear force were neglected.

All tests results for Frame No. 4 are plotted in relation to vertical load values, and thus whenever load is mentioned, it will refer

to the vertical load. In FIGURE 48, load is plotted against horizontal deflection at the top of the columns. A very close correlation between experimental and theoretical values is observed up to the predicted load at which the first plastic hinge is assumed to form. Thereafter, the experimental curve assumes a similar shape to that observed for the beam tests. A sharply defined collapse load is not evident, but rather a gradual transition from the elastic range to the strain-hardening range occurs. FIGURE 49, a plot of load vs. vertical deflection at midspan, shows a similar trend. A larger discrepancy between predicted and measured values is however observed. This is probably due to the fact that deflections were plotted from readings taken with a surveyor's level with an accuracy which is less than would have been obtained from dial readings.

Load vs. curvature relationships are presented in FIGURES 50 to 52 inclusive. As expected, the largest rotations were observed at the top of the right column (FIGURE 52), which was the predicted location of the formation of the first plastic hinge. The load-curvature plot at beam midspan (FIGURE 50), also indicates that the second plastic hinge formed near this location. Since the maximum observed rotation in FIGURE 51 was 5.26×10^{-4} radians/inch, it is obvious that these portions of the frame remained in the elastic range.

FIGURE 53, a plot of load vs. horizontal reaction, shows

excellent correlation of observed values with those predicted, up to the formation of the first plastic hinge at a load of 9.32 kips. The discrepancy observed beyond this load may be attributed to a basic assumption used in calculating theoretical values. Once the plastic hinge forms, it is assumed that the horizontal reaction at the right column remains constant. In actual fact, this does not occur since the effects of strain-hardening enable a larger moment than the theoretical fully-plastic moment to be attained. Measured values are therefore, in all probability, correct.

Moment-curvature relationships are shown for the beam midspan and the right column in FIGURES 54 and 55. The moment-curvature relationship at beam midspan closely follows the theoretical curve up to a moment of 120 inch-kips. Thereafter, a departure from the linear relationship occurs due to residual stresses. Theoretically, this should occur at a moment of 0.77 x 180 = 139 inch-kips. It is also evident from FIGURE 54 that the plastic hinge at midspan had not rotated sufficiently to enter into the strain-hardening range. In FIGURE 55, the moment-curvature relationship in the right column is presented. This curve is similar to the average plot obtained from the beam tests, only at slightly lower values of moment. The difference between the two is no greater than 3 percent, probably due in part to the effects of axial load and shear force.

A general view of Frame No. 4 after testing, is shown in PLATE 12B. From this photograph it is evident that the predicted combined mechanism did indeed form as a result of the formation of plastic hinges near midspan and at the top of the right column.

CHAPTER IX

CONCLUSIONS

9-1 The most significant conclusions based on the results of this investigation are summarized as follows:

(1) In the analysis of a structure loaded with a single concentrated force, the "moment end-slope" relationships provide a relatively simple means of predicting deflections accurately in the plastic range. Of the two frames analyzed in this investigation, the theoretical deflections computed from the "moment end-slope" relationships derived from the beam tests, differed by no more than 7 percent with experimental values. With the "moment end-slope" relationships obtained from the tension test results, the maximum difference noted between theoretical and experimental deflection values was 17 percent.

(2) The most significant factor influencing the accuracy of deflection computations based on the "moment end-slope" relationships, is the value selected as the fully-plastic moment. From the beam tests, the average experimental

value for the fully-plastic moment was 6 percent greater than the theoretical value computed from the tension test results. This difference accounted for an increased accuracy of at least 10 percent in the theoretical deflection calculations.

(3) Deflection calculations based on the "plastic-hinge" method of analysis are satisfactory in predicting deflections up to the formation of the first plastic hinge. Thereafter, predicted values may vary as much as 30 percent from experimental values. In addition, theoretical curves do not follow the same characteristic shape of the experimental curves once the predicted ultimate load is reached.

(4) A clearly defined collapse load was not obtained as predicted by the simple plastic theory. Instead, strain-hardening developed at approximately ultimate load and resulted in an increase in load-carrying capacity that was approximately proportional to deflection.

9-2 Conclusions pertinent to the experimental procedure used in this investigation are summarized as follows:

(1) Use of the "Model TS-M Dual Extensometer" resulted in values obtained for the material properties of the steel used in this investigation which compare favourably with accepted values.

(2) Excellent correlation was observed between the maximum compressive residual stress derived from the stub column tests, and the maximum value obtained by the "method of sections".

(3) Instrumentation designed to measure rotations, loads and deflections functioned favourably. In addition, the lateral support system used provided sufficient restraint for the loads imposed.

(4) Excellent agreement between measured and predicted reaction values was obtained from the strain gauge data. It is, however, essential that the gauges be mounted on parts of the frame which remain in the elastic range.

(5) Computed moment-curvature values at various locations of the frames differed from the average relationship derived from the beam tests by no greater than 3 percent. The effect of shear force and axial load was therefore negligible in the frames tested.

BIBLIOGRAPHY

(1) Longworth, J. "Basic Concepts of Plastic Design," Proceedings, Conference on Recent Developments in Structural Engineering, U. of A., March, 1961.

(2) Sawyer, H. A. Jr., "Post-Elastic Behavior of Wide Flange Steel Beams," Proceedings, A.S.C.E., ST 8, Vol. 87, 1961.

(3) A.S.C.E. Manual No. 41, "Commentary on Plastic Design in Steel", Welding Research Council and the American Society of Civil Engineers, 1961.

(4) Knudsen, K.E., Yang, C.H., Johnston, B.G., Beedle, L.S, "Plastic Strength and Deflections of Continuous Beams," Welding Journal Supplement, Vol. 32, 1953.

(5) Ang, A.H., "Analysis of Frames with Nonlinear Behavior," Proceedings, A.S.C.E., V. 86, EM 3, June, 1960.

(6) Channon, J.R., "The Ultimate Load Capacity of Steel Frames," U. of A. Master Thesis, 1961.

(7) Kraemer, I.F., "The Effects of Strain-Hardening on the Ultimate Load Capacity of Steel Frames," U. of A. Master Thesis, 1962.

(8) Tall, L., "Material Properties of Structural Steel," Fritz Laboratory Report No. 220A.28A, April, 1958.

(9) Beedle, L.S., "Plastic Design of Steel Frames," Wiley, 1958.

(10) Luxion, W.W., Johnston, B.G., "Plastic Behavior of Wide Flange Beams," Welding Journal Supplement, Vol. 27, 1948.

(11) Wang, C.K., "Statically Indeterminate Structures," M^{c}Graw-Hill, 1953.

(12) Civil Engineering Department Staff, Lehigh University, "Structural Steel Design," Fritz Engineering Laboratory Report 354.3.

(13) Gozum, A.T., Huber, A.W., "Material Properties, Residual Stresses, and Column Strength," Lehigh University, Institute of Research, Progress Report, May, 1955.

(14) Beedle, L.S., Huber, A.W., "Residual Stress and the Compressive Properties of Steel," Fritz Engineering Laboratory Report No. 220A.27.

(15) Yang, C.H., Beedle, L.S., Johnston, B.G., "Residual Stress and the Yield Strength of Steel Beams," Welding Journal Supplement, Vol. 31, 1952.

(16) Neal, B.G., "The Plastic Methods of Structural Analysis," Wiley, 1956.

APPENDIX A

CALCULATIONS BASED ON SIMPLE PLASTIC THEORY

A-1 Section Properties (4 I 9.5)

Average section properties, derived from measurements taken on the 4 I 9.5 section, are presented in this section, since subsequent calculations are based on these values. A comparison of measured quantities with Handbook values is given in the following tabulation:

	Actual value	Handbook value
Section depth	4.114 in.	4.00 in.
Flange width	2.764 in.	2.796 in.
Flange thickness	0.287 in.	0.293 in.
Web thickness	0.329 in.	0.326 in.
Area	2.80 in.^{2}	2.76 in.^{2}
Moment of inertia	7.13 in.^{4}	6.7 in.^{4}
Section modulus	3.47 in.^{3}	3.3 in.^{3}
Plastic modulus	4.13 in.^{3}	
Shape factor	1.19	

A-2 Ultimate Load Calculations

In this section, calculations based on the "mechanism method" of calculating ultimate load for the frame specimens and beam specimens,

are presented. Moment diagrams are shown to indicate that the plastic moment has not been exceeded at any section.

a) Frame No. 1

The loading for Frame No. 1 is shown in FIGURE A1(a). Possible plastic hinge locations are at sections 2, 3, and 4. A beam mechanism is formed with plastic hinges at each of these locations (FIGURE A1(b). In this figure, the frame, subjected to the ultimate load P, has been given a virtual vertical displacement, δ, at the beam midspan.

The external work done by the vertical load is thus:

$$W_e = P \times \delta = \frac{P L \Theta}{2} \qquad \left(\text{since } \delta = \frac{L\Theta}{2}\right)$$

Since each plastic hinge at the corners has rotated through an angle Θ, and the hinge at the beam midspan through an angle 2Θ, the total internal work is:

$$W_i = M_p \times \Theta + M_p \times 2\Theta + M_p \times \Theta = 4\, M_p \Theta$$

Equating the external work to the internal work gives:

$$\frac{PL\Theta}{2} = 4\, M_p \Theta \quad \text{from which,} \quad P = \frac{8 M_p}{L}$$

but $M_p = \sigma_y Z$ $\qquad$ ($\sigma_y = 41.1$ ksi, $Z = 4.13$ in.^{3})

Therefore, $M_p = 41.1 \times 4.13 = 170$ inch-kips.

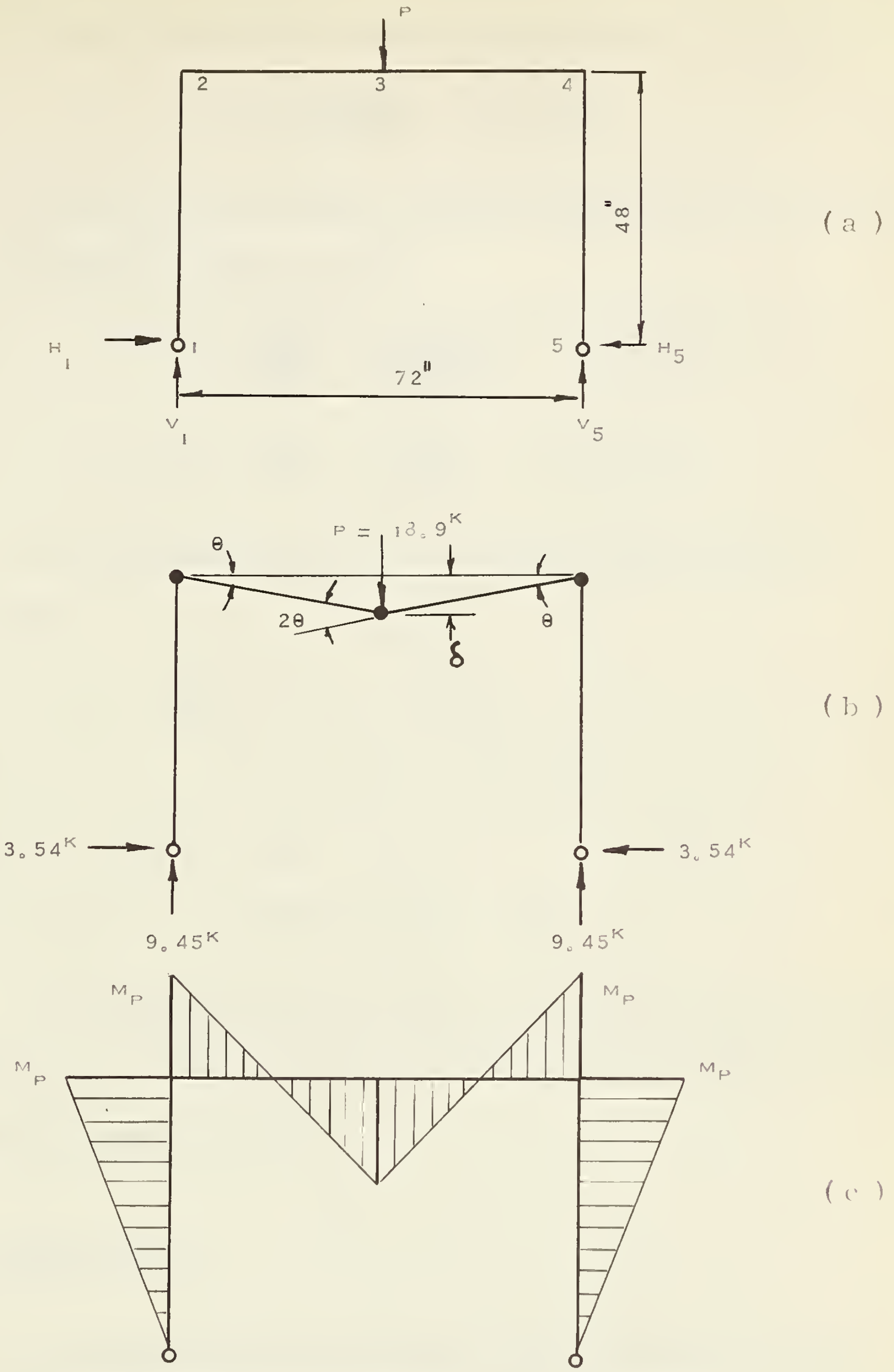

ULTIMATE LOAD ANALYSIS

FRAME NO. I

FIGURE AI

Substituting these values in the equation for P gives:

$$P = \frac{8 \times 170}{72} = 18.9 \text{ kips}$$

The predicted ultimate load for Frame No. 1 then is 18.9 kips.

Solving for the reactions:

$$H_1 = H_5 = \frac{3M_p}{2L} = \frac{3 \times 170}{2 \times 72} = 3.54 \text{ kips.}$$

$$V_1 = V_5 = \frac{P}{2} = \frac{18.9}{2} = 9.45 \text{ kips.}$$

The moment diagram at the ultimate load is shown in FIGURE A1(c).

$$M_3 = 36\ V_1 - 48\ H_1$$

$$= 36 \times 9.45 - 48 \times 3.54$$

$$= 340 - 170$$

$$= 170 \text{ inch-kips} = M_p$$

It is apparent that the plastic moment has not been exceeded at any section of the frame and that the plastic moment acts at the predicted plastic hinge locations.

b) Frame No. 2

The loading for this frame is shown in FIGURE A2(a). There are only two possible plastic hinge locations, at sections 2 and 3. Since two hinges are required to form the collapse mechanism, plastic hinges

must form at both of these sections, resulting in the side-sway or panel mechanism shown in FIGURE A2(b). In this figure, the frame, subjected to the ultimate load P, has been given a virtual horizontal displacement at the top of the left column.

The external work done by the horizontal load is thus:

$$W_e = P \times \delta = \frac{2\ PL\Theta}{3} \qquad \text{since } \delta = \frac{2L\Theta}{3}$$

Since each plastic hinge has rotated through an angle Θ, the total internal work is given by:

$$W_i = M_p \times \Theta + M_p \times \Theta = 2\ M_p\Theta$$

Equating the external work to the internal work gives:

$$\frac{2\ PL\Theta}{3} = 2\ M_p, \text{ from which, } P = \frac{3M_p}{L}$$

Therefore, $P = \frac{3 \times 170}{72} = 7.09$ kips.

The predicted ultimate load for Frame No. 2 then is 7.09 kips.

Solving for the reactions:

$$H_1 = H_4 = \frac{3M_p}{2L} = \frac{3 \times 170}{2 \times 72} = 3.54 \text{ kips}$$

$$V_1 = V_4 = \frac{48 \times 7.09}{72} = 4.72 \text{ kips}$$

The moment diagram for the ultimate load is shown in FIGURE A2(c).

$$M_2 = 48\ P - 72\ V_4$$

$$= 48 \times 7.09 - 72 \times 4.72 = 0$$

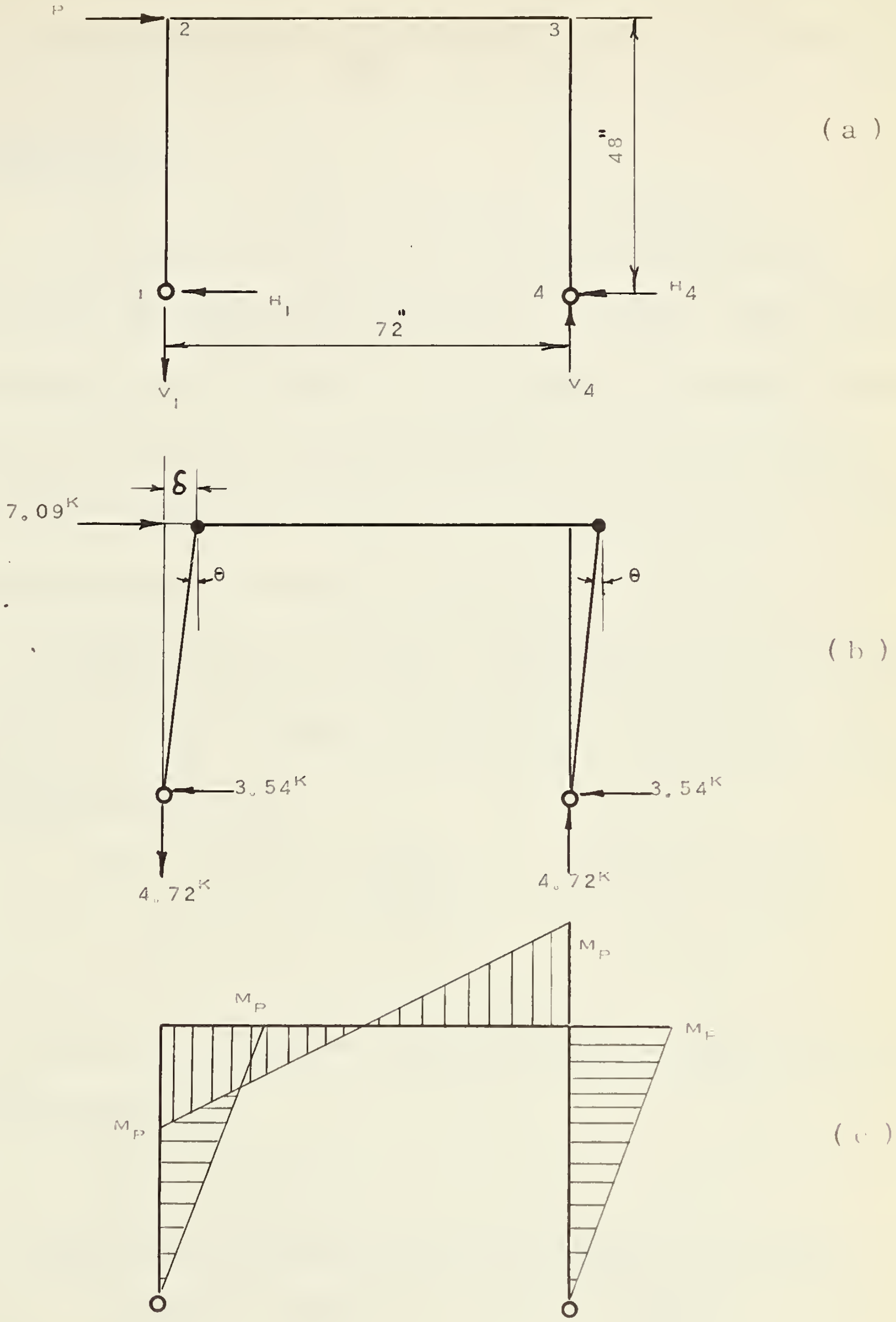

ULTIMATE LOAD ANALYSIS
FRAME NO. 2

FIGURE A2

The plastic moment has not been exceeded at any section of the frame so the ultimate load determined must be the true ultimate load.

c) Frame No. 3

The loading on this frame is shown in FIGURE A3(a). Possible plastic hinge locations are at sections 2, 3, and 4. Since the frame is indeterminate to the first degree, it is necessary for plastic hinges to form at only two of the three possible locations. After analyzing the different possible failure mechanisms, it is found that the side-sway or panel mechanism shown in FIGURE A3(b) forms at the lowest load.

In FIGURE A3(b), the frame, loaded with the ultimate load has been given a virtual horizontal displacement. The external work done by the horizontal load is thus:

$$W_e = P \times \delta = \frac{2\,PL\Theta}{3} \qquad \text{since } \delta = \frac{2L\Theta}{3}$$

Each plastic hinge has rotated through an angle Θ so the total internal work is given by:

$$W_i = 2\,M_p\,\Theta$$

Equating the external work to the internal work gives:

$$\frac{2\,PL\Theta}{3} = 2\,M_p\,\Theta \qquad \text{or, } P = \frac{3M_p}{L}$$

This gives the same ultimate load of 7.09 kips as for Frame No. 2. This is reasonable since side-sway mechanisms formed under

both loading conditions and the horizontal reactions control the formation of this type of mechanism.

Solving for the reactions:

$$H_1 = H_5 = \frac{3M_p}{2L} = \frac{3 \times 170}{2 \times 72} = 3.54 \text{ kips}$$

$$M_1 = 48\,P + 36\,P - 72\,V_5 = O$$

Therefore, $$V_5 = \frac{48\,P + 36\,P}{72} = 8.26 \text{ kips}$$

$$M_5 = 48\,P - 36\,P + 72\,V_1 = O$$

Therefore, $$V_1 = \frac{36\,P - 48\,P}{72} = 1.18 \text{ kips}$$

The moment diagram for the ultimate load is shown in FIGURE A3(c). Moments are plotted on the tension side of the members.

Since $M_2 = M_4 = M_p$

and,
$$\begin{aligned} M_3 &= 48\,H_1 - 36\,V_1 \\ &= 48 \times 3.54 - 36 \times 1.18 \\ &= 170 - 42.5 = 127.5 \text{ inch-kips} = \frac{3}{4} M_p, \end{aligned}$$

it is apparent that the plastic moment has not been exceeded at any section in the frame.

d) Frame No. 4

The loading for Frame No. 4 is shown in FIGURE A4(a). Possible plastic hinge locations are at sections 2, 3, and 4. Since the

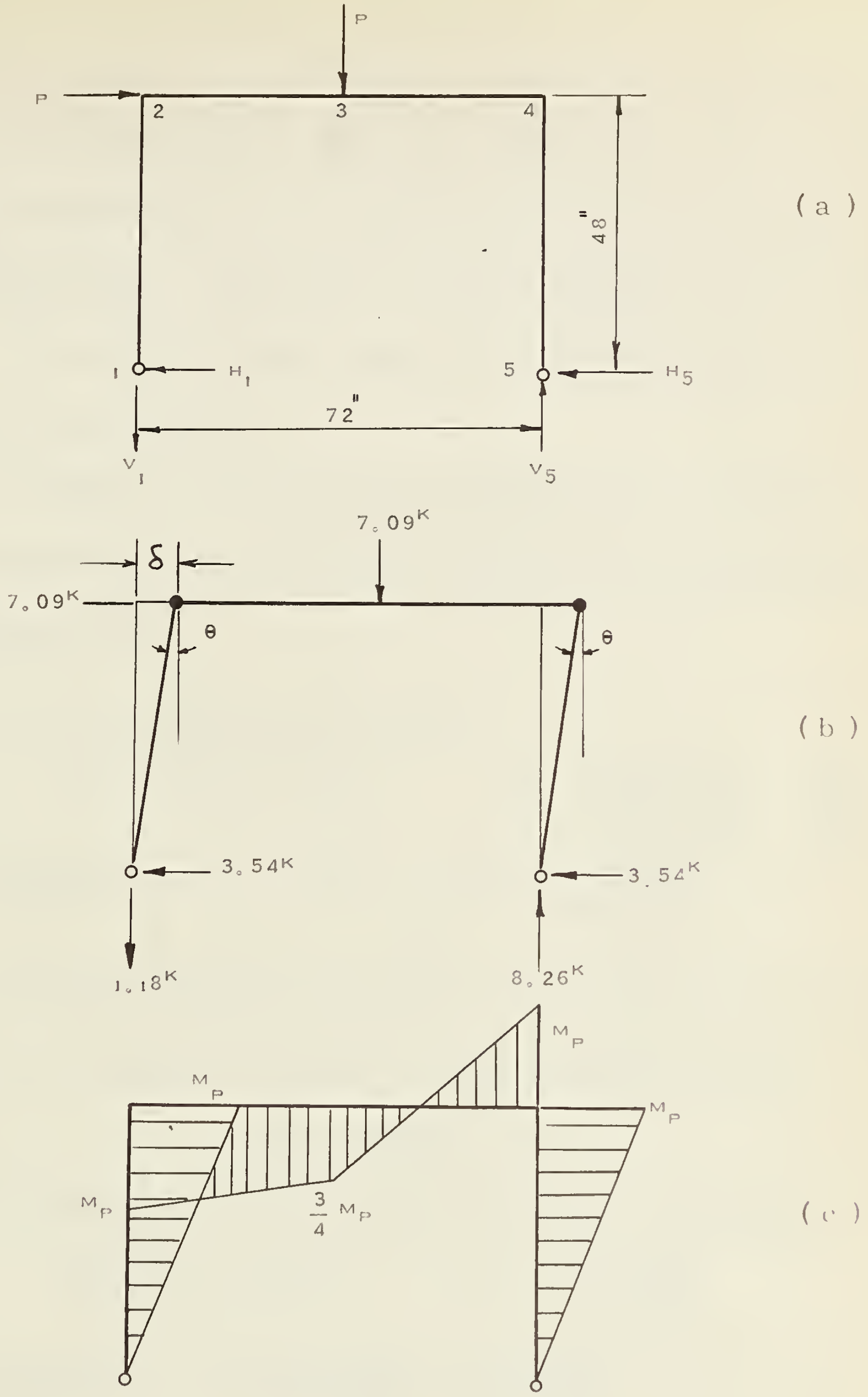

ULTIMATE LOAD ANALYSIS

FRAME NO. 3

FIGURE A3
]

frame is indeterminate to the first degree, it is possible to have two independent mechanisms and one combined mechanism. After analyzing these different possibilities, it is found that the combined mechanism shown in FIGURE A4(b), with plastic hinges at sections 3 and 4 forms at lowest load. Note that the plastic hinges are assumed to form at the corners of the line diagram.

In FIGURE A4(b) the frame, loaded as shown, is given a virtual horizontal displacement δ_2 which results in a vertical displacement at midspan of δ_1.

The total external work done is:

$$W_e = 2P\delta_1 + P\delta_2 \qquad \delta_1 = \frac{L\Theta}{2},\ \delta_2 = \frac{2L\Theta}{3}$$

Therefore, $W_e = PL\Theta + \frac{2}{3} PL\Theta = \frac{5}{3} PL\Theta$

The plastic hinges at the midspan and right corner have each rotated through an angle 2Θ, therefore, the total internal work is:

$$W_i = 4 M_p \Theta$$

Equating the external work to the internal work gives:

$$\frac{5}{3} PL\Theta = 4 M_p \Theta \qquad \text{or,} \quad P = \frac{12}{5} \frac{M_p}{L}$$

Therefore, $P = \frac{12 \times 170}{5 \times 72} = 5.66$ kips.

Thus the predicted ultimate load for Frame No. 4 consists of a horizontal load of 5.66 kips and a vertical load of 11.32 kips.

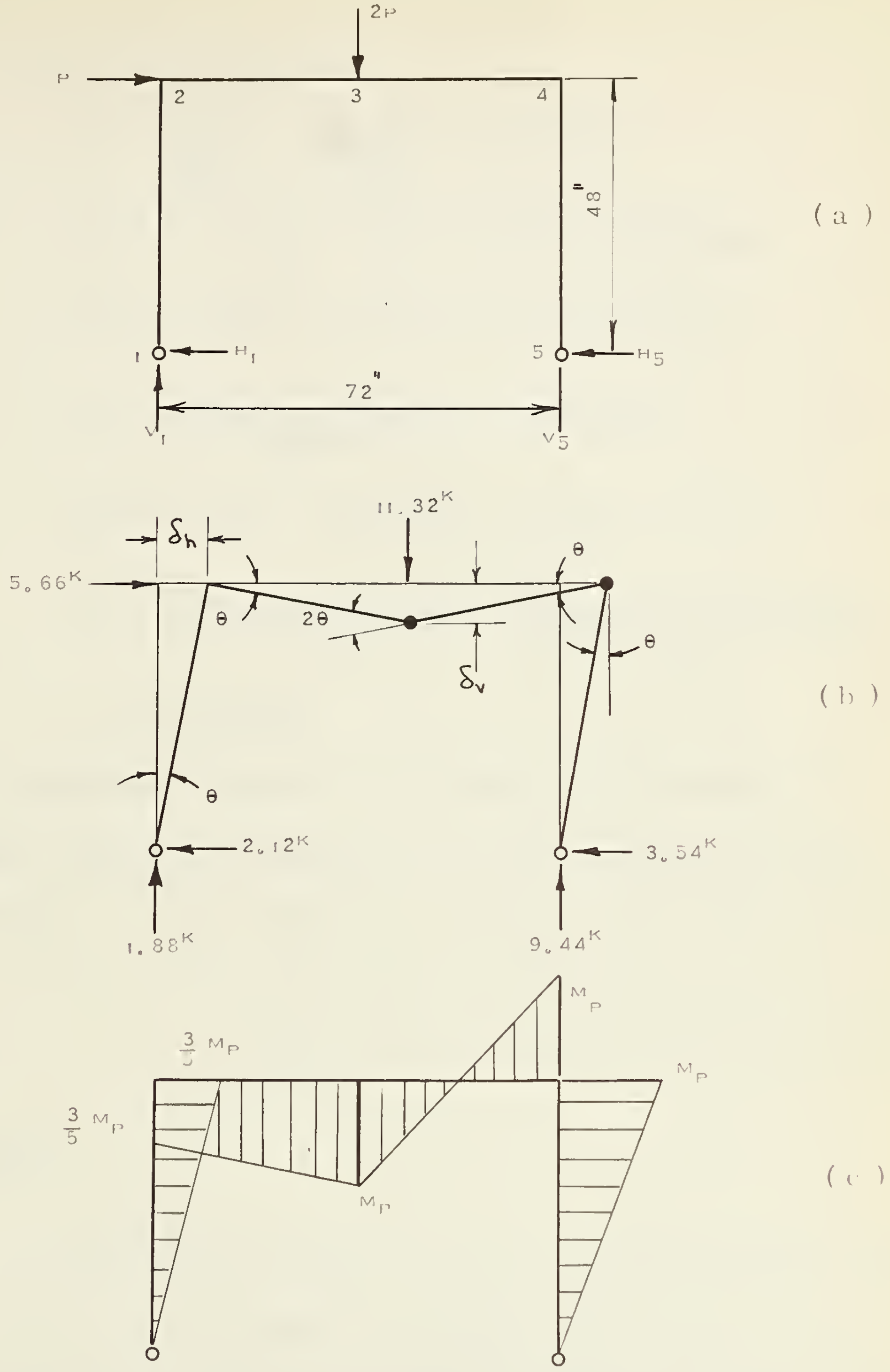

ULTIMATE LOAD ANALYSIS

FRAME NO. 4

FIGURE A4

Solving for the reactions:

$$H_5 = \frac{3\,M_p}{2L} = \frac{3 \times 170}{2 \times 72} = 3.54 \text{ kips}$$

$$H_1 = P - H_5 = 5.66 - 3.54 = 2.12 \text{ kips}$$

$$M_1 = P \times 48 + 2\,P \times 36 - V_5 \times 72 = O$$

$$V_5 = \frac{P \times 48 + 2\,P \times 36}{72} = 9.44 \text{ kips}$$

$$M_5 = P \times 48 - 2\,P \times 36 + V_1 \times 72 = O$$

$$V_1 = \frac{2\,P \times 36 - P \times 48}{72} = \frac{11.32 \times 36 - 5.66 \times 48}{72}$$

$$= 1.88 \text{ kips.}$$

The moment diagram for the ultimate load is shown in FIGURE A4(c). Moments are plotted on the tension side of the frame.

Since $M_2 = H_1 \times \frac{2\,L}{3} = \frac{2.12 \times 2 \times 72}{3} = 102$ inch-kips

$= \frac{3}{5} M_p$, the correct solution has been obtained.

e) Beams

The loading for the beams is shown in FIGURE A5(a). Since the central 18-inch section between the loads is under constant moment, a plastic hinge forms over this entire region resulting in the beam mechanism shown in FIGURE A5(b). The maximum moment as shown in FIGURE A5(c) is:

$$M = \frac{13.5}{45}\,PL$$

[illegible]

$$[illegible]$$

[illegible]

[illegible]

[illegible]

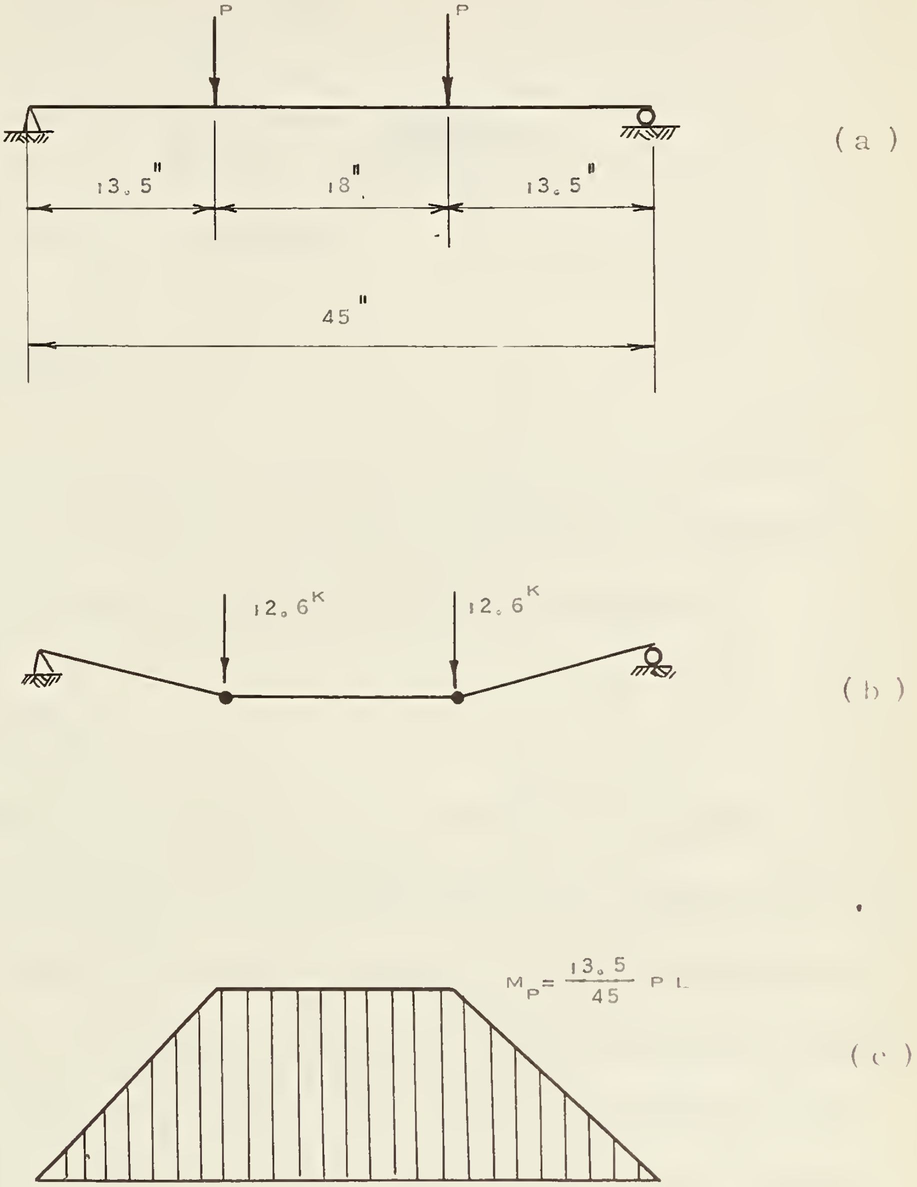

ULTIMATE LOAD ANALYSIS
BEAMS

FIGURE A5

Equating this to the plastic moment,

$$M_p = \frac{13.5}{45} PL \qquad (L = 45 \text{ inches})$$

$$P = \frac{45}{13.5} \frac{Mp}{L} = \frac{45 \times 170}{13.5 \times 45}$$

Therefore, $P = 12.60$ kips.

A-3 Elastic Analysis

Reactions and moments for the frames subjected to unit loads are shown in this section. These calculations are necessary in order to make subsequent theoretical deflection calculations.

a) Frame No. 1

Calculated moments and reactions for the statically indeterminate frame loaded with a unit vertical load at the midspan of the beam are shown in FIGURE A6(a). The frame has been solved using the Müller Breslau method. In FIGURE A6(b) the frame has been made statically determinate by replacing the hinge with a roller at the right support (condition "O"). A horizontal unit load acting to the right at the roller (condition "X_a - 1") produces moments and reactions shown in FIGURE A6(c).

The horizontal deflection at the roller for condition "O", δ_{oa}, can now be solved using the Müller Breslau tables.

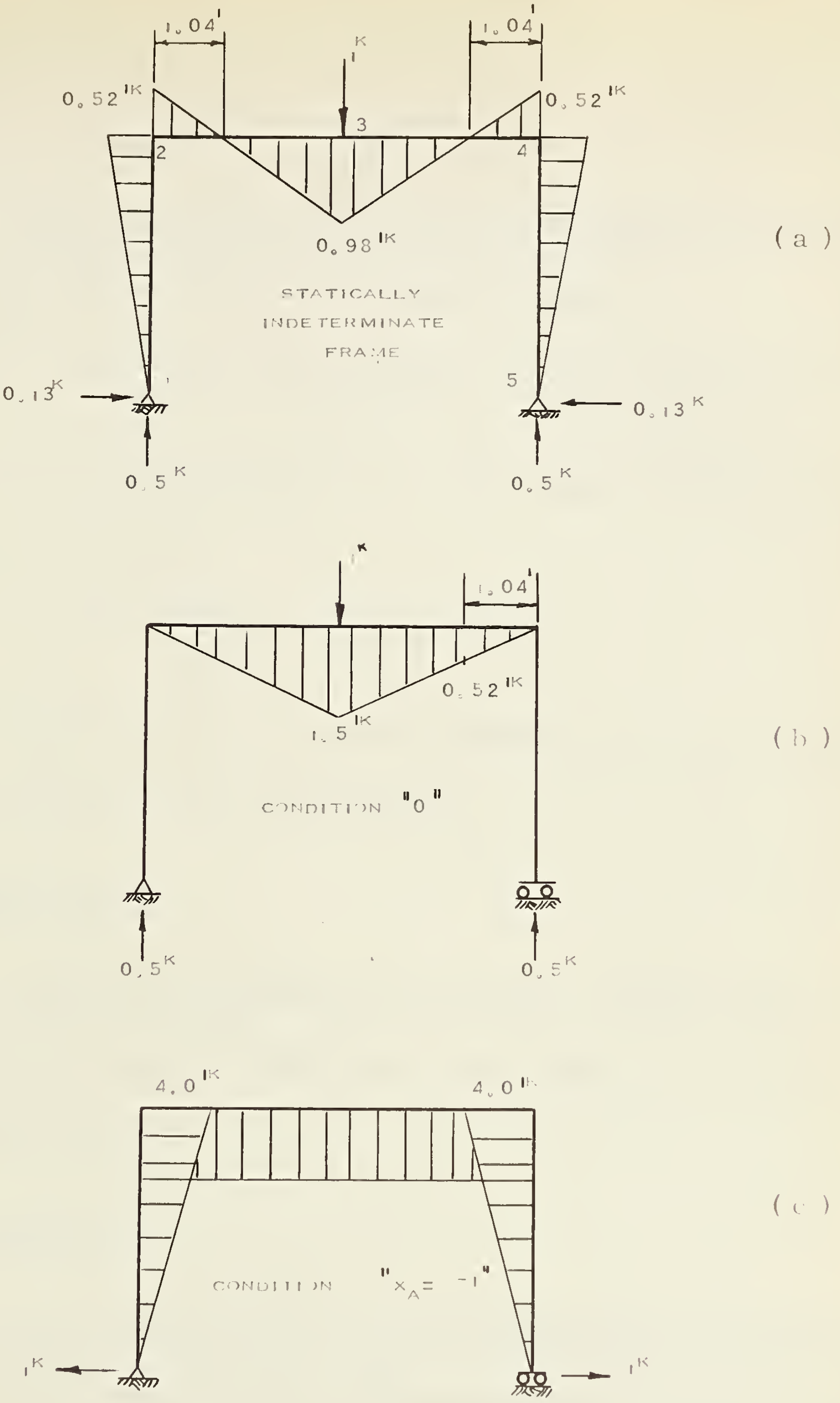

MOMENTS AND REACTIONS FOR UNIT LOAD
FRAME NO. 1

FIGURE A6

$$\delta_{oa} \times EI = \frac{4 \times 1.5 \times 6}{2} = 18$$

The horizontal deflection at the right support for condition "X_a - 1", δ_{aa}, is also solved using the same tables.

$$\delta_{aa} \times EI = \frac{2 \times 4 \times 4^2}{3} + 6 \times 4^2 = 42.67 + 96 = 138.7$$

The horizontal reaction at the right support of the indeterminate frame is therefore:

$$H_5 = \frac{\delta_{oa}}{\delta_{aa}} = \frac{18}{138.7} = 0.13$$

From this value for H_5, the remaining reactions and moments in the indeterminate frame were computed.

b) Frame No. 2

Reactions and moments for Frame No. 2 loaded with a unit horizontal load are shown in FIGURE A7. Calculations are similar to those for Frame No. 1.

c) Frame No. 3

FIGURE A8 shows the reactions and moments calculated for the statically indeterminate frame loaded with unit vertical and horizontal loads as indicated.

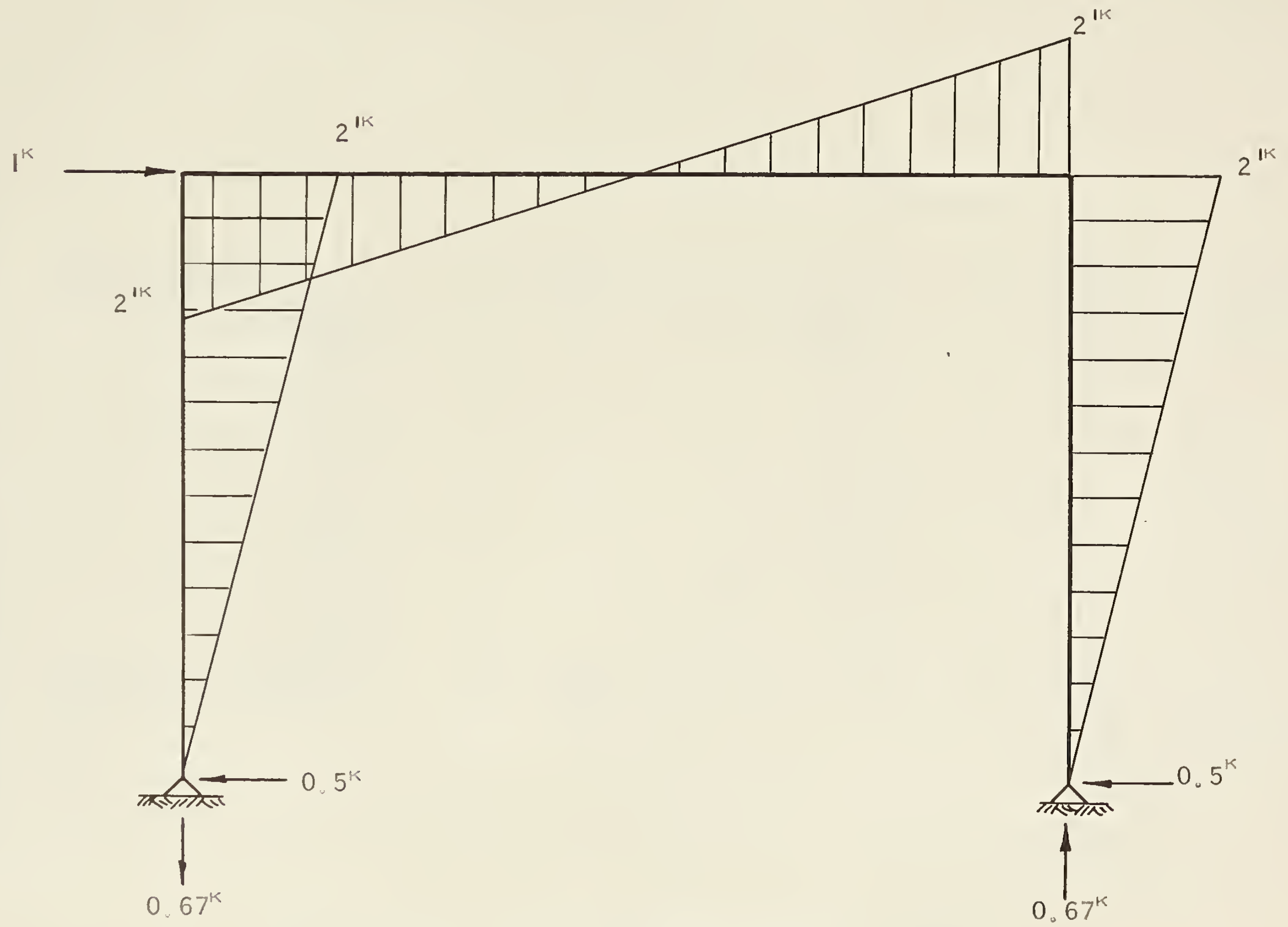

MOMENTS AND REACTIONS FOR UNIT LOAD

FRAME NO. 2

FIGURE A7

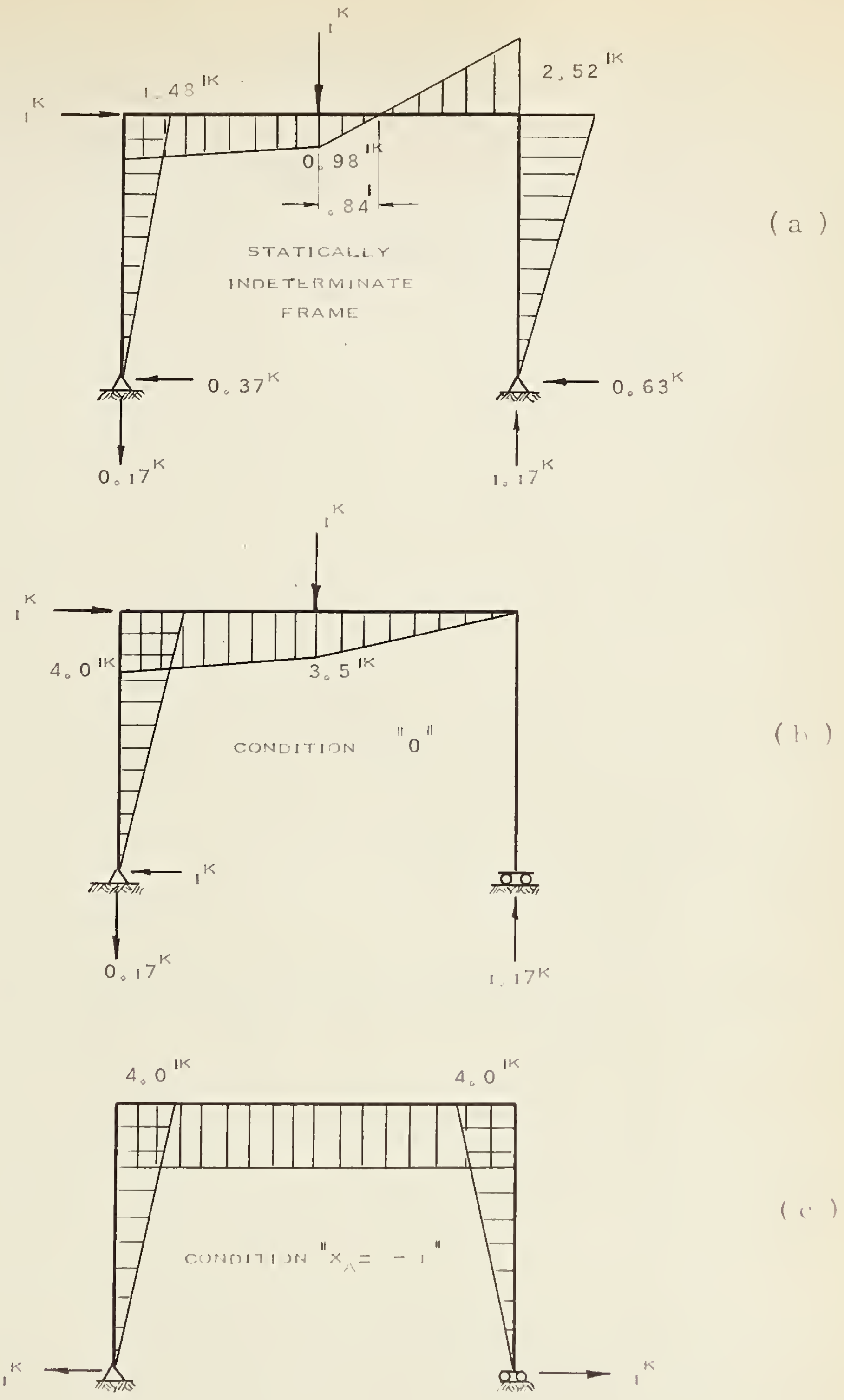

MOMENTS AND REACTIONS FOR UNIT LOAD
FRAME NO. 3

FIGURE A8

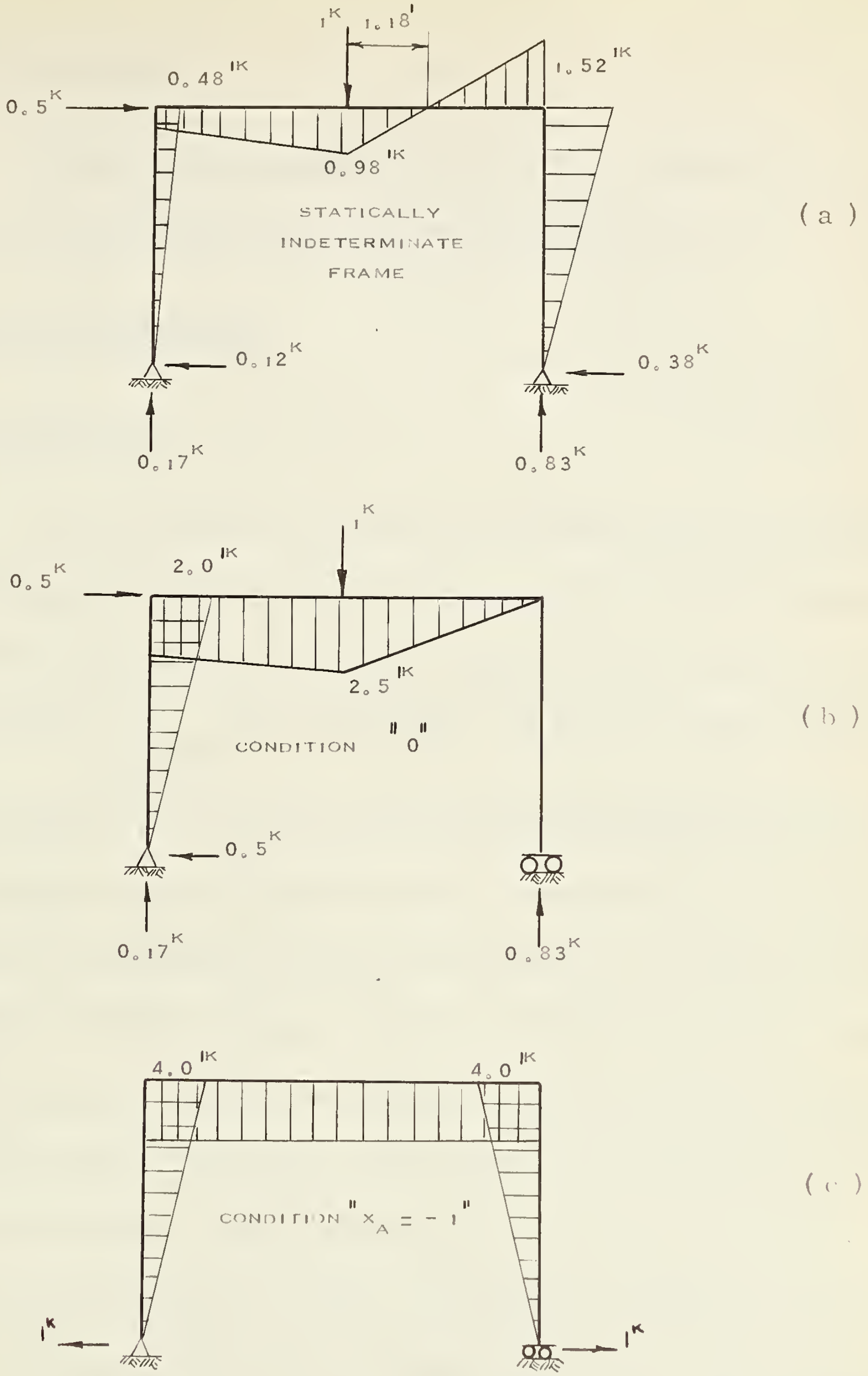

MOMENTS AND REACTIONS FOR UNIT LOAD
FRAME NO. 4

FIGURE A9

d) Frame No. 4

Reactions and moments for Frame No. 4 loaded with a vertical to horizontal load ratio of 2:1 are shown in FIGURE A9.

A-4 Deflection Calculations

a) Frame No. 1

The first plastic hinge will form in this frame at the midspan since the largest bending moment (0.98 foot-kips), for the unit loading, occurs at this section (FIGURE A6(a). This first hinge will form at a predicted load of $\frac{170}{0.98 \times 12} \times 1$ or 14.45 kips. The vertical deflection at the beam midspan for the 14.45 kip load can be determined using the moment diagram shown in FIGURE A6(a). The moments for this load are obtained by multiplying the coefficients shown in this figure by 14.45 kips to obtain the final moments as shown in FIGURE A10(a). By equating the external work done by the unit load in moving through the deflection caused by the 14.45 kip load, to the internal work done by the unit load moments during the same deflection, the value for the vertical deflection at the midspan of the beam, using Müller Breslau tables is:

$$\delta_v \times EI = \frac{2 \times 4 \times 0.52 \times 7.51}{3} + \frac{2 \times 1.04 \times 0.52 \times 7.51}{3} + \frac{3.92 \times 14.15 \times 0.98}{3}$$

$$= 10.4 + 2.71 + 18.1 = 31.21$$

$$\delta_v = \frac{31.21 \times 1728}{29.35 \times 10^3 \times 7.13} = .258'' \qquad \begin{array}{l} E = 29.35 \times 10^3 \text{ ksi (coupon tests)} \\ I = 7.13 \text{ in.}^4 \end{array}$$

The theoretical deflection at the midspan of the beam when the first plastic hinge forms is thus 0.258 inches.

Deflection at the beam midspan at the predicted ultimate load of 18.9 kips has been calculated using slope-deflection equations. The moment diagram for the ultimate load, and a free-body diagram for the frame at ultimate load is shown in FIGURES A10(b) and A10(c), respectively. The slope-deflection equations necessary to solve for the vertical deflection at the ultimate load are as follows:

$$\Theta_{21} = O + O + \frac{2L}{3 \text{x} 3 \; EI} (+M_p) = \frac{2 M_p L}{9 \; EI}$$

$$\Theta_{23} = O + \frac{2\delta v}{L} + \frac{L}{2 \text{x} 3 \; EI} \left(-M_p + \frac{M_p}{2}\right) = \frac{2\delta v}{L} - \frac{M_p \; L}{12 \; EI}$$

$$\Theta_{43} = O - \frac{2\delta v}{L} + \frac{L}{2 \text{x} 3 \; EI} \left(+M_p - \frac{M_p}{2}\right) = -\frac{2\delta v}{L} + \frac{M_p \; L}{12 \; EI}$$

$$\Theta_{45} = O + O + \frac{2L}{3 \text{x} 3 \; EI} (-M_p - O) = \frac{-2 M_p L}{9 \; EI}$$

Clockwise moment and angle change are considered positive. Plastic hinges form simultaneously at sections 2 and 4 to complete the mechanism at ultimate load. Immediately before the formation of these two hinges, continuity still exists at both sections. Therefore, $\Theta_{21} = \Theta_{23}$ and $\Theta_{34} = \Theta_{43}$ just before the collapse mechanism is formed. Equating $\Theta_{21} = \Theta_{23}$ gives:

$$\frac{2 M_p L}{9 \; EI} = \frac{2\delta v}{L} - \frac{M_p L}{12 \; EI}$$

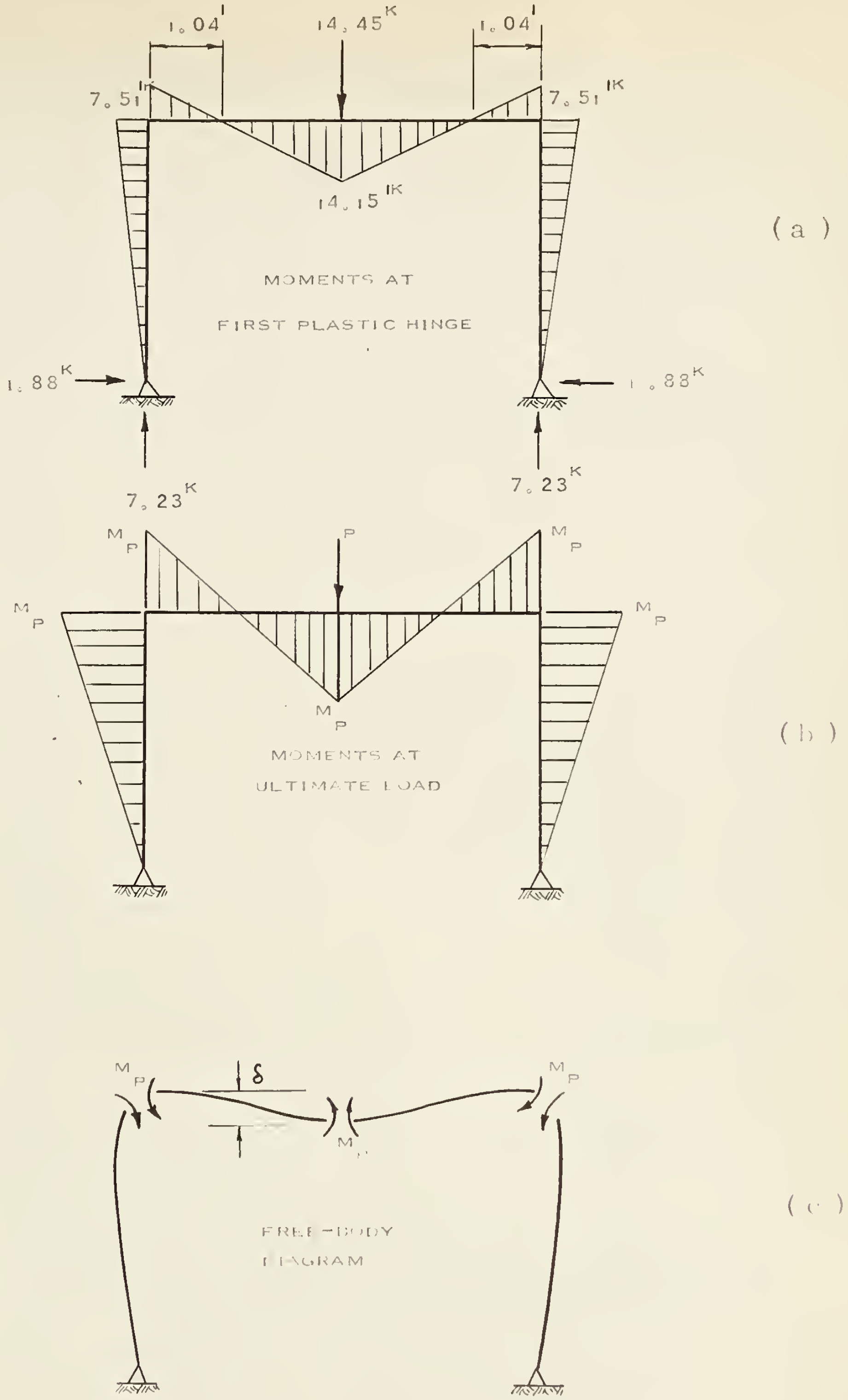

DEFLECTION ANALYSIS

FRAME NO. 1

FIGURE A10

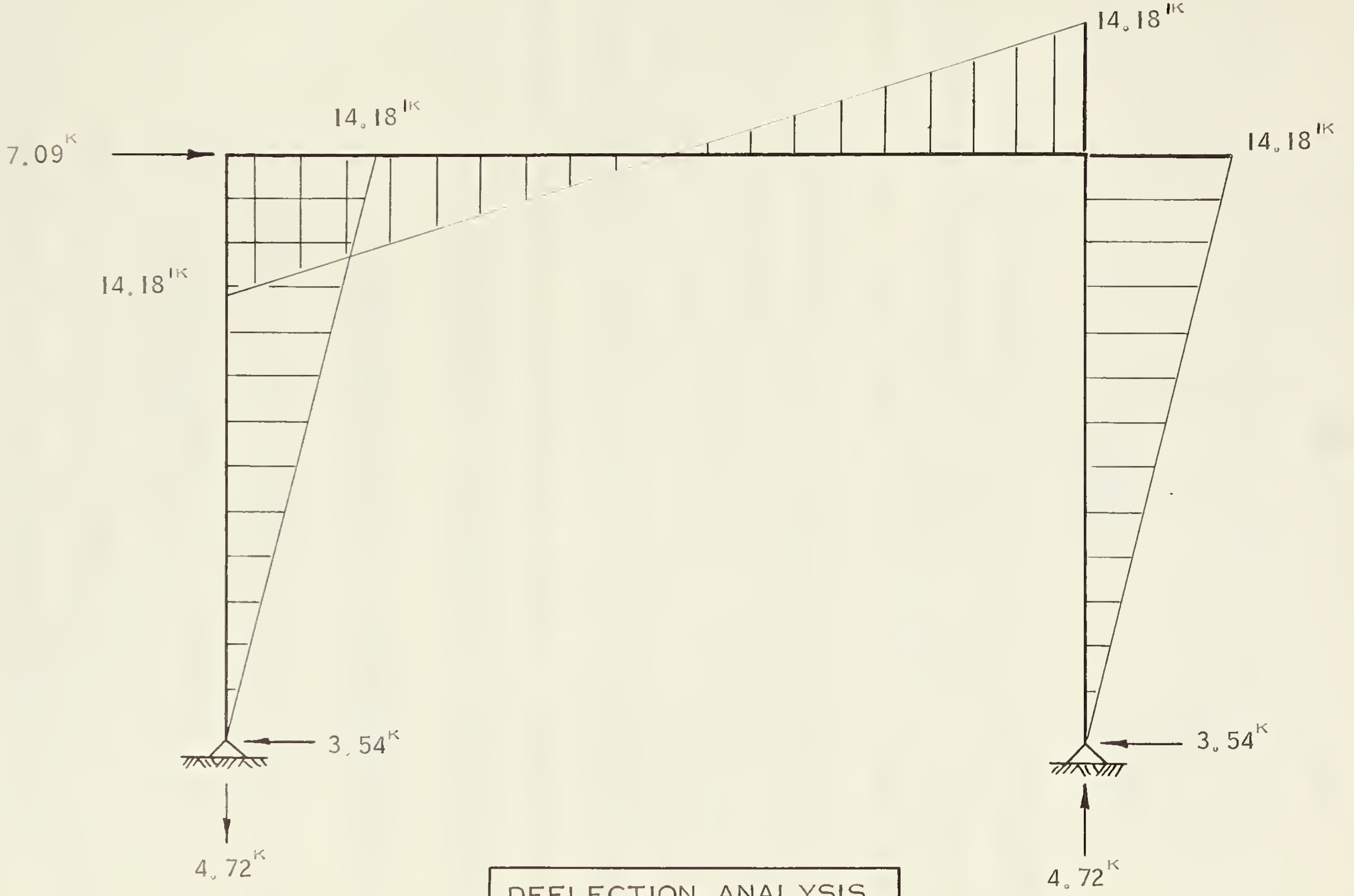

DEFLECTION ANALYSIS
FRAME NO. 2

FIGURE A11

c) Frame No. 3

The first plastic hinge will form in this frame at the top of the right column since the largest bending moment (2.52 foot-kips), for the unit loading, occurs at this section (FIGURE A8(a)). This first hinge will form at a predicted load of $\frac{170}{2.52 \times 12} \times 1$ or, 5.61 kips.

Deflections prior to the formation of the first plastic hinge are readily calculated using the virtual work theory. Moments and reactions for the 5.61 kips load were obtained by multiplying all values shown in FIGURE A8(a) by 5.61. By equating the external work done by the unit load in moving through the horizontal deflection caused by the 5.61 kips load, to the internal work done by the unit load moments during the same deflection, the following value for the horizontal deflection, at the top of the columns, is obtained using Müller Breslau tables:

$$\delta_h \times EI = \frac{4 \times 8.31 \times 2}{3} + \frac{4 \times 14.15 \times 2}{3} + \frac{3 \times 2 \times 22.12}{6}$$

$$- \frac{0.84 \times 5.50 \times 0.56}{6} + \frac{2.16 \times 14.15 \times 4.56}{6}$$

$$= 22.2 + 37.7 + 22.12 - 0.43 + 23.2 = 104.8$$

$$\delta_h = \frac{104.8 \times 1728}{29.35 \times 10^3 \times 7.13} = 0.865 \text{ inches.}$$

Thus, the theoretical horizontal deflection at the top of the columns when the first plastic hinge forms is 0.865 inches.

The theoretical vertical deflection at the midspan of the beam

[illegible]

[illegible]

$$[illegible]$$

[illegible]

$$[illegible]$$

$$[illegible]$$

[illegible]

at the formation of the first plastic hinge is calculated in the same manner. By equating the external work done by the unit load in moving through the vertical deflection caused by the 5.61 kips load, to the internal work done by the unit load moments during the same deflection, the following value for the vertical deflection, at the midspan of the beam, is found:

$$\begin{aligned}
\delta_v \times EI &= \frac{-4 \times 8.31 \times 0.52}{3} - \frac{1.04 \times 0.52\ (16.62 + 7.34)}{6} \\
&\quad + \frac{1.96 \times 0.98\ (11.0 + 7.34)}{6} + \frac{0.84 \times 5.50\ (1.96 + 0.56)}{6} \\
&\quad - \frac{1.12 \times 0.56 \times 7.33}{6} + \frac{1.04 \times 0.52\ (28.30 + 7.33)}{6} \\
&\quad + \frac{4 \times 0.52 \times 14.15}{3} \\
&= -5.75 - 2.16 + 5.87 + 1.94 - 0.77 + 3.21 + 9.81 \\
&= 12.15
\end{aligned}$$

$$\delta_v = \frac{12.15 \times 1728}{29.35 \times 10^3 \times 7.13} = 0.10 \text{ inches.}$$

Thus, the theoretical deflection at beam midspan when the first plastic hinge forms is 0.10 inches.

Deflections at ultimate load are calculated using the slope-deflection equations. FIGURE A13(a) shows the bending moments in the frame at ultimate load, determined previously by the ultimate load analysis. A free-body diagram of the frame is shown in FIGURE A13(b).

The slope-deflection equations required in the solution of the

horizontal and vertical deflections at ultimate load are as follows:

$$\Theta_{21} = O + \frac{3\delta h}{2L} + \frac{2L}{3 \times 3\ EI} \quad (-M_p - O)$$

$$= \frac{3\delta h}{2L} - \frac{2\ M_p L}{9\ EI}$$

$$\Theta_{23} = O + \frac{2\delta v}{L} + \frac{L}{2 \times 3\ EI} \quad \left(M_p + \frac{3\ M_p}{8}\right)$$

$$= \frac{2\delta v}{L} + \frac{11\ M_p L}{48\ EI}$$

$$\Theta_{32} = O + \frac{2\delta v}{L} + \frac{L}{2 \times 3\ EI} \quad \left(-\frac{3}{4} M_p - \frac{M_p}{2}\right)$$

$$= \frac{2\delta v}{L} - \frac{5\ M_p L}{24\ EI}$$

$$\Theta_{34} = O - \frac{2\delta v}{L} + \frac{L}{2 \times 3\ EI} \quad \left(\frac{3\ M_p}{4} - \frac{M_p}{2}\right)$$

$$= \frac{-2\delta v}{L} + \frac{M_p L}{24\ EI}$$

No plastic hinge forms at section 3 so $\Theta_{32} = \Theta_{34}$

$$\frac{2\delta v}{L} - \frac{5\ M_p L}{24\ EI} = \frac{-2\delta v}{L} + \frac{M_p L}{24\ EI}$$

$$\delta_v = \frac{M_p L^2}{16\ EI}$$

$$= \frac{170 \times 72 \times 72}{16 \times 29.35 \times 10^3 \times 7.13} = 0.263 \text{ inches}$$

The theoretical vertical deflection when the collapse mechanism just forms, is thus 0.263 inches.

From FIGURE A9(a), it can be readily determined that the plastic hinge at section 2 will be the last one to form in the collapse

mechanism. Just prior to the formation of this hinge, continuity must exist at section 2, and:

$$\theta_{21} = \theta_{23}$$

$$\frac{3\delta h}{2L} - \frac{2\,M_p\,L}{9\;E\,I} = \frac{2\delta v}{L} + \frac{11\,M_p\,L}{48\;E\,I}$$

with $\delta_v = \frac{M_p\,L^2}{16\;E\,I}$, then:

$$\frac{3\delta h}{2L} = \frac{83\,M_p\,L}{144\;E\,I}$$

$$\delta_h = \frac{83 \times 2 \times 72 \times 72 \times 170}{3 \times 144 \times 29.35 \times 10^3 \times 7.13} = 1.62 \text{ inches.}$$

The theoretical horizontal deflection when the collapse mechanism just forms is thus 1.62 inches.

d) Frame No. 4

The first plastic hinge forms in this frame at section 4, FIGURE A10(a) since the largest bending moment (1.52 foot-kips) for the unit loading acts at this section. The first plastic hinge forms at a predicted vertical load of $\frac{170}{1.52\text{x}12}$ x 1 = 9.32 kips, and thus, at a horizontal load of 4.66 kips.

Deflections prior to the formation of the first plastic hinge are calculated using the virtual work theory. Moments and reactions for the 9.32 kips load were obtained by multiplying all values shown in

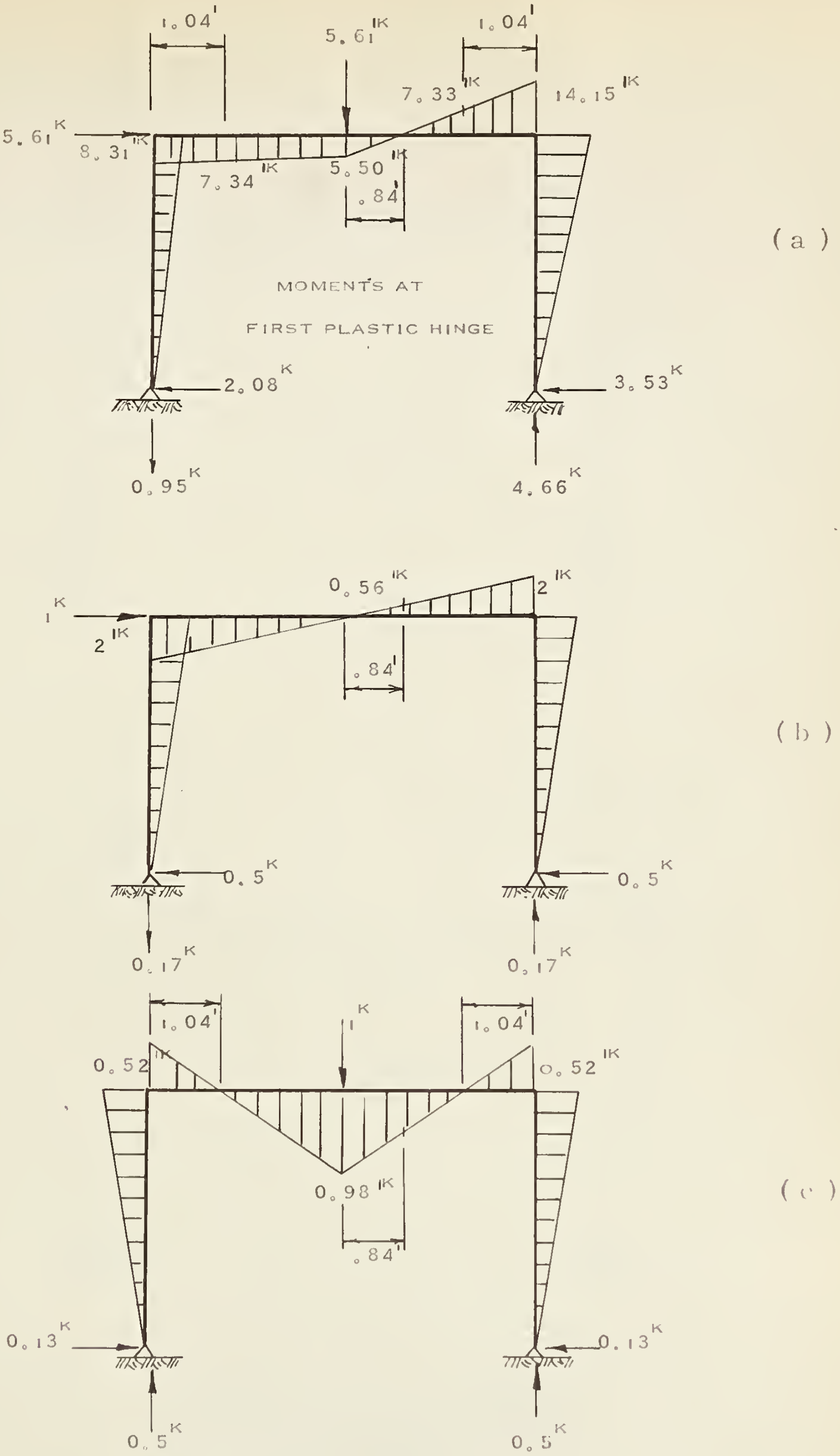

DEFLECTION ANALYSIS
FRAME NO. 3

FIGURE A12

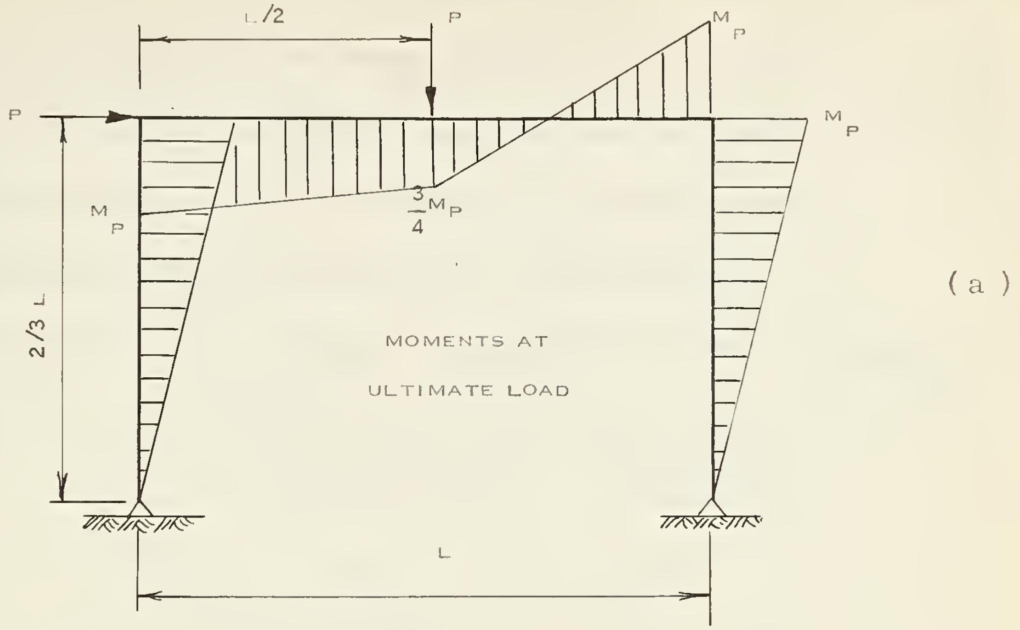

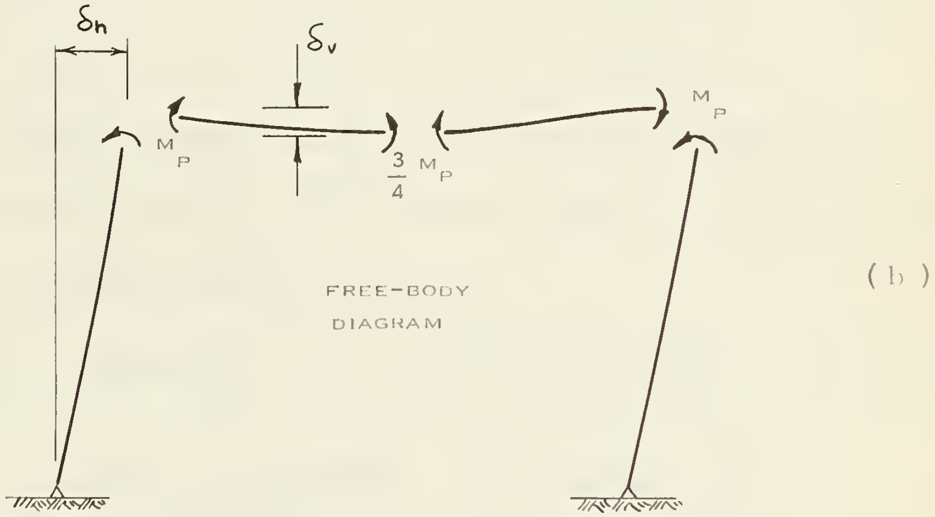

DEFLECTION ANALYSIS
FRAME NO. 3

FIGURE A13

FIGURE A10(a) by 9.32. By equating the external work done by the unit load in moving through the horizontal deflection caused by the 9.32 kips load, to the internal work done by the unit load moments during the same deflection, the following value for the horizontal deflection, at the top of the columns is obtained, using Müller Breslau tables:

$$\delta_h \times EI = \frac{4 \times 4.47 \times 2}{3} + \frac{3 \times 2}{6}(8.94 + 9.13) - \frac{1.18 \times 9.13 \times 0.79}{6}$$

$$+ \frac{1.82 \times 14.15 \times 4.79}{6} + \frac{4 \times 14.15 \times 2}{3}$$

$$= 11.9 + 18.07 - 1.42 + 20.55 + 37.7 = 86.8$$

$$\delta_h = \frac{86.8 \times 1728}{29.35 \times 10^3 \times 7.13} = 0.716 \text{ inches.}$$

The theoretical horizontal deflection at the top of the columns when the first plastic hinge forms is therefore 0.716 inches.

The theoretical vertical deflection at the midspan of the beam immediately prior to the formation of the first plastic hinge is calculated in a similar manner to that of Frame No. 3:

$$\delta_v \times EI = \frac{-4 \times 0.52 \times 4.47}{3} - \frac{1.04 \times 0.52 \times 15.02}{6} + \frac{1.96 \times 0.98 \times 24.34}{6}$$

$$+ \frac{1.18 \times 9.13 \times 2.35}{6} - \frac{0.78 \times 0.39 \times 6.06}{6}$$

$$+ \frac{1.04 \times 0.52 \times 34.36}{6} + \frac{4 \times 0.52 \times 14.15}{3}$$

$$= -3.10 - 1.35 + 7.78 + 4.21 - 0.31 + 3.09 + 9.80 = 20.12$$

$$\delta_v = \frac{20.12 \times 1728}{29.35 \times 10^3 \times 7.13} = 0.166 \text{ inches.}$$

The theoretical vertical deflection at the midspan of the beam when the first plastic hinge forms is therefore 0.166 inches.

Theoretical deflections at ultimate load are calculated using the slope-deflection equations. The moment diagram for the ultimate load, and a free-body diagram for the frame at ultimate load are shown in FIGURES A15(a) and A15(b). The slope-deflection equations required in the solution of the vertical and horizontal deflections are as follows:

$$\Theta_{21} = O + \frac{3\delta h}{2L} + \frac{L}{3x3\ E\,I}\left(-\frac{3}{5}M_p - O\right)$$

$$= \frac{3\delta h}{2L} - \frac{2\ M_p\,L}{15\ E\,I}$$

$$\Theta_{23} = O + \frac{2\delta v}{L} + \frac{L}{2x3\ E\,I}\left(+\frac{3}{5}M_p + \frac{M_p}{2}\right)$$

$$= \frac{2\delta v}{L} + \frac{11\ M_p\,L}{60\ E\,I}$$

$$\Theta_{32} = O + \frac{2\delta v}{L} + \frac{L}{2x3\ E\,I}\left(-M_p - \frac{3M_p}{10}\right)$$

$$= \frac{2\delta v}{L} - \frac{13\ M_p\,L}{60\ E\,I}$$

$$\Theta_{34} = O - \frac{2\delta v}{L} + \frac{L}{2x3\ E\,I}\left(M_p - \frac{M_p}{2}\right)$$

$$= \frac{2\delta v}{L} + \frac{M_p\,L}{12\ E\,I}$$

It can be seen from FIGURE A10(a) that the last plastic hinge forms at section 3. Just prior to the formation of this hinge, continuity must exist at this section, and,

$$\Theta_{32} = \Theta_{34}$$

$$\frac{2\delta_v}{L} - \frac{13\,M_pL}{60\;EI} = \frac{-2\delta_v}{L} + \frac{M_pL}{12\;EI}$$

$$\delta_v = \frac{3\,M_p\,L^2}{40\;EI}$$

$$= \frac{3 \times 170 \times 72 \times 72}{40 \times 29.35 \times 10^3 \times 7.13} = 0.316 \text{ inches.}$$

Therefore, the theoretical vertical deflection at the midspan of the beam when the collapse mechanism forms is 0.316 inches.

No plastic hinge forms at section 2, therefore $\Theta_{21} = \Theta_{23}$:

$$\frac{3\delta_h}{2L} - \frac{2\,M_p\,L}{15\;EI} = \frac{2\delta_v}{L} + \frac{11\,M_p\,L}{60\;EI}$$

but $\delta_v = \dfrac{3\,M_p\,L^2}{40\;EI}$

Therefore $\delta_h = \dfrac{14\,M_p\,L^2}{45\;EI}$

$$\delta_h = \frac{14 \times 170 \times 72 \times 72}{45 \times 29.35 \times 10^3 \times 7.13} = 1.31 \text{ inches.}$$

Therefore, the theoretical horizontal deflection when the collapse mechanism just forms is 1.31 inches.

e) Beams

The deflection at the midspan of a simply-supported beam with two equal concentrated loads symmetrically placed, is given by the expression:

$$\delta = \frac{P\,a}{24\;EI}\left(3\,L^2 - 4\,a^2\right)$$

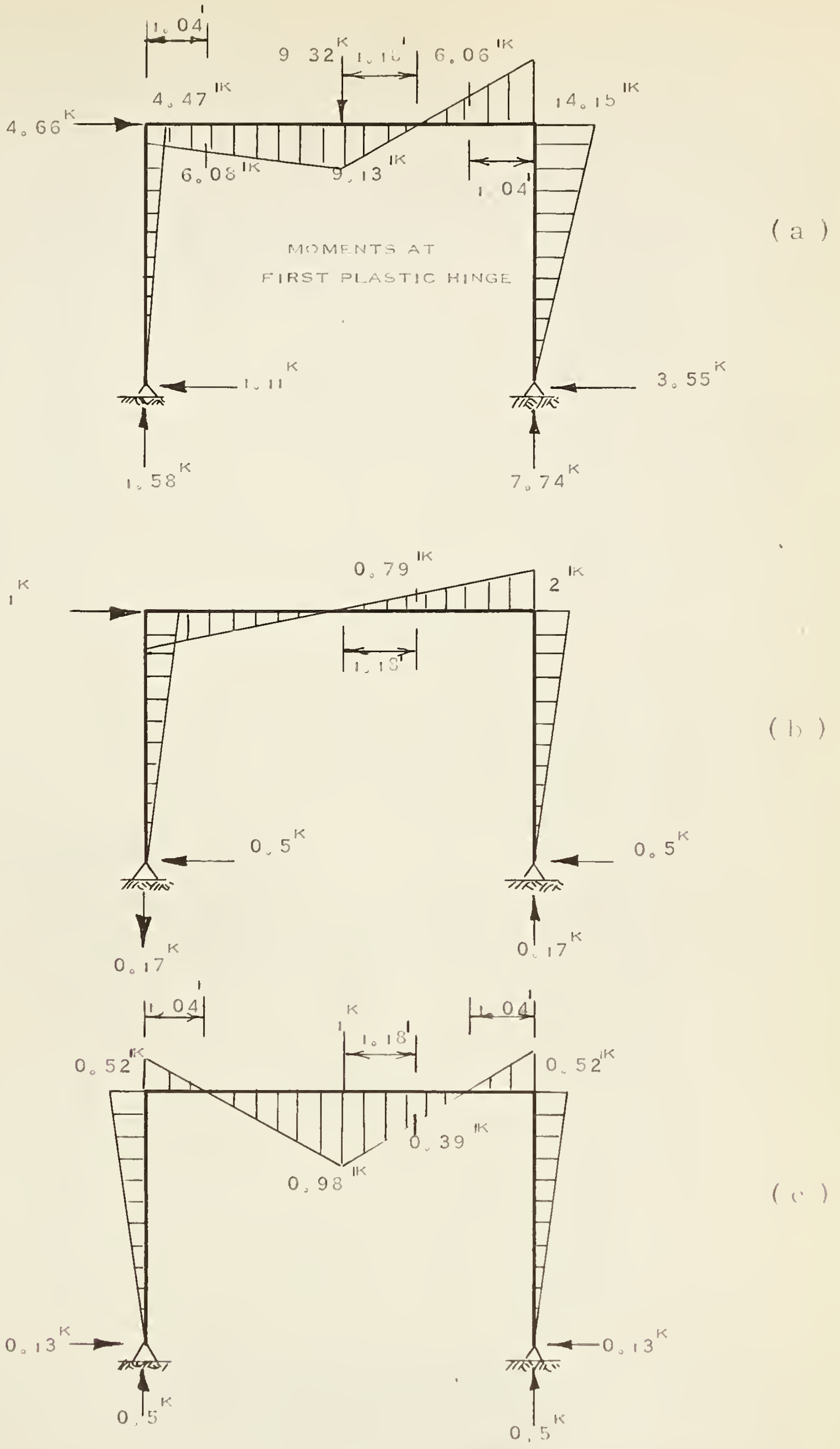

DEFLECTION ANALYSIS
FRAME NO. 4

FIGURE A14

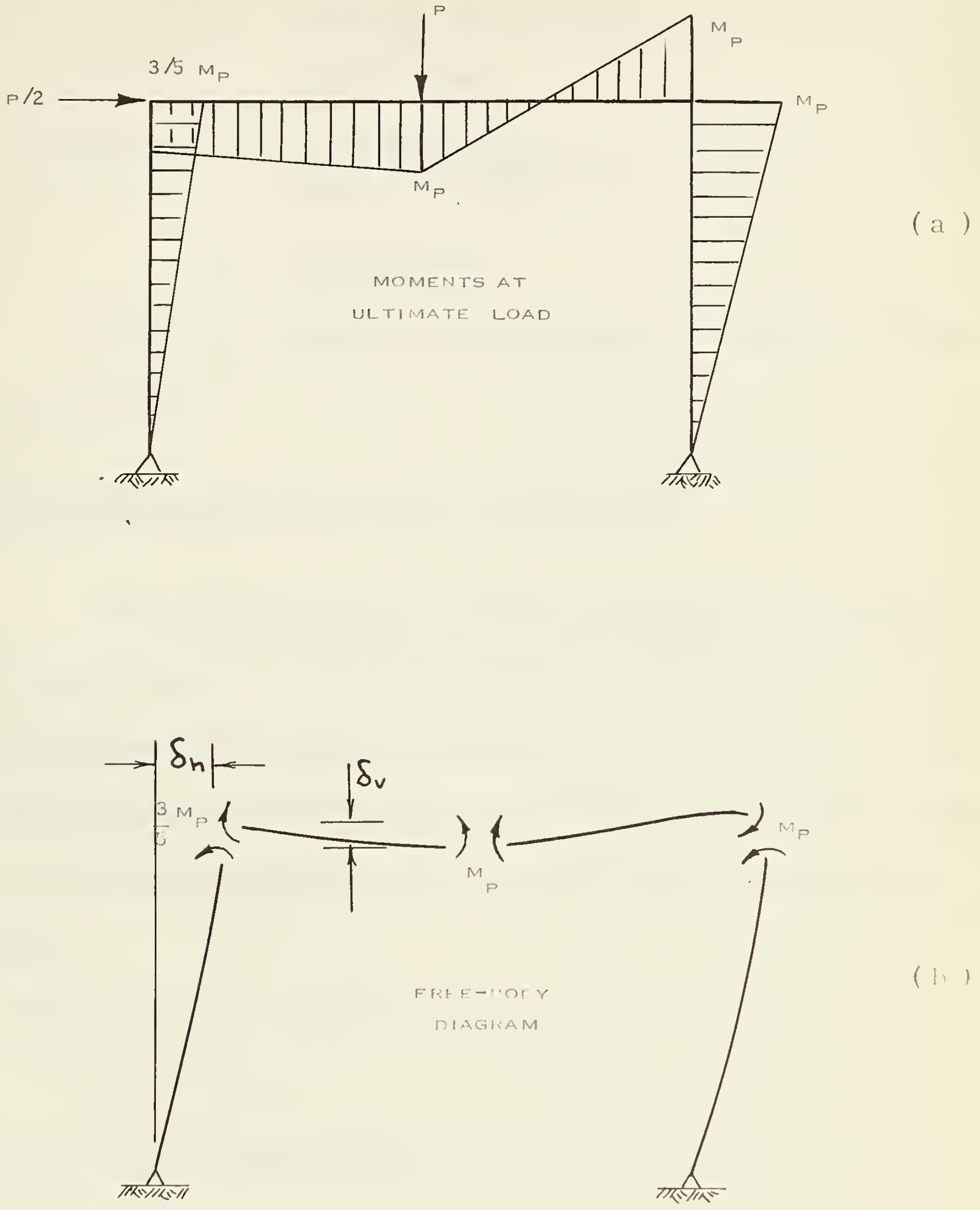

DEFLECTION ANALYSIS
FRAME NO. 4

FIGURE A15

where: L = length of beam

a = distance from one support to the position of the first load

$$\text{Therefore } \delta = \frac{12.60 \times 13.5}{24 \times 29.35 \times 10^3 \times 7.13} \left(3 \times 45^2 - 4 \times 13.5^2 \right)$$

$$= 0.181 \text{ inches.}$$

Therefore, the theoretical deflection at midspan at ultimate load is 0.181 inches.

A-5 Theoretical Moment-Curvature Relationship

The idealized moment-curvature diagram for the 4 I 9.5 section, neglecting strain-hardening, is calculated on the basis of an assumed stress-strain diagram consisting of two straight lines. The calculation of two pairs of M and ϕ values, plus a third limiting M value which satisfactorily determines the moment-curvature relationship, are as follows:

i) Initial yield at outer fibers

$$M_y = \sigma_y S$$

$$= 41,100 \times 3.47$$

$$= 143 \text{ inch-kips}$$

$$\phi_y = \frac{\sigma_y}{d/2} = \frac{2\sigma_y}{E\,d} = \frac{2 \times 41,100}{29.35 \times 10^6 \times 4.11} = 0.681 \times 10^{-3} \text{ rad.}$$

ii) Complete plastification of flanges:

$$M = \sigma_y Z - \frac{1}{3} \sigma_y Z_2$$

where, Z_2 = Statical moment of elastic portion (the web)

$= w\, y_2^2$

w = width of web

y_2 = distance from N.A. to juncture of web and fillets

$$M = 41,100 \times 4.13 - \frac{1}{3} \times 41,100 \times 0.329 \times 1.77^2$$

$= 155.9$ inch-kips

$$\phi = \frac{41,100}{29.35 \times 10^6 \times 1.77} = 0.792 \times 10^{-3} \text{ rad.}$$

iii) Complete plastification of section

$$M_p = \sigma_y Z$$

$= 41,100 \times 4.13$

$= 170$ inch-kips

$$\phi_p = \infty$$

A-6 Calculated Moment-Curvature Relationships

The calculated moment at the midspan of the beam for Frame No. 1 is given by the following expression:

$$M = V_1 \times 36 - H_1 \times 48 + H_1 \times \delta_v$$

where: V_1 = the assumed vertical reaction at the left support ($V_1 = P/2$)

H_1 = the measured horizontal reaction

δ_v = deflection at midspan

36 = one-half of the beam length

48 = column height

The horizontal reaction H_1 is carried by the beam as an axial compressive force. In the plastic range, the beam deflection δ_v becomes larger and the additional beam moment due to this axial force can no longer be neglected.

At the knees of Frame No. 1, the calculated moment is given by:

$$M = H(48-5) = 43H$$

where: H = the measured horizontal reaction

48 = column height

5 = distance from beam centerline to the point at which rotation was measured.

The moments for the remaining three frames were calculated in a manner similar to the above. Corrections due to the measured deflections were made where necessary. In all cases, curvatures were calculated by using the formulas given in Chapters VI and VII. Values for moment at the midspan for the beam tests were calculated by

multiplying the load P by the moment arm of 13.5 inches.

8-7 Calculated Horizontal Reactions

The horizontal reaction at the left support for Frame No. 4 was calculated from the following expression:

$$H_L = \frac{M - V_1 \delta_2}{36}$$

where: H_L = horizontal reaction value to be computed for a given load

M = the value of moment obtained from the strain gauge readings

36 = distance from the pinned-end to the location of the gauges

V_1 = vertical reaction at the left support

δ_2 = horizontal deflection at the location of the strain gauges

$= \frac{36}{48} \delta$, where δ equals the measured horizontal deflection at the top of the column

The vertical reaction at the left support was calculated from the expression given by:

$$V_1 = \frac{M_{℄} - M_L}{36}$$

where: $M_{\mathfrak{L}}$ = the value of moment at the beam midspan obtained from the rotation indicator readings

M_L = the value of moment at the left end of the beam obtained from the rotation indicator readings

36 = one-half of the beam length

A similar calculation to the above was made to compute the horizontal reaction from readings taken from the strain gauges mounted at a distance of 27 inches from the pinned-end. The final value for a given load, was then obtained by averaging the two results.

The above formulas were included only as an illustration of the method used to determine the horizontal reaction at the left column of Frame No. 4. The reaction at the right column, as well as the horizontal reactions for the other frames tested, were calculated in a similar manner. Slight modifications to the above formulas were made where necessary.

APPENDIX B

CALCULATIONS BASED ON MOMENT END-SLOPE RELATIONSHIPS

B-1 Moment-Curvature Relationship

For the 4 I 9.5 section, the value for the moment (M) is expressed in dimensionless form as:

$$\frac{M}{M_{fp}} = 1.334\ N + 0.666\ \frac{\sigma_{f1}}{\sigma_y}$$

where: $N = \dfrac{\text{moment contributed by the web}}{\sigma_y\ A_w\ d}$

M_{fp} = fully-plastic moment

A_w = area of web

d = depth of section = 4.114 inches

σ_y = static level of yield stress

σ_{f1} = average stress in the flange

As a sample computation, consider the case where $e/e_y = 1.0$, i.e. $\phi/\phi_y = 1.0$. From FIGURE 11, $\sigma/\sigma_y = 1.0$, and, by a simple calculation, the average stress in the flange, σ_{f1} is thus computed to be $0.93\ \sigma_y$. Therefore,

$$N = \frac{\sigma_y}{2} \times \frac{A_w}{2} \times \frac{2}{3} \times \frac{2.057 \times 2}{\sigma_y \times A_w \times 4.114}$$

$$= 1/6$$

Hence, $$\frac{M}{M_{fp}} = 1.334 \times \frac{1}{6} + 0.666 \times 0.93 \frac{\sigma_y}{\sigma_y}$$
$$= 0.843,$$

Thus, the ratio M/M_{fp} is equal to 0.843 when the ratio of the total curvature, ϕ, to the curvature at which first yield occurs, ϕ_y, is 1.0. This relatively simple procedure was used to obtain the plot shown in FIGURE 10.

B-2 Deflection Calculations

In this section, sample load-deflection calculations based on the "moment end-slope" relationships are presented for the beam and for Frame Nos. 1 and 2. Only one calculation for each case is given, since all load-deflection values covering a desired range are obtained in a similar manner. Joints are assumed rigid in all cases.

a) Beams

The beam shown in FIGURE B1(a) is subjected to two equally applied loads such that a region of pure moment is achieved in the central portion. The assumed deformed shape is given in FIGURE B1(b). Since the beam is statically determinate, a relatively simple procedure is used to obtain deflection values at the centerline. To illustrate this procedure, a value for deflection will be determined for a load of 15.0 kips, using the "moment end-slope" relationships

derived from the beam tests. For the 4I 9.5 section, the following properties are noted:

$I = 7.13 \text{ in.}^4$ $\qquad \sigma_y = 41,100 \text{ psi}$

$S.F. = 1.19$ $\qquad E = 29.35 \times 10^6 \text{ psi}$

$S = 3.47 \text{ in.}^3$ $\qquad M_{fp} = 180$ inch-kips (experimental)

$M_y = 153$ inch-kips (experimental)

The elastic limit angle-changes for the beam components are:

$$\theta_y^{BC} = \theta_y^{CB} = \frac{M_y L}{2EI} = \frac{153 \times 9}{2 \times 29.35 \times 10^3 \times 7.13}$$

$$= 0.00329 \text{ rad.} = \theta_y^{\circ}$$

$$\theta_y^{AB} = \theta_y^{BA} = \frac{M_y L}{2EI} = \frac{153 \times 13.5}{2 \times 29.35 \times 10^3 \times 7.13}$$

$$= 0.00494 \text{ rad.} = 1.5\,\theta_y^{\circ}$$

For a load of 15.0 kips, the resulting moment at B is $15 \times 13.5 = 202$ inch-kips $= 1.11\, M_{fp}$. Referring to FIGURE B1(b), the equilibrium and continuity requirements at joint B are, respectively,

$$M_{BA} = M_{BC} \quad \ldots\ldots\ldots\ldots\ldots\ldots (8)$$

$$\text{and} \quad \Omega_{BA} = \Omega_{BC} \quad \ldots\ldots\ldots\ldots\ldots\ldots (9)$$

$$\text{Since,} \quad \Omega_{CB} = 0, \qquad \psi_{CB} = \alpha_{CB}$$

$$\text{But,} \quad \psi_{CB} = \psi_{BC} = \alpha_{CB}$$

$$\text{Therefore,} \quad \Omega_{BC} = \alpha_{CB} + \alpha_{BC} \quad \ldots\ldots\ldots\ldots (9a)$$

Both CB and BA have single curvature, therefore FIGURE 16 is used to obtain the "moment end-slope" relationships. For CB,

FIGURE 16 is entered with $M_{ij} = M_{CB} = 1.11\ M_{fp}$ and $M_{ji} = M_{BC} = 1.11\ M_{fp}$. The end-slope corresponding to these moments as given in FIGURE 16 is $\alpha_{ij} = \alpha_{CB} = 13.0\ \theta_y^{CB} = 13.0\ \theta_y^{\circ}$. Since the total joint rotation at the centerline is zero, columns (6) and (7) of Table B are also zero. For member BC, FIGURE 16 is entered with $M_{ij} = M_{BC} = 1.11\ M_{fp}$ and $M_{ji} = M_{CB} = 1.11\ M_{fp}$. The end-slope corresponding to these moments as given by FIGURE 16 is $\alpha_{ij} = \alpha_{BC} = 13.0\ \theta_y^{BC} = 13.0\ \theta_y^{\circ}$. This of course is the same result as obtained above. Hence, by Equation (9a), $\Omega_{ij}/\theta_y^{ij} = \Omega_{BC}/\theta_y^{BC} = 26.0$. The value for $\Omega_{BC}/\theta_y^{\circ}$ is also equal to 26.0 since $\theta_y^{BC} = \theta_y^{\circ}$. In addition, to satisfy equation (9), $\Omega_{BA}/\theta_y^{\circ} = 26.0$ for member BA. But since $\theta_y^{BA} = 1.5\ \theta_y^{\circ}$, $\Omega_{BA}/\theta_y^{BA} = 26.0/1.5 = 17.3$. To complete the analysis for member BA, FIGURE 16 is entered with $M_{ij} = M_{BA} = 1.11\ M_{fp}$ and $M_{ji} = M_{AB} = 0$. The resultant end-slope is thus determined as $\alpha_{ij} = \alpha_{BA} = 2.55\ \theta_y^{BA}$. The derived end-slopes α_{BA} and α_{BC} are then used to obtain the deflection at beam midspan. Since the chord rotation $\psi_{BA} = \Omega_{BA} + \alpha_{BA}$, $\delta_1 = \psi_{BA} \times L_{BA} \times \theta_y^{BA} = (17.3 + 2.55) \times 13.5 \times 0.00494 = 1.32$ inches. Similarly, $\psi_{BC} = \Omega_{BC} - \alpha_{BC}$, and $\delta_2 = \psi_{BC} \times L_{BC} \times \theta_y^{BC} = (26.0 - 13.0) \times 9 \times 0.00329 = 0.385$ inches. Thus, for a load of 15.0 kips, the theoretical deflection at beam midspan is $(1.32 + 0.385) = 1.705$ inches.

An identical precedure is used to obtain the desired number of points for the entire load-deflection curve.

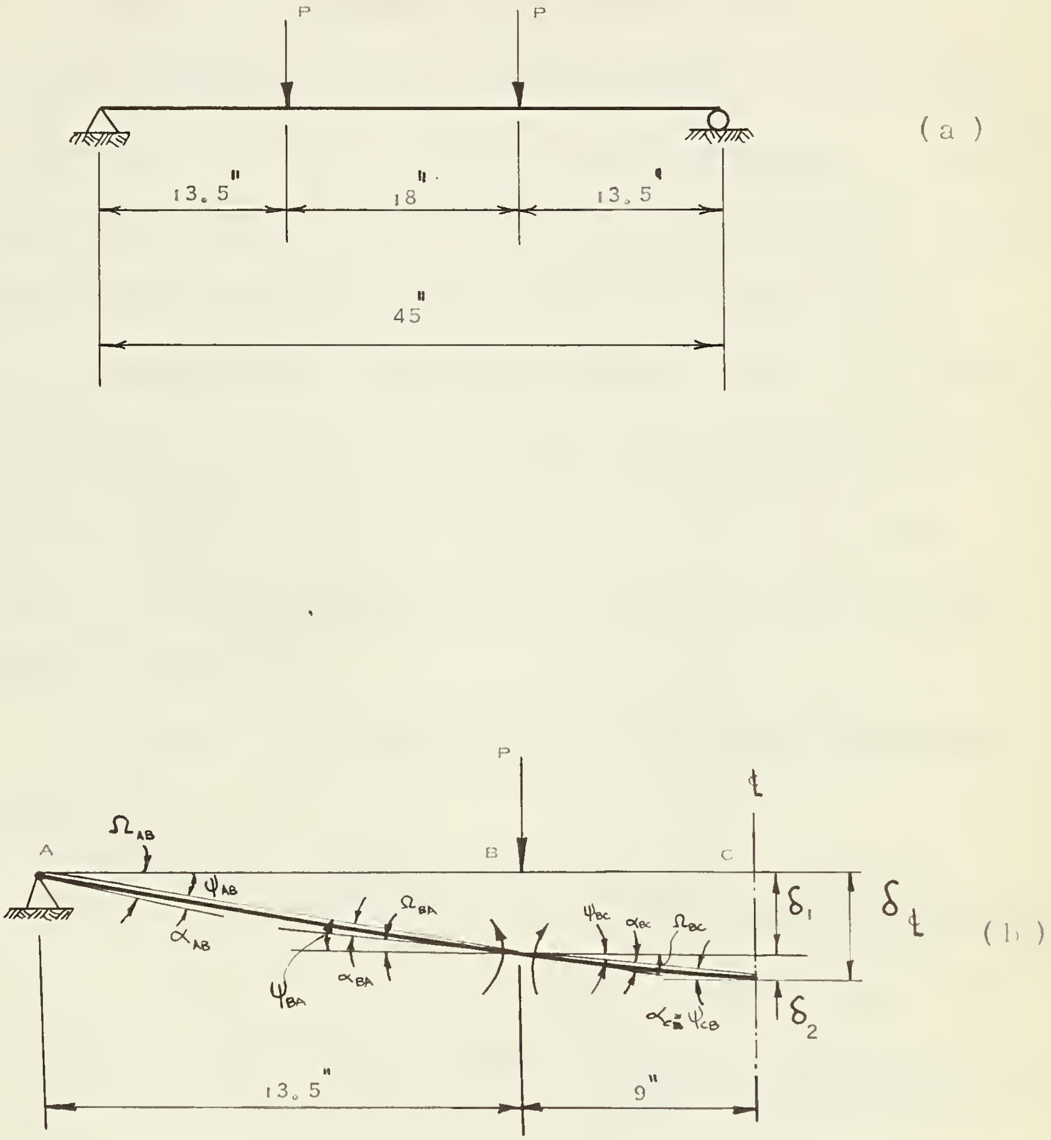

MOMENTS AND DEFORMATIONS FOR BEAM ANALYSIS

FIGURE BI

b) Frame No. 1

Frame No. 1, which was subjected to a concentrated vertical load at midspan, is shown in FIGURE B2(a). The deflected shape of the structure and the correct directions of moments are shown in FIGURE B2(b). The procedure used to determine theoretical values for load-deflection is opposite to that used for the beams in that a deflection is first assumed, rather than a value for load. To illustrate, an assumed value of 3.0 inches as the deflection at midspan will be used with the "moment end-slope" relationships derived from the tension tests. The corresponding values for M_y and M_{fp} are 143 and 170 inch-kips, respectively.

The elastic limit angle-changes for the frame components are as follows:

$$\theta_y^{BC} = \theta_y^{CB} = \theta_y^{CD} = \theta_y^{DC} = \frac{M_y L}{2\,E\,I} = \frac{143 \times 36}{2 \times 29.35 \times 10^3 \times 7.13}$$

$$= 0.0123 \text{ rad.} = \theta_y^{\circ}.$$

$$\theta_y^{AB} = \theta_y^{BA} = \theta_y^{DE} = \theta_y^{ED} = \frac{M_y L}{2\,E\,I} = \frac{143 \times 48}{2 \times 29.35 \times 10^3 \times 7.13}$$

$$= 0.0164 \text{ rad.} = 1.33\, \theta_y^{\circ}$$

The chord displacement angle, ψ_{BC}, shown in FIGURE B2(b) is:

$$\psi_{BC} = \psi_{CB} = 3.0/36 = 0.0834 \text{ rad.} = 6.77\, \theta_y^{\circ}$$

Referring to FIGURE B2 b, the equilibrium and continuity requirements at joint B are, respectively,

$$M_{BA} = M_{BC} \quad \ldots\ldots\ldots\ldots\ldots\ldots(10)$$

and $$\Omega_{BA} = \Omega_{BC} \quad \ldots\ldots\ldots\ldots\ldots\ldots(11)$$

Equations (10) and (11) are solved simultaneously by trial-and-error. As a first approximation, the Moments at joint B, $M_{BA} = M_{BC}$, are assumed to be 1.15 M_{fp}. These values of the moments automatically satisfy Equation (10), and are checked for Equation (11) as follows. Since member BA has single curvature, FIGURE 15 is used, and moment values of $M_{ij} = M_{BA} = 1.15\ M_{fp}$ and $M_{ji} = M_{AB} = O$, result in a corresponding end-slope $\alpha_{ij} = \alpha_{BA} = 4.21\ \theta_y^{BA}$. The total joint rotation at B, $\Omega_{ij} = \Omega_{BA} = 4.21\ \theta_y^{BA}$ is therefore obtained, since $\Omega_{BA} = \alpha_{BA}$. However, since $\theta_y^{BA} = 1.33\ \theta_y^{\circ}$, $\Omega_{BA}/\theta_y^{\circ} = 4.21 \times 1.33 = 5.61$. For member BC, FIGURE 13 is entered with $M_{ij} = M_{BC} = 1.15\ M_{fp}$, and $M_{ji} = M_{CB}$ is assumed to be 1.32 M_{fp}. The end-slope corresponding to these moments is $\alpha_{ij} = \alpha_{BC} = 1.85\ \theta_y^{BC} = 1.85\ \theta_y^{\circ}$. The total joint rotation $\Omega_{ij} = \Omega_{BC}$ is therefore $\Omega_{BC} = \psi_{BC} - \alpha_{BC} = 6.77\ \theta_y^{\circ} - 1.85\ \theta_y^{\circ} = 4.92\ \theta_y^{\circ}$. Since the total joint rotation $\Omega_{CB} = O$, $\psi_{CB} = \alpha_{CB}$. Therefore, FIGURE 13 is entered with $\alpha_{ij} = \alpha_{CB} = 6.77\ \theta_y^{BC}$, and $M_{ji} = M_{BC} = 1.15\ M_{fp}$. The corresponding near-end moment $M_{ij} = M_{CB}$ is thus obtained as 1.38 M_{fp}. Since this value does not agree with the assumed value (1.32 M_{fp}), the procedure is repeated

until convergence of the moments is obtained. The final values for M_{BA} and M_{CB} are thus 1.14 and 1.37 M_{fp}, respectively. These derived moments are then used to compute the load which produces the assumed deflection. From statics, the horizontal reaction at the left column is,

$$H = 1.14 \times 170 \; / \; 48 = 4.04 \text{ kips}$$

and, $$P/2 = \frac{(1.37 + 1.14) \times 170 - 4.04 \times 3.0}{36} = 11.5$$

Therefore, $P = 23.0$ kips.

Thus, a load of 23.0 kips produces a deflection of 3.0 inches. An identical procedure is used to obtain the desired number of points for the entire load-deflection curve for this frame.

c) Frame No. 2

Frame No. 2, which was subjected to a concentrated horizontal load at the top of the left column, is shown in FIGURE B3(a). The deflected shape of the structure and the correct directions of moments are shown in FIGURE B3(b). To illustrate the procedure used to obtain a value for deflection at the top of the column, a load of 7.8 kips is used with the "moment end-slope" relationships derived from the beam tests.

The elastic limit angle-changes for the frame components are as follows:

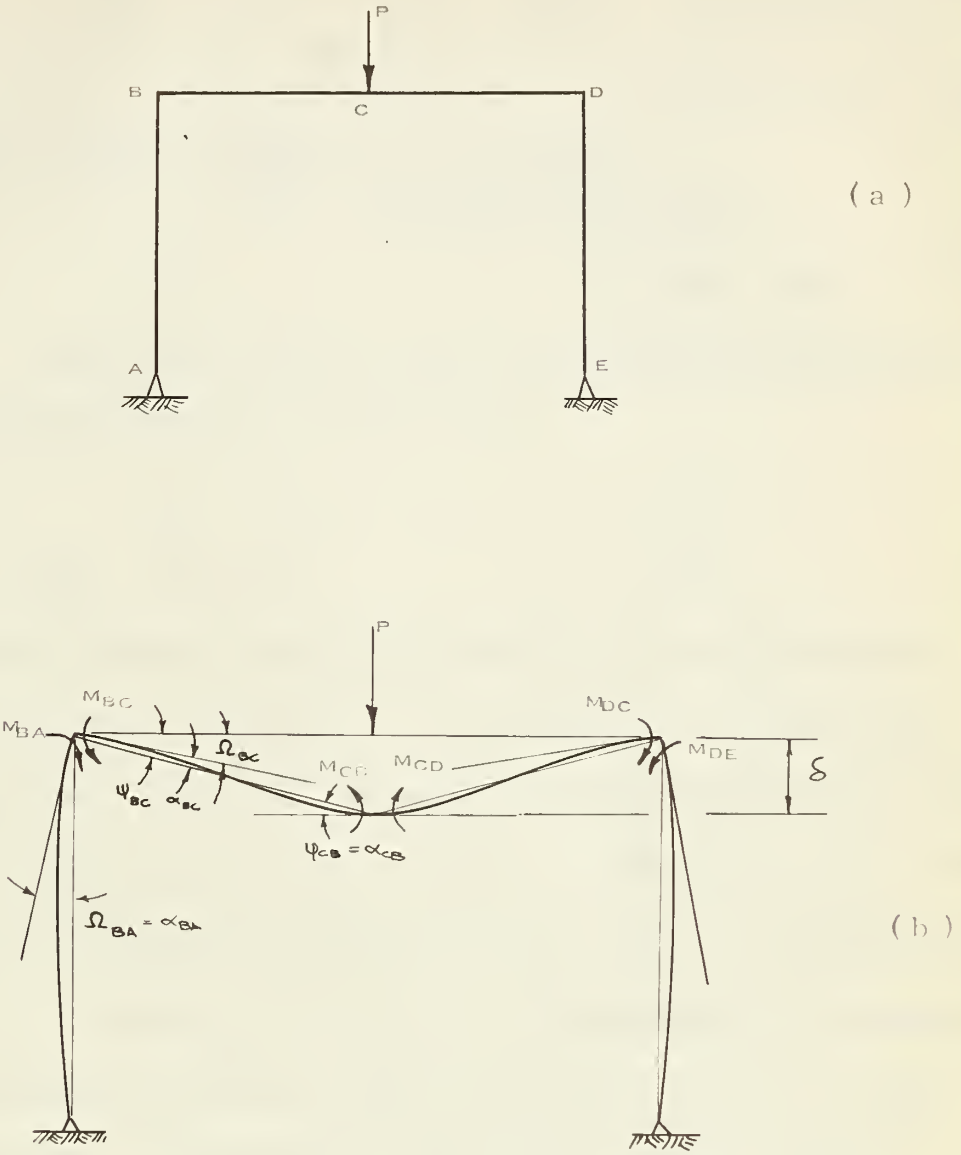

MOMENTS AND DEFORMATIONS FOR FRAME NO. 1

FIGURE B2

$$\Theta_y^{AB} = \Theta_y^{BA} = \Theta_y^{CD} = \Theta_y^{DC} = \frac{M_y L}{2\ EI} = \frac{153 \times 48}{2 \times 29.35 \times 10^6 \times 7.13}$$

$$= 0.01745 \text{ rad.} = \Theta_y^\circ$$

$$\Theta_y^{BC} = \Theta_y^{CB} = \frac{M_y L}{2\ EI} = \frac{153 \times 72}{2 \times 29.35 \times 10^3 \times 7.13}$$

$$= 0.0246 \text{ rad.} = 1.50\ \Theta_y^\circ$$

Referring to FIGURE B3(b), the equilibrium and continuity requirements at joint B are, respectively,

$$M_{BA} = M_{BC} \ldots\ldots\ldots\ldots\ldots\ldots (12)$$

and, $$\Omega_{BA} = \Omega_{BC} \ldots\ldots\ldots\ldots\ldots\ldots (13)$$

For a load of 7.8 kips, the resulting moment at B, assuming equal distribution of load in each column, is 7.8 x 48 / 2 = 187 inch-kips = 1.03 M_{fp}. Since member BC has double curvature, FIGURE 14 is used and since member BA has single curvature, FIGURE 16 is used. For member BC, FIGURE 14 is entered with $M_{ij} = M_{BC} = 1.03\ M_{fp}$ and $M_{ji} = M_{CB} = 1.03\ M_{fp}$ (by symmetry). The end-slope corresponding to these moments as given by FIGURE 16 is $\alpha_{ij} = \alpha_{BC} = 0.69\ \Theta_y^{BC}$. Since $\Omega_{BC} = \alpha_{BC}$, the total joint rotation $\Omega_{ij} = \Omega_{BC} = 0.69\ \Theta_y^{BC}$. But, $\Theta_y^{BC} = 1.50\ \Theta_y^\circ$, therefore, $\Omega_{BC} = 0.69 \times 1.50 = 1.035\ \Theta_y^\circ$. To satisfy Equation (13), $\Omega_{BA}/\Theta_y^\circ = 1.035 = \Omega_{BA}/\Theta_y^{BA}$. To complete the analysis for member BA, FIGURE 16 is entered with $M_{ij} = M_{BA} = 1.03\ M_{fp}$ and $M_{ji} = M_{AB} = 0$. The corresponding end-slope, from FIGURE 16, is $\alpha_{ij} = \alpha_{BA} = 1.36\ \Theta_y^{AB}$. The resultant chord displace-

ment angle, ψ_{BA}, is thus, $\psi_{BA} = \Omega_{BA} + \alpha_{BA} = (1.035 + 1.36) = 2.395\ \Theta_y^{BA}$. With this value for the chord displacement, the horizontal deflection at the top of the columns is calculated to be,

$$\delta = \psi_{BA} \times L_{BA} \times \Theta_y^{BA}$$

$$= 2.395 \times 48 \times 0.01745 = 2.0 \text{ inches.}$$

An identical procedure is used to obtain the desired load-deflection curve for this frame.

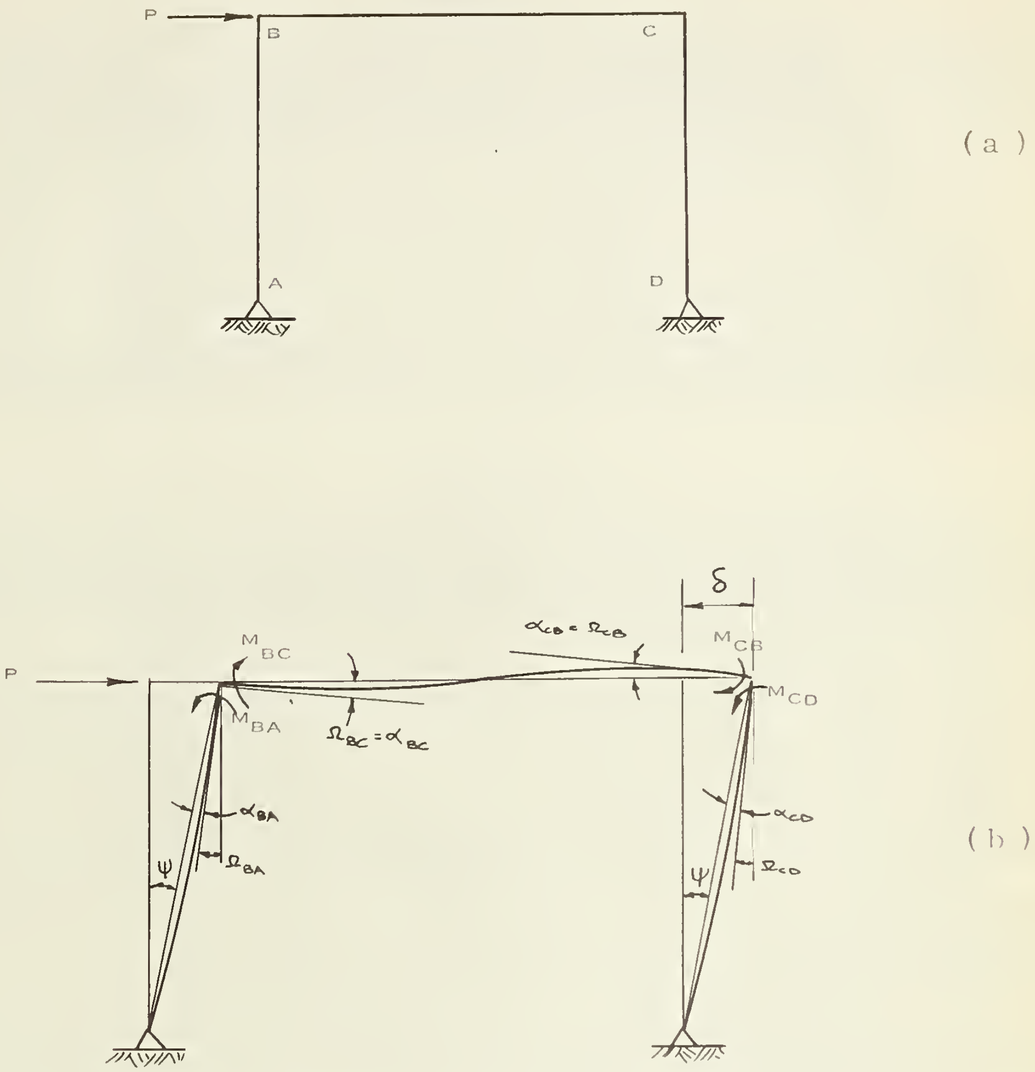

MOMENTS AND DEFORMATIONS FOR FRAME NO 2

FIGURE B3

TABLE B

BEAMS

JOINT	ij	M_{ij}/M_{fp}	M_{ji}/M_{fp}	$\alpha_{ij}/\theta_y^{ij}$	$\Omega_{ij}/\theta_y^{ij}$	$\Omega_{ij}/\theta_y^{\circ}$
(1)	(2)	(3)	(4)	(5)	(6)	(7)
C	CB	1.11	1.11	13.0	0	0
B	BC	1.11	1.11	13.0	26.0	26.0
B	BA	1.11	0	2.55	17.3	26.0

FRAME NO. 1

JOINT	ij	M_{ij}/M_{fp}	M_{ji}/M_{fp}	$\alpha_{ij}/\theta_y^{ij}$	$\Omega_{ij}/\theta_y^{ij}$	$\Omega_{ij}/\theta_y^{\circ}$
B	BA	1.15	0	4.21	4.21	5.61
	BC	1.15	1.32	1.85	4.92	4.92
C	CB	1.38	1.15	6.77	0	0
B	BA	1.13	0	3.72	3.72	4.96
	BC	1.13	1.35	1.41	5.36	5.36
C	CB	1.36	1.13	6.77	0	0
B	BA	1.14	0	4.0	4.0	5.34
	BC	1.14	1.38	1.40	5.37	5.37
C	CB	1.37	1.14	6.77	0	0

FRAME NO. 2

JOINT	ij	M_{ij}/M_{fp}	M_{ji}/M_{fp}	$\alpha_{ij}/\theta_y^{ij}$	$\Omega_{ij}/\theta_y^{ij}$	$\Omega_{ij}/\theta_y^{\circ}$
B	BC	1.03	1.03	0.69	0.69	1.035
	BA	1.03	0	1.36	1.035	1.035

APPENDIX C

COMPUTER PROGRAM FOR MOMENT END-SLOPE RELATIONSHIPS

Calculations used in the derivation of the "moment end-slope" relationships are routine in that for a given pair of end moments, the end-slope is obtained by a numerical integration of the curvature diagram. In deriving these relationships, use of a digital computer is a necessity, since the time involved in a "long-hand" solution would be prohibitive. In order to obtain the "moment end-slope" relationships for the 4 I 9.5 section, a program was written in Fortran for the IBM 1620 digital computer. A brief description of the essential components of this program is presented in this section.

The computer is first instructed to read, and store into memory, values of curvature (ALPHA), and corresponding values of moment (BETA). Two sets of values of the moment-curvature relationship were used as the input data. The first set was the moment-curvature values derived from the tension test results (theoretical); the second set was the moment-curvature values obtained from the beam tests (experimental).

A simply-supported beam with moments applied at both ends, is then divided into a specified number of equally-spaced divisions (FN). For given values of moment at both ends of the span, the moment value at each division point in the beam is determined from either of the

following equations:

(a) Single Curvature

$$Z = (X - Y)\left(\frac{FN - W}{FN}\right) + Y$$

or, (b) Double Curvature

$$Z = X - \frac{W}{FN}(X + Y)$$

where,

Z = value of moment at location W

W = position along beam, i.e. $W \quad 1, \ldots\ldots FN$

X = value of moment at left end

Y = value of moment at right end

For each moment value, Z, a corresponding value for curvature is then obtained, by an interpolation of the moment-curvature values previously stored in the memory unit. Thus, for given end-moments X and Y, a corresponding curvature diagram is obtained.

The reaction (slope) at the left end of the beam (RL), loaded with this curvature diagram, is then determined by a numerical integration procedure. The end-moments are then incremented by a small amount, and the procedure is repeated until the desired range of values is obtained.

A print-out of the actual computer program is shown for the cases of single curvature and double curvature in the following pages.

```
..IDENT TRUCH 920115
..LOAD FORGO CLOCK 9600
C     SINGLE CURVATURE
      DIMENSION ALPHA(25),BETA(25),AA(26)
 4    DO 5 I=1,25
 5    READ,ALPHA(I),BETA(I)
      FN=25.
      N=FN
      N=N+1
      X=0.
25    Y=0.
26    W=0.
      DO 10 J=1,N
      Z=(X-Y)*(FN-W)/FN+Y
      W=W+1.
      K=1
15    IF(Z-BETA(K))16,9,12
 9    AA(J)=ALPHA(K)
      GO TO 10
12    K=K+1
      GO TO 15
16    C=(Z-BETA(K-1))/(BETA(K)-BETA(K-1))*(ALPHA(K)-ALPHA(K-1))
      AA(J)=ALPHA(K-1)+C
10    CONTINUE
      RL=0.
      DO 60 I=1,25
      U=I
60    RL=RL+(AA(I)+AA(I+1))*(.0392-.0016*(U-1.))
      PUNCH,X,Y,RL
      IF(X-1.5)20,21,21
20    X=X+.1
      GO TO 26
21    IF(Y-1.4)40,41,41
40    X=0.
      Y=Y+.1
      GO TO 26
41    GO TO 4
      END
```

```
..IDENT TRUCH 920115
..LOAD FORGO CLOCK 9600
C       DOUBLE CURVATURE
        DIMENSION ALPHA(25),BETA(25),AA(26)
 4      DO 5 I=1,25
 5      READ 70,ALPHA(I),BETA(I)
 70     FORMAT(1X,F5.2,2X,F5.3)
        FN=25.
        N=FN
        N=N+1
        X=0.
25      Y=0.
26      W=0.
        DO 10 J=1,N
        Z=X-(W/FN)*(X+Y)
        W=W+1.
        K=1
        ZZ=Z
        IF (Z)14,15,15
14      Z=-Z
15      IF (Z-BETA(K))16,9,12
 9      AA(J)=ALPHA(K)
        GO TO 17
12      K=K+1
        GO TO 15
16      C=(Z-BETA(K-1))/(BETA(K)-BETA(K-1))*(ALPHA(K)-ALPHA(K-1))
        AA(J)=ALPHA(K-1)+C
17      IF(ZZ)50,10,10
50      AA(J)=-AA(J)
10      CONTINUE
        RL=0.
        DO 60 I=1,25
        U=I
60      RL=RL+(AA(I)+AA(I+1))*(.0392-.0016*(U-1.))
        PUNCH 71,X,Y,RL
 71     FORMAT(F10.5,F10.5,F15.5)
        IF(X-1.5)20,21,21
20      X=X+.1
        GO TO 26
21      IF(Y-1.4)40,41,41
40      X=0.
        Y=Y+.1
        GO TO 26
41      GO TO 4
        END
```

APPENDIX D

TEST RESULTS FROM TENSION TESTS

The average stress-strain relationship (FIGURE 6) for the 4 I 9.5 material used in this investigation was obtained from the tensile test results, which are presented in tabular form in this section. The actual stress-strain curves for each individual coupon are available at the Department of Civil Engineering, University of Alberta, Edmonton, Alberta.

NO.	AREA	UYP (psi)	St. YP(psi)	e_y (in./in.)	e_{st} (in./in.)
KF1	0.120	41, 900	41, 250	0.00164	0.0134
KF2	0.125	45, 200	42, 500	0.00156	0.0129
KF3	0.121	45, 000	42, 800	0.00150	0.0129
KF4	0.127	43, 300	42, 000	0.00148	0.0157
WF5	0.123	41, 900	40, 200	0.00148	0.0128
WF6	0.128	44, 100	41, 300	0.00141	0.0136
WF7	0.118	44, 900	42, 200	0.00141	0.0114
WF8	0.125	44, 200	41, 400	0.00138	0.0108
LF9	0.125	46, 000	43, 600	0.00153	0.0098
LF10	0.118	45, 800	43, 000	0.00156	0.0099
LF11	0.130	48, 100	44, 800	0.00138	0.0113
SF12	0.131	45, 400	41, 800	0.00148	0.0152
SF 13	0.128	44, 900	43, 200	0.00150	0.0143
SF14	0.117	43, 800	40, 800	0.00131	0.0088
KW1	0.207	41, 100	37, 800	0.00134	0.0170
KW2	0.205	44, 600	40, 600	0.00148	0.0161
KW3	0.205	41, 200	37, 700	0.00131	0.0156
KW4	0.208	43, 500	39, 200	0.00138	0.0158
WW5	0.205	44, 100	40, 900	0.00134	0.0154
WW6	0.207	42, 800	39, 000	0.00144	0.0163
WW7	0.207	40, 800	37, 500	0.00137	0.0159
WW8	0.206	41, 000	37, 300	0.00119	0.0177
LW9	0.200	49, 500	44, 800	0.00156	0.0148
LW10	0.200	48, 200	44, 750	0.00156	0.0168
LW11	0.200	45, 750	42, 900	0.00156	0.0185
SW12	0.205	40, 700	38, 200	0.00119	0.0151
SW13	0.205	42, 200	38, 900	0.00141	0.0166
SW14	0.206	43, 200	39, 700	0.00147	0.0163

"F" Denotes coupons cut from flanges

"W" Denotes coupons cut from webs

B29808